

Sabrina Püschmann, BSc

# **Preparation and characterization of J-aggregates on basis of new fluorescent dyes**

## **MASTER'S THESIS**

to achieve the university degree of

Diplom-Ingenieur (Dipl.-Ing.)

Master's degree programme: Technical Chemistry

submitted to

**Graz University of Technology**

Supervisor

Assoc.Prof. kand. Sergey Borisov

Institute of Analytical Chemistry and Food Chemistry

Head of the Institute: Ao.Univ.-Prof. Dipl.-Ing. Dr.techn. Erich Leitner

Graz, September, 2019



“The world is a book and those who do not travel read only one page.”  
- *Augustinus von Thagaste*



---

# Abstract

The aim of this master thesis lays in the synthesis of new  $\pi$ -extended BODIPY's as J-aggregates and the resulting properties characterization. J-aggregates belong to supra-molecular structures with intriguing photophysical properties such as strongly bathochromically shifted absorption and emission, very narrow spectral bands, "superquenching" capabilities. State-of-the-art systems mostly rely on cyanine dyes, J-aggregates based on other dye classes being extremely rare. In this work new fluorescent dyes with functionalities enabling efficient formation of J-aggregates have been synthesized. Photophysical properties of the monomers and J-aggregates have been investigated and their potential for sensing applications evaluated. The J-aggregates showed a large bathochromic shift from red to NIR part of the spectrum and also featured sharp, narrow peaks in absorption and fluorescence in contrast to the monomeric peak. Importantly, the J-aggregates show moderate fluorescence with quantum yields up to 5 %, whereas the monomeric form achieved yields up to 85 %. Formation of J-aggregates both in micellar solutions and in polymers has been demonstrated.



---

# Kurzfassung

Das Ziel dieser Arbeit war die Synthese neuer  $\pi$ -erweiterter BODIPY Farbstoffe als J-Aggregate und die Charakterisierung der daraus resultierenden Eigenschaften. J-Aggregate zählen zu den 'supra-molekularen' Strukturen, mit faszinierenden Eigenschaften, dazu zählen die starke bathochrome Verschiebung der Absorption und Emission, sehr schmale Bandbreiten und die Fähigkeit des 'Superquenchens'. Der aktuelle Stand bezieht sich hauptsächlich auf Cyanin-Farbstoffe, andere Farbstoffklassen sind selten und bilden nur vereinzelt J-Aggregate. Während dieser Arbeit wurden neue Farbstoffe mit verschiedenen funktionellen Gruppen synthetisiert, diese ermöglichen die effiziente J-Aggregat Formierung. Die photophysikalischen Eigenschaften der Monomere und Aggregate wurden untersucht und ihr Potential zur Anwendung als Sensor wurde ermittelt. Die J-Aggregate zeigten eine enorme bathochrome Verschiebung vom roten Bereich des Lichtes in den nahen Infrarot-Bereich des Spektrums. Zusätzlich zeigten diese steile und schmale Peaks in deren Absorptions- und Fluoreszenzspektren im Vergleich zur monomeren Form. Wichtig zu erwähnen ist, dass J-Aggregate mäßige Fluoreszenz zeigen mit Quanten Ausbeuten von maximal 5 %, wohingegen BODIPY Monomere hohe Werte, bis zu 85 % erzielten. Die Bildung von J-Aggregaten wurde sowohl in Tensiden, als auch in Polymeren gezeigt.





---

## **EIDESSTATTLICHE ERKLÄRUNG**

Ich erkläre an Eides statt, dass ich die vorliegende Arbeit selbstständig verfasst, andere als die angegebenen Quellen/Hilfsmittel nicht benutzt, und die den benutzten Quellen wörtlich und inhaltlich entnommenen Stellen als solche kenntlich gemacht habe. Das in TUGRAZonline hochgeladene Textdokument ist mit der vorliegenden Masterarbeit identisch.

## **AFFIDAVIT**

I declare that I have authored this thesis independently, that I have not used other than the declared sources/resources, and that I have explicitly indicated all material which has been quoted either literally or by content from the sources used. The text document uploaded to TUGRAZonline is identical to the present master's thesis.

---

Datum/Date

---

Unterschrift/Signature



---

# Danksagung

Danken möchte ich auf diesem Wege sehr vielen Menschen, alle die den Weg bis dato mit mir verlebt haben, Momente geschaffen und mich zu dem Menschen gemacht haben, der ich heute bin und in Zukunft sein werde.

Beginnen möchte ich bei der gesamten ACFC (Institute of Analytical Chemistry and Food Chemistry), die durch ihren guten Zusammenhalt ein gutes Arbeitsklima bewirkten, in dem man sich sehr wohl fühlte. Auch wegen der Weihnachtsfeiern und voranschreitender Abschlussfeiern, die immer Spaß bereiteten. Auch wegen der Kuchentradition, die ich vermissen werde.

Besonders jedoch bei Sergey, der mich seit meiner Bachelorarbeit, über die Tätigkeit als studentischer Mitarbeiter bis hin zur Masterarbeit begleitete mit seinem vielseitigen Wissen und seinen Ideen, die zur Abschließung dieser spannenden Arbeit führten.

Namentlich möchte ich auch Matthias erwähnen, der einige Vortests in dem Bereich durchgeführt hat, ein paar seiner hergestellten Proben von mir weiterverwendet wurden und den ich immer mit Fragen nerven konnte, wenn ich Unsicherheiten hatte.

Bedanken möchte ich mich auch bei Berni (braun), da ich ein Edukt für einen Versuch von ihm verwendet habe.

Ein weiterer Dank, in diesem Sinne, gilt unserem InstitutsLEITNER (Achtung: Wortspiel) und Ingo Klimant.

Größter Dank gilt meinen Eltern. Ohne sie wäre meine gesamte universitäre Ausbildung nicht möglich gewesen. Meine Eltern unterstützen mich moralisch, ermutigten mich meinen Zielen hinterherzujagen und diese wahr werden zu lassen, und natürlich auch finanziell, ein sehr wichtiger Aspekt über die Jahre.

---

Des Weiteren bedanke ich mich bei meiner gesamten Familie und meinen Freunden, die mich auch ausgehalten haben, als der Stress überhandnahm, mich ablenkten und mit denen ich meine freien Tage oder auch nur einzelne Minuten und Augenblicke genossen habe. Angeblich findet man Freunde fürs Leben während dem Studium und ich glaube, dass ist mir mit meinen Freunden gelungen. Auch wenn sich unsere Wege nach dem Studium teilweise in unterschiedliche Richtungen bewegen werden, werden immer wieder Kreuzungen kommen, an denen wir uns treffen und einen Teil des Weges wieder gemeinsam beschreiten werden.

Danke an euch alle!

Sabrina Püschmann, BSc

Graz, September, 2019

---

# Contents

## Abstract

<b>1</b>	<b>Introduction</b>	<b>1</b>
<b>2</b>	<b>Theoretical Background</b>	<b>3</b>
2.1	Fundamentals of Luminescence . . . . .	3
2.1.1	Physical Background about the Absorption of Light . . . . .	4
2.1.2	Franck-Condon Principle . . . . .	5
2.1.3	The Perrin-Jablonski Diagram . . . . .	6
2.1.4	Characteristics of Fluorescence Emission . . . . .	8
2.1.5	Luminescence Quenching . . . . .	9
2.2	J-aggregates . . . . .	11
2.2.1	Introduction . . . . .	11
2.2.2	Formation and optical properties . . . . .	11
2.2.3	Prime example for J-aggregates: pseudoisocyanine dye (PIC) . . . . .	13
2.2.4	Other examples for J-aggregation and how they differ . . . . .	14
2.2.5	Red and NIR J-aggregates . . . . .	17
2.2.6	Influence of additional surfactants . . . . .	19
2.2.7	Field of applications . . . . .	20
2.3	BODIPY . . . . .	21
2.3.1	Syntheses route . . . . .	21
2.3.2	Modification of the BODIPY core . . . . .	22
<b>3</b>	<b>Materials and Methods</b>	<b>24</b>
3.1	List of used solvents . . . . .	24
3.2	NMR Solvents . . . . .	24
3.3	List of used Chemicals . . . . .	25
3.3.1	List of Surfactants . . . . .	26
3.3.2	List of Polymers . . . . .	26
3.4	Chromatography . . . . .	27
3.4.1	Thin Layer Chromatography (TLC) . . . . .	27
3.4.2	Flash Column Chromatography . . . . .	27

3.5	Photophysical Measurements . . . . .	27
3.5.1	Absorption . . . . .	27
3.5.2	Emission and Excitation . . . . .	28
3.5.3	Lifetime . . . . .	28
3.5.4	Quantum Yield . . . . .	28
3.6	Structural Characterization . . . . .	29
3.6.1	Nuclear Magnetic Resonance Spectroscopy (NMR) . . . . .	29
3.6.2	High Resolution Mass Spectrometry (HR-MS) . . . . .	29
<b>4</b>	<b>Experimental</b>	<b>30</b>
4.1	Synthesis of symmetrical BODIPY derivatives . . . . .	30
4.1.1	Cl-rigid m-decyloxy BODIPY (21) . . . . .	30
4.1.2	1,3,7,9-Tetramethyl m-decyloxy BODIPY (22) . . . . .	32
4.1.3	2,5,8,11-tetraoxatridecan-13-yl-4-methylbenzenesulfonate: Tos TEG (23) . . . . .	33
4.1.4	4-((2,5,8,11-tetraoxatridecan-13-yl)oxy)benzaldehyde: TEG Benzaldehyde (24) . . . . .	33
4.1.5	Cl-rigid m-TEG BODIPY (25) . . . . .	34
4.1.6	4-propylphenyl m-TEG BODIPY (27) . . . . .	35
4.1.7	3,4-dihydro-6-TEG-naphthalen-1(2H)-one (28) . . . . .	36
4.1.8	7-TEG-3-phenyl-pyrrole (29) . . . . .	37
4.1.9	TEG-m-perfluoro BODIPY (31) . . . . .	38
4.1.10	p-Tolyl ethynyl sulfone (33) . . . . .	39
4.1.11	2-Tosylbicyclo[2,2,2]octa-2,5-diene (34) . . . . .	40
4.1.12	Ethyl-4,7-dihydro-4,7-ethano-2H-isoindole-1-carboxylate (35) . . . . .	40
4.1.13	2-Methyl-4,7-dihydro-4,7-ethano-2H-isoindole (36) . . . . .	41
4.1.14	Different attempts to synthesize 14-(4-decyloxy)phenyl-7-7-difluoro-5,9-dimethyl-1,7,10,13-tetrahydro-4H-diethano[1,3,2]diazaborino diisoindole (37) . . . . .	42
4.1.15	retro Diels-Alder . . . . .	44
4.2	Synthesis of asymmetrical BODIPY derivatives . . . . .	45
4.2.1	9-chloro-13-(4-(decyloxy)phenyl)-5,5-difluoro-1,3-dimethyl-12-phenyl-5,11-dihydro-5l4,6l4-indeno[2',1':4,5]pyrrolo[2,1-f]pyrrolo[1,2-c][1,3,2]diazaborinine (39) via different attempts . . . . .	45
4.2.2	method 2 . . . . .	46
4.2.3	p-(4-((2,5,8,11-tetraoxatridecan-13-yl)oxy)styryl)-(4-(decyloxy)phenyl)-difluoro-trimethyl-5H-dipyrrolo diazaborinine (42) . . . . .	47
4.3	Synthesis of amphiphilic BODIPYs . . . . .	48
4.3.1	Cl-rigid m-decyloxy B-TEG BODIPY (43) . . . . .	48
4.3.2	Cl-rigid m-TEG B-decyloxy BODIPY (44) . . . . .	49
4.3.3	Cl-rigid m-perfluoro B-TEG BODIPY (46) . . . . .	50

---

4.3.4	Tetramethyl m-decyloxy B-TEG BODIPY (47)	51
4.4	Preparation of J-aggregates	52
4.4.1	J-aggregate formation in various surfactants	52
4.4.2	J-aggregate formation in various polymers	52
<b>5</b>	<b>Results and Discussion</b>	<b>54</b>
5.1	Synthetic Considerations	54
5.1.1	Synthesis of BODIPY dyes	54
5.1.2	Attempted Synthesis of Asymmetrical BODIPY	58
5.1.3	Substitution of Fluorine with Alcohols	59
5.2	Dye Characterization	62
5.2.1	Absorption and Emission Spectra	62
5.2.2	Quantum Yield	64
5.2.3	Fluorescence Lifetime	64
5.3	Formation of J-aggregates	65
5.3.1	Aggregates with Surfactants	65
5.3.2	Formation of J-aggregates in Polymers	77
5.4	Photophysical Properties of the J-aggregates	84
5.4.1	Absorption and Emission Spectra	84
5.4.2	Quantum Yields	87
5.4.3	Fluorescence Lifetime	87
<b>6</b>	<b>Conclusion and Outlook</b>	<b>88</b>
<b>7</b>	<b>References</b>	<b>90</b>
<b>8</b>	<b>List of Figures</b>	<b>99</b>
<b>9</b>	<b>List of Tables</b>	<b>103</b>
<b>10</b>	<b>Appendix</b>	<b>105</b>
10.1	Supporting Information	105
10.1.1	Attempts to couple alcohol at the boron center	105
10.1.2	Synthesis of Ethyl-4,7-dihydro-2H-4,7-ethanoisindole-1-carboxylate (35)	106
10.1.3	Synthesis 14-(4-decyloxy)phenyl-7,7-difluoro-5,9-dimethyl-1,7,10,13-tetrahydro-4H-diethano[1,3,2]diazaborino diisindole (37)	106
10.2	Remaining Absorption and Emission Spectra	107
10.3	NMR Spectra	108
10.3.1	Compound 21	108
10.3.2	Compound 22	110
10.3.3	Compound 23	113

---

---

10.3.4	Compound 24 . . . . .	115
10.3.5	Compound 25 . . . . .	116
10.3.6	Compound 27 . . . . .	118
10.3.7	Compound 28 . . . . .	120
10.3.8	Compound 33 . . . . .	121
10.3.9	Compound 34 . . . . .	122
10.3.10	Compound 35 . . . . .	123
10.3.11	Compound 36 . . . . .	126
10.3.12	Compound 37 . . . . .	127
10.3.13	Compound 38 . . . . .	128
10.3.14	Compound 42 . . . . .	129
10.3.15	Compound 43 . . . . .	130
10.3.16	Compound 44 . . . . .	132
10.3.17	Compound 45 . . . . .	134
10.3.18	Compound 47 . . . . .	135
10.4	MS Data . . . . .	136
10.4.1	Compound 21 . . . . .	136
10.4.2	Compound 22 . . . . .	138
10.4.3	Compound 25 . . . . .	140
10.4.4	Compound 27 . . . . .	143
10.4.5	Compound 38 . . . . .	147
10.4.6	Compound 43 . . . . .	149
10.4.7	Compound 44 . . . . .	151
10.4.8	Compound 45 . . . . .	152
10.4.9	Compound 46 . . . . .	156
10.4.10	Compound 47 . . . . .	158



---

# 1 Introduction

Nowadays novel sensing and imaging based on fluorescence in the near-infrared region is of high interest. Advantage of NIR is the low interference of impurities and especially in field of bio medicine, where tumor cells could be detected easily [1]. Another broad and interesting field are solar cells, because a huge amount of sunlight is part of the light in the NIR region [2].

In general are BODIPY derivatives one of the most important chromophore dye class, because of their strong UV absorbance and the dyes emit fluorescence characterized by sharp peaks yielding in high quantum yields (60-90 %). By tuning the BODIPY core a bathochromical shift is easily accomplished [3]. By further forming J-aggregates, a even higher shift can be obtained. During the last decades J-aggregates, first introduced in the 30s by Jelley [4] and Scheibe [5], get more and more attention by supramolecular approaches and their wide field of possible applications. The aggregated form, a ordered cluster of molecular dyes, has unique properties, like a huge bathochromical shift with narrow width, a negligible Stokes shift and "superquenching". Due to their strong light absorption, these aggregates have attracted attention in the filed of photographic processes as spectral sensitization with silver halides [6] and also are interesting for artificial light harvesting systems [7, 8].

Until now, mostly cyanine dyes are reported [9] to form the highly ordered structures, other dye classes only show rarely dyes, which enable the capability to form J-aggregates. Porphyrins [10, 11], chlorins [12], perylene bisimides [13] count as examples. Also with azaBODIPYs a success was achieved, however does the formation take several weeks [14].

The latest achievement was by modifying the cyanine dye structure to gain an amphiphilic character, the hydrophobic and hydrophilic parts should control the structural ordering after self-assembling. Amphiphilic dyes can be used in various applications, like in light harvesting systems or for dye sensitized solar cells [15].



---

## 2 Theoretical Background

### 2.1 Fundamentals of Luminescence

The references in this chapter and the following subchapters are derived from [16–18]. Therefore, only other references will be cited separately.

What is Luminescence? The principle is based on the emission of photons with energies in the ultraviolet, visible or infrared region. An electron in the molecule is excited from the ground state ( $S_0$ ) to an electronically higher excited state ( $S_n$ ) by an external source of energy. During relaxation back into the ground state the electron loses energy in form of heat or electromagnetic radiation, also called luminescence.

There are different types of luminescence: electroluminescence (excitation occurs in an electrical field), chemoluminescence (after a chemical process), bioluminescence (e.g. fireflies) and the most important one is photoluminescence. In case of photoluminescence, light is used as the energy source. A distinction is drawn between fluorescence, a spin allowed relaxation of the electron, delayed-fluorescence and phosphorescence, a spin forbidden process.

Other possibilities of the electron pathway are internal conversion (IC), intersystem crossing (ISC) and intramolecular charge transfer. The mentioned categories will be further described in section 2.1.3 and in figure 2.1.

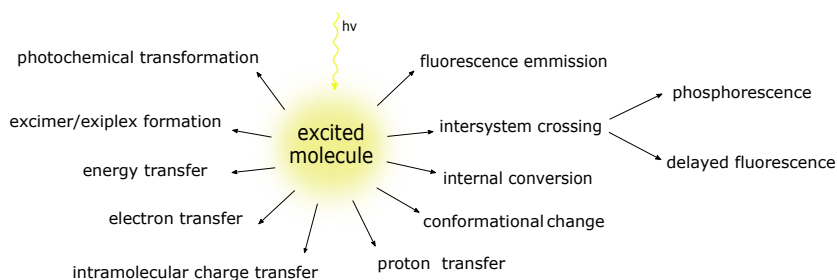


**Figure 2.1:** Possible de-excitation processes after excitation of a molecule

The term dye or lumiphore is used, when a photon of the visible (VIS) range (380 – 740 nm) is absorbed by the molecule.

### 2.1.1 Physical Background about the Absorption of Light

During the absorption of a photon the electron in the orbital of the molecule changes the location of the ground state to an unoccupied orbital of a higher state.

Orbitals of  $\pi$  and  $\sigma$  origin need to be distinguished. Whereas  $\sigma$  orbitals can be formed in different ways, with two s atomic orbitals, one s and one p or from two p atomic orbitals in a collinear axis. In contrast, the  $\pi$  orbital is only formed from two overlapping p orbitals. Non-bonding (n) electrons occur in case of heteroatoms, like oxygen or nitrogen. These orbitals obtain different energies (the \* denotes the anti-bonding molecule), which are in following order:

$$n \rightarrow \pi^* < \pi \rightarrow \pi^* < n \rightarrow \sigma^* < \sigma \rightarrow \pi^* < \sigma \rightarrow \sigma^*$$

In case of absorption and fluorescence spectroscopy the so-called Highest Occupied Molecular Orbital (HOMO) and the Lowest Unoccupied Molecular Orbital (LUMO) are of importance.

During a transition from one molecular orbital (MO) to another the spin of an excited electron remains generally unchanged, leading to a total spin quantum number of zero ( $S = \sum s_i$ , with  $s_i = +\frac{1}{2}$  or  $s_i = -\frac{1}{2}$ ). Therefore, the multiplicity ( $M = 2S + 1$ ) of the ground state and excited state equals 1. In this case, the excited state is called singlet state.

Although, a transition, which changes the spin-orientation, resulting in an state with two unpaired electrons with parallel spin are spin forbidden, can occur due to the "spin-orbit coupling". Here the total spin quantum number is 1 and the multiplicity is 3, therefore the excited state is called triplet state. According to the Hund's Rule three states of equal energy can be observed with lower energy than that of a singlet state.

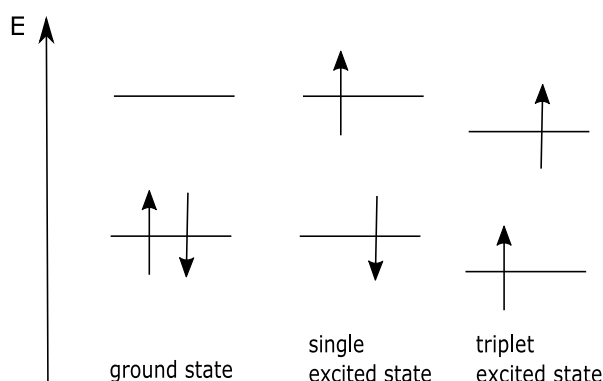


**Figure 2.2:** Differences in states (Hund's rule) and spin orientation in the excited states

## Selection rules

For electron transitions two selection rules can be applied, they can be spin-forbidden and symmetry-forbidden which lead to a decrease in their probability to occur.

In the first case, the spin-forbidden transition, transitions between states of different multiplicities are not allowed, like in singlet-triplet transitions. However, a weak interaction between wavefunctions of different multiplicities is present, which is a result of the spin-orbit coupling (see 2.1.1 and in section 2.1.3 *Intersystem crossing*).

The second rule implies that a transition is forbidden because of the symmetry. Such transitions can be observed due to vibronic coupling.

The efficiency of the absorption of the light at a certain wavelength can be determined with the Lambert-Beer equation:

$$A = \log\left(\frac{I_0}{I}\right) = \epsilon \cdot c \cdot d \quad (2.1)$$

A	absorbance
$I_0$	intensity of entering light in absorbing medium
I	intensity leaving the absorbing medium
$\epsilon$	molar absorption coefficient [ $l \text{ mol}^{-1} \text{ cm}^{-1}$ ]
c	concentration of absorbing species [ $\text{mol l}^{-1}$ ]
d	thickness of absorbing medium [cm]

The absorbance is defined as the decadic logarithm of the ratio of the light intensity before ( $I_0$ ) and after (I) the sample. The molar absorption coefficient  $\epsilon$  displays the ability of the dye to absorb light. The law also includes the optical path length (which is in general 1 cm) through the sample and the dye concentration.

Due to aggregation or the presence of other absorbing species the linear dependence of the law can be disobeyed.

### 2.1.2 Franck-Condon Principle

Motions of electrons are faster than those of the nuclei, states the Born-Oppenheimer approximation. The excitation of an electron to an anti bonding molecular orbital happens within  $10^{-15}$  s. The fundamentals of the Franck-Condon principle declare that an electronic transition occurs without changes in the location of the nuclei in the molecule or in the environment. The resulting vertical transitions are shown in an energy diagram, in which the potential energy curve is a function of the configuration. The width of an absorption band depends on

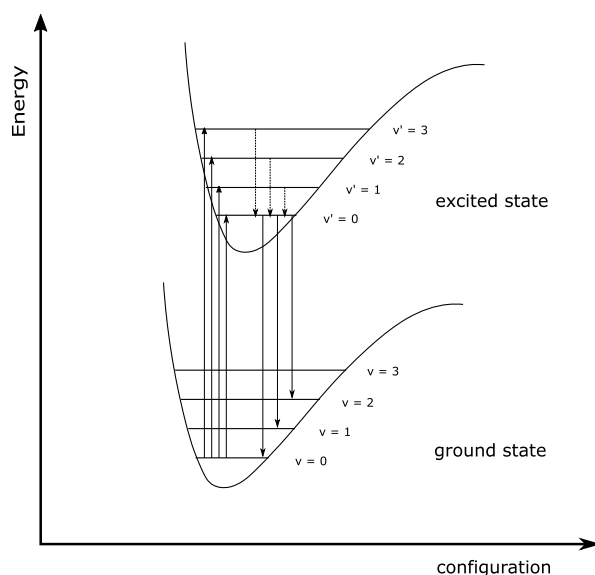


**Figure 2.3:** Illustration of the possible transitions according to the Franck-Condon principle

homogeneity, due to a continuous set of vibrating sublevels, and inhomogeneous broadening, due to fluctuations of the structure of the solvent shell.

### 2.1.3 The Perrin-Jablonski Diagram

After the absorbance of light and resulting excitation from the ground state in a higher electronic state, the de-excitation under emission of energy can happen in various ways. This can either have a radiative or non-radiative origin. The Perrin-Jablonski diagram, seen in figure 2.4, is a common and easy way to show this possible transition processes. In the next chapters the different ways of de-excitations are described in detail.

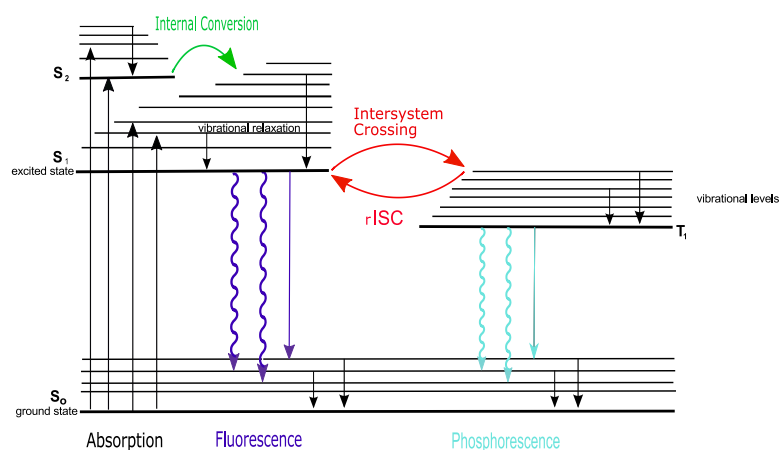


**Figure 2.4:** Perrin-Jablonski diagram showing the de-excitation possibilities

## Non-radiative processes

### *Internal Conversion (IC)*

A transition between two electronic states of the same spin multiplicity from a higher to a lower vibrational level can be observed. Because of a larger energy gap between  $S_1$  and  $S_0$ , it is less efficient than a conversion from  $S_2$  to  $S_1$  and can compete with other processes, like fluorescence and ISC to the triplet state and resulting phosphorescence.

### *Intersystem Crossing (ISC)*

During this de-excitation process, the electron jumps from the  $S_1$  state to the triplet state, which has a different multiplicity. Processes like phosphorescence can follow. This pathway is in general forbidden, unless the spin-orbit coupling is large enough. Spin-orbit coupling is about the interaction of spins and the motion of orbital around the nucleus. Due to the electromagnetic interference between the electric field, where the electron moves freely, and the spin of the electron a shift in the energy levels is the consequence and ISC can be possible [19]. The presence of heavy atoms and collision with solvent molecules favor the ISC.

## Radiative processes

### *Fluorescence*

Fluorescence is the relaxation and resulting emission from the  $S_1$  to the ground state ( $S_0$ ). The fluorescence spectrum is bathochromical shifted compared to the absorption spectrum. The reason can be found in an energy loss to the environment during the vibrational relaxation.

### *Delayed fluorescence*

Instead of a direct de-excitation to the ground state, like it is the case for fluorescence, a reversed ISC from the  $T_1$  to the  $S_1$  can be observed and is followed by a relaxation to the ground state. A transition is only possible, if the energy gap between those different states is small and when the lifetime of the triplet state is long enough. Another difference is that the emission has a longer decay time than conventional fluorescence. The delayed fluorescence emission is temperature dependent, therefore with increasing temperature the efficiency increases. Another possibility which leads to a delayed fluorescence is the triplet-triplet annihilation. After collision of two molecules in the triplet state enough energy is generated to return to the singlet state.

### *Phosphorescence*

Phosphorescence, the relaxation of a higher triplet state to the ground state, is observed particularly at lower temperatures. In this case, the decay lifetime can be up to seconds or

even minutes. The low energy levels, compared to that of the singlet state, lead to a shift to higher wavelengths in the phosphorescence spectrum.

### 2.1.4 Characteristics of Fluorescence Emission

#### Lifetime

As already described, during the absorption of photons electrons are exhilarated to an excited state. The relaxation back into the ground state is not observed immediately. This specific period of time, that the species remains in the excited state is called lifetime  $\tau$ . The radiative and non-radiative processes, described in the Perrin-Jablonski diagram, follow a rate constant  $k$ , which has a different denotation depending on the process (radiative processes  $k_r^S$  and non-radiative  $k_{nr}^S$ ). The rate of the vanishing excited molecules can be described with following equation:

$$-\frac{d[A^*]}{dt} = (k_r^S + k_{nr}^S)[A^*] \quad (2.2)$$

Integration of equation 2.2 leads to an expression, which describes the exponential decay of the electron back to the ground state after pulse light excitation:

$$[A^*] = [A_0^*] \exp\left(-\frac{t}{\tau_S}\right) \quad (2.3)$$

$[A^*]$	concentration of species A in the excited state $[\frac{mol}{l}]$
$[A_0^*]$	concentration of excited molecules at time= 0
t	time [s]
$\tau_S$	lifetime of the excited state $S_1$

#### Quantum yield

The quantum yield is defined as the part of excited molecules, that return back to the ground state under emission of fluorescence photons. A ratio of emitted to absorbed photons is given. The competitive de-excitation reactions lower the quantum yield. An increase of the temperature has also a negative impact.

$$\phi_F = \frac{\text{number of emitted photons}}{\text{number of absorbed photons}} = \frac{k_r^S}{k_r^S + k_{nr}^S} = k_r^S \tau_S \quad (2.4)$$



The quantum yield can be determined either with an absolute method via an integrating sphere set-up or relative method by comparison to a standard with known QY.

### Stokes Shift

The Stokes shift describes the difference between the peak maximum of the fluorescence and the absorption spectrum.

### 2.1.5 Luminescence Quenching

In the previous chapters only de-excitation pathways without inter-molecular interactions were described. Therefore another competitive process can occur, the so-called quenching. This process includes the presence of a quencher molecule and a fast transfer from a donor to an corresponding acceptor (e.g. electron, energy, proton transfer). Due to this interaction the quantum yield decreases.

The environment of a molecule can be analyzed qualitatively and quantitatively (via a kinetic model).

The two main types will be described in the following chapters, the static and dynamic quenching.

#### Static Quenching

The quenching molecule and the fluorescent molecule in the ground state react to a complex, which leads to the loss of luminescence. The fluorescence intensity is affected, however the lifetime is unaffected. This effect is concentration dependent. An application of static quenching is the determination of micellar aggregation numbers.

#### Dynamic Quenching

During dynamic quenching a quencher (Q) molecule collides with an excited lumiphore  $M^*$  and the energy is transferred from the donor (D), which is the excited molecule, to the acceptor (A), the quencher. During this process the luminescence is erased. Both the lifetime and fluorescence intensity are decreased. The process is diffusion controlled.

This quenching mechanism can be described with the Stern-Volmer equation and the corresponding plot:

$$\frac{\phi_0}{\phi} = \frac{I_0}{I} = 1 + k_q \tau_0 [Q] = 1 + K_{SV} [Q] \quad (2.5)$$

whereas  $I$  denotes the fluorescence intensities with and without the quencher,  $\phi$  the quantum yields in both cases and  $K_{SV}$  the Stern-Volmer constant.

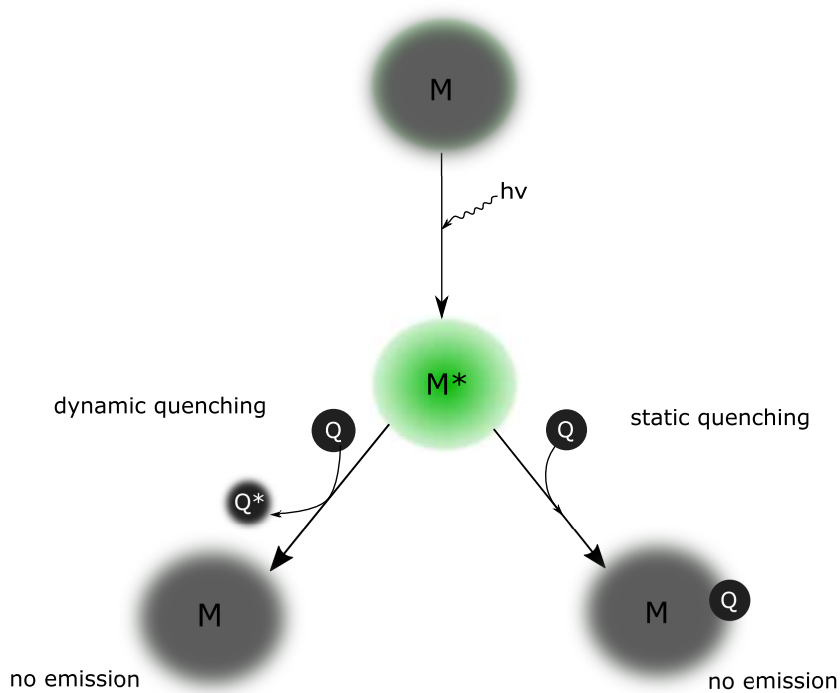


**Figure 2.5:** Mechanism of static and dynamic quenching

## 2.2 J-aggregates

### 2.2.1 Introduction

J-aggregates were first discovered in the 1930s independently by Jelley [4, 20], where the name derived from, and Scheibe [5, 21]. Nowadays many researches became interested in this topic, especially in the field of dye chemistry and supramolecular chemistry. The nanomaterials are formed by highly ordered clusters of the dye molecules. This aggregated molecules show totally different spectral properties in comparison to the monomers and disordered assemblies [9], which will be described in detail later. A variety of dyes, such as chlorins [8, 12, 22], cyanines [9, 23], perylene bisimides [13, 24–26], phthalocyanines [27], porphyrins [10, 11, 28, 29], derivatives of naphthalenes and fluorenes [30] already have been investigated [31]. With BODIPY [3, 32, 33] chromophores it is possible to generate J-aggregates, which absorb and emit in the near-Infrared region (780-1400 nm).

Until now the morphology, size and number of aggregation units are still not fully understood and discussed in many papers. With several analytical techniques the determined aggregation numbers do not match the geometrical size of the aggregates.

### 2.2.2 Formation and optical properties

A lot of different assumptions were made about the allegation of J-aggregates, until Förster [34] concluded, that the monomers are aligned parallel or slightly inclined. The formation takes place due to  $\pi$ - $\pi$  dispersive interaction of highly polarizable groups and electrostatic interactions between opposite charges, leading to a joining of their centers via a *head-to-tail* or *shifted plates* arrangement of the aggregates.

Kasha [35] suggested an exciton model (illustrated in figure 2.6) for the different energy levels during electronic transitions of molecular H- and J-type dimers. Because of electronic devolution a splitting in energy levels can be seen in the Kasha-model. The transition to higher or lower excitation levels can be allowed or forbidden, depending on the molecular axis of the aggregate and the angle between the dipoles.

In case of opposite directions of dipoles the vector sum is zero resulting in a forbidden transition to a lower level. Parallel alignment (also called sandwich structure) of dipoles lead to transitions in upper levels and a blue shift in absorption can be observed. Such non-fluorescent dyes are called H-aggregates, named after the hypsochromic shift.

An allowed transition to the lower excited level would be the result if dipoles are in line with the molecular axis and lead to a red-shift of the absorption peak.

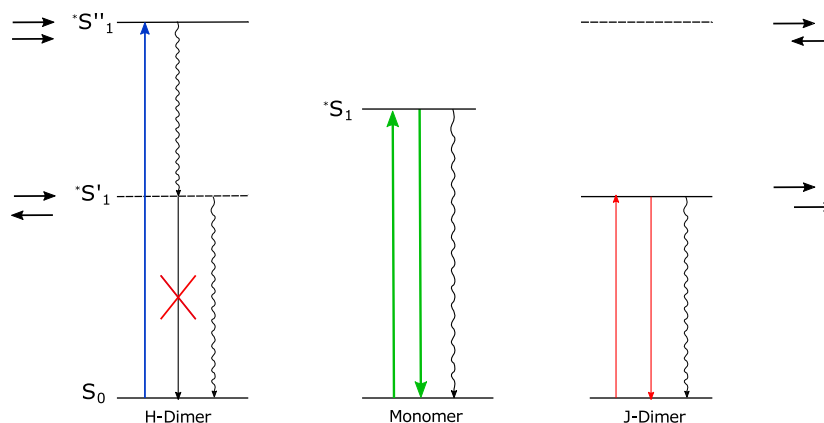


**Figure 2.6:** Illustration of the Kasha model during electron transitions of H- and J- dimers

To gain stable H- and J-aggregates is often difficult in solution, they mostly exist only at high dye concentrations. Furthermore in most cases the monomer form is present additionally to the aggregated forms. During formation of J-aggregates dimers can be found as intermediates [36], sometimes already light induces a shift to the aggregated form. Another possibility to decrease the concentration of dimer and monomer resulting in an increase of J-form is by adding salt [37]. The final structure of aggregates can be guided by several parameters, like addition of salt, temperature [38, 39], pH-value [40], polarity and used solvent [40].

This highly ordered configuration of J-aggregates acts as one unit with a strongly increased dipole moment [31]. The excitons of electronic transitions is the cause for the unique properties. Reason here for is the exciton motion along the molecular chain, the excitation is no longer localized on one monomer, however delocalized over the whole chain length. Leading to very narrow (10-20 nm in width) and almost symmetrical absorption bands. A huge bathochromic shift of about 100 nm to the red can be observed. Their fluorescence spectra match the absorption spectra and therefore show also a narrow width. The absorption and emission are similar because no vibrational modes are active and thus no energy losses take place. Therefore they show a really small or even negligible Stokes shift in fluorescence spectra.

In contrast, H-aggregates are formed side-by-side and can be easily identified in an absorption spectra by the hypsochromic shift, meaning to shorter wavelengths. So an interpretation of the aggregate type can be made while looking at the absorption spectrum, an general example can be seen in figure 2.7.

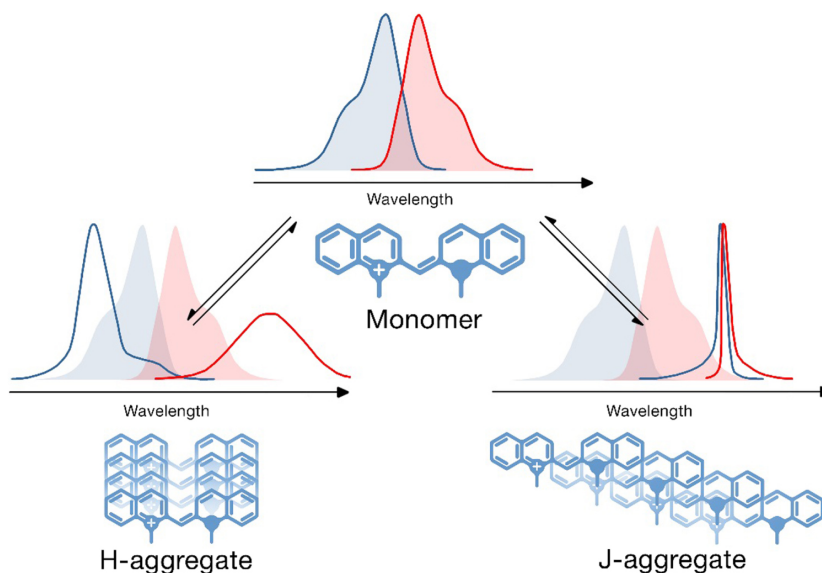


**Figure 2.7:** Schematic representation of differences in absorption (blue) and fluorescence (red) spectra after formation of H- and J-aggregates from cyanine dye monomers [9]

J-aggregates also show other features, like an increase in absorbance compared to their monomers and the decrease of radiative lifetime on picoseconds time scale [41]. This effect is also called 'superradiance' [42, 43]. Here it is the matter of a collective emission phenomenon, compilations of atoms or molecules have ultrafast radiative decays compared to the emission of lone atoms, because the amplitudes in those acquisitions add up to form a large dipole. Highly polarized emission is caused by high optical anisotropy [44, 45]. A clear statement about the quantum yield of J-aggregates can not be made, they vary in a broad range. Nevertheless is it possible to raise the fluorescence quantum yields by improving the structural order whilst the formation occurs in surfactant micellar solutions.

An interesting point to determine the fluorescence abilities represents the exciton self-trapping [46] in highly static disordered formations at lower temperatures. The self-trapping has quenching as a consequence.

### 2.2.3 Prime example for J-aggregates: pseudoisocyanine dye (PIC)

PIC is a well investigated dye [47] in the field of J-aggregation, especially via absorption and fluorescence spectroscopy, but also with different methods of imaging techniques and single-molecule spectroscopy. An overview about different experiments on PIC examples can be found in the review *J-aggregates: From Serendipitous Discovery to Supramolecular Engineering of Functional Dye Materials* p. 3379-3384 from Würthner et al. [31] and would go beyond the scope of this master thesis.

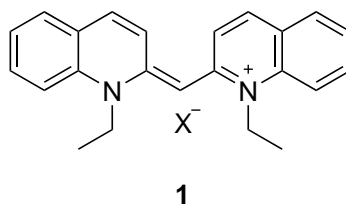


**Figure 2.8:** Structure of one of the most studied dyes for J-aggregate formation, the pseudoisocyanine (PIC), X = Counter-anion, like Cl or I

It was possible for Scheibe and his coworkers to determine the chain length of PIC aggregates by fluorescence quenching experiments due to the fact, that the energy is transferred in the chain and large Stern-Volmer constants could be measured. This effect was also apparent with other J-aggregates and is now known as 'superquenching' [48, 49]. They also stated that the increase of dye concentration has an increasing impact on the chain length.

With this particular dye Förster was able to predict the orientation of such aggregates, a parallel arrangement to the aggregate direction [34], as already mentioned above.

Nevertheless Würthner et al. concluded that the size and structure of aggregates by PIC dyes are a result of the conditions, such as temperature, concentration, pH value and ionic strength, during experiment. For example in infinite dilute solutions H- and J-aggregates can be found in equilibrium [31].

#### 2.2.4 Other examples for J-aggregation and how they differ

Various other cyanine (*gr. cyanos = blue*) dyes, except from PCI, are established for the formation of J-aggregates. The general constitution consists of an aromatic heterocyclic donor connecting to an acceptor by a polymethine chain. The number of vinylene units determine the color of the dyes. Via modifications of the basic structure the bathochromic shift can be more intensified. This alterations could be fulfilled with insertions of different substituents at the quinoline ring, by expanding the  $\pi$ -extended systems, as well as by increasing the quantity of methyl groups in the chain. Already with the addition of one unit a bathochromic shift of about 100 nm can be achieved, therefore a shift to the NIR-region could be possible. The chain extension unfortunately decreases the stability of the molecules. After altering the basic building block cyanine can be neutral, cationic or anionic. The structure need to be rigid to perform good aggregation, however it is not allowed to be too bulky, because if no planar structure is possible no stacking of molecules is either [9]. That rule is valid for all classes to be able to form J-aggregates.

The main reason for cyanine dyes to form J-aggregates in water is the hydrophobic effect, non-polar molecules try to avoid the interaction with water molecules [50].

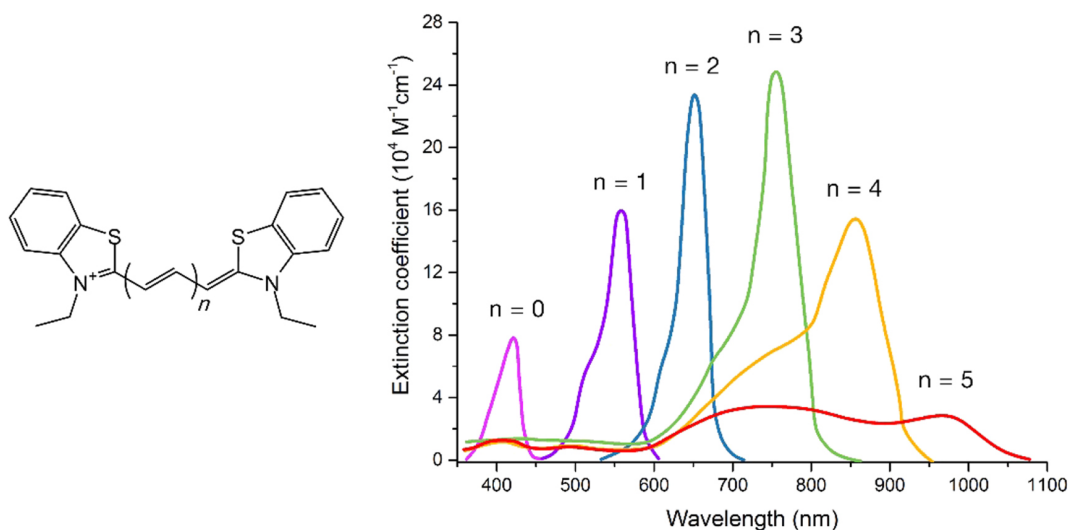


**Figure 2.9:** Illustration of the influence of the quantity of vinylene units at cyanine dye derivatives on absorption spectrum. The addition leads to a bathochromic shift of the maxima [9]

To get an insight of the dependency of concentration the dye 5,5',6,6'-tetrachloro-1,1'-diethyl-3,3'-di(4-sulfobutyl)benzimidazolocarbo-cyanine (TDBC) was investigated via UV-Vis spectroscopy. This dye is very suitable compared to PIC, because no undesired dimers or H-aggregates are formed. While the concentration of the dye gets increased, the ratio of J-aggregate to monomer ascends [51].

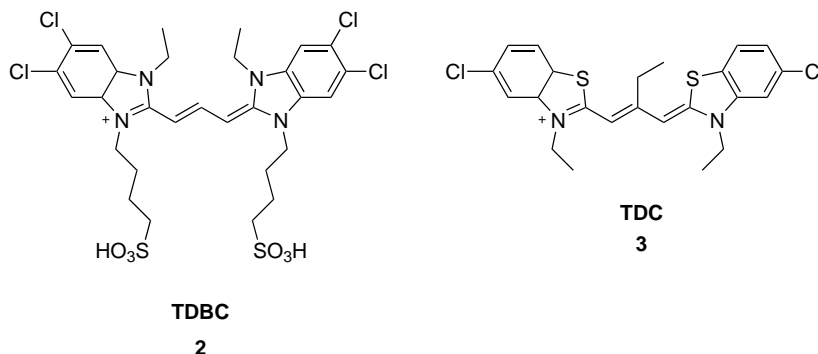


**Figure 2.10:** Structure of TDBC (**2**) and TDC (**3**), cyanine derivatives

Another cyanine dye that need to be mentioned is the 3,3',9-triethyl-5,5'-dichlorothiacyanine (TDC). Particularly is the fact that three different temperature-dependent J-aggregate types can be seen in the spectra [31].

The latest achievement in modifications of cyanine dyes was to synthesize amphiphilic structures, which was also the intention behind this master thesis, generate new fluorescent dyes on basis of BODIPY structure with hydrophobic and hydrophilic chains. Amphiphilic dyes are really promising, because of the broad range of applications [7, 15, 52].

The micellar morphology after self-assembly in aqueous solution can be controlled by the chain lengths and kind of substituents of the polar and non-polar side groups. Structures like vesicles, tubes or bundles of tubes can be build up by virtue of the hydrophobic effect. This self-assembled amphiphilic dyes have the unique characteristics of J-aggregates and could play an important role in synthesized light harvesting systems (LHS) (see 2.2.7).

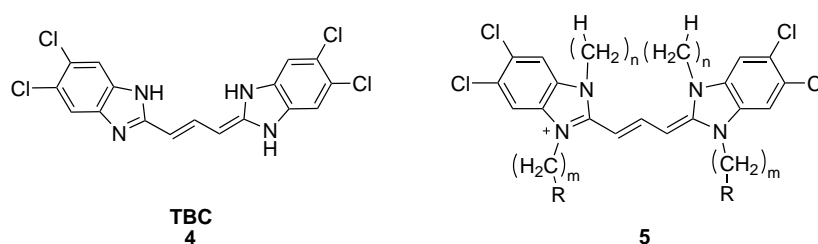


**Figure 2.11:** Structure of an amphiphilic dye based on TBC (**4**) with a hydrophobic chain and hydrophilic one, where  $R = \text{COO}^-$  ( $\text{COOH}$ ),  $\text{SO}_3^-$  ( $\text{SO}_3\text{Na}$ )

Suitable examples for amphiphilic J-aggregates were synthesized by von Berlepsch and Dähne [53], they are derivatives of the 5,5',6,6'-tetrachloro-benzimidacarbocyanine (TBC) (**4**) in figure 2.11 due to the fact that even in low concentration the formation of J-aggregates can easily be accomplished. The final aggregated form subordinate on the surrounding environment. To investigate the morphology and structure of amphiphilic dyes von Berlepsch et al. first used the cryogenic transmission electron microscopy (cryo-TEM) and achieved a huge breakthrough [53–55]. The samples, preferentially biological probes, are cooled down to cryogenic temperature (below  $-180^\circ\text{C}$ ) and after examination with an electron beam the resulting image can be detected and analyzed. The image gives information about the structure, particle size, morphology etc [56].

Chromophores with short non-polar substituents show similar behavior than classical J-aggregates, meaning that only one red-shifted J-band can be seen due to a planar structure of the aggregate. For other derivatives a tubular form with chirality was observable, in this case more J-band peaks are visible in the absorption spectrum. However, the fluorescence emission shows only the peak for the one with the lowest energy [7].

To summarize, cyanine dyes show many promising features and could be applied in a broad range of fields. An example delivers the property to transport exciton over a long chain length and 'superquenching', therefore those are important as sensor materials. The color change after formation to the aggregated state, deriving from the huge bathochromic shift, can also be useful.



On the other hand, cyanine dyes show only moderate photostability and after a long storage period the morphology can change.

To mention another dye class that is suitable to form J-aggregates with unique optical properties, the perylene bisimides. Actually no fluorescence is observable in solid state with that class, however microcrystalline powders are accessible that demonstrates quantum yields up to 70%. Perylene bisimides tend to form H-aggregates, nevertheless with different techniques a shift to J-aggregates can be accomplished. Perylene dyes consist of an enlarged aromatic system and the insertion of bulky substituents or hydrogen bondings can cause a large shift. Also attainable by changing the solvent polarity, chain length, concentration or temperature [24, 25].

### 2.2.5 Red and NIR J-aggregates

Nowadays the shift to lower energies (to higher wavelengths) are of great interest, especially in the field of biomedical applications [57], e.g. to detect tumor cells, but also in the field of renewable energies [58], like solar cells. Why near-Infrared anyway? Interferences and impurities absorb in the lower wavelength regions, therefore a high sensitivity of detection is granted in the NIR-region (780 - 1400 nm).

One approach to generate such dyes, that are capable to absorb in the NIR-region, is to stabilize cyanine dyes with polymethylene bridges via cyclization, because solely the introduction of further vinylene-units would cause a destabilization of the dye. Other possibilities are either to introduce branched heterocyclic systems or to attach donor substituents, like  $OCH_3$ ,  $N(CH_3)_2$ , etc., to create the bathochromic shift [59]. Oppositely, substituents on sulfur basis and  $NO_2$  block the formation of J-aggregates.

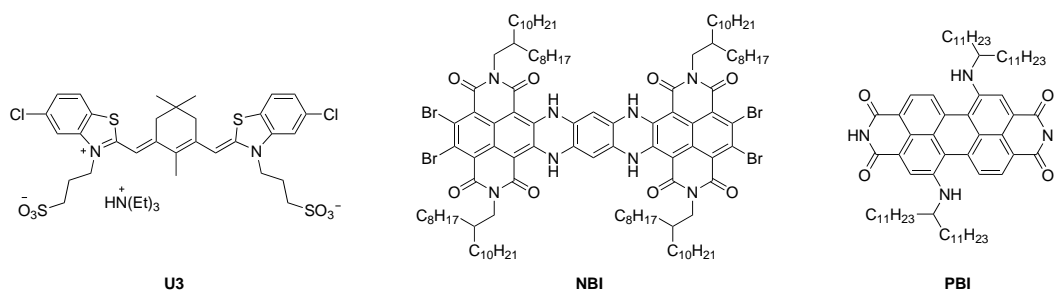


**Figure 2.12:** Examples of J-aggregates absorbing and emitting in NIR-region

With this methods it was possible to synthesize J-aggregates absorbing and emitting in the red and NIR-range. For example, by cyclization of a cyanine derivative (U3, see figure 2.12) with a absorption maxima shift of 120 nm was synthesized, which is used as NIR-photodetector

[60]. A absorption and emission spectrum of U3 compared with TDBC (=F1) can be found in figure 2.13.

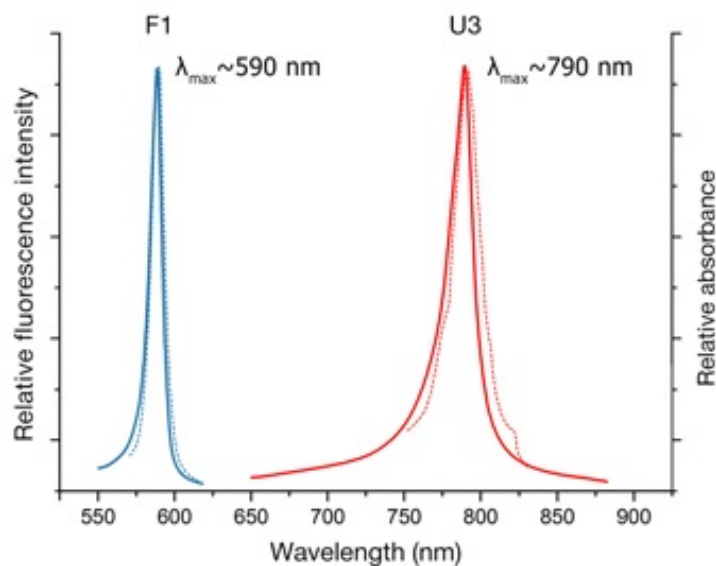


**Figure 2.13:** Comparison of the J-aggregates of dyes U3 and TDBC (2) [60]

Also the rylene class shows interesting examples of dyes (NBI and PBI [13]) with a huge bathochromic shift after J-aggregate formation. With NBI an absorption maximum of over 900 nm was achieved [61]. The structures can be found in figure 2.12.

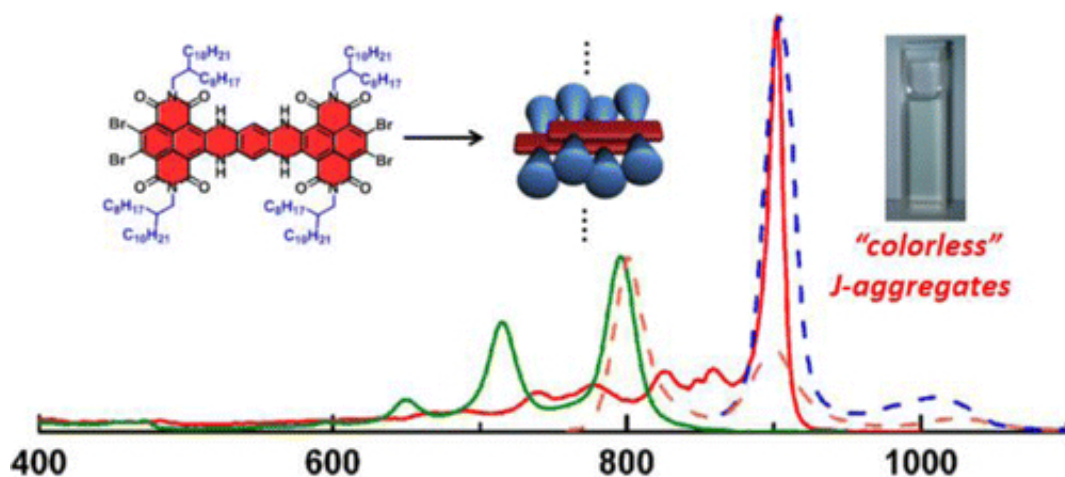


**Figure 2.14:** Absorbance (solid lines) and fluorescence (dashed lines) of J-aggregates in n-hexane and monomer in  $\text{CHCl}_3$  of NBI [61]

Figure 2.14 shows the absorption (solid line) and emission spectra (dashed line) of the monomeric form (green) and J-aggregate form (red) for NBI.

A summary of the spectral properties of the mentioned dyes as monomers and J-aggregates can be found in table 2.1.

**Table 2.1:** Properties of NIR J-aggregates compared to their monomeric form

dye	monomer				J-aggregate		
	$\lambda_{abs}$ [nm]	$\epsilon$ [l/mol cm]	$\lambda_{em}$ [nm]	QY [%]	$\lambda_{abs}$ [nm]	QY [%]	Stokes Shift [nm]
U3	670	216 000			790		3
NBI	796	190 000	801	8	902	2	2
PBI	702	34 900	760	10	822	not emissive	

Another impressive dye class that absorbs in this special range of wavelength are BODIPYs. Details can be found in chapter 2.3.

### 2.2.6 Influence of additional surfactants

The addition of surfactants to solutions lead often to self-aggregation resulting in a different structure compared to the separated forms.

This phenomena can also be found with dyes, which form J-aggregates. A mixture of TDBC (**2**) and N,N-dimethyl-n-alkyl betain show a higher molecular order of the aggregates [62].

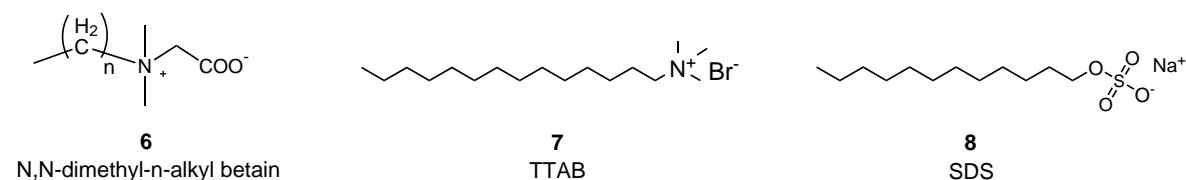


**Figure 2.15:** Structure of the surfactant N,N-dimethyl-n-alkyl betain, of trimethyl tetradecyl ammonium bromide (TTAB) (**7**) and sodium dodecyl sulphate (SDS) (**8**)

A separate investigation shows that the addition of sodium dodecyl sulphate (SDS), an anionic surfactant, to trimethyl tetradecyl ammonium bromide (TTAB) leads to the formation of single tubules structure with larger diameters. After storage over a long period of time the structure goes through a transition. Addition of cationic TTAB a vesicular structure is formed only after three days [54, 55]. It is assumed, that a destroyed molecular order and an increase of the membrane flexibility is caused by the opposite charge of the surfactant.

However two different substituents, which only vary in one carbon atom, were analyzed and both show individual behavior. Concluding, no prediction of other dyes, different surfactants or in other solvents can be made. Therefore further investigations are necessary.

### 2.2.7 Field of applications

Due to the fact that various dye classes are able to form J-aggregates, a huge diversity of dyes can be synthesized, which deliver a broad field of applications.

J-aggregates could be used as photoreducers [63], for biosensing [48, 64], chemical sensing, artificial light harvesting systems [7, 65], photovoltaic systems [66–69], nonlinear optics [70] and many more.

Over a long period of time cyanine dyes (preferentially PIC (**1**)) were used in silver halide photography, which is mentioned in nearly every paper concerning J-aggregates [63, 71–73], because it was the first huge breakthrough. These formed J-aggregates are able to reduce metal cations and absorb a huge amount of light. Through photoinduced electron transfer from the excited dye aggregate to the silver halide, a reduction to the atom level occurs, followed by a crystallization on the dye surface.

The advantage of J-aggregates is the fast exciton transfer along the chain. Due to that fact, J-aggregates have several epithets, like 'superquenching' and 'supersensitizers', which leads to required abilities for sensing applications.

With light harvesting systems (LHS) it is possible to comprehend the processes taking place in photosynthesis [74, 75]. To be sure that a high effectiveness is enabled the dye molecules need to fulfill two properties. First, a self-assembly of the molecules to a highly ordered structure, preferentially with a large surface area to absorb a huge amount of light. Secondly, an instantaneous energy transfer to the desired position for following processes [76].

This principle is further used in photovoltaic systems, such as organic solar cells.

Several attempts have been made, for instance the synthesis of chlorophyll-like derivatives [77]. However the difficulty was to synthesis dyes, which are able to satisfy the two conditions, ordered packages after self arrangement and the exciton migration along huge distances.

A progress was achieved after J-aggregates were discovered. They show high efficiency as optical antennas, because of their self-aggregation in aqueous solution and their unique resulting ordered structure, which is the cause for excitons to move freely along the molecular chain. Especially the latest achievement in dye modification need to be mentioned: amphiphilic structures to form aggregates [7]. In contrast to the previous dyes already low concentrations are sufficient to build up the typical formation.

Near Infrared absorbing dyes are suitable in the field of biological and medical imaging [78, 79]. This dyes inherit low energies that can go deeper into the sample and in this wavelength region low impurities and background will be interfering. Therefore cancer cells could be identified early. However until now researchers struggle with the fact that NIR J-aggregates have a low stability and are of high costs.

## 2.3 BODIPY

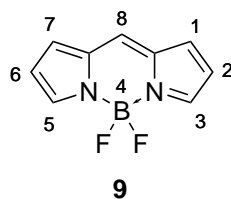


**Figure 2.16:** General structure of the BODIPY core

4,4-difluoro-4-bora-3a,4a-diaza-s-indacene (BODIPY) dyes count as one of the most important chromophore classes. The first BODIPY dyes were invented in the late 60s [80]. These dye class absorb strongly UV-light and are able to emit fluorescence characterized by sharp peaks (520 - 600 nm) with excellent quantum yields. With simple modifications of the BODIPY core, like insertion of bulky substituents to generate a rigid structure, via introducing electron donating groups or by extending the  $\pi$ -system, a bathochromic shift is attainable. BODIPYs inherit the abilities to be insensitive to pH and polarity resulting in a high stability. Chemosensors [81, 82], laser dyes [83, 84], labeling agents [85] and fluorescent switches [86] are a few application possibilities to name.

Disadvantages in the field of biotechnology could be observed, because just a few are water soluble and most emit less than 600 nm, whereas higher wavelengths would be desirable.

### 2.3.1 Syntheses route

To synthesize BODIPYs several approaches are possible, which are already well established [83, 87].

First, via condensation of pyrroles with acyl chlorids leading to the unstable intermediate **12**, followed by a complexation step with boron trifluoride diethyl etherate.

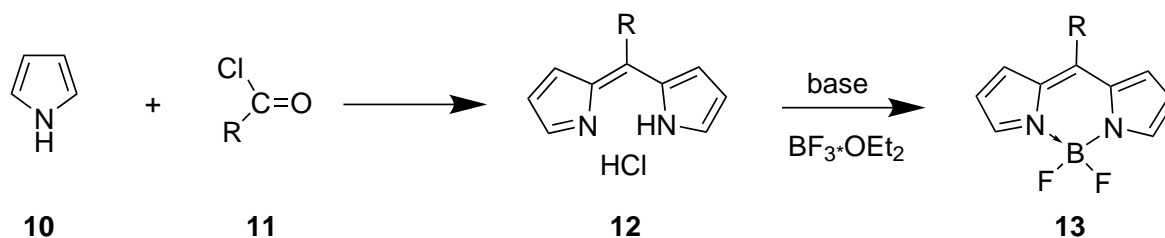


**Figure 2.17:** Synthesis of the BODIPY core via a condensation reaction with acyl chlorid (**11**)

The most common way, shown in figure 2.18, is the reaction of an aromatic aldehyde with a pyrrole. A reduction step is required afterwards, for instance with p-chloranil, ensures milder

conditions, or DDQ. Last step is the complexation in a basic environment. The whole reaction is an one-pot synthesis, followed by an easy work-up. Unfortunately the yields are quite low.

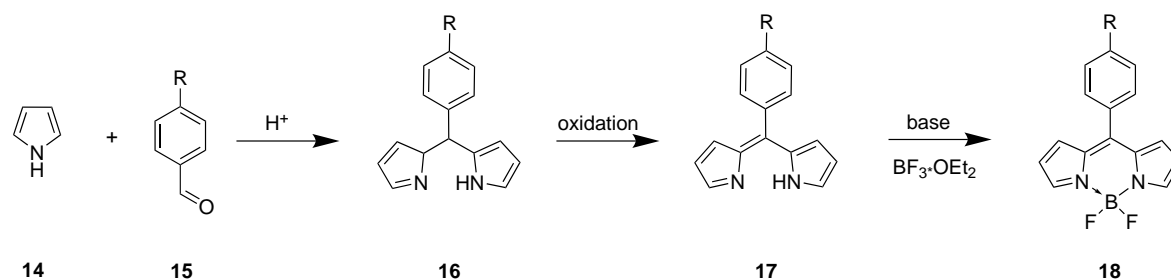


**Figure 2.18:** The most common way to synthesize BODIPY

With different aldehydes a huge variation of *meso*-substituted BODIPYs can be synthesized, meaning that BODIPYs can be modified to fulfill a special purpose.

The mentioned syntheses route only yields symmetrical products, to produce unsymmetrical BODIPY dyes another approach is necessary. The first step is to generate the ketopyrrole intermediate. After this reaction a condensation in the presence of a Lewis acid (e.g.  $POCl_3$ ) of the other pyrrole is carried out [88, 89]. Another possibility is to simply execute that reaction in an one-pot synthesis equal to the common way mentioned before, in contrast both pyrroles react simultaneously with the aldehyde. This way is easier, however the isolation of the unsymmetrical product from the side products is problematic.

### 2.3.2 Modification of the BODIPY core

To tune the properties it is only necessary to modify the BODIPY structure. Absorption spectra show a sharp band with high molar absorption coefficients and high fluorescence quantum yields (60-90 %). BODIPY dyes are photochemically stable, dissolve in most solvents and possess the lifetime of about a few ns [90]. In general, no aggregation can be observed, however the goal of this master thesis was to synthesize new BODIPY structures, which form J-aggregates in defined conditions.

Introduction of substituents at the *meso* position has an effect on the quantum yield, but not on the absorption or emission wavelength. Through increase of the rigidity and hindrance of rotation it is possible to attain higher quantum yields. An extension of the  $\pi$ -conjugated system has also an impact on the spectrum shift, as well as electron-donating groups.

The 3- and 5-position can be easily substituted via nucleophilic reaction leading to a bathochromic shift and a change in the quantum yield.

The fluor-atom on the boron-center can be exchanged. The substitution with alcohol takes place after reaction with aluminium- or boron trichloride, they are known as B-OR compounds [91, 92].

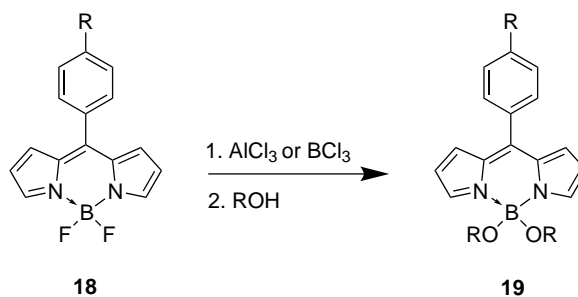


**Figure 2.19:** Reaction scheme of the substitution of fluorine with an alcohol

Hence there are so many different modifications that can be done at the BODIPY core, many possible derivatives can be synthesized with different properties. For instance, introduction of different phenols in the meso position results in pH sensitive dyes. The featuring substituents can have a negative or a positive effect on quantum yield, spectrum shift, stability, etc. Therefore with required features a shift to the NIR-region is feasible [79], the broad field of applications of NIR dyes was already mentioned.

A lot of possible modifications and there effects can be found in [3].

---

## 3 Materials and Methods

The used chemicals and solvents during this master thesis were described in the tables below.

### 3.1 List of used solvents

**Table 3.1:** List of Solvents

Solvent	abbr.	Supplier	CAS-Number
Acetone		Fisher chemicals	67-64-1
Chloroform	CHCl <sub>3</sub>	Roth	67-66-3
Cyclohexane	CH	Fisher chemicals	110-82-7
Dichlormethane	DCM	Fisher chemicals	75-09-2
Dimethylformamide	DMF	Roth	68-12-2
Dimethylsulfoxide	DMSO	Roth	67-68-5
Ethyl acetate	EA	Fisher chemicals	141-78-6
H <sub>2</sub> O distilled			
n-Heptane		Roth	142-82-5
n-Hexane		Promochem	110-54-3
Novec 7200		3M	163702-05-4
Novec 7500		3M	297730-93-9
Tetrahydrofuran	THF	Fisher chemicals	109-99-9
Toluene		Fisher chemicals	108-88-3

### 3.2 NMR Solvents

Chloroform D: + 0.03 % TMS, 99.80 % D, Eurisotop

Methylene chloride D<sub>2</sub>: 99.90 % D, Eurisotop



## 3.3 List of used Chemicals

Table 3.2: List of used chemicals

Chemical	abbr.	Supplier	CAS-Number
1,3-Cyclohexadiene		Fluorochem	592-57-4
1,8-Diazabicyclo[5.4.0]undec-7-ene	DBU	Fluka	6674-22-2
2,3-Dichloro-5,6-dicyanobenzoquinone	DDQ	Sigma-Aldrich	84-58-2
2,4-Dimethylpyrrole		Sigma-Aldrich	625-82-1
2,5,8,11-Tetraoxatrideca-13-ol		Fluorochem	23783-42-8
3-Phenyl-2H-azirene		Matthias	
4-(Decyloxy)benzaldehyde		TCI	24083-16-7
4-Hydroxybenzaldehyde		Sigma-Aldrich	123-08-0
4-Perfluorononyloxybenzaldehyde		Matthias	
4-Phenyl-2-(4-propylphenyl)-1H-pyrrole		Berni	
6-Chloro-3-phenyl-1,4-dihydroindeno pyrrole		Matthias	
Aluminiumchloride	AlCl <sub>3</sub>	Fluka	7446-70-0
Bis(trimethylsilyl)acetylene		TCI	14630-40-1
Borontrichloride	BCl <sub>3</sub>	Sigma-Aldrich	10294-34-5
Boron trifluoride diethyl etherate	BF <sub>3</sub> OEt <sub>2</sub>	Sigma-Aldrich	109-63-7
Cl-rigid m-perfluoro BODIPY		Matthias	
Ethyl isocyanoacetate		Sigma-Aldrich	2999-46-4
Glacial acetic acid		Roth	64-19-7
Hydrochloric acid 1M	HCl	Sigma-Aldrich	7647-01-0
Indium chloride	InCl <sub>3</sub>	Andi	12672-70-7
Indocyanine green		TCI	3599-32-4
Lithium diisopropylamide	LDA	Sigma-Aldrich	4111-54-0
Lithiumaluminium hydrid	LiAlH <sub>4</sub>	Inorganic Chemistry	16853-85-3
N,N-Diisopropylethylamine	DIPEA	TCI	7087-68-5
n-Decanol		TCI	112-30-1
p-Chloranil		ICTM	118-75-2
Piperidine		Sigma-Aldrich	110-89-4
Potassium carbonate	K <sub>2</sub> CO <sub>3</sub>	Sigma-Aldrich	584-08-7
Potassium tert-butoxide		Sigma-Aldrich	865-47-4
p-Toluenesulfonic acid		Sigma-Aldrich	6192-52-5
p-Toluenesulfonylchloride		TCI	98-59-9
Sodium chloride sat.	NaCl	VWR chemicals	7647-14-5
Sodium hydride	NaH	TCI	7646-69-7
Sodium hydrocarbonate sat.	Na <sub>2</sub> CO <sub>3</sub>	VWR chemicals	144-55-8

Continued on next page

**Table 3.2 – continued from previous page**

<b>Chemical</b>	<b>abbr.</b>	<b>Supplier</b>	<b>CAS-Number</b>
Sodium hydroxide	NaOH	VWR chemicals	1310-73-2
Sodium sulfate	NaSO <sub>4</sub>	Roth	7757-82-6
Tetrabutylammonium chloride		Sigma-Aldrich	1112-67-0
Triethylamine	TEA	Roth	121-44-8
Trifluoroacetic acid	TFA	TCI	76-05-1

### 3.3.1 List of Surfactants

**Table 3.3:** List of Surfactants

<b>Surfactant</b>	<b>abbr.</b>	<b>Supplier</b>	<b>CAS-Number</b>
Polyethylene glycol oleyl ether	Brij 93	Aldrich	9004-98-2
Polyoxyethylene Sorbitan Trioleate	Tween	TCI	9005-70-3
Sodium dodecyl sulfate	SDS	Merck	151-21-3
Ethylene oxide propylene oxide copolymer	Pluronic	Aldrich	9003-11-6
Polyethylene glycol tert-octylphenyl ether	Triton X-100	Aldrich	9002-93-1
Sorbitan Monooleate	Span 80	TCI	1338-43-8

### 3.3.2 List of Polymers

**Table 3.4:** List of Polymers

<b>Polymer</b>	<b>Supplier</b>	<b>CAS-Number</b>
Cellulose acetate average M.W. 100,000	ACROS organics	9004-35-7
Hydrogel D4	ABCR	556-67-2
PolyHEMA average M.W. 300,000	Sigma-Aldrich	25249-16-5
Polystyrene (PS) average M.W. 260,000	Scientific Polymer Cat	9003-53-6
Silicone preparation:		
Poly(dimethylsiloxane)vinyl dimethylsiloxy terminated	ABCR	68083-19-2
Methylhydrosiloxane-dimethylsiloxane-copolymer, 25-35 %	ABCR	68037-59-2
1,3,5,7-Tetravinyl-1,3,5,7-tetramethylcyclotetrasiloxane, 97 % (retarder)	ABCR	2554-05-5
Platinum (0)-1,3-divinyl-1,1,3,3-tetramethyl-disiloxane complex solution	Sigma-Aldrich	66478-92-2

## 3.4 Chromatography

### 3.4.1 Thin Layer Chromatography (TLC)

Thin layer chromatography was used to monitor the reaction progress in defined time intervals. Probes were detected by UV light on TLC silica plates from Merck (silica gel 60  $F_{254}$ ).

### 3.4.2 Flash Column Chromatography

Further purification can be accomplished via flash column chromatography. The used silica gel derived from Roth (0.035 – 0.070 mm, 60 Å). Approximately the 100-fold (calculated by amount of crude product) of silica was used. The needed solvents can be estimated by polarity and  $R_f$ -value.

## 3.5 Photophysical Measurements

### 3.5.1 Absorption

Absorption spectra were recorded by an UV-VIS spectrophotometer, the Varian Cary 50 conc, using Cary WinUV software. A fast or medium scan mode with baseline correction (using solvent as blank sample) was adjusted. The samples were placed in 100-OS cuvettes from Hellma Analytics with a path length of 1 cm.

#### Molar Absorption Coefficient

To determine the molar absorption coefficient ( $\epsilon$ ), the synthesized dyes were dissolved in THF resulting in a concentration of  $2 * 10^{-5}$  M and a corresponding spectrum was recorded. Via the Lambert-Beer law (eq. 2.1) the molar absorption coefficient can be calculated. In case of J-aggregates, the spectrum was recorded in water to get  $\epsilon$ .

#### Temperature Dependency Measurements

Temperature dependent measurements were carried out via an UV-VIS spectrophotometer. To generate the desired temperature water circulated and was either cooled down or heated up via Julabo F 25. The exact temperature was measured with a single cell peltier accessory from Varian. The measurement took place in a 1 mm cuvette, which was sealed and provided from Hellma Analytics.

## Flow Cell Measurements

A flow cell was equipped with a blank foil and a coated foil, for baseline correction blank foils on both sides was measured. Nitrogen or humid atmosphere was passed through and the signal was recorded over an hour. To generate a humid atmosphere sat. KCl solution was filled in a "Übergucker" and placed before the flow cell.

### 3.5.2 Emission and Excitation

The emission and excitation spectra were measured on a Fluorolog<sup>®</sup>3 spectrofluorometer from Horiba Scientific which was equipped with a R2658 photomultiplier by Hamamazu. Fluorescence cuvettes from Hellma (type 100-QS, 10 mm) with screw-caps were used.

### 3.5.3 Lifetime

Via TCSPC (time-correlated single photon counting) fluorescence lifetime was determined. A Fluorolog<sup>®</sup>3 Spectrofluorometer equipped with a NanoLED light source N-635L controlled by a DeltaHub module and a NL-C2 Pulsed Diode Controller from Horiba Scientific was used. Data analysis was carried out with a DAS6 decay analysis software from Horiba Scientific. The data were fitted with an exponential fit to get a linear slope. To record the prompt fluorescence signal a scattering suspension of Poly(1-vinylpyrrolidone-co-styrene) from Aldrich in water was used.

### 3.5.4 Quantum Yield

#### Relative QY

Quantum yields were measured relatively to a fluorescent dye with a known fluorescence quantum yield (standard), which is in the wavelength range of the measured species. In case of the prepared J-aggregates, indocyanine green ( $\phi = 0,132$  in ethanol [93]) was used. On the other hand, the dye tert-butyl-BODIPY from Tanja Rappitsch, Institute of Analytical Chemistry and Food Chemistry TU Graz, with a quantum yield of 0,94 in THF was used for the synthesized BODIPY derivatives.

The relative quantum yield was calculated via following equation:

$$\phi_C = \phi_R \cdot \frac{E_C B_R n_C^2}{E_R B_C n_R^2} \quad (3.1)$$

- E        integrated area  
B        absorption related term ( $1-10^{abs}$ )  
n        refractive index of solvent

The indices C and R represents the investigated compound and reference, respectively.

### **Absolute QY**

For the absolute method an integrating sphere set-up, the Quanta- $\phi$  by Horiba Scientific, was used, which allows detection of all absorbed photons and emitted photons of the sample. The sample, a foil coated with J-aggregate, was placed in that set-up. Four measurements need to be recorded in total. First, the sample was excited at a certain wavelength and the emission spectrum was recorded. Afterwards a transmission filter (20%) was put in between and an excitation spectrum is recorded. The same measurements need to be carried out with a blank foil. The program was able to calculate the resulting QY.

## **3.6 Structural Characterization**

### **3.6.1 Nuclear Magnetic Resonance Spectroscopy (NMR)**

$^1\text{H}$ -NMR and  $^{13}\text{C}$ -NMR spectra were measured on a 300 MHz Bruker AVANCE III instrument, which was equipped with an autosampler. An internal standard ( $\text{CDCl}_3$  or  $\text{CD}_2\text{Cl}_2$ ) was used to interpret the chemical shifts  $\delta$  (ppm). For analysis the software MestReNova NMR was utilized.

### **3.6.2 High Resolution Mass Spectrometry (HR-MS)**

Structural analyses of the synthesized dyes were performed with a Micromass TofSpec 2E MALDI/TOF (Time-of-Flight) mass spectrometer by Bruker. These measurements were carried out by Ing. Karin Bartl from the Institute of Chemistry and Technology of Materials, Graz Technical University. External calibration was done with a mixture of poly(ethyleneglycol)s (PEG). The received data were evaluated with MassLynx software V4.1 by Waters.

---

## 4 Experimental

In this chapter, the experimental procedures for the synthesis that were carried out successfully during this master thesis will be described. Synthesis that failed or did not yield the desired product will be discussed in the following chapter (see chapter 5) and the corresponding experimental procedures can be found in the appendix (see chapter 10) of this thesis, as well as all recorded NMR and MS spectra.

### 4.1 Synthesis of symmetrical BODIPY derivatives

All synthesis concerning BODIPY need to be performed in dark surrounding, because pyrrole is not stable while exposed to light. Therefore this synthesis were carried out with aluminum foil wrapped around the glass ware.

#### 4.1.1 Cl-rigid m-decyloxy BODIPY (21)

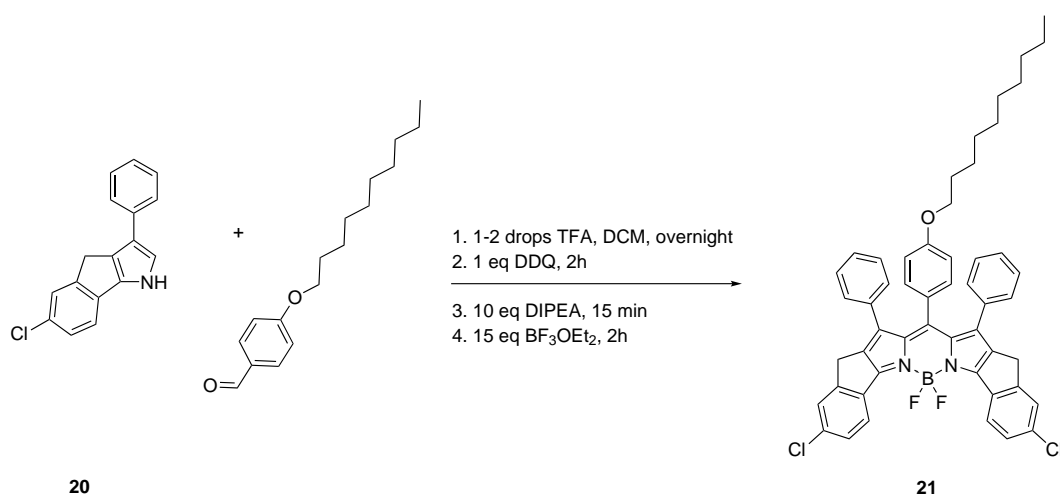


Figure 4.1: Synthesis of Cl-rigid m-decyloxy BODIPY (21)

After evacuating and flushing with Argon (Ar) three times, 300 mg (1.13 mmol, 2 eq) 6-chloro-3-phenyl-1,4-dihydroindeno[1,2]pyrrole (**20**), prepared by Matthias Schwar, were dissolved in dry DCM (20 ml), resulting in a green-yellow colored solution. The aldehyde, 4-(decyloxy)benzaldehyde (592.68  $\mu$ mol, 164  $\mu$ L, 1.05 eq), was added to the solution. After adding two drops of Trifluoro acetic acid (TFA) the color changed to red. The mixture was stirred over night.

The reaction progress was controlled via TLC. After full conversion 2,3-dichlor-5,6-dicyano-1,4-benzochinon DDQ (128 mg, 564.46  $\mu$ mol, 1 eq) was added. After 2h a color change to green could be observed. Adding N,N-Diisopropylethylamine DIPEA (983  $\mu$ L, 5.64 mmol, 10 eq) results in a violet color change. After 15 min boron trifluoride diethyl etherate  $\text{BF}_3\text{OEt}_2$  (1.04 mL, 8.47 mmol, 15 eq) was added dropwise and stirred for 2h.

The blue-colored fraction was extracted with  $\text{H}_2\text{O}$ . Some of the impurities were separated by passing the solution through silica gel and  $\text{Na}_2\text{SO}_4$ . The solvent was removed by rotary evaporation.

The crude product was purified by flash column chromatography (silica-gel, CH : toluene, 3 : 1) yielding in blue-green crystals.

Yield: 104.7 mg (22,6 %), blue-green crystals

$^1\text{H}$  NMR (300 MHz, Methylene Chloride- $d_2$ )  $\delta$  8.31 (d,  $J = 8.5$  Hz, 2H), 7.54 – 7.45 (m, 4H), 6.97 – 6.87 (m, 6H), 6.84 – 6.68 (m, 6H), 5.96 (d,  $J = 8.0$  Hz, 2H), 3.67 (t,  $J = 6.5$  Hz, 2H), 3.57 (s, 4H), 1.64 (t,  $J = 6.9$  Hz, 2H), 1.37 – 1.30 (m, 14H), 0.88 (s, 3H).

$^{13}\text{C}$  NMR (76 MHz,  $\text{CD}_2\text{Cl}_2$ )  $\delta$  136.22, 130.16, 129.94, 129.09, 129.09, 128.15, 114.21, 113.88, 32.49, 31.72, 30.55, 30.27, 29.91, 29.86, 26.51, 23.24, 14.46, 14.46.

MALDI-TOF:  $m/z$  calc. for  $\text{C}_{51}\text{H}_{45}\text{BCl}_2\text{F}_2\text{N}_2\text{O}$  is 820.2979, found: 820.5513

## 4.1.2 1,3,7,9-Tetramethyl m-decyloxy BODIPY (22)

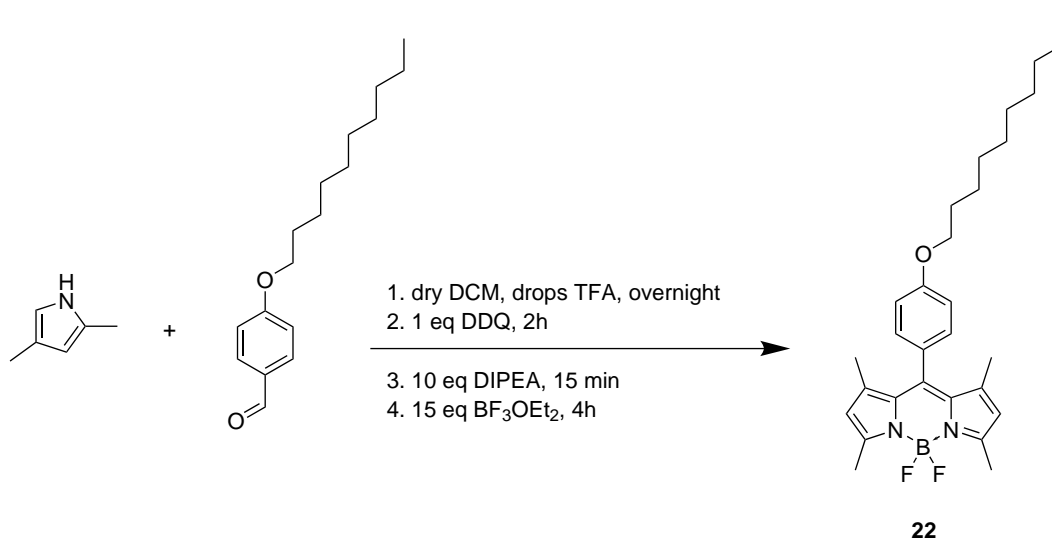


**Figure 4.2:** Synthesis of tetramethyl m-decyloxy BODIPY (**22**)

500 mg 2,4-dimethylpyrrole (5.26 mmol, 541  $\mu$ L, 2 eq) were dissolved in dry DCM under inert atmosphere in a Schlenk tube. Afterwards 4-(decyloxy)benzaldehyde (2.76 mmol, 762  $\mu$ L, 1.05 eq) was added. To generate an acidic environment two drops of TFA were added and stirred over night. On the next day, DDQ (596.5 mg, 2.63 mmol, 1 eq), DIPEA (26.28 mmol, 4.58 ml, 10 eq) and BF<sub>3</sub> diethyl etherate (39.41 mmol, 4.86 ml, 15 eq) were added dropwise. The reaction progress after every step was controlled via TLC and UV-VIS spectrum. The reaction was shut down by extraction with water and sat. NaHCO<sub>3</sub>, for better phase separation. The work-up took longer, because the phase boundary was difficult to determine. After drying the organic phase over Na<sub>2</sub>SO<sub>4</sub> and removing the solvent by rotary evaporation, the crude product was purified by flash column chromatography with the solvents cyclohexane and toluene (yellow fractions).

Yield: 254.4 mg (20.2 %), orange metallic crystals

<sup>1</sup>H NMR (300 MHz, Methylene Chloride-d<sub>2</sub>)  $\delta$  7.24-7.11 (m, 2H), 7.08-6.95 (m, 2H), 6.01 (s, 2H), 4.00 (t, J = 6.6 Hz, 2H), 2.50 (s, 6H), 1.80 (p, J = 6.7 Hz, 2H), 1.45 (s, 6H), 1.41-1.05 (m, 14H), 0.95-0.83 (m, 3H).

<sup>13</sup>C NMR (76 MHz, CD<sub>2</sub>Cl<sub>2</sub>)  $\delta$  160.46, 155.66, 143.99, 132.39, 129.77, 127.17, 121.56, 115.67, 68.79, 54.00, 32.50, 30.16, 30.01, 29.91, 29.84, 26.62, 23.28, 14.90, 14.46.

MALDI-TOF: m/z calc. for C<sub>29</sub>H<sub>39</sub>BF<sub>2</sub>N<sub>2</sub>O is 80.3129, found: 480.3309



### 4.1.3 2,5,8,11-tetraoxatridecan-13-yl-4-methylbenzenesulfonate: Tos TEG (23)

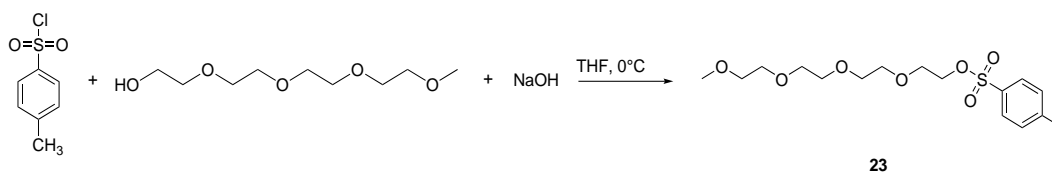


**Figure 4.3:** Synthesis of Tos TEG (**23**)

5.00 g 2,5,8,11-tetraoxatridecan-13-ol (24 mmol, 4.8 mL) were dissolved in 10 mL dry THF in a Schlenk tube and cooled down to 0°C. 10 mL of an aqueous sodium hydroxide solution (1.92 g, 48 mmol, 2 eq) were added dropwise. In a second Schlenk tube p-Toluensulfonyl chloride (5.94 g, 31.21 mmol, 1.30 eq) was dissolved in the same amount of dry THF. The solution was added dropwise to the first at 0°C, slowly heated up to room temperature and stirred for 2h. The work-up was accomplished by an extraction with water/ethyl acetate (3x). The organic phase was further extracted with a HCl-solution (2x), dried over Na<sub>2</sub>SO<sub>4</sub>, filtered and evaporated.

Yield: 8.49 g (97.6 %), colorless oil

<sup>1</sup>H NMR (300 MHz, Methylene Chloride-*d*<sub>2</sub>) δ 7.77 (d, J = 8.2 Hz, 2H), 7.36 (d, J = 8.0 Hz, 2H), 4.20 – 4.02 (m, 2H), 3.63 (dd, J = 5.7, 3.7 Hz, 2H), 3.61 – 3.34 (m, 12H), 3.31 (s, 3H), 2.43 (s, 3H).

### 4.1.4 4-((2,5,8,11-tetraoxatridecan-13-yl)oxy)benzaldehyde: TEG Benzaldehyde (24)

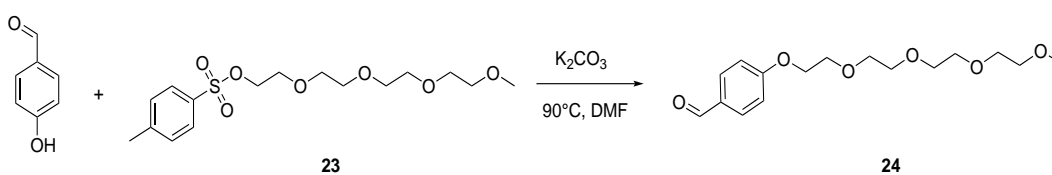


**Figure 4.4:** Synthesis of TEG Benzaldehyde (**24**)

4-Hydroxybenzaldehyde (1.00 g, 8.19 mmol, 1 eq), Tos TEG (**23**) (3.26 g, 9 mmol, 1.10 eq) and K<sub>2</sub>CO<sub>3</sub> (2.26 g, 16.38 mmol, 2 eq) were loaded in a Schlenk flask under Ar. To the reaction 20 mL dry DMF were added and stirred at 90°C over night.

The suspension was slowly cooled down to RT. Afterwards the reaction was extracted with water and ethyl acetate. The organic phase was washed intensively with water and a small

amount of NaCl for better phase separation. This layer was dried over  $\text{Na}_2\text{SO}_4$ , filtered and the solvent was removed. No further purification was necessary.

Yield: 1.34 g (52.2 %)

$^1\text{H}$  NMR (300 MHz, Methylene Chloride- $d_2$ )  $\delta$  9.86 (s, 1H), 7.82 (d,  $J = 8.6$  Hz, 2H), 7.08 – 6.98 (m, 2H), 4.20 (t,  $J = 4.7$  Hz, 2H), 3.85 (t,  $J = 4.8$  Hz, 2H), 3.68 (dd,  $J = 6.3, 3.2$  Hz, 2H), 3.63 – 3.41 (m, 10H), 3.32 (s, 3H).

#### 4.1.5 Cl-rigid m-TEG BODIPY (25)

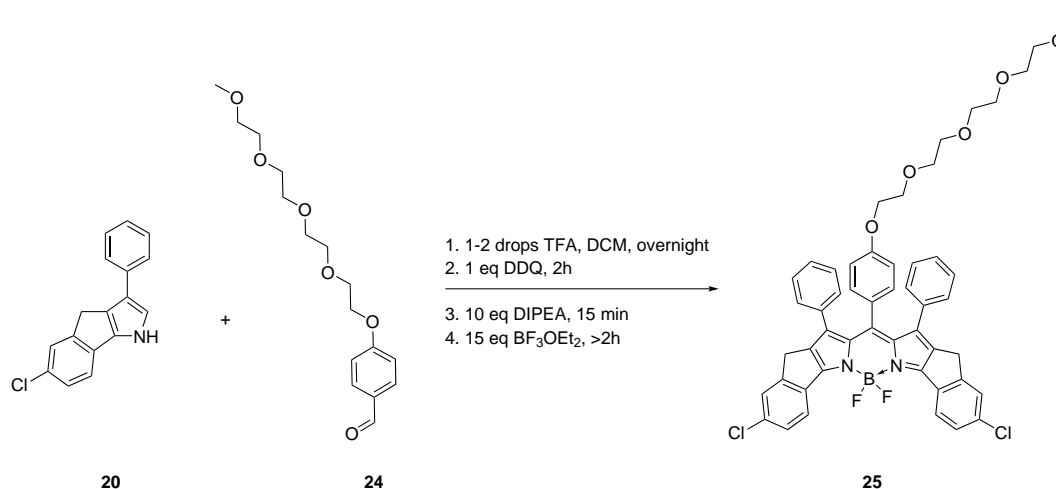


**Figure 4.5:** Synthesis of Cl-rigid m-TEG BODIPY (25)

250 mg (940.77  $\mu\text{mol}$ , 2 eq) pyrrole (**20**) and 154 mg (493.9  $\mu\text{mol}$ , 1.05 eq) TEG benzaldehyde were dissolved in 20 mL dry DCM in an inert Schlenk flask. After a drop of TFA the color changed from yellow to red and the mixture stirred over night.

After adding DDQ (106.78 mg, 470.38  $\mu\text{mol}$ , 1 eq) the oxidation took 2h. The complexation with DIPEA (4.70 mmol, 820  $\mu\text{L}$ , 10 eq) and  $\text{BF}_3\text{OEt}_2$  (7.06 mmol, 895  $\mu\text{L}$ , 15 eq) took 2.5 h. The mixture was poured in  $\text{H}_2\text{O}$  and extracted three times. After drying and removal of the solvent, the crude product (745.6 mg) was purified via column chromatography (silica-gel, CH : EA, 1 : 2).

Yield: 110 mg (26.8 %), blue metallic crystals

$^1\text{H}$  NMR (300 MHz, Methylene Chloride- $d_2$ )  $\delta$  8.40 – 8.22 (m, 2H), 7.56 – 7.45 (m, 4H), 6.94 (q,  $J = 6.0$  Hz, 6H), 6.79 (dt,  $J = 14.0, 5.0$  Hz, 6H), 6.00 (d,  $J = 8.6$  Hz, 2H), 3.87 – 3.77 (m, 2H), 3.75 – 3.69 (m, 2H), 3.67 (s, 4H), 3.64 – 3.51 (m, 12H), 3.35 (s, 3H).

$^{13}\text{C}$  NMR (76 MHz,  $\text{CD}_2\text{Cl}_2$ )  $\delta$  159.82, 153.09, 135.85, 135.36, 133.98, 131.88, 129.42, 128.75,

127.99, 126.72, 125.49, 124.26, 113.67, 72.51, 71.34, 71.20, 71.13, 71.00, 70.05, 68.02, 54.00, 30.25.

MALDI-TOF:  $m/z$  calc. for  $C_{50}H_{43}BCl_2F_2N_2O_5$  is 870.2519, found: 870.4746

#### 4.1.6 4-propylphenyl m-TEG BODIPY (**27**)

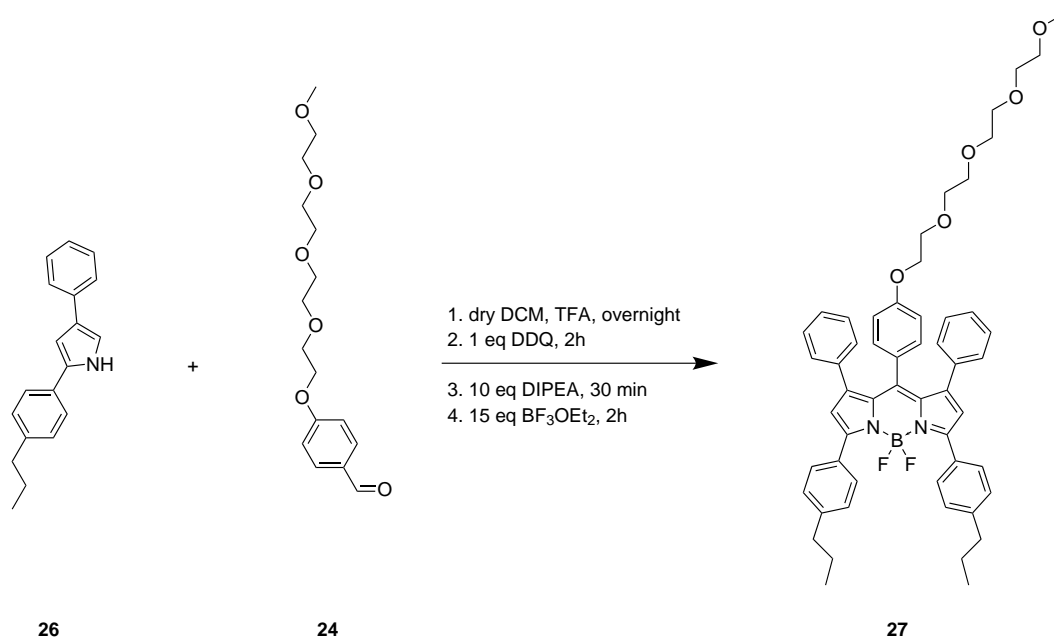


**Figure 4.6:** Synthesis of 4-propylphenyl m-TEG BODIPY (**27**)

4-phenyl-2-(4-propylphenyl)-1H-pyrrole (**26**), was synthesized by Bernhard Müller, during his work at the Institute of Analytical Chemistry and Food Chemistry at the TU Graz. In an evacuated and with Ar flooded Schlenk flask 500 mg of the pyrrole (1.91 mmol, 2 eq) were dissolved in dry DCM. The previously prepared TEG benzaldehyde (313.2 mg, 1 mmol, 1.05 eq) and TFA were added. The mixture was stirred over night. After adding 220 mg DDQ (956.51  $\mu$ mol, 1 eq) the color changed to blue. The complexation with boron trifluoride diethyl etherate (1.77 mL, 14.35 mmol, 15 eq) in a basic environment (DIPEA, 1.67 mL, 9.57 mmol, 10 eq) took 2.5 h.

After extraction with water, the organic layer was dried with  $Na_2SO_4$  and the solvent was removed. The crude BODIPY was purified via flash column chromatography.

Yield: 134.4 mg (16.3 %), pink-green solid

$^1H$  NMR (300 MHz, Methylene Chloride- $d_2$ )  $\delta$  7.77 (d,  $J = 7.9$  Hz, 4H), 7.28 (d,  $J = 7.9$  Hz, 4H), 6.94 (p,  $J = 6.1$  Hz, 6H), 6.80 (h,  $J = 6.1, 5.5$  Hz, 6H), 6.56 (s, 2H), 6.02 (d,  $J = 8.3$  Hz, 2H), 3.82 (dd,  $J = 5.9, 3.6$  Hz, 2H), 3.76-3.45 (m, 14H), 3.35 (s, 3H), 2.73-2.57 (m, 4H), 2.05

(s, 6H), 1.68 (s, 4H)

solvent residues detected (DCM)

$^{13}\text{C}$  NMR (76 MHz,  $\text{CD}_2\text{Cl}_2$ )  $\delta$  160.04, 157.20, 148.35, 145.16, 136.49, 135.74, 134.23, 130.74, 129.99, 129.94, 129.43, 128.78, 127.82, 126.66, 125.58, 123.77, 113.67, 72.52, 71.35, 71.13, 70.03, 68.02, 59.22, 38.52, 32.74, 30.27, 27.02, 24.99, 23.77, 14.34.

MALDI-TOF:  $m/z$  calc. for  $\text{C}_{54}\text{H}_{57}\text{BF}_2\text{N}_2\text{O}_5$  is 862.4338, found: 862.4902

#### 4.1.7 3,4-dihydro-6-TEG-naphthalen-1(2H)-one (**28**)

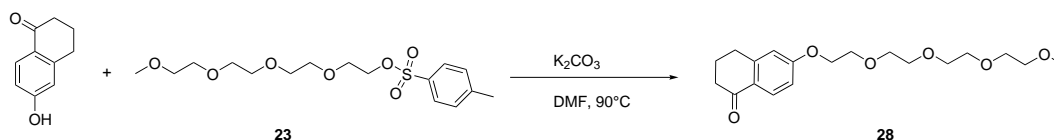


**Figure 4.7:** Synthesis of TEG-3,4-dihydronaphthalen (**28**)

6-Hydroxy-1-tetralone (1.50 g, 9.25 mmol), compound **23** (3.70 g, 10.17 mmol, 1.10 eq) and potassium carbonate (2.59 g, 18.50 mmol, 2 eq) were handed in a Schlenk flask, where inert atmosphere was guaranteed. To dilute the compounds dry DMF (25 mL) was added. The solution had a red-brown color. The suspension was heated up to  $90^\circ\text{C}$  and stirred over night. After TLC control the reaction was cooled down to RT. The solution was extracted with water and ethyl acetate. The organic phase was washed with water (adding a small amount of sat. NaCl), dried and exempt from solvent. No further purification was necessary, the product can be used directly for the next step.

Yield: 2.49 g (76,5 %), brown oil

$^1\text{H}$  NMR (300 MHz, Methylene Chloride- $d_2$ )  $\delta$  7.93 (d,  $J = 8.7$  Hz, 1H), 6.87 – 6.63 (m, 2H), 4.17 (dd,  $J = 5.7, 3.6$  Hz, 2H), 3.89 – 3.77 (m, 2H), 3.71 – 3.44 (m, 12H), 3.33 (d,  $J = 2.5$  Hz, 3H), 2.96 – 2.79 (m, 2H), 2.56 (dd,  $J = 7.3, 5.6$  Hz, 2H), 2.09 (p,  $J = 6.3$  Hz, 2H).

## 4.1.8 7-TEG-3-phenyl-pyrrole (29)

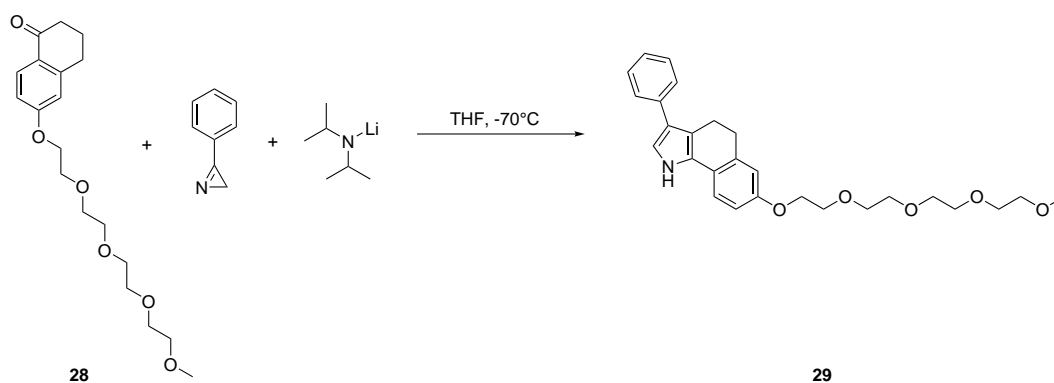


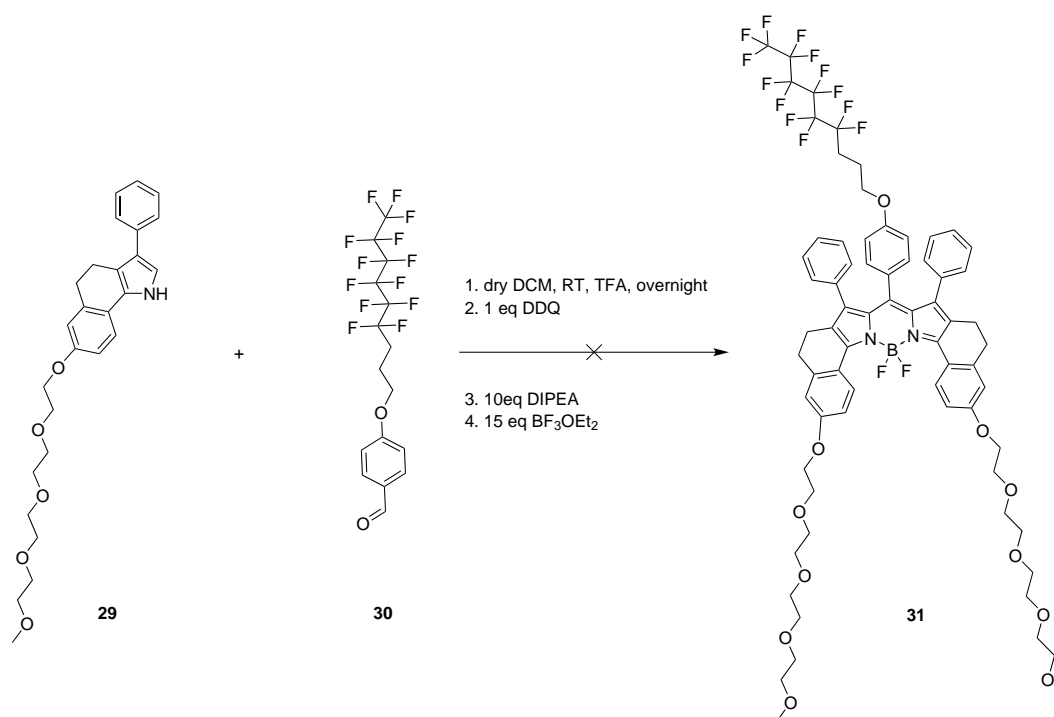
**Figure 4.8:** Synthesis of 7-TEG-3-phenyl-pyrrole (29) with azirine and LDA

After providing an inert system, compound **28** was dissolved in 15 mL dry THF. The reaction was cooled down to  $-70^{\circ}\text{C}$  and 717  $\mu\text{L}$  lithium diisopropylamide (1.43 mmol, 2.00 M, 1.01 eq) were added. After 15 min 1.07 mL 3-phenyl-2H-azirine (184.67 mmol, 1.20 eq) were pipetted to the solution. 30 min later the reaction was heated up to RT and stirred for another 40 min. The reaction was shut down with 10 mL  $\text{H}_2\text{O}$ . A neutralization was achieved with 1 M HCl. The product was extracted with DCM and water, followed by a drying step and removal of the solvent.

The reaction was controlled via TLC, the pyrrole was detected with vanilin/sulfuric acid (spot turns pink). The crude product was purified with flash column chromatography (CH : EA, 1 : 2). The product need to be stored in a freezer to avoid decomposition.

Yield: 190.8 mg (29.8 %), orange-brown oil

## 4.1.9 TEG-m-perfluoro BODIPY (31)

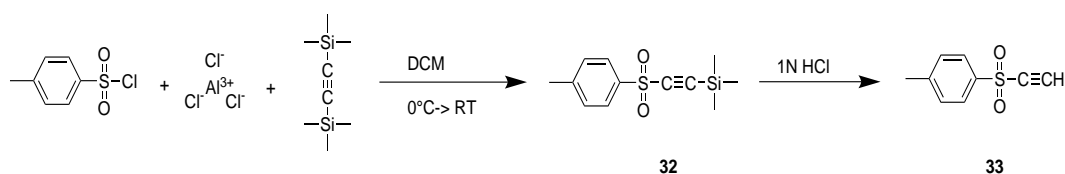


**Figure 4.9:** Synthesis of TEG rigid m-perfluoro BODIPY (31)

103 mg 4-(Tridecafluoronyl)oxy benzaldehyde ( $174.39 \mu\text{mol}$ , 1.05 eq), provided by Matthias Schwar, and compound **29** (150 mg,  $332.18 \mu\text{mol}$ , 2 eq) were dissolved in 15 mL dry DCM. The reaction stirred over night. To oxidize the system DDQ ( $37.7 \text{ mg}$ ,  $166.09 \mu\text{mol}$ , 1 eq) was added.

To complex the compound DIPEA ( $289 \mu\text{L}$ , 1.66 mmol, 10 eq) and  $\text{BF}_3\text{OEt}_2$  ( $316 \mu\text{L}$ , 2.49 mmol, 15 eq) were added dropwise. No product could be identified.

The solution was extracted with water, dried and solvent was removed via rotary evaporation. A product was tried to isolate with flash column chromatography (silica-gel, CH : DCM, 1 : 2 + 1 % MeOH). Different fractions could be collected, however no product could be determined.

4.1.10 p-Tolyl ethynyl sulfone (**33**)

**Figure 4.10:** Synthesis of p-Tolyl ethynyl sulfone (**33**)

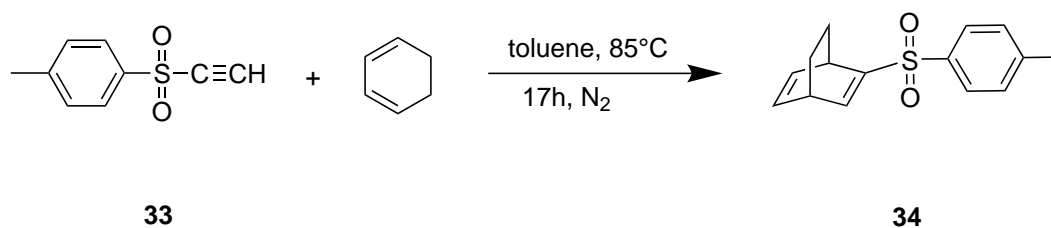
p-Toluenesulfonyl (15 g, 78.68 mmol) was added to powdered AlCl<sub>3</sub> (10.5 g, 78.68 mmol) in a round flask in 60 mL DCM. The resulting yellow solution was maintained at RT for 30 min. This mixture was transferred in a dropping funnel and slowly added (over 30 min) to an ice-cold solution of bis(trimethylsilyl)acetylene (16.05 mL, 70.81 mmol, 0.90 eq) in the same amount DCM. The color changed from colorless to dark red. The reaction stirred for 24 hours at room temperature.

Afterwards the solution was poured on a mixture of crushed ice (60 g) and 1 N HCl (60 mL). The organic phase was separated and extracted several times with water and then dried over Na<sub>2</sub>SO<sub>4</sub>. After removal of the solvent under reduced pressure a brown solid participate.

The product was purified in smaller portions with flash column chromatography. The product was eluted with CH : EA (8 + 1). Intermediate **32** could also be isolated and was again converted to the product by repeating the last step (adding HCl).

Yield: 7.82 g (55 %), white-slightly brown crystalline solid

<sup>1</sup>H NMR (300 MHz, Chloroform-*d*): δ 7.90 (d, J = 8.2 Hz, 2H), 7.39 (d, J = 8.0 Hz, 2H), 3.45 (s, 1H), 2.47 (s, 3H).

4.1.11 2-Tosylbicyclo[2,2,2]octa-2,5-diene (**34**)Figure 4.11: Synthesis of 2-Tosylbicyclo[2,2,2]octa-2,5-diene (**34**)

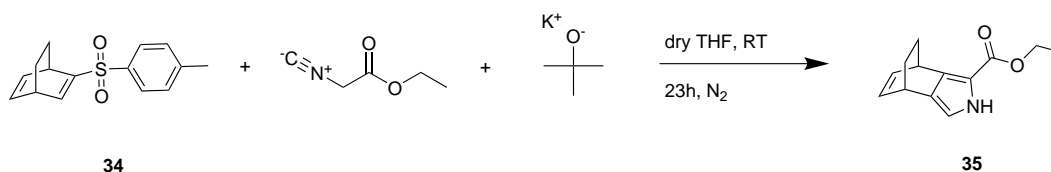
A solution of 1,3-cyclohexadiene (1.23 mL, 12.90 mmol) and compound **34** in dry toluene (40 mL) was heated to 85°C for 17 hours under N<sub>2</sub> atmosphere. The solvent was removed via rotary evaporation and a yellow oil was obtained. No further purification step was necessary, the product was directly used for the next step.

Yield: 1.94 g (89.5 %), yellow oil

<sup>1</sup>H NMR (300 MHz, Chloroform-*d*): δ 7.93 – 7.83 (m, 1H), 7.70 (d, *J* = 8.0 Hz, 2H), 7.27 (d, *J* = 7.7 Hz, 2H), 6.23 (tt, *J* = 7.6, 3.9 Hz, 2H), 3.93 – 3.80 (m, 2H), 2.41 (s, 3H), 1.35 (dtd, *J* = 14.1, 7.9, 7.1, 4.0 Hz, 2H), 1.29 – 1.11 (m, 2H).

4.1.12 Ethyl-4,7-dihydro-4,7-ethano-2H-isoindole-1-carboxylate (**35**)

Mechanism according to the Barton-Zard reaction.

Figure 4.12: Synthesis of BCOD fused pyrrole (**35**)

Compound **34** (1.10 g, 4.23 mmol) and ethyl isocyanate (1.31 mL, 11.83 mmol, 2.80 eq) were dissolved in dry THF (22 mL) at 0°C under inert atmosphere. To the stirring solution potassium tert-butoxide (2.6g, 21.13 mmol, 1 M) and dry THF were added. The mixture was stirred for 23 hours at room temperature.

The reaction progress was controlled via TLC and MS. After product formation, the solution was poured into 1 M HCl and extracted with chloroform. The organic layer was washed with sat. NaHCO<sub>3</sub>, water and brine. Afterwards dried over Na<sub>2</sub>SO<sub>4</sub> and the solvent was removed.



Followed by the purification step via flash column chromatography (silica-gel, CH : DCM 1 + 4) and recrystallization from CHCl<sub>3</sub>/hexane.

Yield: 518 mg (56 %),

<sup>1</sup>H NMR (300 MHz, Chloroform-*d*):  $\delta$  8.48 (s, 1H), 6.57 (d, *J* = 2.6 Hz, 1H), 6.50 (q, *J* = 4.5, 4.1 Hz, 2H), 4.44-4.35 (m, 1H), 4.30 (t, *J* = 7.2 Hz, 2H), 3.93-3.81 (m, 1H), 1.54 (s, 2H), 1.47 (ddd, *J* = 13.0, 6.3, 4.1 Hz, 2H), 1.36 (d, *J* = 7.2 Hz, 3H).

<sup>13</sup>C NMR (76 MHz, CDCl<sub>3</sub>)  $\delta$  161.81, 136.64, 136.32, 135.54, 131.57, 114.30, 112.92, 77.16, 59.99, 33.78, 33.41, 27.24, 26.56, 14.70.

This reaction was carried out with potassium tert-butoxide. The same procedure was tried with DBU instead, but no product was formed (details can be found in the appendix).

#### 4.1.13 2-Methyl-4,7-dihydro-4,7-ethano-2H-isoindole (36)

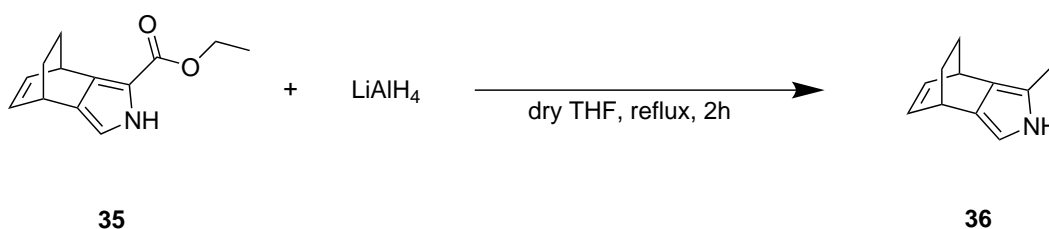


**Figure 4.13:** Reduction of Ethyl-4,7-dihydro-4,7-ethano-2H-isoindole-1-carboxylate

LiAlH<sub>4</sub> (380 mg, 10.36 mmol, 5eq) was added in small portions over half an hour to a stirring solution of compound **35** (415 mg, 2.07 mmol, 1 eq) in dry THF (48 mL) under argon. The reaction was refluxed for 2h and then controlled by MS. The mixture was slowly cooled down to room temperature and to neutralize the excess of LiAlH<sub>4</sub>, water (24 mL) was added dropwise. The residue was filtered and washed with EtOAc (3x). The organic phase was separated and washed with water (5x) and brine, dried over sodium sulfate and concentrated at reduced pressure. No further purification step was necessary.

<sup>1</sup>H NMR (300 MHz, Chloroform-*d*)  $\delta$  7.19 (s, 1H), 6.49 (td, *J* = 7.7, 6.1 3.7 Hz, 2H), 6.32 (d, *J* = 2.2 Hz, 1H), 3.84-3.61 (m, 2H), 2.21 (s, 3H), 1.62-1.49 (m, 4H).

MS (APCI): *m/z*: 159 [M]<sup>+</sup>, 131 [M-C<sub>2</sub>H<sub>4</sub>]<sup>+</sup>

#### 4.1.14 Different attempts to synthesize 14-(4-decyloxy)phenyl-7,7-difluoro-5,9-dimethyl-1,7,10,13-tetrahydro-4H-diethano[1,3,2]diazaborino diisoindole (37)

##### 1. method

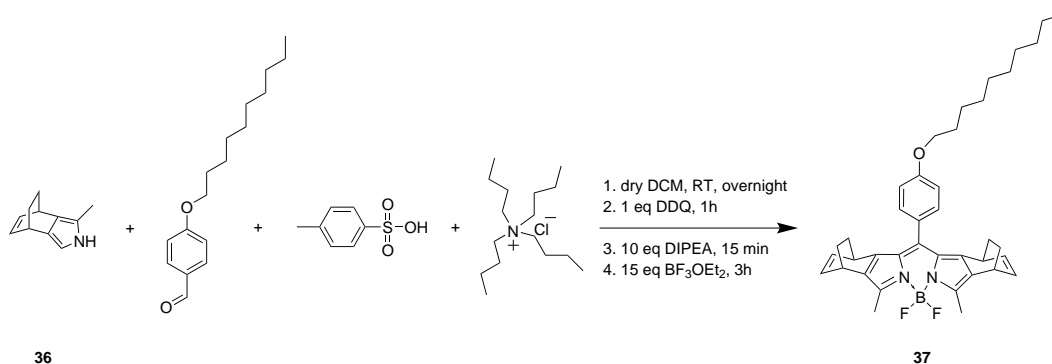


**Figure 4.14:** Method 1 to synthesis compound **37**

In a Schlenk flask, under inert atmosphere, 5.00 mg 2-methyl-4,7-dihydro-4,7-ethano-2H-isoindole (31.40  $\mu\text{mol}$ , 2 eq) were dissolved in dry DCM (0.5 mL). 4-(Decyloxy)benzaldehyde (4.5  $\mu\text{L}$ , 16.49  $\mu\text{mol}$ , 1.05 eq), tertbutylammonium chloride (190  $\mu\text{g}$ , 0.04 eq) and p-toluenesulfonic acid (340  $\mu\text{g}$ , 1.57  $\mu\text{mol}$ , 0.10 eq) were added and stirred over night.

The reaction was controlled via MS (APCI):  $m/z$ : 560 [M], 577 [M+Cl]

DDQ (4 mg, 15.71  $\mu\text{mol}$ , 1 eq) was added and stirred for 1 hour. After addition of DIPEA (27.5  $\mu\text{L}$ , 157.09  $\mu\text{mol}$ , 10 eq) a red-green color was observable. The complexation with  $\text{BF}_3\text{OEt}_2$  (29  $\mu\text{L}$ , 235.63  $\mu\text{mol}$ , 15 eq) took 3 hours and lead to a burgundy-violet solution. The mixture was extracted with water (3x), sat.  $\text{NaHCO}_3$  (2x), sat.  $\text{NaCl}$  and again with water. The organic phase was dried and removed with reduced pressure.

A purification with flash column chromatography was carried out, however the product could not be isolated.

##### 2. method

The addition of ethanol should enhance the product yield [94]. Also to test the more suitable oxidation reagent, either DDQ or p-chloranil, synthesis with both were performed and the one with DDQ can be found in the appendix.

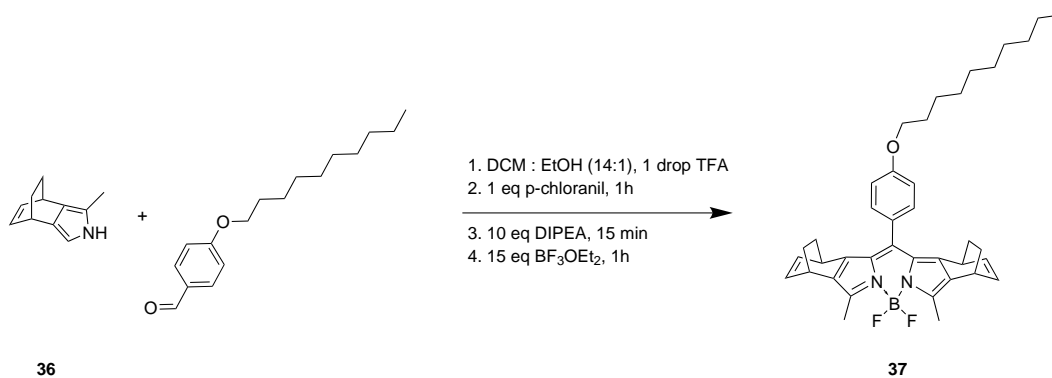


**Figure 4.15:** Synthesis of compound (**37**) with method 2

Compound **35** (50.00 mg, 314.01  $\mu\text{mol}$ , 2 eq) was dissolved in dry DCM (16 mL) and small amount of dry ethanol (1.14 mL), 14 : 1, in a Schlenk tube under inert atmosphere. 4-(Decyloxy)benzaldehyde (45.00  $\mu\text{L}$ , 164.85  $\mu\text{mol}$ , 1.05eq) and a drop TFA were added. The mixture was stirred over night at room temperature.

After oxidation with p-chloranil (38.60 mg, 157.0  $\mu\text{mol}$ , 1 eq), ethanol was removed under reduced pressure, because the alcohol interferes with the complexation step. The solid was again dissolved in dry DCM and DIPEA (274  $\mu\text{L}$ , 1.57 mmol, 10 eq) was added to guarantee a basic surrounding. BF<sub>3</sub> diethyl etherate (291  $\mu\text{L}$ , 2.36 mmol, 15 eq) was added dropwise to the solution for the complexation. The mixture was extracted with water, prepurified with a small column (silica, DCM) and the solvent was removed.

The reaction progress was monitored with TLC (CH : EA, 4 + 1).

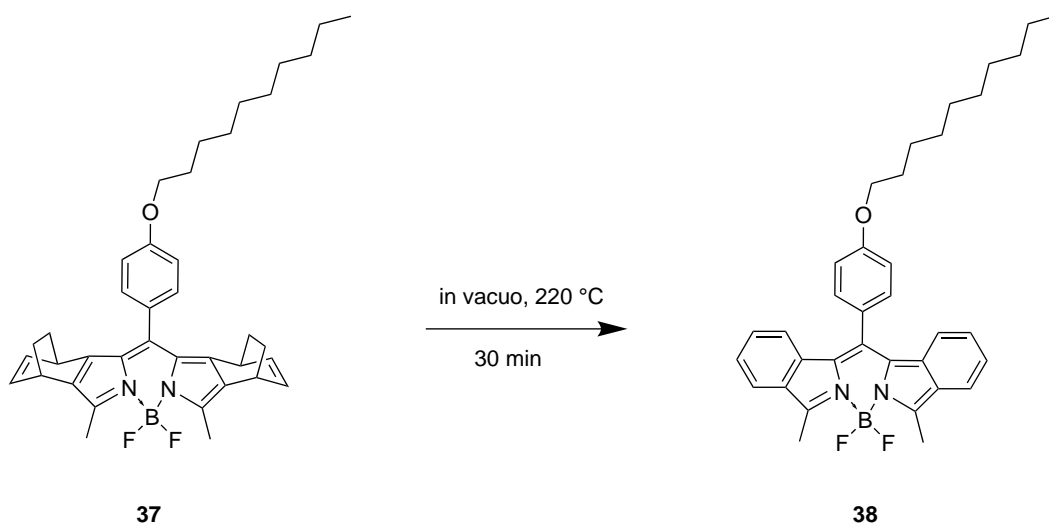
The crude product was purified with flash column chromatography (silica-gel, CH + 1 % EA). However no clean product could be isolated and the product containing impurities was therefore used in the next step as soon as possible.

Yield: 37.2 mg (39 %), violet product

Adding ethanol results in a higher yield than with the conventional method. However the product was difficult to isolate and instable. The purification steps lead to product losses.

<sup>1</sup>H NMR (300 MHz, Methylene Chloride-*d*<sub>2</sub>)  $\delta$  7.36 – 7.30 (m, 2H), 7.04 (dt, J = 9.5, 3.6 Hz, 2H), 6.41 (t, J = 6.9 Hz, 2H), 6.11 (q, J = 6.3 Hz, 2H), 4.07 (q, J = 6.2 Hz, 2H), 3.87 – 3.81 (m, 2H), 2.87 – 2.78 (m, 2H), 2.47 (s, 6H), 2.09 – 1.95 (m, 4H), 1.89 – 1.82 (m, 2H), 1.71 – 1.64 (m, 4H), 1.35 (s, 14H), 0.81 (s, 3H).

## 4.1.15 retro Diels-Alder

**Figure 4.16:** retro Diels-Alder reaction

The product from previous step, compound **37** (34 mg), was heated in a Büchi contained in vacuo. Prior to this the container was filled with nitrogen.

The product was purified via flash column chromatography (silica, CH : DCM, 7 + 1), the column was wrapped with aluminum foil to exclude light. A structure with presumably one aromatized ring was isolated as side product. The fractions were recorded via UV-VIS spectroscopy, the product showed a peak at 604 nm and side product at 557 nm.

Compound **38** is not stable while exposed to light and has therefore be stored in darkness.

$^1\text{H}$  NMR (300 MHz, Methylene Chloride- $d_2$ )  $\delta$  7.70 (dd,  $J = 18.4, 8.5$  Hz, 2H), 7.57 – 7.28 (m, 4H), 7.31 – 6.86 (m, 6H), 4.30 (dt,  $J = 13.8, 6.7$  Hz, 2H), 2.92 (d,  $J = 3.2$  Hz, 3H), 1.88 (h,  $J = 6.5$  Hz, 2H), 1.81 – 1.62 (m, 3H), 1.33 (s, 14H), 0.88 (s, 3H).

MALDI-TOF:  $m/z$  calc. for  $\text{C}_{35}\text{H}_{39}\text{BF}_2\text{N}_2\text{O}$  is 522.3130, found: 522.3608

## 4.2 Synthesis of asymmetrical BODIPY derivatives

### 4.2.1 9-chloro-13-(4-(decyloxy)phenyl)-5,5-difluoro-1,3-dimethyl-12-phenyl-5,11-dihydro-5λ4,6λ4-indeno[2',1':4,5]pyrrolo[2,1-f]pyrrolo[1,2-c][1,3,2]diazaborinine (39) via different attempts

#### method 1

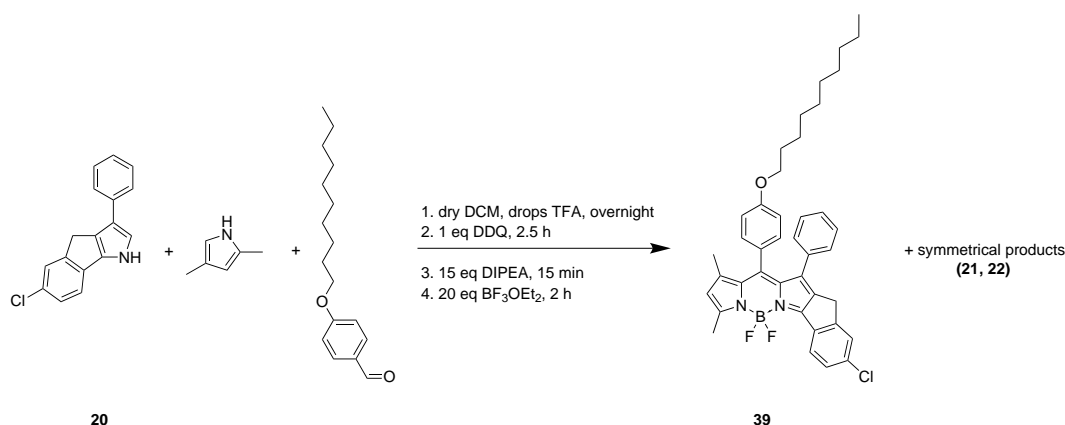


**Figure 4.17:** Synthesis of asymmetric compound (39) with two different pyrroles (method 1)

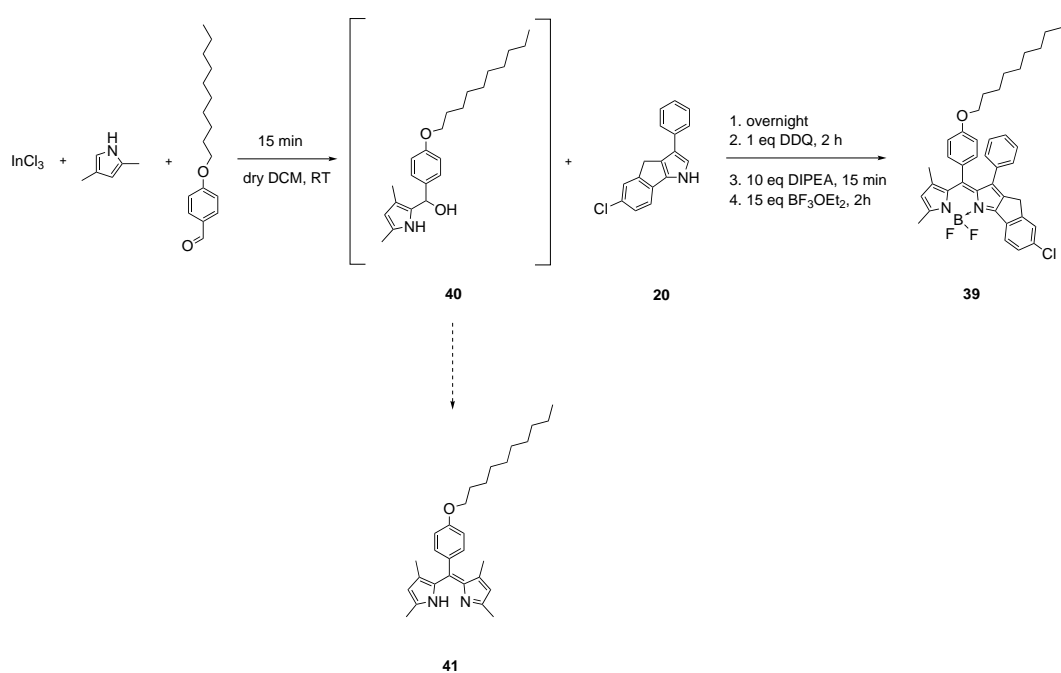
Under inert atmosphere, compound **20** (400 mg, 1.51 mmol, 1 eq), 2,4-dimethylpyrrole (110  $\mu$ L, 1.51 mmol, 1 eq) and 4-(decyloxy)benzaldehyde (440  $\mu$ L, 1.58 mmol, 1.05 eq) were dissolved in dry DCM (20 mL). Two drops of TFA were added and the solution was stirred overnight during light exclusion.

The compound was oxidized with DDQ (350 mg, 1.51 mmol, 1 eq) over 2.5 hours. Adding DIPEA (3.93 mL, 22.58 mmol, 15 eq) and BF<sub>3</sub>OEt<sub>2</sub> (3.81 mL, 30.10 mmol, 20 eq) results in a violet solution. The mixture was extracted with water + sat. NaCl and sat. NaHCO<sub>3</sub>, dried over Na<sub>2</sub>SO<sub>4</sub> and the organic solvent was removed under reduced pressure.

The reaction progress was controlled by TLC (CH + EA, 4 + 1) and UV/VIS-spectroscopy.

The product was attempted to be purified via flash column chromatography (CH : n-heptane, 7 + 1 + 3 % ethylacetate), however the asymmetrical and symmetrical products could not be separated.

## 4.2.2 method 2

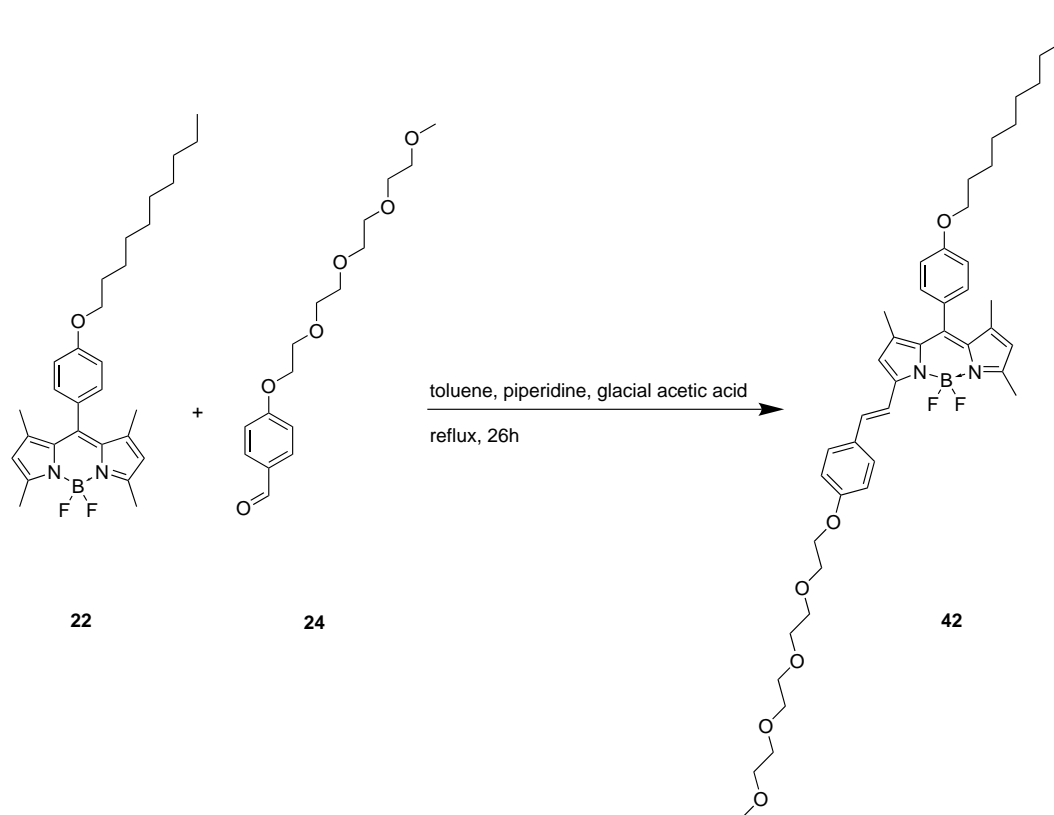


**Figure 4.18:** Synthesis of compound **39** via the intermediate (4-(decyloxy)phenyl)(3,5-dimethyl-1H-pyrrol-2-yl)methanol

115  $\mu\text{L}$  (1.58 mmol, 1 eq) 2,4-dimethylpyrrole and 457  $\mu\text{L}$  (1.66 mmol, 1.05 eq) 4-(decyloxy)benzaldehyde were submitted in a Schlenk flask under inert atmosphere. 0.10 eq  $\text{InCl}_3$  (34.87 mg, 157.65  $\mu\text{mol}$ ) and dry DCM (20 mL) were added. After maximum 15 minutes compound **20** (419 mg, 1.13 mmol, 1 eq) must be added, otherwise product **41** is synthesized. A color change to dark red was observed. The reaction was stirred overnight.

The compound was complexed, first by oxidation with DDQ (358 mg, 1.58 mmol, 1 eq), followed by adding DIPEA (2.75 mL, 15.77 mmol, 10 eq) and boron trifluoride diethyl etherate (3.00 mL, 23.65 mmol, 15 eq) to the mixture. The reaction progress was detected by TLC (CH + EA, 4 + 1). A violet color after the last step was noticed. To neutralize the excess of  $\text{InCl}_3$  sodium hydroxide (190 mg) was added.

An extraction with water + sat.  $\text{NaCl}$ ,  $\text{NaHCO}_3$  and again water followed. The organic layer was dried and removed under reduced pressure. The product was tried to purify via flash column chromatography (CH : toluene, 2 : 1 + 0.5 % DCM). The isolation of a pure asymmetrical product was not possible.

**4.2.3 p-(4-((2,5,8,11-tetraoxatridecan-13-yl)oxy)styryl)-(4-(decyloxy)phenyl)-difluoro-trimethyl-5H-dipyrrolo diazaborinine (42)**

**Figure 4.19:** Condensation of dimethyl m-decyloxy BODIPY (**22**) with TEG benzaldehyde (**24**)

Compounds **22** (40 mg, 83.26  $\mu\text{mol}$ , 1 eq) and **24** (29.91 mg, 95.74  $\mu\text{mol}$ , 1.15 eq) were refluxed for 26 hours in a mixture of toluene (5 mL), piperidine (111  $\mu\text{L}$ ) and glacial acetic acid (92  $\mu\text{L}$ ) together with a small amount of molecular sieve to trap water. After cooling down to room temperature, the product was purified with flash column chromatography (CH : EA, 2 + 1).

Yield: 5 mg (8 %), violet

$^1\text{H}$  NMR (300 MHz, Methylene Chloride- $d_2$ )  $\delta$  7.53 (t,  $J = 6.2$  Hz, 2H), 7.49 – 7.37 (m, 1H), 7.28 (d,  $J = 11.4$  Hz, 1H), 7.18 (d,  $J = 3.0$  Hz, 2H), 7.02 (d,  $J = 8.4$  Hz, 2H), 6.94 (d,  $J = 8.5$  Hz, 2H), 6.62 (s, 1H), 6.04 (s, 1H), 4.15 (q,  $J = 4.7$  Hz, 2H), 4.01 (t,  $J = 6.6$  Hz, 2H), 3.83 (q,  $J = 7.0, 5.9$  Hz, 2H), 3.75 – 3.41 (m, 14H), 3.33 (s, 3H), 2.54 (s, 3H), 2.02 (d,  $J = 14.4$  Hz, 6H), 1.52 (d,  $J = 7.5$  Hz, 14H), 0.83 (s, 3H).

### 4.3 Synthesis of amphiphilic BODIPYs

#### 4.3.1 Cl-rigid m-decyloxy B-TEG BODIPY (43)

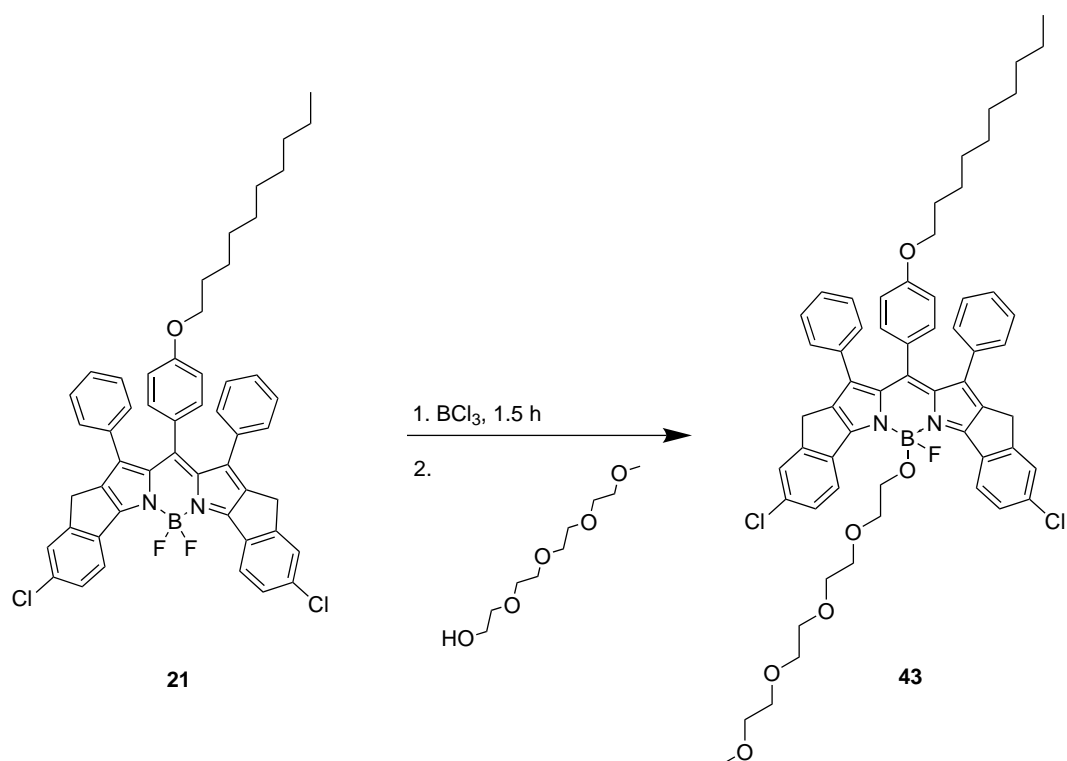


**Figure 4.20:** Synthesis of an amphiphilic BODIPY, the Cl-rigid m-decyloxy B-TEG BODIPY (**43**)

15 mg (18.26  $\mu\text{mol}$ ) Cl-rigid m-decyloxy BODIPY (**21**) were dissolved in dry DCM (8 mL) under inert atmosphere.  $\text{BCl}_3$  solution in heptane (18.26  $\mu\text{L}$ , 18.26  $\mu\text{mol}$ , 1 M) was added and stirred for 1.5 hours. The reaction progress was detected by TLC and UV/VIS-spectroscopy, where a shift of 14 nm was recorded.

To attach the hydrophilic part, 2,5,8,11-tetraoxatridecan-13-ol (71.7  $\mu\text{L}$ , 365.1  $\mu\text{mol}$ , 20 eq) was added and stirred for another hour. The mixture was thoroughly washed with water, dried ( $\text{Na}_2\text{SO}_4$ ) and the solvent was removed via rotatory evaporation.

Yield: 17.5 mg (94.9 %), blue-green powder

$^1\text{H}$  NMR (300 MHz, Methylene Chloride- $d^2$ )  $\delta$  8.74 (d,  $J = 8.3$  Hz, 2H), 7.52 (d,  $J = 12.3$  Hz, 4H), 6.97 – 6.92 (m, 6H), 6.85 – 6.73 (m, 6H), 5.97 (d,  $J = 8.3$  Hz, 2H), 3.67 (t,  $J = 6.4$  Hz, 2H), 3.56 (s, 4H), 1.65 (s, 3H), 1.34 – 1.29 (m, 16H), 1.25 (d,  $J = 8.0$  Hz, 16H), 0.89 (s, 3H).  
 $^{13}\text{C}$  NMR (76 MHz,  $\text{CD}_2\text{Cl}_2$ )  $\delta$  160.18, 158.92, 153.29, 140.26, 139.52, 135.94, 134.82, 133.76, 131.65, 129.22, 127.86, 126.63, 126.26, 123.01, 113.41, 68.20, 54.53, 54.17, 53.45, 53.09, 32.33,



30.09, 26.35, 23.10, 14.29, 1.16.

MALDI-TOF m/z: theoretical [M-H] is 1007.4150, measured [M-H]: 1007.3290

### 4.3.2 Cl-rigid m-TEG B-decyloxy BODIPY (44)

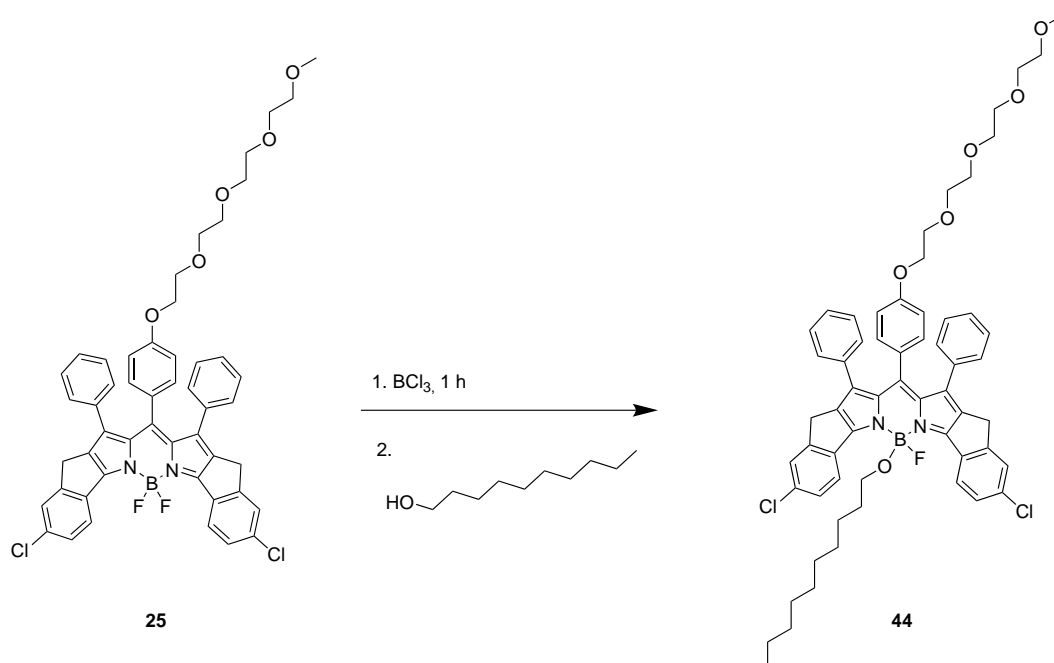


**Figure 4.21:** Synthesis of Cl-rigid m-TEG B-decyloxy BODIPY (**44**)

To a solution of Cl-rigid m-TEG BODIPY (**25**) (25 mg, 28.68  $\mu\text{mol}$ ) in dry DCM (15 mL)  $\text{BCl}_3$  (29  $\mu\text{L}$ , 28.68  $\mu\text{mol}$ , 1 M) was added and stirred in an inert atmosphere for an hour. A color change from turquoise to green was observed, which was also detected by a bathochromical shift of 15 nm. 20 eq 1-decanol (110  $\mu\text{L}$ , 573.65  $\mu\text{mol}$ ) were added. The reaction was stopped after 2.5 hours by extraction of the product in organic phase and extensively washed with water. The solvent was dried and removed under reduced pressure.

Yield: 28.2 mg (97 %), dark green powder

$^1\text{H}$  NMR (300 MHz, Methylene Chloride- $d_2$ )  $\delta$  8.72 (dd,  $J = 10.7, 8.1$  Hz, 2H), 7.55 – 7.42 (m, 4H), 6.95 (dq,  $J = 9.4, 4.8, 3.9$  Hz, 6H), 6.85 – 6.74 (m, 6H), 6.01 (d,  $J = 8.3$  Hz, 2H), 3.99 – 3.76 (m, 3H), 3.74 – 3.43 (m, 14H), 3.35 (s, 2H), 1.70 – 1.42 (m, 2H), 1.40 – 1.13 (m, 16H), 0.97 (s, 3H), 0.87 (q,  $J = 6.6$  Hz, 4H).

$^{13}\text{C}$  NMR (76 MHz,  $\text{CD}_2\text{Cl}_2$ )  $\delta$  153.51, 140.50, 136.17, 134.98, 134.04, 131.81, 129.43, 129.21, 128.41, 128.09, 126.89, 126.46, 113.72, 71.25, 70.10, 68.05, 54.00, 43.76, 32.50, 30.27, 30.14, 29.92, 23.27, 14.46, 1.35.

## 4.3.3 Cl-rigid m-perfluoro B-TEG BODIPY (46)

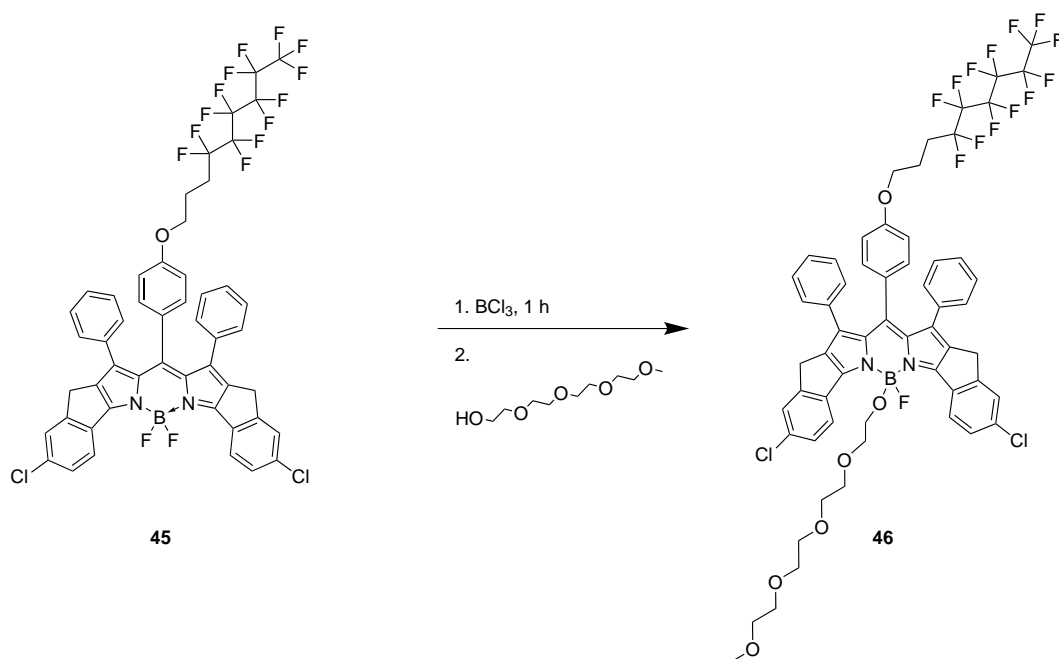


**Figure 4.22:** Synthesis of Cl-rigid m-perfluoro B-TEG BODIPY (46)

Compound **45** was synthesized by Matthias Schwar. After an inert atmosphere in a Schlenk flask was guaranteed, the BODIPY dye (25 mg, 24  $\mu\text{mol}$ ) was dissolved in dry DCM (15 mL) and  $\text{BCl}_3$  (24  $\mu\text{L}$ , 24  $\mu\text{mol}$ , 1 M) was added. The solution stirred for an hour. The alcohol, 2,5,8,11-tetraoxatridecan-13-ol (94.5  $\mu\text{L}$ , 480  $\mu\text{mol}$ , 20 eq), was added. The exchange of substituents took 1.5 hours. To stop the reaction, extraction with water was profoundly carried out. The organic phase was dried and removed.

Yield: 21.9 mg (74.2 %), dark green powder

$^1\text{H}$  NMR (300 MHz, Methylene Chloride- $d_2$ )  $\delta$  8.36 – 8.24 (m, 2H), 7.62 – 7.39 (m, 4H), 7.04 – 6.86 (m, 6H), 6.83 – 6.70 (m, 6H), 5.97 (dd,  $J = 8.9, 2.4$  Hz, 2H), 3.76 (t,  $J = 5.9$  Hz, 2H), 3.56 (s, 4H), 2.27 (tt,  $J = 19.1, 7.7$  Hz, 2H), 1.99 (dq,  $J = 12.0, 6.1$  Hz, 2H).

Compound **45** : MALDI-TOF:  $m/z$  calc. for  $\text{C}_{50}\text{H}_{30}\text{BCl}_2\text{F}_{15}\text{N}_2\text{O}$  is 1040.1596, found: 1048.1130

$^1\text{H}$  NMR of compound **46** showed same spectrum as compound **45**, probably due to the fact that it was not stable during the analysis. TLC, UV-VIS spectroscopy and MS analysis confirmed the product formation.

Compound **46**: MALDI-TOF:  $m/z$  calc. for  $\text{C}_{59}\text{H}_{48}\text{BCl}_2\text{F}_{14}\text{N}_2\text{O}_6$   $[\text{M}-\text{H}]^+$  is 1227.2769, found: 1227.2571

## 4.3.4 Tetramethyl m-decyloxy B-TEG BODIPY (47)

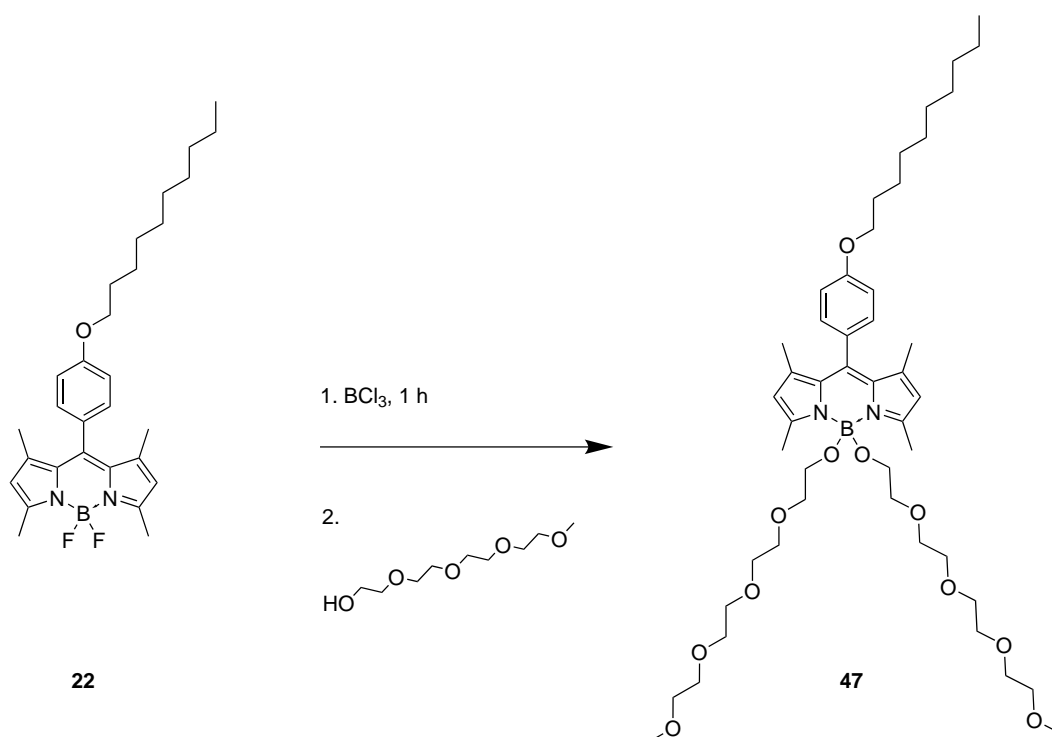


**Figure 4.23:** Coupling reaction of 1,3,7,9-tetramethyl m-decyloxy BODIPY (**22**) with 2,5,8,11-tetraoxatridecanol

The previously synthesized BODIPY derivative (25 mg, 52  $\mu\text{mol}$ ), **22**, was dissolved in dry DCM (25 mL).  $\text{BCl}_3$  (52  $\mu\text{L}$ , 52  $\mu\text{mol}$ , 1M) was added to the solution and stirred for an hour. A shift of 5 nm in the absorption spectrum was detected.

2,5,8,11-tetraoxatridecan-13-ol (204.5  $\mu\text{L}$ , 1.04  $\mu\text{mol}$ , 20 eq) was added and the reaction mixture stirred for 2 hours. The work-up was performed by extraction of impurities with water (10 x), drying over  $\text{Na}_2\text{SO}_4$  and removal of the solvent by rotary evaporation.

Yield: 10 mg, orange-green powder

$^1\text{H}$  NMR (300 MHz, Methylene Chloride- $d_2$ )  $\delta$  7.19 – 7.13 (m, 2H), 7.02 – 6.97 (m, 2H), 5.97 (d,  $J = 9.4$  Hz, 2H), 3.99 (d,  $J = 7.0$  Hz, 4H), 3.57 (dd,  $J = 12.7, 6.8$  Hz, 6H), 3.44 (s, 2H), 2.50 (t,  $J = 9.9$  Hz, 6H), 1.80 (s, 6H), 1.56 – 1.38 (m, 16H), 1.31 (d,  $J = 15.6$  Hz, 28H), 0.88 (s, 3H).

## 4.4 Preparation of J-aggregates

To analyze the J-aggregate formation of the synthesized and characterized products, a stock solution of the respective dyes in 3 mL acetone were prepared.

### 4.4.1 J-aggregate formation in various surfactants

#### Preparation of the stock solutions of surfactants

200 mg of surfactant (Pluronic, SDS, Brij 93, Tween 85, Triton X-100 and Span 80) were dissolved in 5 mL acetone, except in case of Span 80 and SDS additionally 2 mL H<sub>2</sub>O were added.

#### Determination of the ideal dye concentration and amount of surfactant

By varying the amount of the surfactant Pluronic from 0 - 10 mg with a defined concentration of dye ( $2 \times 10^{-5}$  M) the ideal amount of surfactant can be determined via UV/Vis-spectroscopy. Same principle goes for the concentration determination. The concentration varies with defined amount of surfactant (0.1 mg).

#### J-aggregate formation in presence of different surfactants

An defined amount of stock solution, to achieve a concentration of  $2 \times 10^{-5}$  M, was transferred in a 3 mL vial. 0.1 mg surfactant, acetone and finally 2.5 ml water were added. The acetone was removed by blowing nitrogen through the solution and a spectrum was recorded to detect the aggregation. The test was also accomplished without the addition of a surfactant.

To get an insight of the influence of dye aggregation in the presence of other dyes, a mixture of two dyes with and without surfactant were also carried out.

### 4.4.2 J-aggregate formation in various polymers

#### Preparation of stock solutions and foils

The polymer was weighed in a 20 mL vial in THF to yield a 10 wt% solution. Hydrogel D4, Polystyrene and cellulose acetate were prepared this way, except in case of PolyHEMA the polymer was dissolved in THF and water (9 + 1). A defined amount of dye stock solution of compounds **25**, **43**, **44**, **45** and **46** was added to 150 mg polymer to yield a 1 wt% solution. After removal of acetone, the "cocktails" were knife bladed on a Mylar foil (wet film thickness

0.5 mil (12.5  $\mu\text{m}$ ). The coated foils were characterized both in a dry state and swollen in water via UV/Vis-spectroscopy and via Fluorolog.

In case for compounds **43**, **45** and **46** also "cocktails" of 5 w% dye in 6 % D4 were prepared. A different procedure was followed with the silicone rubber. For the stock solution, 1 g of the vinyl-terminated PDMS, 40  $\mu\text{L}$  Hydride-PDMS (co-polymer) were dissolved in 2 mL DCM. The dyes **25**, **43**, **45** and **46** (approximately 0.7 mL of the stock solution) were transferred in a vial and acetone was removed. 200 mg silicon polymer stock solution, 2  $\mu\text{L}$  methylvinylcyclosiloxane (retarder) and 2  $\mu\text{L}$  Pt-cat were added (see table 3.4). Within 10 minutes the "cocktail" need to be knife bladed with a 3 mil knife.

---

## 5 Results and Discussion

The aim of this thesis was to synthesize new BODIPY dyes, which are able to form the highly ordered structures of J-aggregates. In the last decades researchers were able to synthesize dyes of different classes, like perylene bisimides, porphyrins and cyanines, which were able to form J-aggregates. The formation was also observed with azaBODIPYs, however this took several weeks [14]. This type of aggregation is very interesting, because of their unique properties, like a huge bathochromic shift with a small band width.

In the first part of this chapter the synthesis of various synthesized BODIPY dyes will be discussed, as well as the difficulties and possible improvements. Followed by a section of the synthesis of amphiphilic BODIPY derivatives and formation of J-aggregates.

Finally, the characterization of the synthesized BODIPYs and of the J-aggregates formed with surfactants and in various polymers will be analyzed.

### 5.1 Synthetic Considerations

#### 5.1.1 Synthesis of BODIPY dyes

The synthetic route to generate BODIPYs is already well established [81, 85]. It can be either accomplished via condensation of pyrroles with acyl chlorides, followed by a complexation step to get the BODIPY core (see figure 2.17) or by reaction of an aromatic aldehyde with a pyrrole in an acidic environment, which is followed by an oxidation. After complexation in a basic surrounding the reaction leads to the BODIPY core, see figure 2.18, which is the most common way and was also utilized during this thesis.

As already mentioned, the second approach was used to synthesize the BODIPY dyes **21**, **22** and **25**, for the last one the benzaldehyde was not commercially available, therefore previous reaction steps are necessary, which are described in **Synthesis of TEG-benzaldehyde**.

An overview of the reaction steps for BODIPY synthesis is illustrated in figure 5.1.

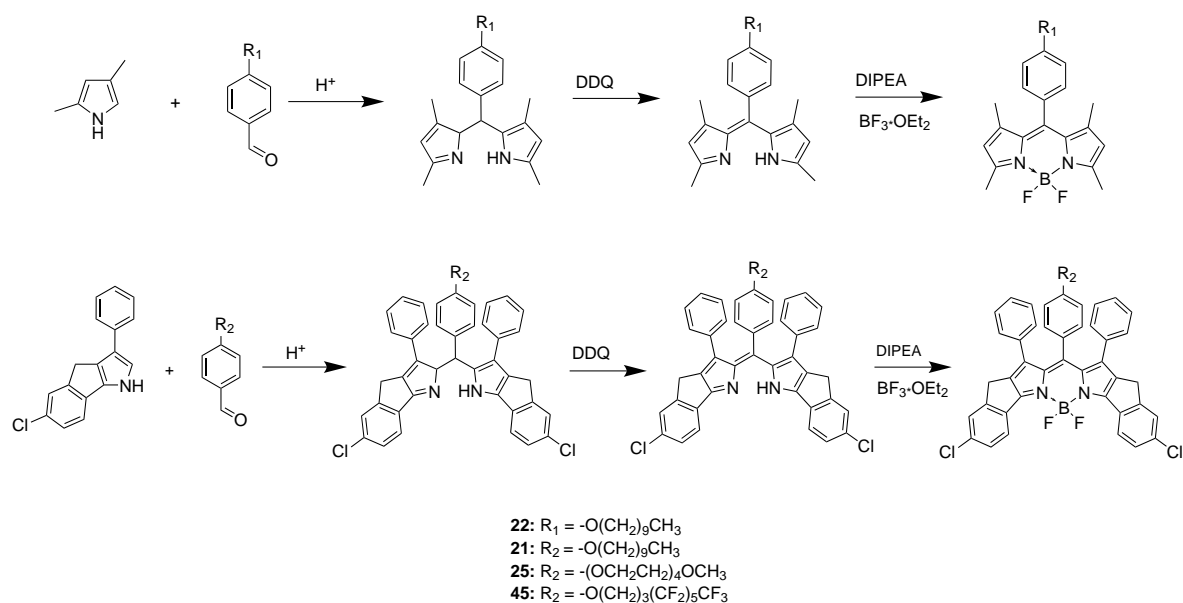


**Figure 5.1:** Overview of the reactions steps to synthesize symmetrical BODIPY derivatives, with different pyrroles and aldehydes, the 4-(hydroxy)benzaldehyde and TEG benzaldehyde, which was synthesized beforehand

The synthesis took two days and has to be conducted under inert atmosphere and exclusion of light, because the pyrrole is sensitive and will degrade. The first attempts during this thesis did not work out, due to the fact, that the boron trifluoride diethyl etherate was older and therefore the complexation was not successful. However after a new one arrived, the reaction worked out in moderate yields, like those in literature [3].

According to Jameson and Dzyuba [95] the overall reaction time for BODIPY synthesis can be reduced to only 5 minutes.

An attempt to increase the yield of this synthesis was by adding ethanol to the standard procedure [94], which went really well. After oxidation the alcohol need to be removed, otherwise the complexation step is hindered. However the dye was not stable and after purification a lot of product was lost, the overall reaction and all necessary steps will be discussed in the following section. Another improvement can be achieved by using p-chloranil as oxidation reagent instead of DDQ. Chloranil has the advantages of being cheaper and less side products are formed.

BODIPY dye with extended  $\pi$ -System

The whole reaction pathway, described in this section, can be found in 5.2.

The first two reaction steps were executed like in literature [96]. Bis(trimethylsilyl)acetylene was converted with *p*-toluenesulonyl and  $\text{AlCl}_3$  to the intermediate which was converted to **32** after pouring the solution in 1N HCl *p*-tolyl ethynyl sulfone was gained.

A Diels-Alder reaction of **33** with 1,3-cyclohexadiene followed in toluene at  $85^\circ\text{C}$ , no further purification was necessary. The Diels-Alder adduct was treated with ethyl isocyanoacetate in presence of  $\text{K}^+\text{OtBu}^-$  yielding the pyrrole via the Barton-Zard mechanism. This two steps were performed according to literature [97]. Ethyl-4,7-dihydro-4,7-ethano-2H-isoindole-1-carboxylate was further reduced with excess of  $\text{LiAlH}_4$  to **36** [98]. The reaction was controlled via MS, the theoretical peak should be at 159.1 and at 159 a peak was detected.

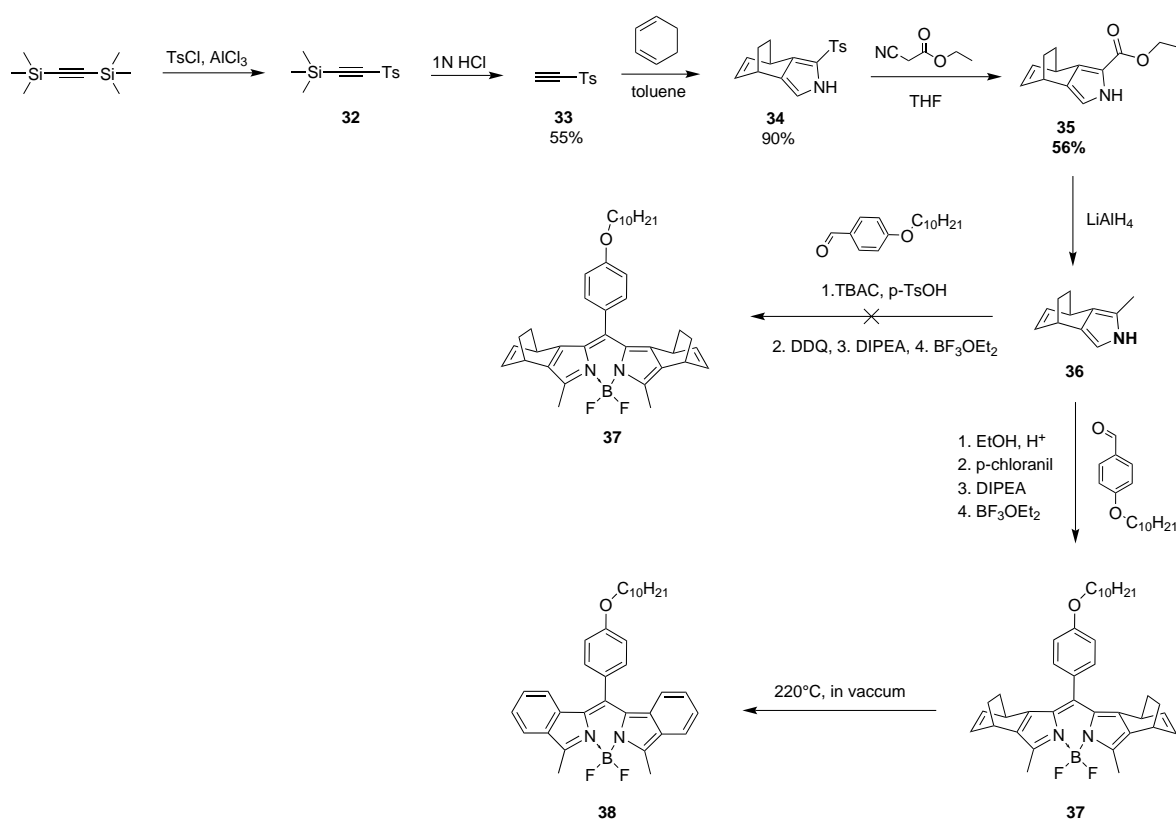


**Figure 5.2:** Overview of 14-(4-(decyloxy)phenyl)-7,7-difluoro-5,9-dimethyl-7H-[1,3,2]diazaborinino[4,3-a:6,1-a']diisoindole synthesis

To synthesize the BODIPY structure two different methods were accomplished. The one typical to the standard procedure, with two little differences: first, a small amount of ethanol was added (14 + 1) and second, instead of DDQ *p*-chloranil was used for the oxidation step. It turned out, that this were the better reaction conditions for BODIPY synthesis. However, the product was difficult to isolate, after certain time the product decompose, therefore the



purification was impossible.

The other method, was in presence of tertbutylammonium chloride and p-toluenesulfonic acid, where no product could get isolated.

The last step was a retro Diels-Alder reaction to extend the  $\pi$  system of the BODIPY, which was easily achieved by heating the pink solid up to 200°C under vacuum. As side product, the compound with only one aromatic ring could also be observed (557 nm). Unfortunately, this dye (604 nm) is hardly suitable for further modification, since it is highly photolabile, even substitution on the boron center would not enhance the stability.

### Synthesis of TEG-benzaldehyde

Via nucleophile substitution of 2,5,8,11-tetraoxatridecan-13-ol with p-toluenesulfonyl chloride it was possible to synthesize tosyl TEG (**23**) in excellent yields ( $\sim 98\%$ ). No further purification step was necessary. In a second step the synthesized compound was coupled with 4-hydroxybenzaldehyde at 90°C over night resulting in the desired product.

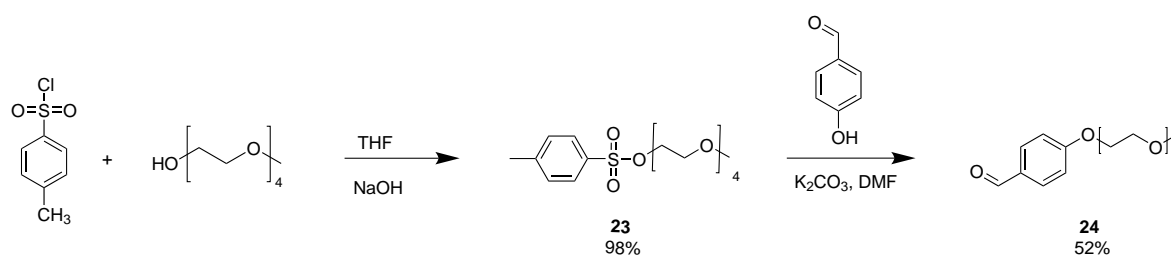


**Figure 5.3:** Overview of TEG-benzaldehyde synthesis

### Synthesis of TEG-m-perfluoro BODIPY

The aim during this synthesis was to generate a pyrrole with a hydrophilic substituent to get an amphiphilic BODIPY ground structure. First, the previously synthesized tosyl TEG reacted with 6-hydroxy-1-tetralone via nucleophilic substitution to 3,4-dihydro-6-TEG-naphthalen-1(2H)-one in good yields. Next, the pyrrole was synthesized by activation with lithium diisopropylamide and coupling with 3-phenyl-2H-azirine, which is toxic and need to be handled carefully. The purification step need to be carried out quickly, because the crude pyrrole is not stable. The product has to be stored in a freezer.

During the last step of the BODIPY synthesis, **29** reacted with 4-(tridecafluoronyl)oxy benzaldehyde. The system was oxidized with DDQ and and complexation of the resulted dye was attempted. However, no product was isolated.

Reason could be the older batch of  $\text{BF}_3\text{OEt}_2$ . The reaction was not repeated, due to the fact that the used pyrrole was already consumed.

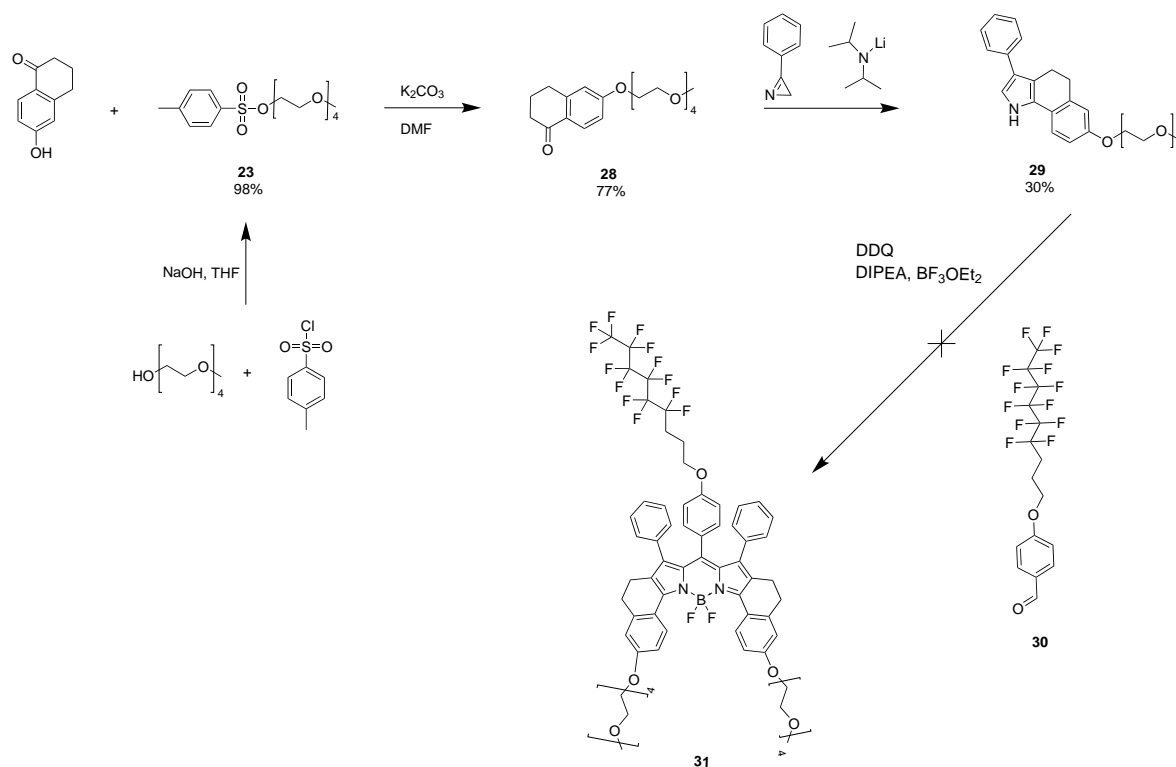


**Figure 5.4:** Attempted synthesis of TEG-m-perfluoro BODIPY

### 5.1.2 Attempted Synthesis of Asymmetrical BODIPY

To synthesize asymmetrical BODIPYs the second method worked out better, the procedures can be found in the experimental part of this thesis (see 4.2.1) and the synthetic route of the second method is also shown in figure 5.5. Here the 2,4-dimethylpyrrole reacted with the aldehyde in presence of indium chloride to form the alcohol intermediate. The time window to only synthesis the intermediate and not the tetramethyl BODIPY derivative is really small and need to be detected fast. The difficult part was to isolate the asymmetric compound, because the symmetrical ones elute at the same time. By forming stable ketons [99], the synthesize of the asymmetrical derivative would be improved and the possibility to form symmetric BODIPYs should be decreased drastically.

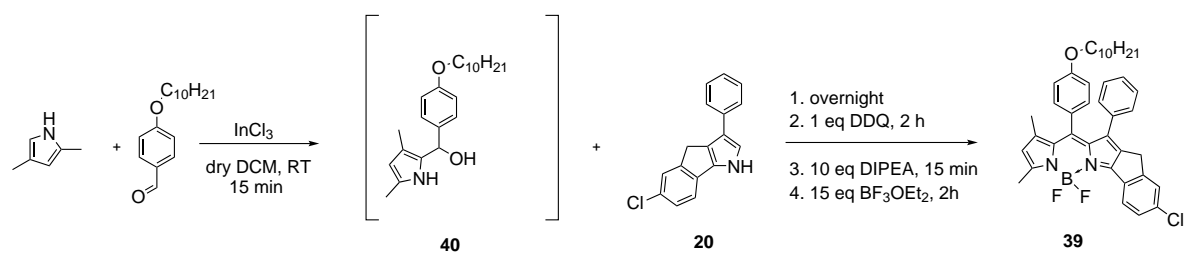
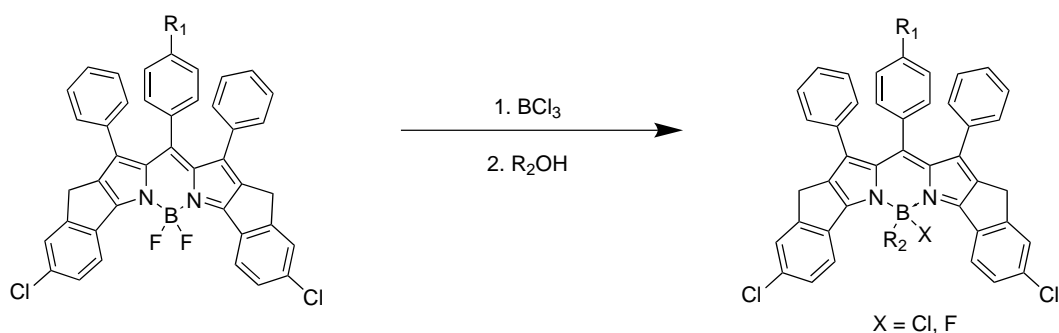


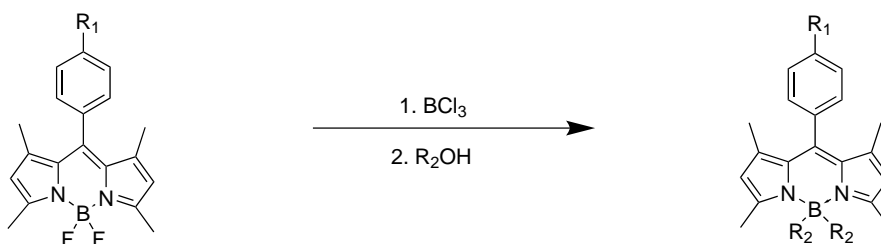
**Figure 5.5:** Attempted synthesis of an asymmetrical BODIPY

### 5.1.3 Substitution of Fluorine with Alcohols

The aim of this task was to introduce alcohols at the boron center by formation of B-O bonds to synthesize amphiphilic BODIPY derivatives. Amphiphilic BODIPYs have the advantage of self-aggregation, because of their hydrophilic and hydrophobic parts. The synthesis route is already reported in various papers [91, 92, 100] and the synthetic route during this work is illustrated in figure 5.6.



- 43:**  $R_1 = -O(CH_2)_9CH_3$ ,  $R_2 = -(OCH_2CH_2)_4OCH_3$   
**44:**  $R_1 = -(OCH_2CH_2)_4OCH_3$ ,  $R_2 = -O(CH_2)_9CH_3$   
**46:**  $R_1 = -O(CH_2)_3(CF_2)_5CF_3$ ,  $R_2 = -(OCH_2CH_2)_4OCH_3$



- 47:**  $R_1 = -O(CH_2)_9CH_3$ ,  $R_2 = -(OCH_2CH_2)_4OCH_3$

**Figure 5.6:** Coupling of the previously synthesized dyes at the boron center with alcohols

The first attempts were carried out by converting the alcohol with sodium hydride to the

corresponding alcoholate, while the dye reacted with boron trichloride for 20 min in DCM. After chlorination the alcoholate was added, however the expected bathochromic shift of the UV spectra was not observed. After TLC control several spots were detected and an assignment was difficult to make. After purification no product was isolated, which was due to the fact that the chlorine reacts with the silica. It was assumed that the 1 M  $\text{BCl}_3$  solution is too aggressive and mostly ligand is formed. Another observation was that  $\text{BCl}_3$  is not stable over a long storage time in DCM and therefore does not play the important role during the reaction. A test with different reaction condition was conducted to gain insight of the optimal conditions. After adding alcohol the second halogenated substituent on the boron center was tried to convert again to fluorine by adding tetra butyl ammonium fluoride, to prevent the problem during purification. The reactions were accomplished at  $0^\circ\text{C}$ , room temperature and at  $60^\circ\text{C}$ . Also the influence of adding triethyl amine was tested. However, no improvement could be achieved. The most promising approach was found to be to increase the reaction time (activation step) and then to directly add the alcohol and not the alcoholate.

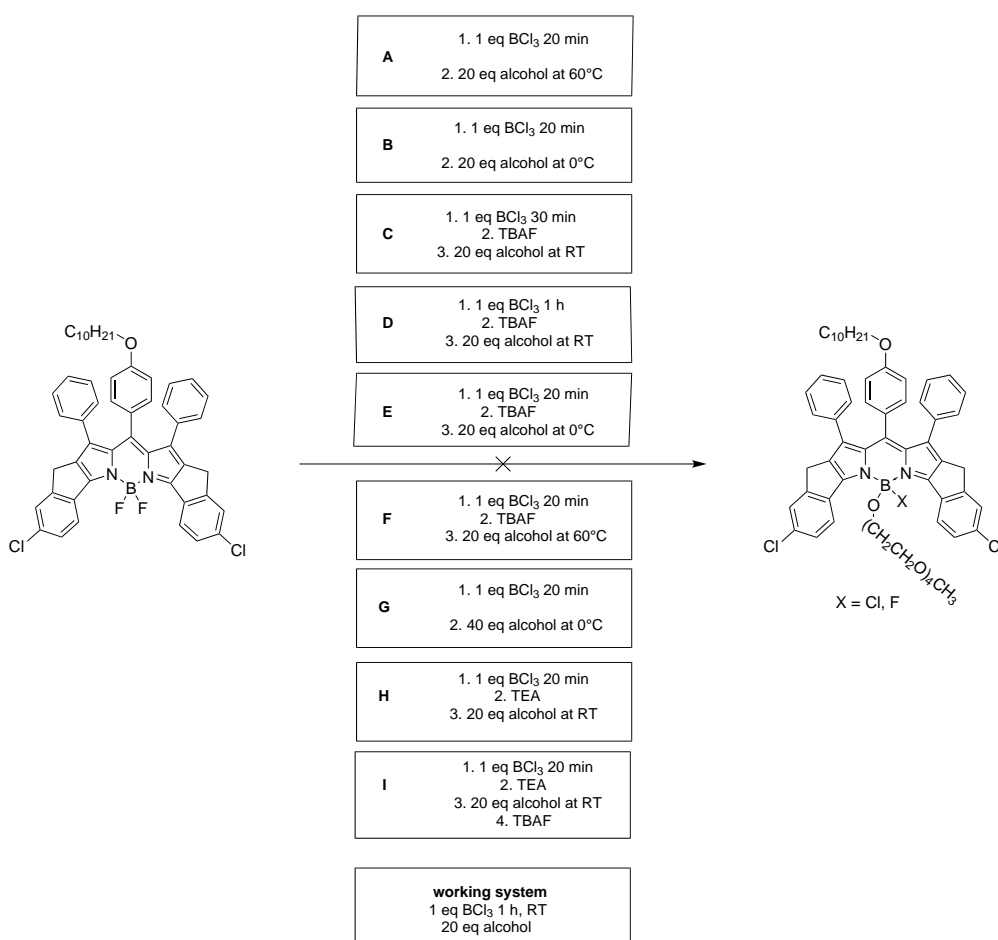


**Figure 5.7:** Optimization of the reaction conditions for synthesis of amphiphilic BODIPYs

To conclude, the reaction was carried out by substitution of fluorine by chlorine atom with  $\text{BCl}_3$  (stored in heptane) for one hour and afterwards adding the alcohol. The product can not be further purified via column chromatography since it was found to decompose on silica-gel presumably losing the alkoxy chain. Therefore, to remove the impurities the organic layer need to be carefully washed with water to get rid mainly of the excess of the alcohol as well as the excess of boron trichloride. With this method the desired products could be synthesized, which was verified by NMR measurement (see appendix). In case of the dyes with rigid structures (**43**, **44** and **46**) one fluorine was substituted. Dye **47** showed two substituents, because the structure is not that sterically hindered.

## 5.2 Dye Characterization

For photophysical characterization of the synthesized dyes absorption and emission spectra were recorded, with these methods the molar absorption coefficients, fluorescence lifetimes and relative quantum yields were determined. All measurements were performed in solution (THF).

An overview of the results can be found in table 5.1.

**Table 5.1:** Overview photophysical properties of the synthesized dyes (Monomer)

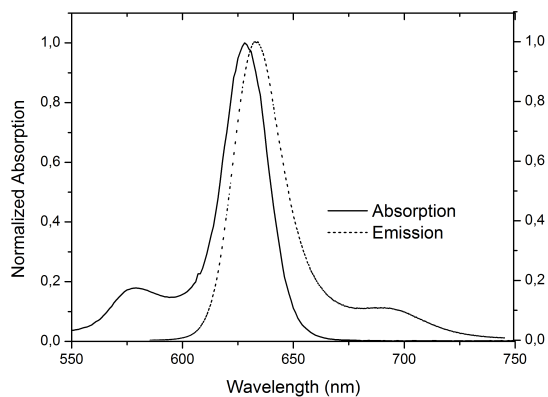
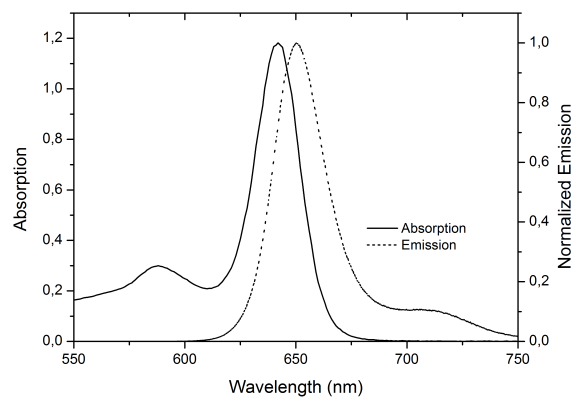
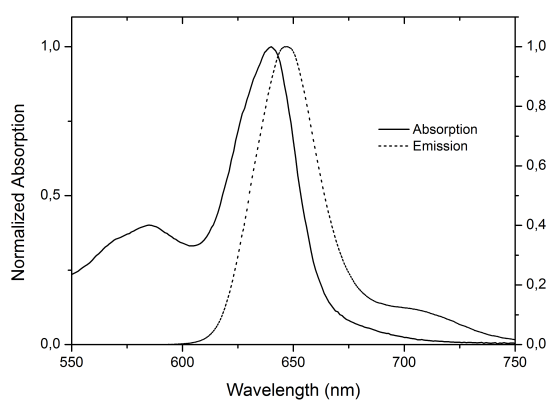
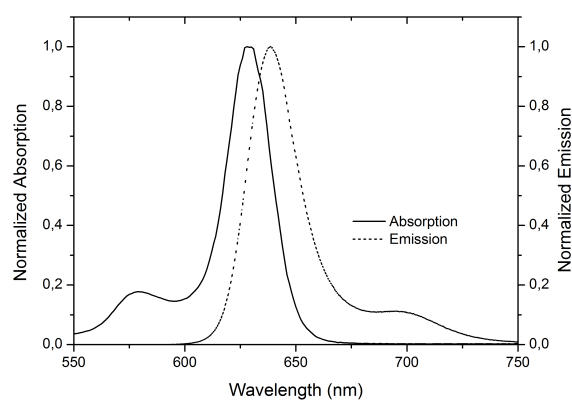
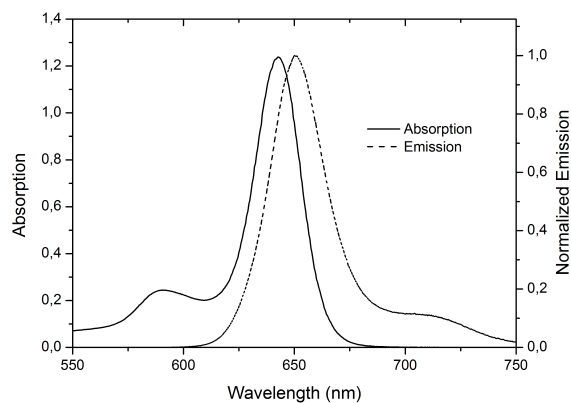
compound	$\lambda_{abs}$ [nm]	$\epsilon$ [l/mol cm]	$\lambda_{em}$ [nm]	QY [%]	lifetime [ns]
<b>21</b>	631	107900			8,8
<b>22</b>	501	62400			4,5
<b>25</b>	628	160800	639	68	9,7
<b>27</b>	568	36700			4,2
<b>38</b>	604	62800			4,6
<b>43</b>	644	59100	650	42	7,4
<b>44</b>	640	45150	646	26	6,4
<b>45</b>	631	153000	639	65	8,6
<b>46</b>	645	133600	650	85	9,6
<b>47</b>	501	12941			5,0

### 5.2.1 Absorption and Emission Spectra

A bathochromic shift of the absorption maxima, which can be seen in figure 5.8, was achieved by synthesis of amphiphilic compounds. By introduction of a hydrophilic chain at the boron center in case of m-TEG BODIPY (**25**) or hydrophilic with the other two BODIPYs a shift of around 10 nm was obtained.

As already known, BODIPYs emit fluorescence characteristically by sharp peaks. The typical emission maxima lay between 520-600 nm [3], with the synthesized dyes a maximum of 650 nm was achieved. The Stokes shift of this dyes are really small (5-11 nm).

In case of compound **44**, Cl-rigid m-TEG B-decyloxy BODIPY, the spectrum shows a broader peak.

(a) compound **25** m-decyloxy(b) compound **43** m-decyloxy B-TEG(c) compound **44** m-TEG B-decyloxy(d) compound **45** m-perfluoro(e) compound **46** m-perfluoro B-TEG

**Figure 5.8:** Absorption (solid) and Emission (dashed) spectra of the synthesized dyes in their monomeric form (in THF)

### 5.2.2 Quantum Yield

Quantum yields measured in THF vary in a broad range. The range goes from lowest results with 26 % to the highest with 85 %. As reference tert-butyl BODIPY from Tanja Rappitsch with a known QY of 94 % was used.

As already known from literature [3, 90], BODIPY dyes inherit excellent quantum yields (60-90 %), which can also be seen with the synthesized dyes during this thesis, see table 5.1. By introduction of a substituent on the boron center a decrease in quantum yield can be observed, except for compound **46**, where the amphiphilic structure yields in a higher QY. Dye **44** shows the lowest QY value, probably due to tendency of the dye to form H-aggregates already in solution (see figure 5.8c).

### 5.2.3 Fluorescence Lifetime

The fluorescence lifetimes of the monomeric forms are quite high and range from 4.2 - 9.7 ns, which is in the range of literature known BODIPYs (1-10 ns)[90]. Amphiphilic derivatives show shorter lifetimes than their corresponding compound with only the substituent in meso position, except of the perfluoro derivative, here the addition of the hydrophilic chain enhance the lifetime, which also matches the results deriving from the QY measurements. The dyes with rigid structure show higher values.

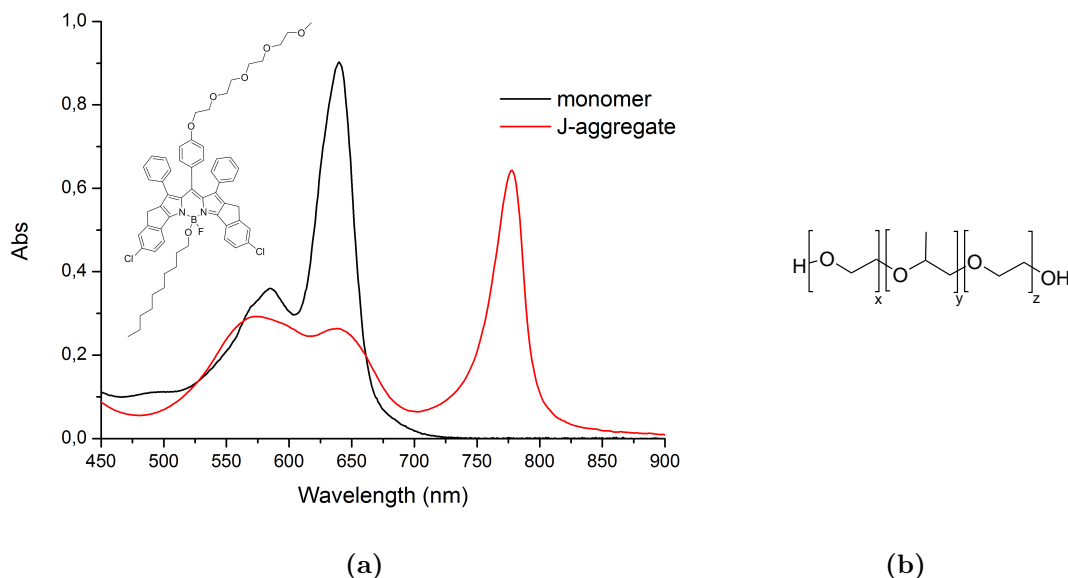


## 5.3 Formation of J-aggregates

In this chapter the synthesized dyes were tried to form the desired aggregates with surfactants and in polymers resulting in the unique properties, described in the theoretical part of this master thesis.

### 5.3.1 Aggregates with Surfactants

De Rossi et al [62] claimed, that J-aggregate inherit a higher molecular order by adding surfactants. Therefore experiments with and without various surfactants were carried out and compared.



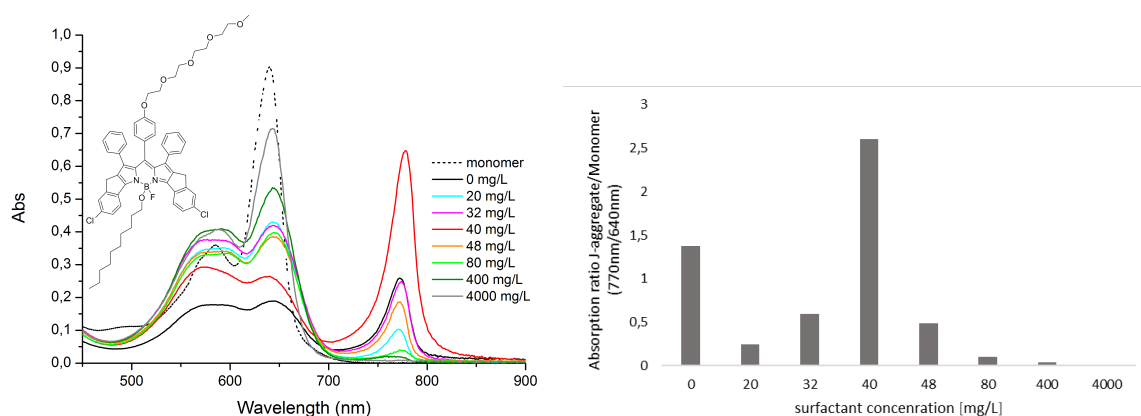
**Figure 5.9:** (a) Absorption spectrum of compound **44**, representing the monomer in THF (black) and after J-aggregation in water in the presence of Pluoronic (red)  
 (b) Structure of Pluoronic

Figure 5.9a shows compound **44** before (in THF) and after J-aggregate formation (in water) in presence of surfactant (Pluoronic). The spectrum shows the characteristic absorption band at about 780 nm (red line) after forming the J-aggregate. Whereas the monomer shows an absorption maximum at around 640 nm (black line). A bathochromic shift of almost 140 nm (!) was achieved after the highly ordered structure is formed.

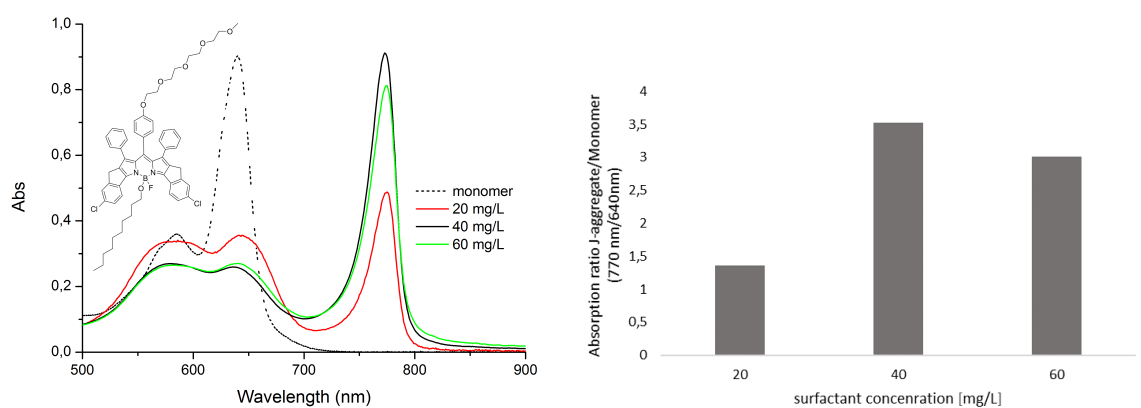
## Determination of the Surfactant Concentration

First, a suitable amount of surfactant need to be determined. Therefore, to an aqueous solution (2.5 mL) of compound **44**, with a dye concentration of  $2 \times 10^{-5}$  M, different amounts of Pluronic were added (0, 20, 32, 40, 48, 80 and 400 mg/L). By adding 4000 mg/L surfactant no aggregation can be observed. The test was also carried out with SDS instead, however only with 20, 40 and 60 mg/L of surfactant.

The corresponding absorption spectra were recorded. As shown in figure 5.10a, already without adding a surfactant the dye forms J-aggregates. With 40 mg/L the best dye - surfactant proportion was determined. The same result showed the test with SDS (see figure 5.10c)



(a) Determination of the optimal surfactant concentration with Pluronic in water with compound **44** ( $c = 2 \times 10^{-5}$  M), the dashed line represents the monomeric form in THF (b) Plot of the absorption ratio (ratio of J-aggregate at 770 nm to monomer at 640 nm) vs. the surfactant concentration [mg/L]

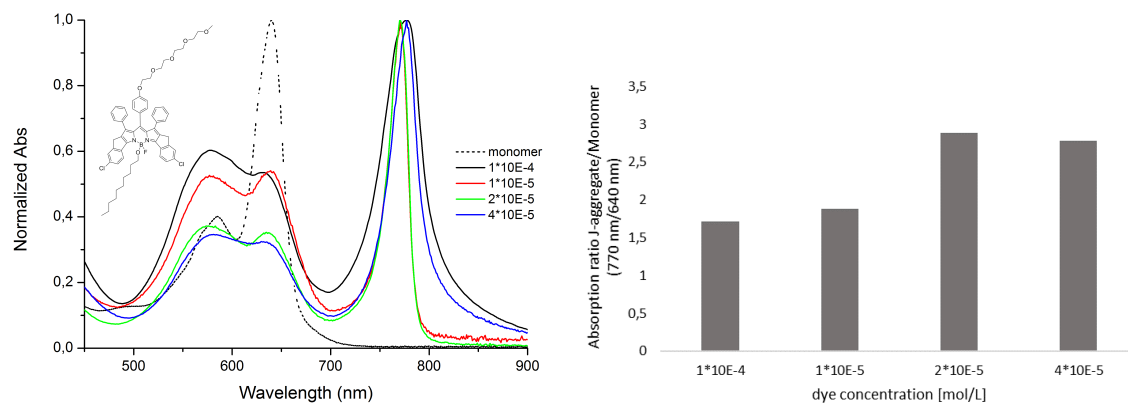


(c) Ideal amount of surfactant (SDS) verification with compound **44** in water, with defined dye conc ( $2 \times 10^{-5}$  M). (d) Plot of the absorption ratio (ratio of J-aggregate at 770 nm to monomer at 640 nm) vs. the SDS concentration [mg/L]

**Figure 5.10:** Determination of the optimal surfactant concentration with Pluronic and SDS

## Determination of the Dye Concentration

Now that we know, that with adding 40 mg/L surfactant the best results are achieved, the question of the optimal dye concentration need to be answered. It was found that the concentration, which was used during the previously tests, achieved the best results, as it can be seen in figure 5.11a. During this measurements Brij 93 was used as surfactant.



(a) Absorption spectrum with different concentrations of compound **44** with Brij 93 as surfactant (b) Plot of the absorption ratio (ratio of J-aggregate at 770 nm to monomer at 640 nm) vs. the dye concentration [mol/L]

Lower and higher concentrations lead to broader peaks. Even though the conc. at  $4 \times 10^{-5} M$  has a larger red shift, nevertheless the peak is broader, which can be seen at full width at half maximum (FWHM). The selected concentration,  $2 \times 10^{-5} M$ , yield in a value of 21.6 nm and  $4 \times 10^{-5} M$  shows a FWHM of 31.9 nm. In case of  $1 \times 10^{-5} M$  the monomeric portion is higher.

### Influence of Surfactant Nature on J-aggregates Formation

During this measurements the dependency of surfactants was determined. In total, six different surfactants were tested, the used surfactants are shown in table 3.3 and the structures in figure 5.12. The structure of Pluoronic can be found in figure 5.9b.

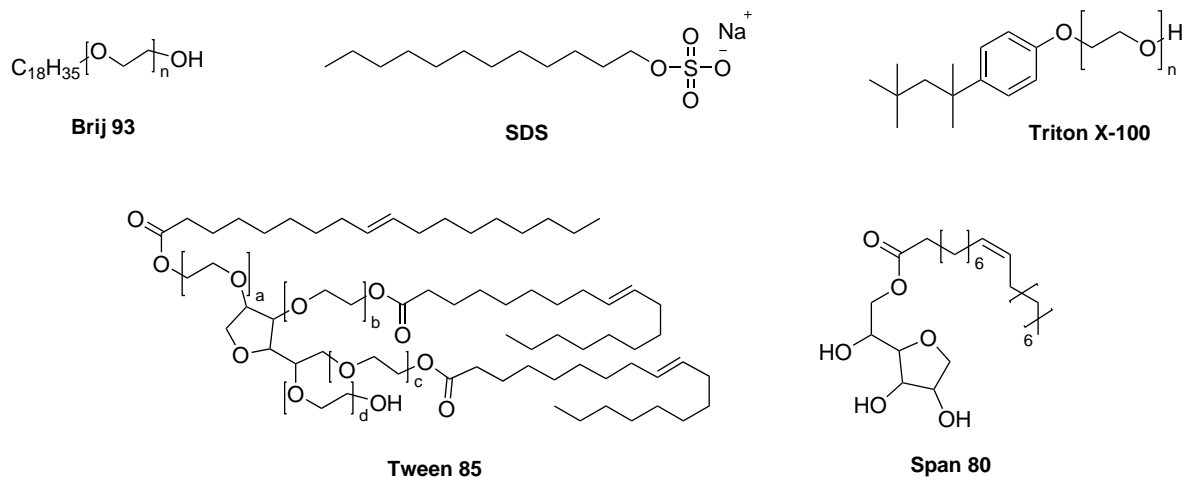


**Figure 5.12:** Structure of the used surfactants: Brij 93, SDS, Triton X-100, Tween 85 and Span 80

Brij 93, SDS and Tween 85 showed the best results and were used for the following tests. Brij 93 and Tween 85 are non-ionic surfactants, whereas SDS is an anionic one. As already investigated, 40 mg/L of surfactant and a dye concentration of  $2 \times 10^{-5} M$  showed the best results and were prepared in an aqueous solution. Eleven different dyes were analyzed, compounds **21**, **25**, **43**, **44**, **45** and **46** formed J-aggregates with and without surfactants and a huge bathochromic shift can be observed. After preparation, absorption spectra of each compound were recorded and show the dependency of used surfactants.

Color change upon the formation of J-aggregates is exemplified in Fig. 5.10 for dye **25**. As can be seen, the color intensity after formation of J-aggregates fades, due to the bathochromic shift and disappearance of the monomer absorption.

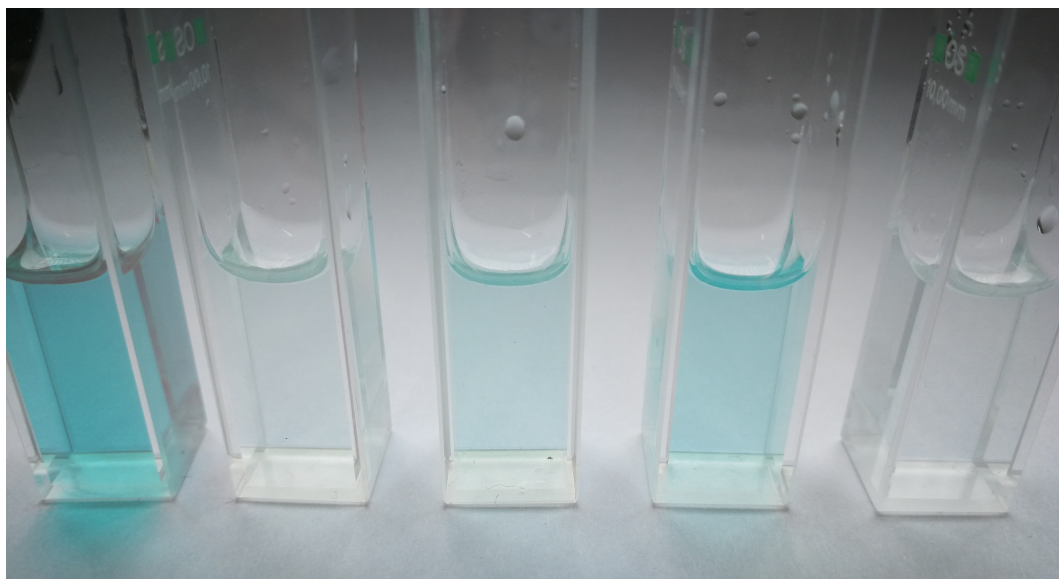


**Figure 5.13:** Dye **25** before (in THF) and after J-aggregation (in water) with different surfactants: 1. monomer, 2. without surfactant, 3. Brij 93, 4. SDS and 5. Tween 85 (from left to right). Uncolored solutions indicate disappearance of the monomer absorption and strong absorption in NIR part of the spectrum.

Already without adding surfactants J-aggregates are formed, however after addition the aggregates show a higher structural order.

Dye **25** shows self-aggregation even without a hydrophobic counter part. The hydrophobic BODIPY core is already enough for the hydrophilic TEG-part to organize a highly ordered structure and is almost entirely converted to the aggregated form. Tween 85 was the only exception. In case of the perfluoro derivatives broader peaks can be observed, in contrast to the typical sharp peaks, seen with the other compounds. As well as with compound **25**, the amphiphilic dye **46** only forms the aggregated conformation.

J-aggregates are predominantly formed. In some cases, formation of H-aggregates (characterized by broadening of the absorption band and hypsochromic shift) is also observed, depending on the used surfactant (see figure 5.14).

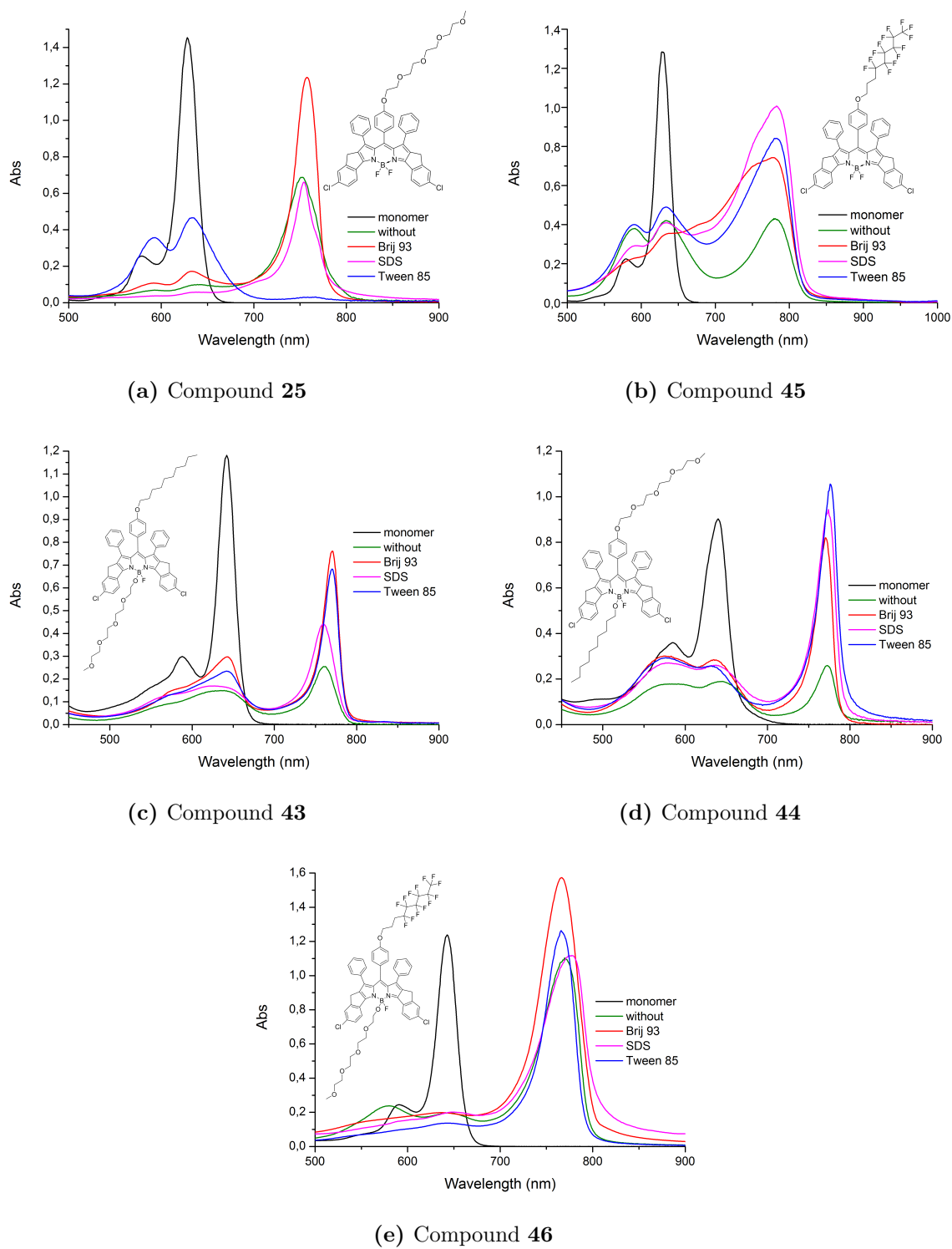


**Figure 5.14:** Absorption spectra of dye aggregates ( $c = 2 \times 10^{-5} M$ ) with different surfactants (40 mg/L) in water, the black lines represent the monomeric forms in THF with the same dye concentration.

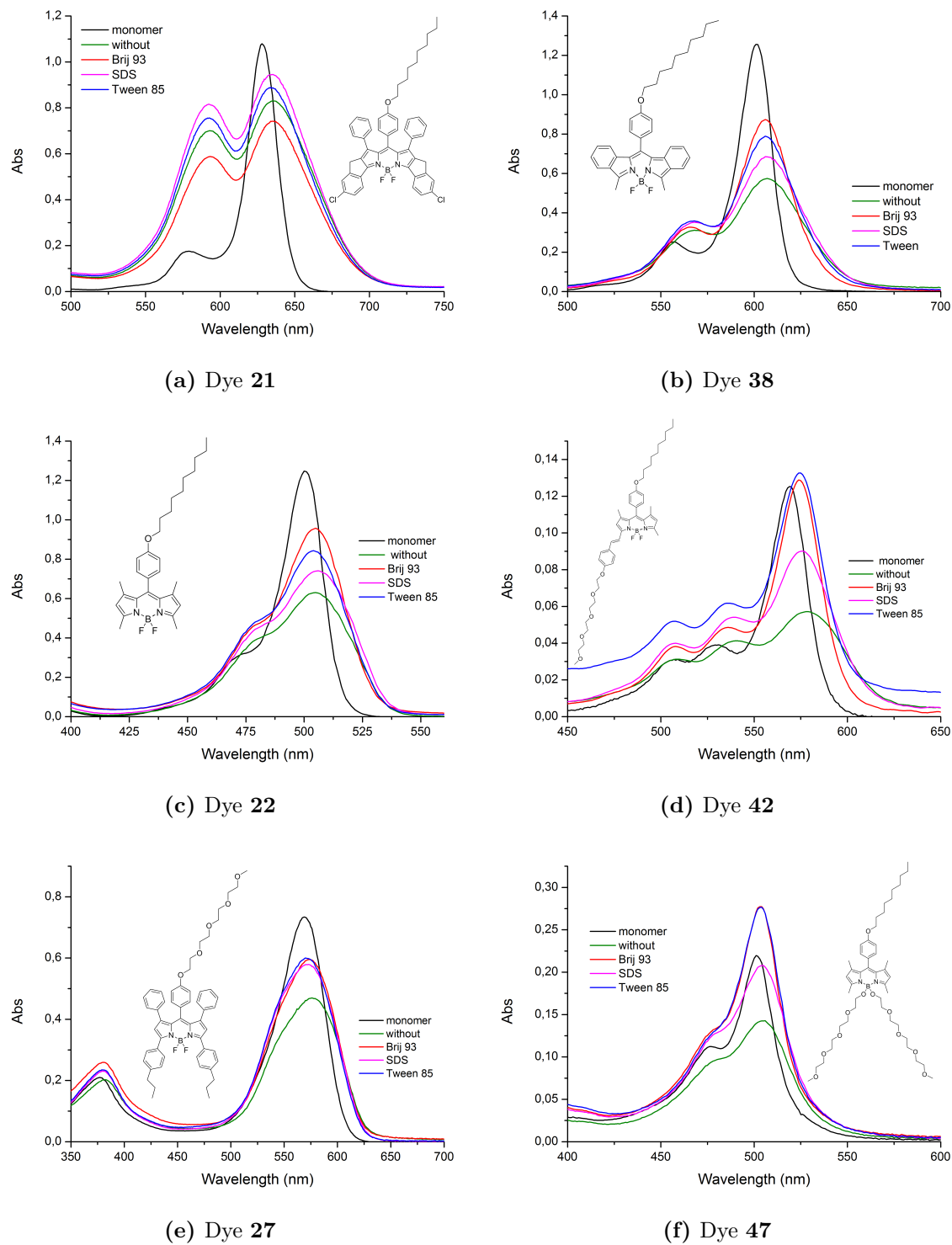


**Figure 5.15:** Absorption spectra of remaining dyes, which did not lead to formation of J-aggregates with different surfactants. The monomers are represented as a black line.

J-aggregates are formed with similar absorption spectra, independent on whether the hydrophobic chain is in meso-position and the hydrophilic in B-O-position or other way round.

J-aggregation only occurs when the structure has a hydrophilic or very hydrophobic perfluoroalkyl chain in meso-position, without any B-O substituent.

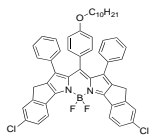
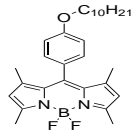
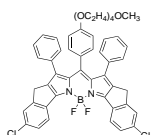
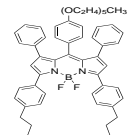
For dye **21**, decyloxy in meso-position and without a hydrophilic group at boron center (see figure 5.15 a), no J-aggregation can be observed. However by introduction of TEG at the center, the tendency to form J-aggregates gets improved. The same trend is valid for the perfluoro derivative. Without TEG there are also some H-aggregates formed, however with - there is only J-aggregation.

In case of perfluoro derivatives the absorption bands are broader, e.g. compound **46** with Brij 93 shows a FWHM of 46.4 nm, however the absorption intensity is much higher than the one of the other dyes.

All dyes shown in figure 5.15 do not form J-aggregates due to their structure.

Concluding, the BODIPY structure need to be  $\pi$ -extended at the right position and rigid to form J-aggregate, therefore the following tests and characterizations were carried out with the five BODIPY derivatives shown in 5.14.

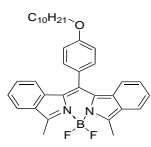
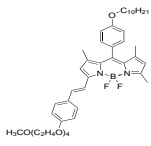
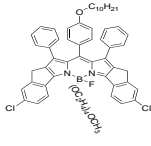
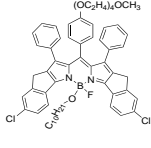
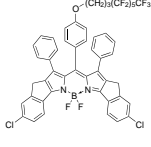
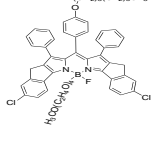
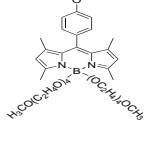
**Table 5.2:** Overview of attempts to form J-aggregates with different surfactants  
(+++ : forms almost exclusively; ++ : forms in moderate amount ; + some dye in this form can be found; no sign - none of this form can be found)

		H-aggregates	M/D	J-aggregates
<b>21</b>		without	+	/+
		Brij 93	+	/+
		SDS	+	/+
		Tween 85	+	/+
<b>22</b>		without		/+++
		Brij 93		/+++
		SDS		/+++
		Tween 85		/+++
<b>25</b>		without		+++
		Brij 93		++
		SDS		+++
		Tween 85	+	+
<b>27</b>		without		+++
		Brij 93		+++
		SDS		+++
		Tween 85		+++

Continued on next page



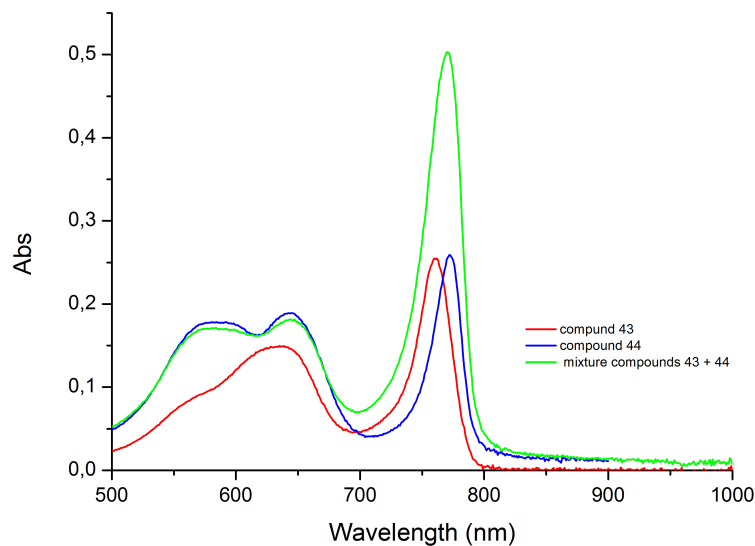
Table 5.2 – continued from previous page

		H-aggregates	M/D	J-aggregates
38		without	+	/++
		Brij 93	+	/++
		SDS	+	/++
		Tween 85	+	/++
42		without	+	/+
		Brij 93	+	/++
		SDS	+	/++
		Tween 85	+	/++
43		without	+	+
		Brij 93	+	++
		SDS	+	++
		Tween 85	+	++
44		without	+	+
		Brij 93	+	++
		SDS	+	++
		Tween 85	+	++
45		without	+	+
		Brij 93		++
		SDS	+	++
		Tween 85	+	++
46		without	+	++
		Brij 93		+++
		SDS		+++
		Tween 85		+++
47		without	+++	
		Brij 93	+++	
		SDS	+++	
		Tween 85	+++	

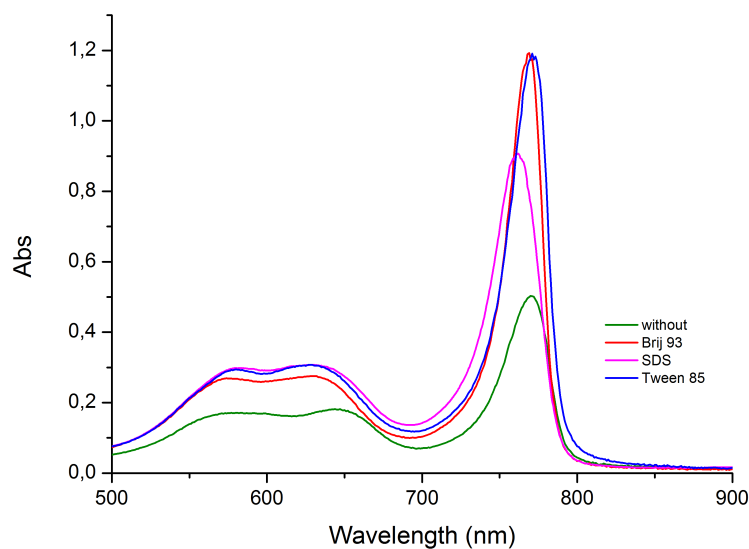
M = monomer

D = dimer

To see the influence of mixed dye aggregates, compound **43** and **44** (1 : 1) were put together and the resulting absorption spectra were recorded (see figure 5.16). After mixing the two compounds the absorption peaks covers the peaks of the individual compounds. In case of all surfactants almost only the aggregated form is present.



(a) Comparison of the mixture with the individual compounds after J-aggregate formation without surfactant



(b) 1 : 1 mixture of compounds **43** and **44** with different surfactants

**Figure 5.16:** Absorption spectra of 1 : 1 mixture of compounds **43** and **44**

## Resonance Light Scattering

To confirm the formation of J-aggregates, a light scattering measurement was performed with dye **25** in presence of Brij 93 in water. This method is very selective and sensitive towards investigation of solutions of aggregates and is only observed for extended aggregates of chromophores. In addition, the shape and size can be determined [101]. This method is performed in synchronous-scan mode and  $90^\circ$  geometry of the spectrofluorometer. Light from an excitation source passes through a solution and the scattered light is detected at the excitation wavelength. This effect can be seen near or at the absorption maxima and increases in case of strong electronic coupling of chromophores in aggregates resulting in a spectra, which resemble this of the absorption spectra (see 5.17).

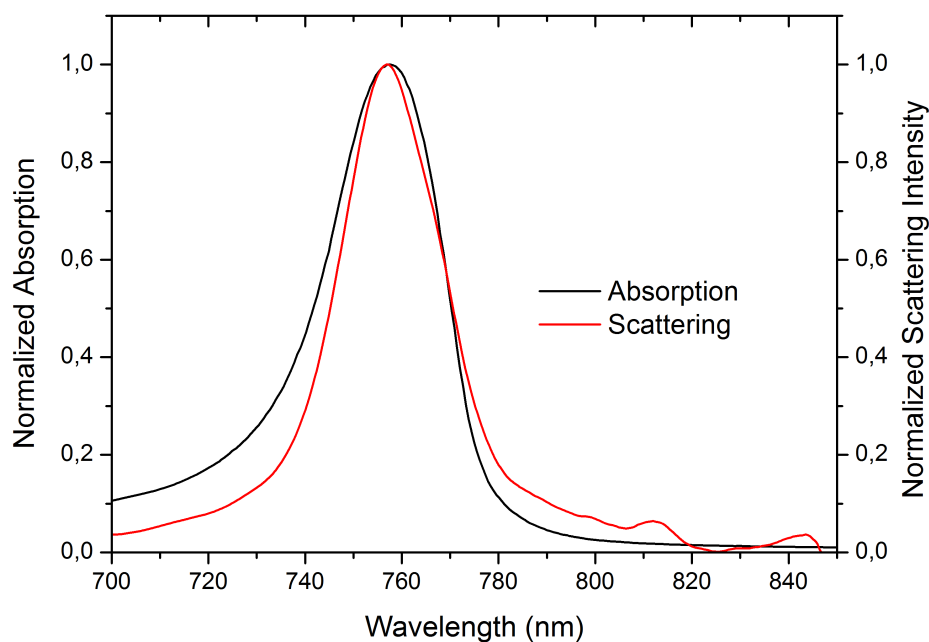
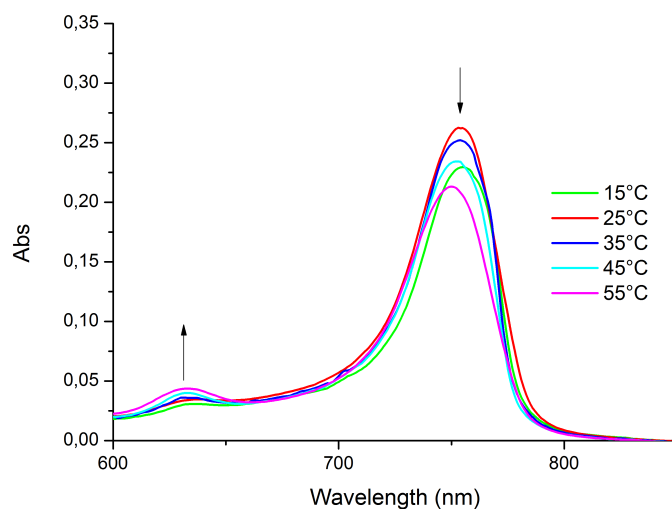


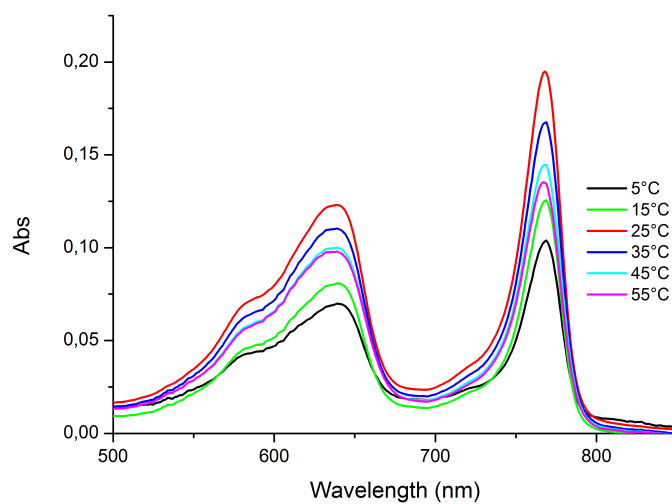
**Figure 5.17:** Absorption and light scattering spectra of dye **25** with Brij 93

### Temperature Dependency of Aggregates with Surfactants

As it can be seen in figure 5.18, with increasing temperature the J-aggregate decreases and more monomer is formed. Such temperature dependence is typical, at higher temperature the equilibrium shifts and more monomer is formed. The situation is more complex since there are also H-aggregates present.



(a)



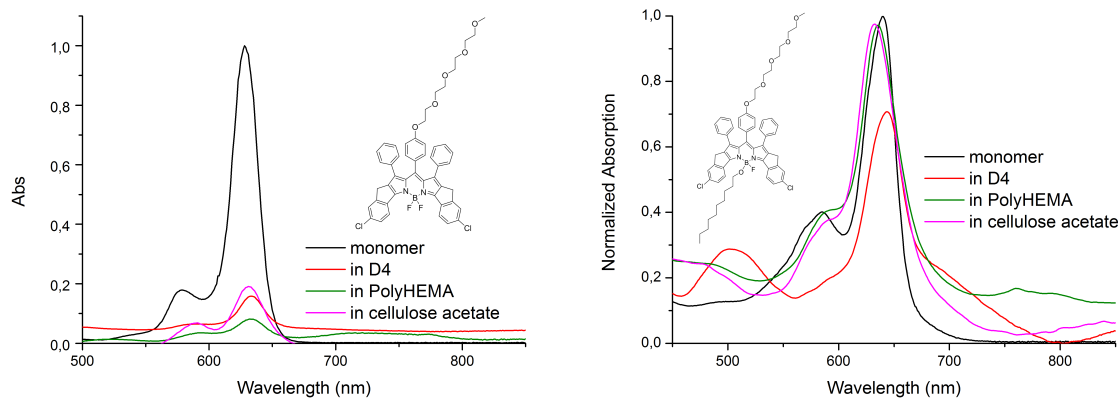
(b)

**Figure 5.18:** Temperature dependency detected via recording of absorption spectra.

(a) shows compound **25** with surfactant Brij 93, (b) compound **43** with Brij 93

### 5.3.2 Formation of J-aggregates in Polymers

The task was to generate aggregates in polymers and find out, if a higher structural order can be achieved, because it would be very interesting for practical applications to obtain J-aggregates in polymers, not only in solutions. The dyes, which already formed J-aggregates with surfactants were investigated. 1 w% dye was incorporated in different polymers (see table 3.4). After foil preparation the absorption spectra were recorded. It was found that polystyrene is not a suitable matrix for formation of J-aggregates for any of the dyes.



(a) Dye **25** in different polymers showing no J-aggregation

(b) Dye **44** in different polymers showing no J-aggregation

**Figure 5.19:** Absorption spectra of dyes **25** and **44** with different polymers show no formation of J-aggregates

In case of BODIPY derivatives with TEG in *meso* position there was no aggregation formation in any polymers observable, neither with the amphiphilic derivative **44**.

Figure 5.20 shows that in silicone rubber and Hydrogel D4 a characteristic peak in NIR is clearly visible. but still some monomer and H-aggregate peaks are present.

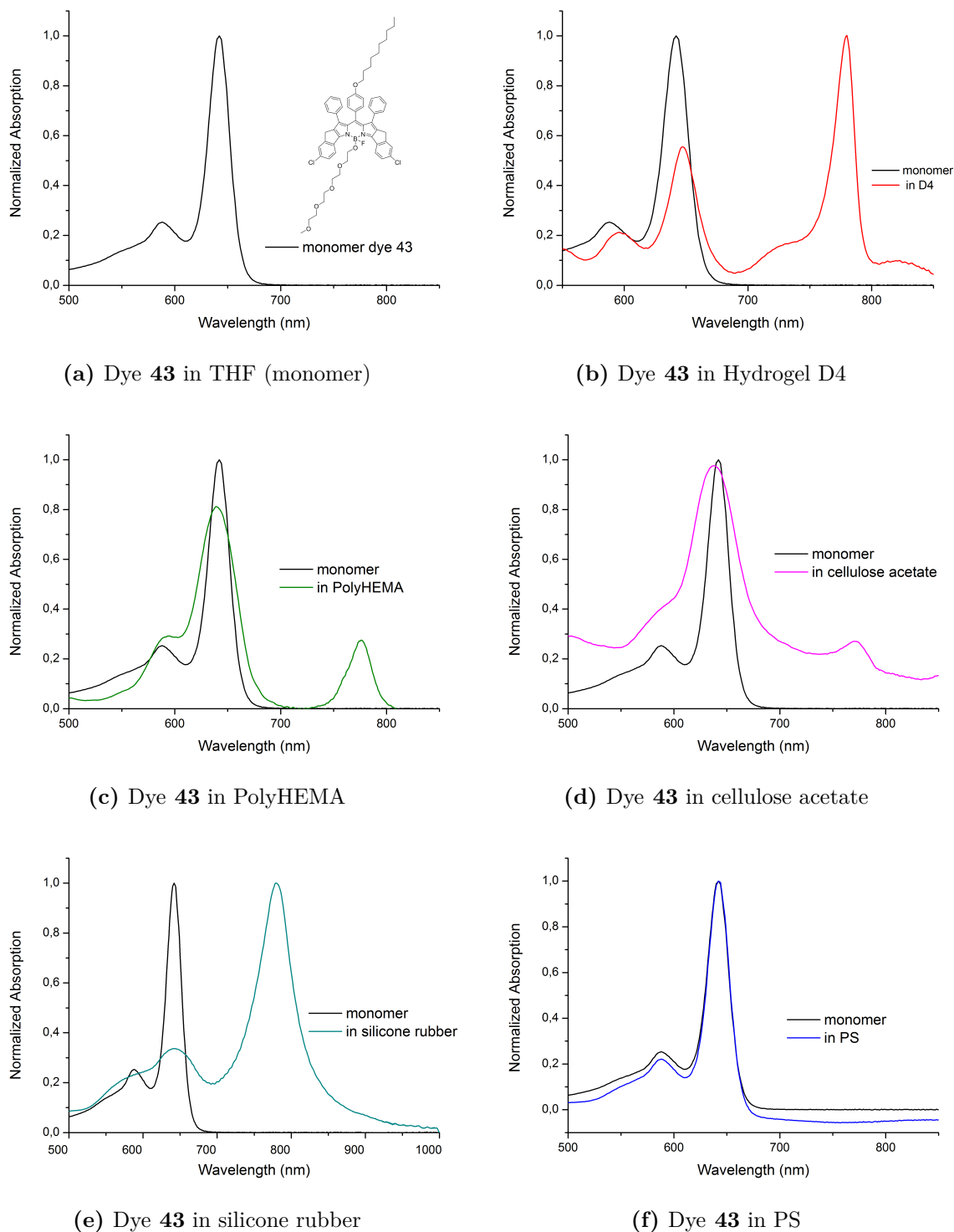
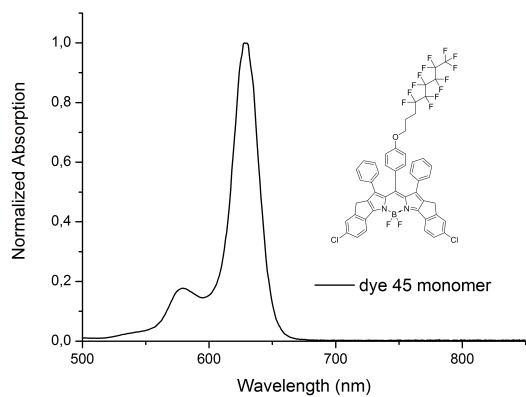
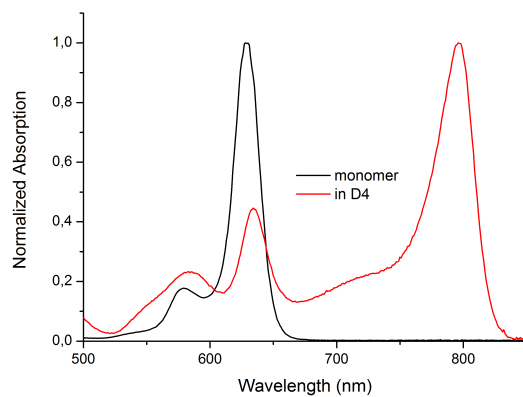


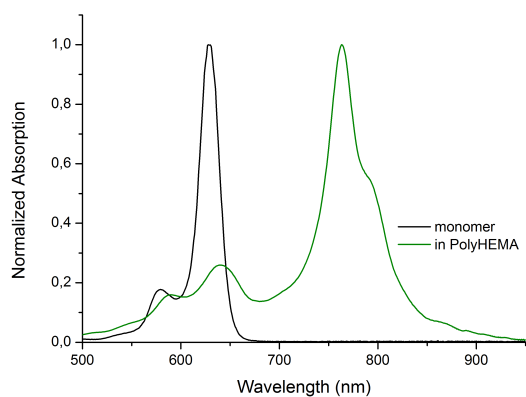
**Figure 5.20:** Comparison of J-aggregate formation via absorption spectra of dye **43** with Hydrogel D4 (b), PolyHEMA (c), cellulose acetate (d), silicon rubber (e) and PS (f) with the monomeric form in THF (black)



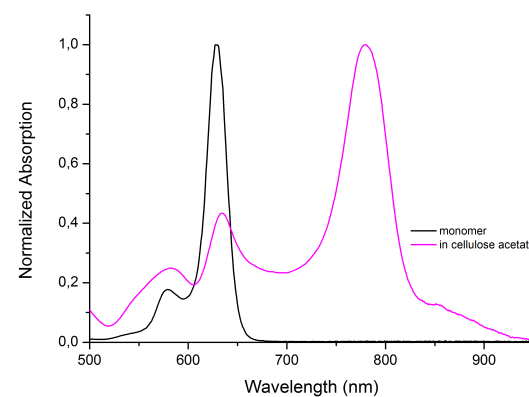
(a) dye 45 in THF (monomer)



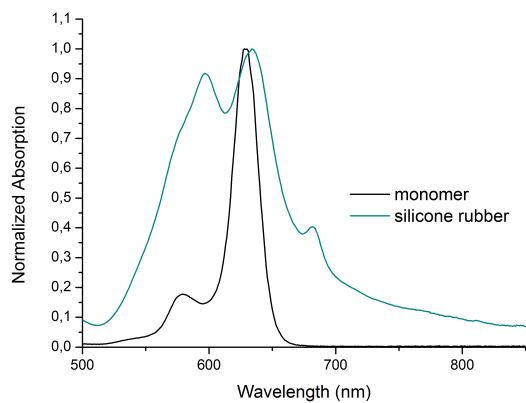
(b) dye 45 in Hydrogel D4



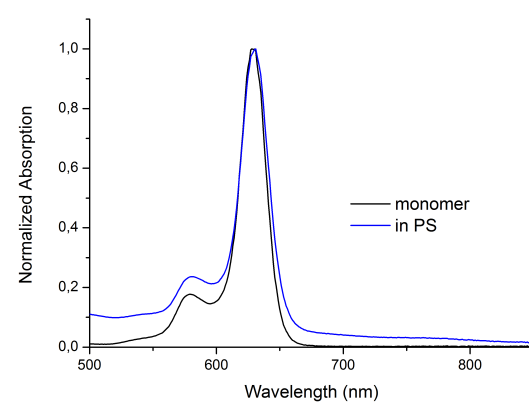
(c) dye 45 in PolyHEMA



(d) dye 45 in cellulose acetate



(e) dye 45 in silicone rubber



(f) dye 45 in PS

**Figure 5.21:** Comparison of J-aggregate formation via absorption spectra of dye 45 with Hydrogel D4 (b), PolyHEMA (c), cellulose acetate (d), silicon rubber (e) and PS (f) with the monomeric form in THF (black)

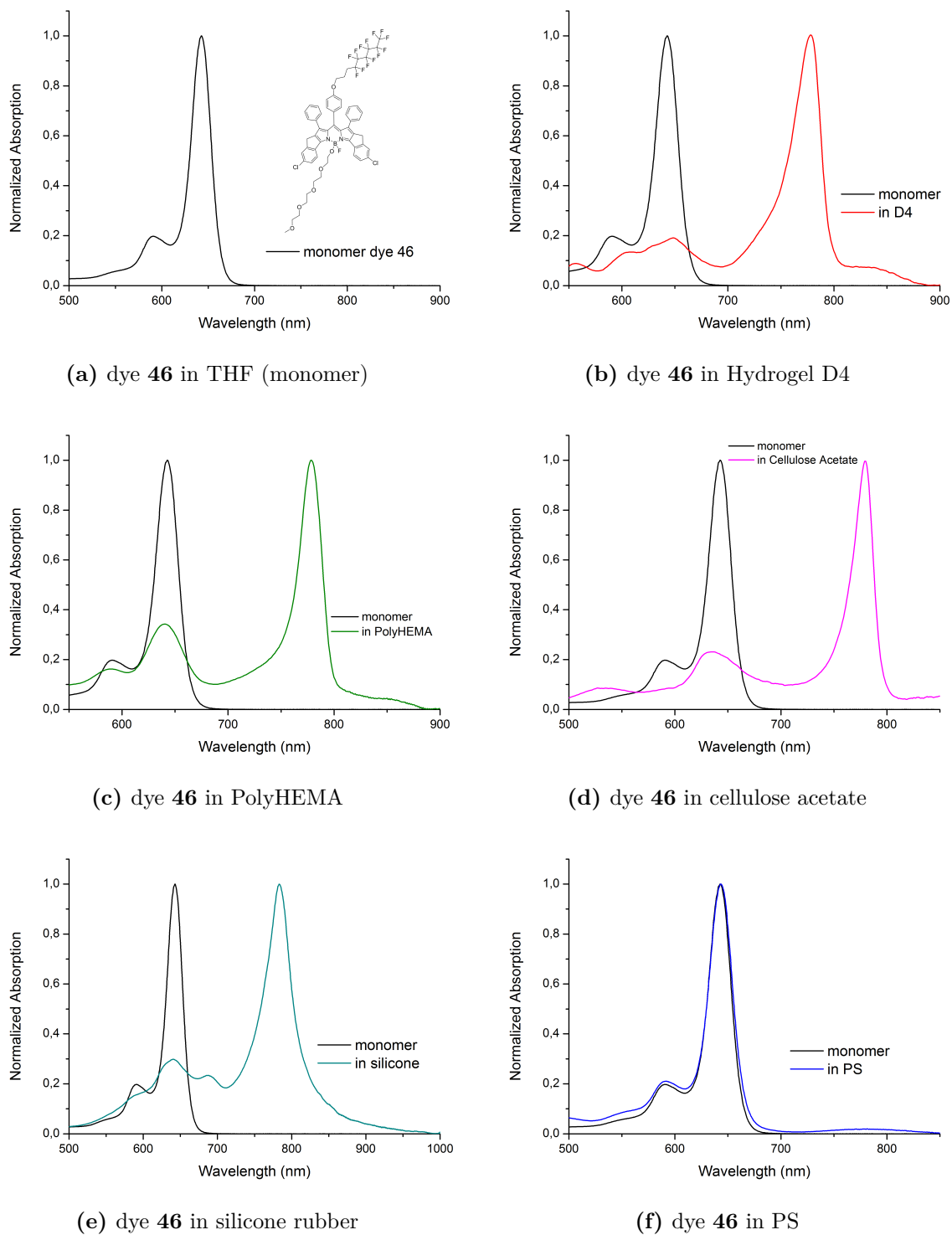


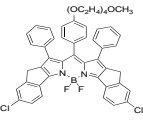
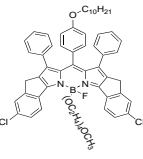
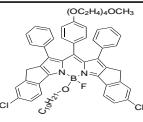
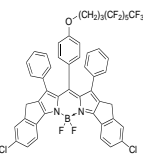
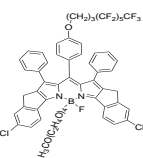
**Figure 5.22:** Comparison of J-aggregate formation via absorption spectra of dye **46** with Hydrogel D4 (b), PolyHEMA (c), cellulose acetate (d), silicon rubber (e) and PS (f) with the monomeric form in THF (black)



Only the perfluoro derivatives, dye **45** and **46**, show J-aggregation in polyHEMA and cellulose acetate. Reason could be the hydrophobic perfluoro chain.

Even though silicone showed good results with compound **43** and **46**, the foils did not dry entirely and were difficult to handle. The resulting peaks are broader than the classical sharp peaks of J-aggregates. Dye **46** showed the formation of other species in minor concentration (peak at around 690 nm), which are probably dimers.

**Table 5.3:** Overview of attempts to form J-aggregates with different polymers  
(+++ : forms almost exclusively; ++: forms in moderate amount ; + some dye in this form can be found; no sign - none of this form can be found)

	Polymer	H-aggregates	Monomer	J-aggregates
<b>25</b> 	D4		+++	
	PolyHEMA		+++	
	cellulose acetate		+++	
<b>43</b> 	D4		+	++
	PolyHEMA		++	+
	cellulose acetate		+++	
	silicone rubber	+		
<b>44</b> 	D4	+	++	
	PolyHEMA		+++	
	cellulose acetate		+++	
<b>45</b> 	D4	(+)	+	++
	PolyHEMA		+	++
	cellulose acetate	(+)	+	++
	silicone rubber	+	+	
<b>46</b> 	D4			+++
	PolyHEMA		+	++
	cellulose acetate		+	++
	silicone rubber		+	++
	PS		+++	

### Temperature Dependency of J-aggregates with Polymers

2 w% dye **43** was incorporated in D4, which swells in water. The measurement was carried out in dry and wet conditions. In case of dry state there is much more monomer than in water. After this measurement, it can be stated, that foils in water show higher aggregate formation than without water (see figure 5.23), therefore measurement of the dynamic response to humidity changes was carried out in a flow-through cell (see the following section).

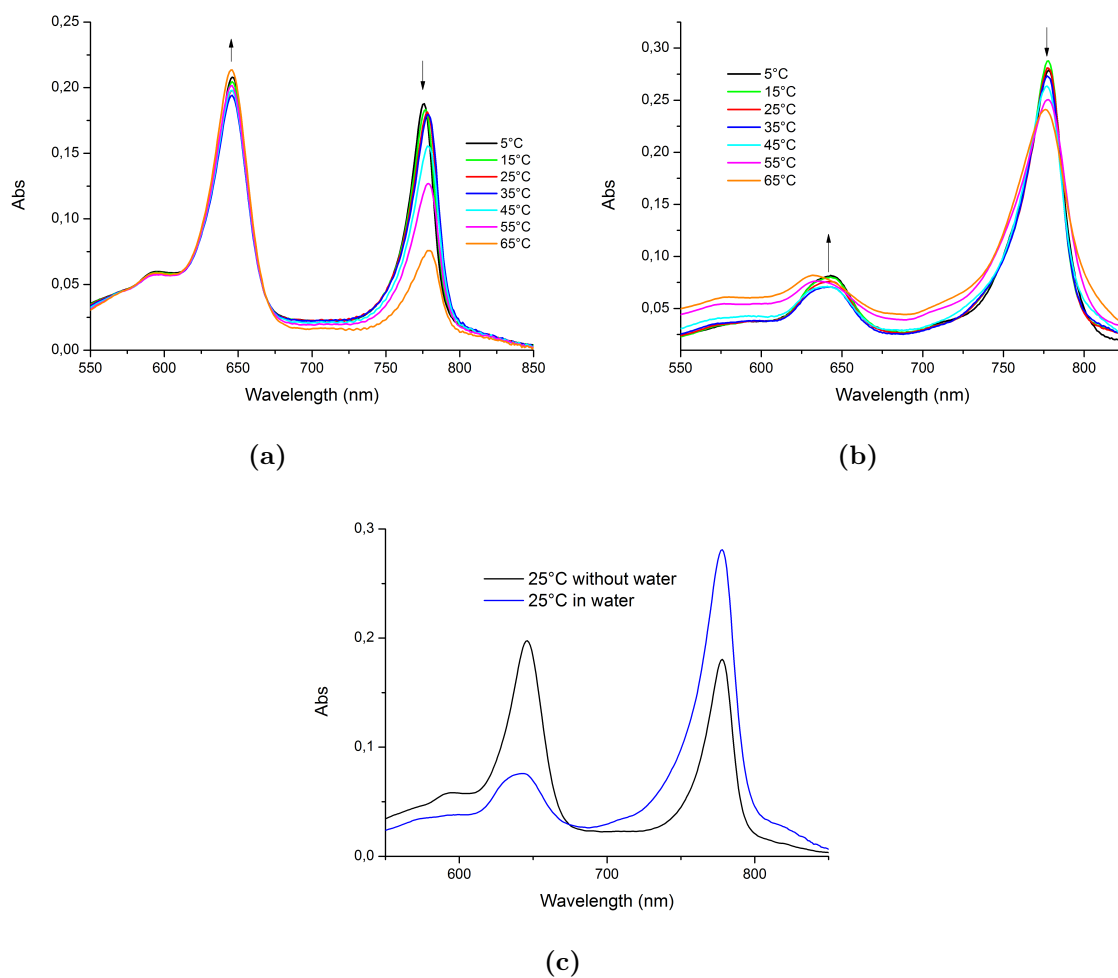


**Figure 5.23:** Absorption spectra shows in (a) and (b) - for the 2% of **43** in hydrogel D4, measured in dry state and in water, respectively. (c) shows the comparison at 25°C in dry state and in water

### Dynamic response to humidity changes

The aim of this measurement was to identify the dependency of moisture on the aggregated and monomeric forms. Therefore, a foil with 2 w% dye **43** in 10 % Hydrogel D4 was prepared and the changing absorption intensity at 780 nm was detected over time in inert and with humid atmosphere, generated by a sat. KCl-solution (85 % humidity).

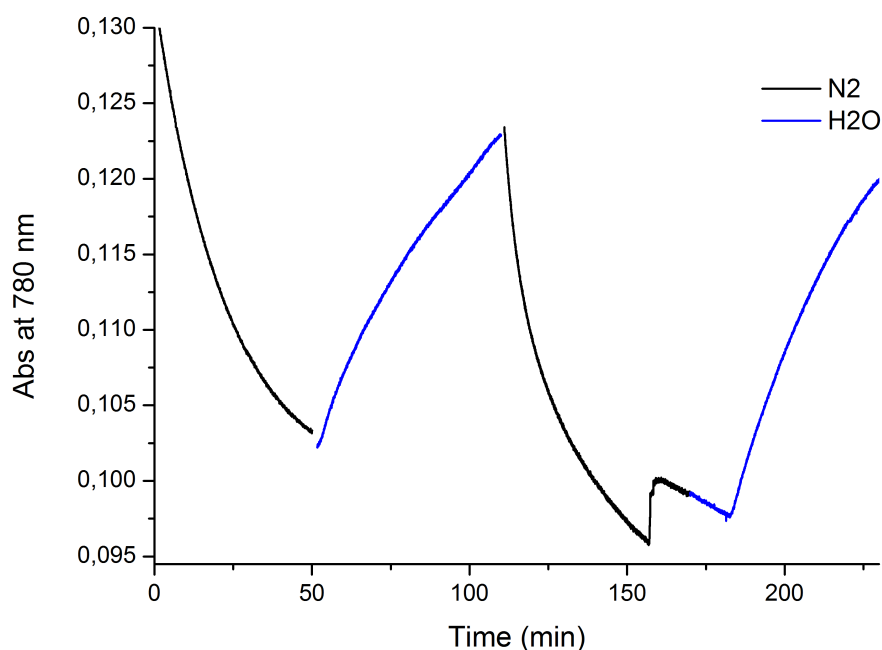


**Figure 5.24:** Dynamic response with alternating inert and 85 % humid atmosphere. Detected absorption plotted against time.

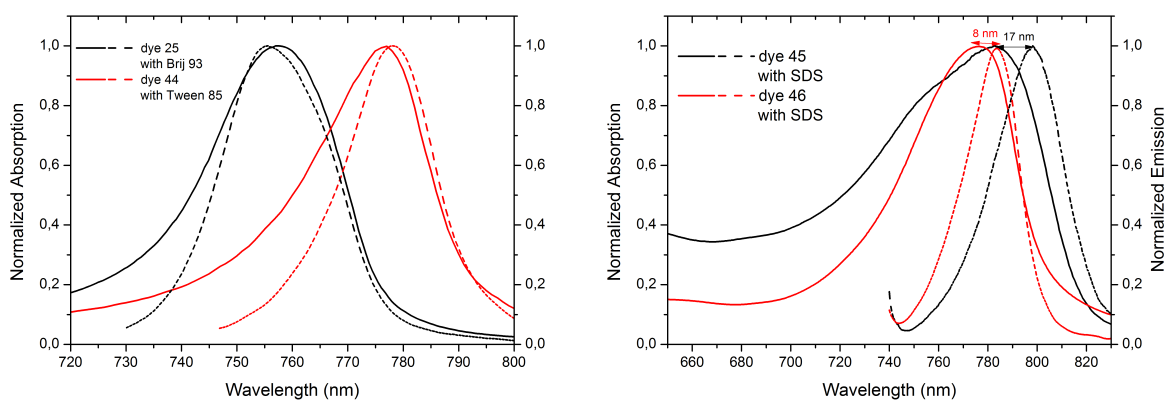
As it can be seen in figure 5.24, while nitrogen runs through the set-up a decrease of the absorption intensity can be observed. By passing through humid atmosphere the intensity increases. Monomer will show the exactly opposite trend. As a result, those dyes can be used as moisture sensors, however with a really slow response time. After around 150 min a sharp increase and again slowly decrease can be seen, because the set-up failed shortly.

## 5.4 Photophysical Properties of the J-aggregates

The aim of this thesis was to generate J-aggregates with different surfactants, as well with polymers. In this chapter the prepared aggregates were characterized according to their photophysical properties.

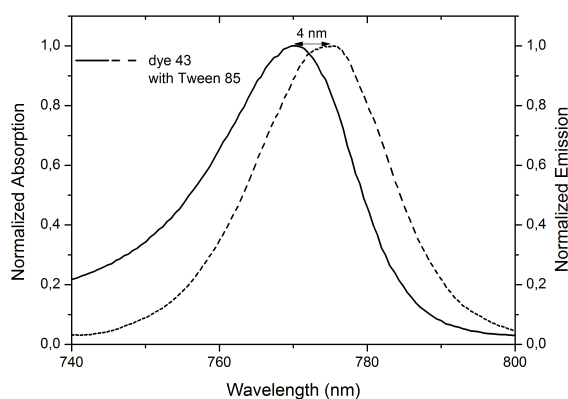
### 5.4.1 Absorption and Emission Spectra

In this section only the spectra with surfactants, which achieved the highest shift, for the individual dye are shown, the remaining spectra can be found in the appendix (see 10.2).



(a) m-TEG derivatives with surfactants Brij 93 and Tween 85

(b) m-perfluoro derivatives with SDS



(c) Compound **43** with Tween 85

**Figure 5.25:** Absorption (solid line) and Emission (dashed line) spectra with the best surfactants, respectively

During this measurement the emission spectra were recorded in front face orientation, because spectra with higher resolution were obtained. The excitation took place at 730 nm, except for compound **25**, where 715 nm was adjusted. However, in the next chapter, for better comparison to reference values, the typical 90° setting was adjusted. The sample were excited at 740 nm and 725 nm, respectively.

The recording of emission spectra was difficult, because the device and light source are not suitable in the NIR region. To obtain an useful spectrum the slits had to be small and a few cycles need to be recorded. Since the Stokes shift is very small and the bands narrow, it is not easy to select the excitation wavelength where the absorption is still reasonable but no artifacts from scattered light are detected.

Compounds with a perfluoro chain (dye **45** and **46**) show a higher order of aggregation in apolar surfactants. Whereas m-TEG BODIPY (**25**) compared to the amphiphilic derivative (**44**) show an opposite trend. Therefore a real prognosis can not be made.

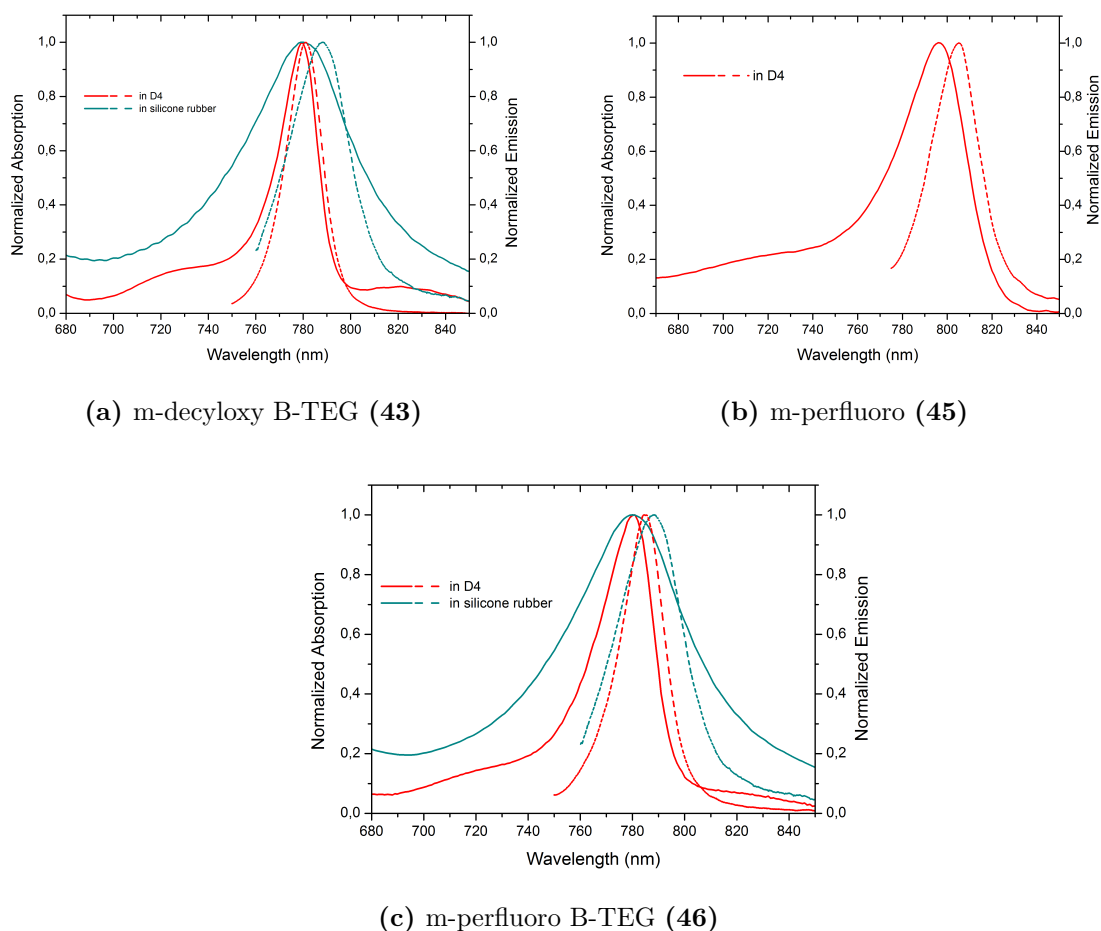


**Figure 5.26:** Absorption (solid) and Emission (dashed line) spectra of m-decyloxy B-TEG, m-perfluoro and m-perfluoro B-TEG in Hydrogel D4 or silicone

All spectra confirm that after forming J-aggregates very small Stokes shift can be seen.

Table 5.4 and 5.5 give an overview of the results.

**Table 5.4:** Overview photophysical properties of J-aggregates with surfactants

compound	surfactant	$\lambda_{abs}$ [nm]	$\lambda_{em}$ [nm]	$QY_{rel}$ [%]
25	without	752	752	0,37
	Brij 93	757	756	13
	SDS	754	753	1,5
43	without	761	771	1,6
	Brij 93	771	773	4,8
	SDS	759	768	3,4
44	Tween 85	770	774	4,0
	Brij 93	770	773	1,1
	SDS	773	778	0,69
45	Tween 85	777	778	0,95
	without	781	797	1,2
	Brij 93	778	787	2,0
46	SDS	782	798	1,7
	Tween 85	780	791	1,9
	without	770	773	3,5
43 + 44	Brij 93	767	777	4,7
	SDS	776	784	2,8
	Tween 85	767	776	3,9
43 + 44	Brij 93	769	772	5,4

**Table 5.5:** Overview photophysical properties of J-aggregates with polymers

compound	polymer	$\lambda_{abs}$ [nm]	$\lambda_{em}$ [nm]	$QY_{abs}$ [%]
43	Hydrogel D4	779	781	1,9
	Silicone	780	788	2,1
45	Hydrogel D4	796	805	
	Cellulose Acetate	780	783	
46	Hydrogel D4	781	785	
	PolyHEMA	778	779	
	Cellulose Acetate	780	783	
	Silicone	780	788	0,59

### 5.4.2 Quantum Yields

The relative QY were determined without and with different surfactants in water and calculated via eq. 3.1, described in section 3.5.4.

As reference indocyanine green with a quantum yield of 13,2 % in ethanol [93] was used.

The calculated relative QY vary in a broad range and strongly depend on the nature of the dye and surfactant. All results can be found in table 5.4.

The non-ionic surfactant Brij 93 shows the highest quantum yields with all dyes, whereas the yields in water are really low, the only exception is compound **46**.

In general, dyes with hydrophobic substituents in meso position tend to have higher yields. Compared to the monomeric form, where the QY are in the range between 26-85 %, after aggregation the fluorescence decreases in most cases by about 10 fold. However the measured QY for those dyes are relatively high compared to dyes known from literature, which absorb and emit in the NIR region of the spectrum. As already mentioned in the theoretical part of this thesis, NBI, which also forms J-aggregates, only achieved a quantum yield of 2 % [61]. Some other dyes are not even emissive [13].

A huge disadvantage during this measurements was the limitation of the light source and the PMT detector at high wavelengths. Another reason for the low quantum yields can be the inner filter effects (e.g. reabsorption of the emitted light), which can have an huge influence on the quantum yields. The refractive index for the investigated compound is also not entirely correct, because the one of water was adopted, however also the surfactant has an impact.

For the absolute QY, three samples were measured. 2 w% dye **43** in Hydrogel D4 in water, dye **43** in silicone, as well as compound **46** in silicone. The yields were quite low (see table 5.5). Dye **43** in silicone, with 2.1 % achieved the highest value.

### 5.4.3 Fluorescence Lifetime

The fluorescence lifetimes of J-aggregates are dramatically shortened. They are in the ps range and can not be fitted easily. The device and light are not suitable in this range, therefore the results can not be trusted entirely.

---

## 6 Conclusion and Outlook

Within the scope of this work eleven new BODIPY dyes were synthesized, five of them were able to form J-aggregates. Structures without a  $\pi$ -extended system do not show formation of J-aggregates. Concluding that the structure need to be rigid and  $\pi$ -extended to be able for the formation. The amphiphilic character enhance the probability and result in a bathochromic shift of the spectrum.

The five dyes form J-aggregates in aqueous solution in presence and sometimes in absence of surfactants, in certain cases even in polymers. Characteristic strong bathochromic shift is observed. Absorption spectra are shifted to the NIR region with maxima at approximately 770 nm after formation of J-aggregates with surfactants as well as in polymers (monomer at about 640 nm). So it is an easy way to synthesize dyes which can absorb and emit in the NIR region. Absorption and emission in this region of the light is preferential for many applications due to reduced background noise, less influence of impurities, deeper tissue penetration (in medical applications) and less scattering of excitation and emission light. The resulting Stokes shifts are negligible small.

The measured quantum yields of the monomers were found to be from moderate to high. After coupling the alcohol to the boron center, the yields get lower, except for the perfluoro derivative, where an opposite trend can be observed. This can be seen for the lifetime as well for the quantum yield. After forming the highly ordered structures, the J-aggregates, the measured quantum yields and the lifetimes are drastically declined, however are moderately high in some cases, considering the long wavelength of emission and that some of those known from literature are not even emissive or achieved really low QYs.

In general the light scattering spectrum resembles the absorption spectrum, which was also seen during this thesis.

Typical J-aggregate behavior was detected during this thesis, like temperature dependency and strong light scattering. While increasing the temperature the aggregated form is not that stable anymore and more monomer is formed. Dyes incorporated in a hydrogel show humidity-dependent monomer/J-aggregate equilibrium (higher humidity - more aggregate), which can be potentially utilized for humidity sensing but is slow in response.



---

The potentially promising asymmetrical BODIPYs, which may be able to terminate the J-aggregation, could not be synthesized during this work and should be further investigated. The separation from the symmetrical byproducts was not possible, this could be improved by synthesizing the stable ketone intermediate and further converting to the asymmetrical product. Probably both fluorine atoms will be substituted by alcohol, because the structure provides more space than the rigid structure of the synthesized products during this work.

During this thesis a new dye class was investigated, amphiphilic BODIPY dyes, resulting in the first extensive study of J-aggregate formation with BODIPYs.

Concluding, J-aggregates formed with BODIPY dyes show a high potential, as well as for sensing applications, particularly considering the NIR fluorescence.

---

## 7 References

1. Luo, S., Zhang, E., Su, Y., Cheng, T. & Shi, C. A review of NIR dyes in cancer targeting and imaging. *Biomaterials* **32**, 7127–7138 (2011).
2. Xiang, H., Cheng, J., Ma, X., Zhou, X. & Chruma, J. J. Near-infrared phosphorescence: materials and applications. *Chemical Society Reviews* **42**, 6128–6185 (2013).
3. Loudet, A. & Burgess, K. BODIPY Dyes and Their Derivatives: Syntheses and Spectroscopic Properties. *Chemical Reviews* **107**, 4891–4932 (2007).
4. Jelley, E. Spectral absorption and fluorescence of dyes in the molecular state. **138**, 1009–1010 (1936).
5. Scheibe, G. Variability of the absorption spectra of some sensitizing dyes and its cause. **49**, 563 (1936).
6. *J-aggregates* (ed Kobayashi, T.) (World Scientific, Singapore ; River Edge, NJ, 1996). 228 pp.
7. Kirstein, S. & Daehne, S. J-aggregates of amphiphilic cyanine dyes: Self-organization of artificial light harvesting complexes. *International Journal of Photoenergy* **2006**, 1–21 (2006).
8. Miyatake, T., Tanigawa, S., Kato, S. & Tamiaki, H. Aqueous self-aggregates of amphiphilic zinc 31-hydroxy- and 31-methoxy-chlorins for supramolecular light-harvesting systems. *Tetrahedron Letters* **48**, 2251–2254 (2007).
9. Bricks, J. L., Slominskii, Y. L., Panas, I. D. & Demchenko, A. P. Fluorescent J-aggregates of cyanine dyes: basic research and application review. *Methods and Applications in Fluorescence*. doi:10.1088/2050-6120/aa8d0d (2018).
10. Ohno, O., Kaizu, Y. & Kobayashi, H. J-aggregate formation of a water-soluble porphyrin in acidic aqueous media. *The Journal of Chemical Physics* **99**, 4128–4139 (1993).
11. Maiti, N. C., Mazumdar, S. & Periasamy, N. J- and H-Aggregates of Porphyrin-Surfactant Complexes: Time-Resolved Fluorescence and Other Spectroscopic Studies. *The Journal of Physical Chemistry B* **102**, 1528–1538 (1998).
12. Huber, V., Katterle, M., Lysetska, M. & Würthner, F. Reversible Self-Organization of Semisynthetic Zinc Chlorins into Well-Defined Rod Antennae. *Angewandte Chemie International Edition* **44**, 3147–3151 (2005).

- 
13. Wang, H., Kaiser, T. E., Uemura, S. & Würthner, F. Perylene bisimide J-aggregates with absorption maxima in the NIR. *Chemical Communications*, 1181 (2008).
  14. Chen, Z., Liu, Y., Wagner, W., Stepanenko, V., Ren, X., Ogi, S. & Würthner, F. Near-IR Absorbing J-Aggregate of an Amphiphilic BF<sub>2</sub>-Azadipyromethene Dye by Kinetic Cooperative Self-Assembly. *Angewandte Chemie International Edition* **56**, 5729–5733 (2017).
  15. Abdel-Mottaleb, M. M. S. & Hafez, H. S. J-Aggregates of Amphiphilic Cyanine Dyes for Dye-Sensitized Solar Cells: A Combination between Computational Chemistry and Experimental Device Physics. *International Journal of Photoenergy* **2014**, 1–6 (2014).
  16. Valeur, B. *Molecular Fluorescence: Principles and Applications* 399 pp. (Wiley-VCH Verlag GmbH, 2001).
  17. Albani, J. R. *Principles and Applications of Fluorescence Spectroscopy: Albani/Principles* doi:10.1002/9780470692059 (Blackwell Publishing Ltd, Oxford, UK, 2007).
  18. Lakowicz, J. R. & Masters, B. R. Principles of Fluorescence Spectroscopy, Third Edition. *Journal of Biomedical Optics* **13**, 029901 (2008).
  19. Majumdar, S., Majumdar, H., Österbacka, R. & McCarthy, E. in *Reference Module in Materials Science and Materials Engineering* (Elsevier, 2016). doi:10.1016/B978-0-12-803581-8.00577-4.
  20. Jelley, E. Molecular, nematic and crystal states of 1:1'-diethyl-y-cyanine chloride. **139**, 631 (1937).
  21. Scheibe, G. Über die Veränderlichkeit der Absorptionsspektren in Lösungen und die Nebenvalezen als ihre Ursache. **50**, 212–219 (1937).
  22. Röger, C., Müller, M. G., Lysetska, M., Miloslavina, Y., Holzwarth, A. R. & Würthner, F. Efficient Energy Transfer from Peripheral Chromophores to the Self-Assembled Zinc Chlorin Rod Antenna: A Bioinspired Light-Harvesting System to Bridge the “Green Gap”. *Journal of the American Chemical Society* **128**, 6542–6543 (2006).
  23. Steiger, R., Pugin, R. & Heier, J. J-aggregation of cyanine dyes by self-assembly. *From manipulation in two dimensions to attempt to understand the origin of life - in honour of the 90th birthday of Hans Kuhn* **74**, 484–491 (2009).
  24. Yagai, S., Seki, T., Karatsu, T., Kitamura, A. & Würthner, F. Transformation from H- to J-Aggregated Perylene Bisimide Dyes by Complexation with Cyanurates. *Angewandte Chemie International Edition* **47**, 3367–3371 (2008).
  25. Kaiser, T. E., Stepanenko, V. & Würthner, F. Fluorescent J-Aggregates of Core-Substituted Perylene Bisimides: Studies on Structure-Property Relationship, Nucleation-Elongation Mechanism, and Sergeants-and-Soldiers Principle. *Journal of the American Chemical Society* **131**, 6719–6732 (2009).

26. Yan, Q., Cai, K. & Zhao, D. Supramolecular aggregates with distinct optical properties from PDI oligomers of similar structures. *Physical Chemistry Chemical Physics* **18**, 1905–1910 (2016).
27. Zhang, X.-F., Xi, Q. & Zhao, J. Fluorescent and triplet state photoactive J-type phthalocyanine nano assemblies: controlled formation and photosensitizing properties. *Journal of Materials Chemistry* **20**, 6726 (2010).
28. Micali, N., Romeo, A., Lauceri, R., Purrello, R., Mallamace, F. & Scolaro, L. M. Fractal Structures in Homo- and Heteroaggregated Water Soluble Porphyrins. *The Journal of Physical Chemistry B* **104**, 9416–9420 (2000).
29. Koti, A. S. R. & Periasamy, N. Self-Assembly of Template-Directed J-Aggregates of Porphyrin. *Chemistry of Materials* **15**, 369–371 (2003).
30. Deng, Y., Yuan, W., Jia, Z. & Liu, G. H- and J-Aggregation of Fluorene-Based Chromophores. *The Journal of Physical Chemistry B* **118**, 14536–14545 (2014).
31. Würthner, F., Kaiser, T. E. & Saha-Möllner, C. R. J-aggregates: From Serendipitous Discovery to Supramolecular Engineering of Functional Dye Materials. *Wiley-VCH Verlag GmbH & Co* **50**, 3376–3410 (2011).
32. Awuah, S. G., Polreis, J., Biradar, V. & You, Y. Singlet Oxygen Generation by Novel NIR BODIPY Dyes. *Organic Letters* **13**, 3884–3887 (2011).
33. Lu, H., Mack, J., Yang, Y. & Shen, Z. Structural modification strategies for the rational design of red/NIR region BODIPYs. *Chem. Soc. Rev.* **43**, 4778–4823 (2014).
34. Forster, T. Energiewanderung und Fluoreszenz. *Naturwissenschaften* **33**, 166–175 (1946).
35. Kasha, M., Rawls, H. R. & Ashraf El-Bayoumi, M. The exciton model in molecular spectroscopy. *Pure and Applied Chemistry* **11**, 371–392 (1965).
36. Shapiro, B. I. Block building of polymethine dye aggregates. *Nanotechnologies in Russia* **3**, 139–150 (2008).
37. Slavnova, T. D., Chibisov, A. K. & Görner, H. Kinetics of Salt-Induced J-aggregation of Cyanine Dyes. *The Journal of Physical Chemistry A* **109**, 4758–4765 (2005).
38. Scheblykin, I., Varnavsky, O., Verbouwe, W., De Backer, S., Van der Auweraer, M. & Vitukhnovsky, A. Relaxation dynamics of excitons in J-aggregates revealing a two-component Davydov splitting. *Chemical Physics Letters* **282**, 250–256 (1998).
39. Passier, R., Ritchie, J. P., Toro, C., Diaz, C., Masunov, A. E., Belfield, K. D. & Hernandez, F. E. Thermally controlled preferential molecular aggregation state in a thiocarbocyanine dye. *The Journal of Chemical Physics* **133**, 134508 (2010).
40. Guo, X. m. Effect of solvent influence on J-aggregate of tetra-p-hydroxyphenylporphyrin (THPP) under different pH. *Journal of Molecular Structure* **892**, 378–383 (Dec. 15, 2008).

- 
41. Kometani, N., Nakajima, H., Asami, K., Yonezawa, Y. & Kajimoto, O. Luminescence Properties of the Mixed J-Aggregate of Two Kinds of Cyanine Dyes in Layer-by-Layer Alternate Assemblies. *The Journal of Physical Chemistry B* **104**, 9630–9637 (2000).
  42. Gross, M. & Haroche, S. Superradiance: An essay on the theory of collective spontaneous emission. *Physics Reports* **93**, 301–396 (1982).
  43. Fidler, H., Knoester, J. & Wiersma, D. A. Superradiant emission and optical dephasing in J-aggregates. *Chemical Physics Letters* **171**, 529–536 (1990).
  44. Díaz-García, M. E. & Badía-Laiño, R. in *Encyclopedia of Analytical Science (Third Edition)* (eds Worsfold, P., Poole, C., Townshend, A. & Miró, M.) 309–319 (Academic Press, Oxford, 2019). doi:10.1016/B978-0-12-409547-2.11182-5.
  45. Scheblykin, I., Drobizhev, M., Varnavsky, O., Van der Auweraer, M. & Vitukhnovsky, A. Reorientation of transition dipoles during exciton relaxation in J-aggregates probed by fluorescence anisotropy. *Chemical Physics Letters* **261**, 181–190 (1996).
  46. Sorokin, A. V., Pereverzev, N. V., Grankina, I. I., Yefimova, S. L. & Malyukin, Y. V. Evidence of Exciton Self-Trapping in Pseudoisocyanine J-Aggregates Formed in Layered Polymer Films. *The Journal of Physical Chemistry C* **119**, 27865–27873 (2015).
  47. Von Berlepsch, H., Böttcher, C. & Dähne, L. Structure of J-Aggregates of Pseudoisocyanine Dye in Aqueous Solution. *The Journal of Physical Chemistry B* **104**, 8792–8799 (2000).
  48. Jones, R. M., Bergstedt, T. S., Buscher, C. T., McBranch, D. & Whitten, D. Superquenching and Its Applications in J-Aggregated Cyanine Polymers. *Langmuir* **17**, 2568–2571 (2001).
  49. Lu, L., Helgeson, R., Jones, R. M., McBranch, D. & Whitten, D. Superquenching in Cyanine Pendant Poly(l-lysine) Dyes: Dependence on Molecular Weight, Solvent, and Aggregation. *Journal of the American Chemical Society* **124**, 483–488 (2002).
  50. Kruse, A. & Dinjus, E. Hot compressed water as reaction medium and reactant. *The Journal of Supercritical Fluids* **39**, 362–380 (2007).
  51. De Rossi, U., Moll, J., Spieles, M., Bach, G., Dähne, S., Kriwanek, J. & Lisk, M. Control of the J-Aggregation Phenomenon by variation of the N-alkyl-substituents. *Journal für Praktische Chemie/Chemiker-Zeitung* **337**, 203–208 (1995).
  52. Nazeeruddin, M., Zakeeruddin, S., Lagref, J.-J., Liska, P., Comte, P., Barolo, C., Viscardi, G., Schenk, K. & Graetzel, M. Stepwise assembly of amphiphilic ruthenium sensitizers and their applications in dye-sensitized solar cell. *Michael Graetzel Festschrift, a tribute for his 60th Birthday, Dye Sensitized Solar Cells* **248**, 1317–1328 (2004).
  53. Von Berlepsch, H., Böttcher, C., Quart, A., Burger, C., Dähne, S. & Kirstein, S. Supramolecular Structures of J -Aggregates of Carbocyanine Dyes in Solution. *The Journal of Physical Chemistry B* **104**, 5255–5262 (2000).

54. Von Berlepsch, H., Böttcher, C., Quart, A., Regenbrecht, M., Akari, S., Keiderling, U., Schnablegger, H., Dähne, S. & Kirstein, S. Surfactant-Induced Changes of Morphology of J-Aggregates: Superhelix-to-Tubule Transformation. *Langmuir* **16**, 5908–5916 (2000).
55. Von Berlepsch, H., Regenbrecht, M., Dähne, S., Kirstein, S. & Böttcher, C. Surfactant-Induced Separation of Stacked J-Aggregates. Cryo-Transmission Electron Microscopy Studies Reveal Bilayer Ribbons. *Langmuir* **18**, 2901–2907 (2002).
56. Kuntsche, J., Horst, J. C. & Bunjes, H. Cryogenic transmission electron microscopy (cryo-TEM) for studying the morphology of colloidal drug delivery systems. *Advanced characterization techniques* **417**, 120–137 (2011).
57. Ribeiro, T., Raja, S., Rodrigues, A. S., Fernandes, F., Farinha, J. P. S. & Baleizão, C. High performance NIR fluorescent silica nanoparticles for bioimaging. *RSC Advances* **3**, 9171–9174 (2013).
58. Li, Y., Lin, J.-D., Che, X., Qu, Y., Liu, F., Liao, L.-S. & Forrest, S. R. High Efficiency Near-Infrared and Semitransparent Non-Fullerene Acceptor Organic Photovoltaic Cells. *Journal of the American Chemical Society* **139**, 17114–17119 (Nov. 29, 2017).
59. Bricks, J. L., Kachkovskii, A. D., Slominskii, Y. L., Gerasov, A. O. & Popov, S. V. Molecular design of near infrared polymethine dyes: A review. *Dyes and Pigments* **121**, 238–255 (2015).
60. Wenus, J., Ceccarelli, S., Lidzey, D. G., Tolmachev, A. I., Slominskii, J. L. & Bricks, J. L. Optical strong coupling in microcavities containing J-aggregates absorbing in near-infrared spectral range. *Coupled States of Excitons, Photons, and Plasmons in Organic Structures* **8**, 120–126 (2007).
61. Cai, K., Xie, J. & Zhao, D. NIR J-Aggregates of Hydroazaheptacene Tetraimides. *Journal of the American Chemical Society* **136**, 28–31 (2014).
62. De Rossi, U. & Daehne, S. Increased Coupling Size in J-aggregates through N-n-Alkyl Betaine Surfactants. *Langmuir* **12**, 1159–1165 (1996).
63. Eachus, R. S., Marchetti, A. P. & Muentner, A. A. The photophysics of silver halide imaging materials. *Annual Review of Physical Chemistry* **50**, 117–144 (1999).
64. Achyuthan, K. E. *et al.* Fluorescence superquenching of conjugated polyelectrolytes: applications for biosensing and drug discovery. *Journal of Materials Chemistry* **15**, 2648 (2005).
65. Lim, J., Paleček, D., Caycedo-Soler, F., Lincoln, C. N., Prior, J., von Berlepsch, H., Huelga, S. F., Plenio, M. B., Zigmantas, D. & Hauer, J. Vibronic origin of long-lived coherence in an artificial molecular light harvester. *Nature Communications* **6**, 7755 (2015).

- 
66. Deing, K. C., Mayerhöffer, U., Würthner, F. & Meerholz, K. Aggregation-dependent photovoltaic properties of squaraine/PC61BM bulk heterojunctions. *Physical Chemistry Chemical Physics* **14**, 8328 (2012).
  67. Chen, G., Sasabe, H., Lu, W., Wang, X.-F., Kido, J., Hong, Z. & Yang, Y. J-aggregation of a squaraine dye and its application in organic photovoltaic cells. *Journal of Materials Chemistry C* **1**, 6547 (2013).
  68. Más-Montoya, M. & Janssen, R. A. J. The Effect of H- and J-Aggregation on the Photophysical and Photovoltaic Properties of Small Thiophene-Pyridine-DPP Molecules for Bulk-Heterojunction Solar Cells. *Advanced Functional Materials* **27**, 1605779 (2017).
  69. Saccone, D., Galliano, S., Barbero, N., Quagliotto, P., Viscardi, G. & Barolo, C. Polymethine Dyes in Hybrid Photovoltaics: Structure-Properties Relationships. *European Journal of Organic Chemistry* **2016**, 2244–2259 (2016).
  70. Würthner, F., Wortmann, R. & Meerholz, K. Chromophore Design for Photorefractive Organic Materials. *ChemPhysChem* **3**, 17–31 (2002).
  71. Muentner, A. A., Brumbaugh, D. V., Apolito, J., Horn, L. A., Spano, F. C. & Mukamel, S. Size dependence of excited-state dynamics for J-aggregates at silver bromide interfaces. *The Journal of Physical Chemistry* **96**, 2783–2790 (Apr. 1, 1992).
  72. Lanzafame, J. M., Muentner, A. A. & Brumbaugh, D. V. The effect of J-aggregate size on photoinduced charge transfer processes for dye-sensitized silver halides. *Confined Excitations in Molecular and Semiconductor Nanostructures* **210**, 79–89 (1996).
  73. TANI, T. Formation and Behavior of J-aggregated Cyanine Dyes in Silver Halide Photographic Materials. *Journal of The Society of Photographic Science and Technology of Japan* **70**, 287–294 (2007).
  74. Pullerits, T. & Sundström, V. Photosynthetic Light-Harvesting Pigment-Protein Complexes: Toward Understanding How and Why. *Accounts of Chemical Research* **29**, 381–389 (1996).
  75. Hashimoto, H., Sugai, Y., Uragami, C., Gardiner, A. T. & Cogdell, R. J. Natural and artificial light-harvesting systems utilizing the functions of carotenoids. *Journal of Photochemistry and Photobiology C: Photochemistry Reviews* **25**, 46–70 (2015).
  76. Ishida, Y., Shimada, T., Masui, D., Tachibana, H., Inoue, H. & Takagi, S. Efficient Excited Energy Transfer Reaction in Clay/Porphyrin Complex toward an Artificial Light-Harvesting System. *Journal of the American Chemical Society* **133**, 14280–14286 (2011).
  77. Sengupta, S. & Würthner, F. Chlorophyll J-Aggregates: From Bioinspired Dye Stacks to Nanotubes, Liquid Crystals, and Biosupramolecular Electronics. *Accounts of Chemical Research* **46**, 2498–2512 (2013).

78. Hilderbrand, S. A., Kelly, K. A., Weissleder, R. & Tung, C.-H. Monofunctional Near-Infrared Fluorochromes for Imaging Applications. *Bioconjugate Chemistry* **16**, 1275–1281 (2005).
79. Bertolino, C. A., Caputo, G., Barolo, C., Viscardi, G. & Coluccia, S. Novel Heptamethine Cyanine Dyes with Large Stokes' Shift for Biological Applications in the Near Infrared. *Journal of Fluorescence* **16**, 221–225 (2006).
80. Treibs, A. & Kreuzer, F.-H. Difluorboryl-Komplexe von Di- und Tripyrrylmethenen. *Justus Liebigs Annalen der Chemie* **718**, 208–223 (1968).
81. Qi, X., Jun, E. J., Xu, L., Kim, S.-J., Joong Hong, J. S., Yoon, Y. J. & Yoon, J. New BODIPY Derivatives as OFF-ON Fluorescent Chemosensor and Fluorescent Chemodosimeter for Cu<sup>2+</sup>: Cooperative Selectivity Enhancement toward Cu<sup>2+</sup>. *The Journal of Organic Chemistry* **71**, 2881–2884 (2006).
82. Boens, N., Leen, V. & Dehaen, W. Fluorescent indicators based on BODIPY. *Chem. Soc. Rev.* **41**, 1130–1172 (2012).
83. Shah, M., Thangaraj, K., Soong, M.-L., Wolford, L. T., Boyer, J. H., Politzer, I. R. & Pavlopoulos, T. G. Pyrromethene-BF<sub>2</sub> complexes as laser dyes:1. *Heteroatom Chemistry* **1**, 389–399 (1990).
84. Boyer, J. H., Haag, A. M., Sathyamoorthi, G., Soong, M.-L., Thangaraj, K. & Pavlopoulos, T. G. Pyrromethene-BF<sub>2</sub> complexes as laser dyes: 2. *Heteroatom Chemistry* **4**, 39–49 (1993).
85. Yee, M.-c., Fas, S. C., Stohlmeyer, M. M., Wandless, T. J. & Cimprich, K. A. A Cell-permeable, Activity-based Probe for Protein and Lipid Kinases. *Journal of Biological Chemistry* **280**, 29053–29059 (2005).
86. Golovkova, T. A., Kozlov, D. V. & Neckers, D. C. Synthesis and Properties of Novel Fluorescent Switches. *The Journal of Organic Chemistry* **70**, 5545–5549 (2005).
87. Wood, T. E. & Thompson, A. Advances in the Chemistry of Dipyrrens and Their Complexes. *Chemical Reviews* **107**, 1831–1861 (2007).
88. Leen, V., Braeken, E., Luckermans, K., Jackers, C., Van der Auweraer, M., Boens, N. & Dehaen, W. A versatile, modular synthesis of monofunctionalized BODIPY dyes. *Chemical Communications*, 4515 (2009).
89. Hall, M. J., McDonnell, S. O., Killoran, J. & O'Shea, D. F. A Modular Synthesis of Unsymmetrical Tetraarylazadipyrromethenes. *The Journal of Organic Chemistry* **70**, 5571–5578 (2005).
90. Ulrich, G., Ziessel, R. & Harriman, A. Die vielseitige Chemie von Bodipy-Fluoreszenzfarbstoffen. *Angewandte Chemie* **120**, 1202–1219 (2008).



- 
91. Lundrigan, T. & Thompson, A. Conversion of F-BODIPYs to Cl-BODIPYs: Enhancing the Reactivity of F-BODIPYs. *The Journal of Organic Chemistry* **78**, 757–761 (2013).
  92. Tahtaoui, C., Thomas, C., Rohmer, F., Klotz, P., Duportail, G., Mély, Y., Bonnet, D. & Hibert, M. Convenient Method To Access New 4,4-Dialkoxy- and 4,4-Diaryloxy-diazas-indacene Dyes: Synthesis and Spectroscopic Evaluation. *The Journal of Organic Chemistry* **72**, 269–272 (2007).
  93. Rurack, K. & Spieles, M. Fluorescence Quantum Yields of a Series of Red and Near-Infrared Dyes Emitting at 600-1000 nm. *Analytical Chemistry* **83**, 1232–1242 (2011).
  94. Radunz, S., Andresen, E., Würth, C., Koerdt, A., Tschiche, H. R. & Resch-Genger, U. Simple Self-Referenced Luminescent pH Sensors Based on Upconversion Nanocrystals and pH-Sensitive Fluorescent BODIPY Dyes. *Analytical Chemistry* **91**, 7756–7764 (2019).
  95. Jameson, L. P. & Dzyuba, S. V. Expeditious, mechanochemical synthesis of BODIPY dyes. *Beilstein Journal of Organic Chemistry* **9**, 786–790 (2013).
  96. Chen, Z. & Trudell, M. L. A Simplified Method for the Preparation of Ethynyl P-Tolyl Sulfone and Ethynyl Phenyl Sulfone. *Synthetic Communications* **24**, 3149–3155 (1994).
  97. Okujima, T., Jin, G. & Hashimoto, Y. Synthesis of 4,7-dihydro-2H-isoindole derivatives via Diels-Alder reaction of tosylacetylene. *Heterocycles* **70**, 619–626 (2006).
  98. Shen, Z., Röhr, H., Rurack, K., Uno, H., Spieles, M., Schulz, B., Reck, G. & Ono, N. Boron-Diindomethene (BDI) Dyes and Their Tetrahydrobicyclo Precursors—en Route to a New Class of Highly Emissive Fluorophores for the Red Spectral Range. *Chemistry – A European Journal* **10**, 4853–4871 (2004).
  99. Nicolaou, K., Claremon, D. & Papahatjis, D. A mild method for the synthesis of 2-ketopyrroles from carboxylic acids. *Tetrahedron Letters* **22**, 4647–4650 (1981).
  100. Goze, C., Ulrich, G., Mallon, L. J., Allen, B. D., Harriman, A. & Ziessel, R. Synthesis and Photophysical Properties of Borondipyrromethene Dyes Bearing Aryl Substituents at the Boron Center. *Journal of the American Chemical Society* **128**, 10231–10239 (2006).
  101. Collings, P. J., Gibbs, E. J., Starr, T. E., Vafek, O., Yee, C., Pomerance, L. A. & Pasternack, R. F. Resonance Light Scattering and Its Application in Determining the Size, Shape, and Aggregation Number for Supramolecular Assemblies of Chromophores. *The Journal of Physical Chemistry B* **103**, 8474–8481 (1999).



---

## 8 List of Figures

2.1	De-excitation processes . . . . .	3
2.2	Spin orientation . . . . .	4
2.3	Franck-Condon principle . . . . .	6
2.4	Jablonski Diagram . . . . .	6
2.5	Quenching . . . . .	10
2.6	Illustration of the Kasha model during electron transitions of H- and J- dimers	12
2.7	Differences in spectra of H- and J-aggregates . . . . .	13
2.8	PIC . . . . .	14
2.9	influence of vinylene units on absorption spectrum . . . . .	15
2.10	cyanine derivatives . . . . .	15
2.11	Structure of amphiphilic cyanine dye . . . . .	16
2.12	Structures of U3, PBI 1 and 3 . . . . .	17
2.13	Spectrum of U3 . . . . .	18
2.14	Spectrum of NBI . . . . .	18
2.15	Structure surfactants and TTAB . . . . .	19
2.16	Structure of BODIPY . . . . .	21
2.17	BODIPY synthesis via condensation with acyl chlorid . . . . .	21
2.18	Synthesis of BODIPY . . . . .	22
2.19	Sub of F with alcohol . . . . .	23
4.1	Synthesis of compound 21 . . . . .	30
4.2	Synthesis of compound 22 . . . . .	32
4.3	Synthesis of compound 23 . . . . .	33
4.4	Synthesis of compound 24 . . . . .	33
4.5	Synthesis of compound 25 . . . . .	34
4.6	Synthesis of compound 27 . . . . .	35
4.7	Synthesis of compound 28 . . . . .	36
4.8	Synthesis of compound 29 . . . . .	37
4.9	Synthesis of compound 31 . . . . .	38
4.10	Synthesis of compound 33 . . . . .	39
4.11	Synthesis of compound 34 . . . . .	40
4.12	Synthesis of compound 35 . . . . .	40

---

4.13	Synthesis of compound 36 . . . . .	41
4.14	Synthesis of compound 37: method 1 . . . . .	42
4.15	Synthesis of compound 37: method 2 . . . . .	43
4.16	Synthesis of compound 38 . . . . .	44
4.17	Synthesis of compound 39: method 1 . . . . .	45
4.18	Synthesis compound 39: method 2 . . . . .	46
4.19	Synthesis of compound 42 . . . . .	47
4.20	Synthesis of compound 43 . . . . .	48
4.21	Synthesis of compound 44 . . . . .	49
4.22	Synthesis of compound 46 . . . . .	50
4.23	Synthesis of compound 47 . . . . .	51
5.1	General synthesis of symmetrical BODIPYs . . . . .	55
5.2	Synthetic route for dye 38 . . . . .	56
5.3	Benzaldehyde synthesis . . . . .	57
5.4	TEG-m-perfluoro BODIPY . . . . .	58
5.5	Attempted synthesis of an asymmetrical BODIPY . . . . .	59
5.6	Overview of amphiphilic BODIPY dye synthesis . . . . .	59
5.7	Optimization of the reaction conditions for synthesis of amphiphilic BODIPYs .	60
5.8	Absorption (solid) and Emission (dashed) spectra of the synthesized dyes in their monomeric form (in THF) . . . . .	63
5.9	(a) Absorption spectrum of compound 44, representing the monomer in THF (black) and after J-aggregation in water in the presence of Pluoronic (red) (b) Structure of Pluoronic . . . . .	65
5.10	Determination of the optimal surfactant concentration with Pluoronic and SDS	66
5.12	Used surfactants . . . . .	68
5.13	Color change after J-aggregation . . . . .	69
5.14	Absorption spectra of dye aggregates ( $c= 2 * 10^{-5}M$ ) with different surfactants (40 mg/L) in water, the black lines represent the monomeric forms in THF with the same dye concentration. . . . .	70
5.15	Remaining Absorption spectra . . . . .	71
5.16	Absorption spectra of 1 : 1 mixture of compounds 43 and 44 . . . . .	74
5.17	Light Scattering . . . . .	75
5.18	Temperature dependency of J-aggregates with surfactants . . . . .	76
5.19	Absorption spectra of dyes 25 and 44 with different polymers show no formation of J-aggregates . . . . .	77
5.20	Absorption spectra compound 43 with different polymers . . . . .	78
5.21	Absorption spectra of compound 45 with polymers . . . . .	79
5.22	Absorption spectra of compound 46 with different polymers . . . . .	80

---

---

5.23	Absorption spectra shows in <b>(a)</b> and <b>(b)</b> - for the 2% of <b>43</b> in hydrogel D4, measured in dry state and in water, respectively. <b>(c)</b> shows the comparison at 25°C in dry state and in water . . . . .	82
5.24	Flow Cell Measurement . . . . .	83
5.25	Absorption (solid line) and Emission (dashed line) spectra with the best surfactants, respectively . . . . .	84
5.26	Absorption (solid) and Emission (dashed line) spectra of m-decyloxy B-TEG, m-perfluoro and m-perfluoro B-TEG in Hydrogel D4 or silicone . . . . .	85
10.1	Absorption (solid line) and Emission (dashed line) spectra of dyes in water in presence of different surfactants . . . . .	107
10.2	<sup>1</sup> H NMR of compound 21 . . . . .	108
10.3	APT of compound 21 . . . . .	109
10.4	<sup>1</sup> H NMR of compound 22 . . . . .	110
10.5	COSY of compound 22 . . . . .	111
10.6	APT of compound 22 . . . . .	112
10.7	<sup>1</sup> H NMR of compound 23 . . . . .	113
10.8	COSY of compound 23 . . . . .	114
10.9	<sup>1</sup> H NMR of compound 24 . . . . .	115
10.10	<sup>1</sup> H NMR of compound 25 . . . . .	116
10.11	APT of compound 25 . . . . .	117
10.12	<sup>1</sup> H NMR of compound 27 . . . . .	118
10.13	APT of compound 27 . . . . .	119
10.14	<sup>1</sup> H NMR of compound 28 . . . . .	120
10.15	<sup>1</sup> H NMR of compound 33 . . . . .	121
10.16	<sup>1</sup> H NMR of compound 34 . . . . .	122
10.17	<sup>1</sup> H NMR of compound 35 . . . . .	123
10.18	COSY of compound 35 . . . . .	124
10.19	APT spectrum of compound 27 . . . . .	125
10.20	<sup>1</sup> H NMR of compound 36 . . . . .	126
10.21	<sup>1</sup> H NMR of compound 37 . . . . .	127
10.22	<sup>1</sup> H NMR of compound 38 . . . . .	128
10.23	<sup>1</sup> H NMR of compound 42 . . . . .	129
10.24	<sup>1</sup> H NMR of compound 43 . . . . .	130
10.25	APT of compound 43 . . . . .	131
10.26	<sup>1</sup> H NMR of compound 44 . . . . .	132
10.27	APT of compound 44 . . . . .	133
10.28	<sup>1</sup> H NMR of compound 45 . . . . .	134
10.29	<sup>1</sup> H NMR of compound 47 . . . . .	135
10.30	Whole MS compound 21 . . . . .	136

10.31MS compound 21 . . . . .	137
10.32MS compound 22 . . . . .	138
10.33MS compound 22 . . . . .	139
10.34MS compound 25 . . . . .	140
10.35MS compound 25 . . . . .	141
10.36MS compound 25 . . . . .	142
10.37MS compound 27 . . . . .	143
10.38MS compound 27 . . . . .	144
10.39MS compound 27 . . . . .	145
10.40MS compound 27 . . . . .	146
10.41MS compound 38 . . . . .	147
10.42MS compound 38 . . . . .	148
10.43MS compound 43 . . . . .	149
10.44MS compound 43 . . . . .	150
10.45MS compound 44 . . . . .	151
10.46MS compound 45 . . . . .	152
10.47MS compound 45 . . . . .	153
10.48MS compound 45 . . . . .	154
10.49MS compound 45 . . . . .	155
10.50MS compound 46 . . . . .	156
10.51MS compound 46 . . . . .	157
10.52MS compound 47 . . . . .	158
10.53MS compound 47 . . . . .	159

---

## 9 List of Tables

2.1	Properties of NIR J-aggregates compared to their monomeric form . . . . .	19
3.1	List of Solvents . . . . .	24
3.2	List of used chemicals . . . . .	25
3.3	List of Surfactants . . . . .	26
3.4	List of Polymers . . . . .	26
5.1	Overview photophysical properties of the synthesized dyes (Monomer) . . . . .	62
5.2	Overview of attempts to form J-aggregates with different surfactants (+++: forms almost exclusively; ++: forms in moderate amount ; + some dye in this form can be found; no sign - none of this form can be found) . . . . .	72
5.3	Overview of attempts to form J-aggregates with different polymers (+++: forms almost exclusively; ++: forms in moderate amount ; + some dye in this form can be found; no sign - none of this form can be found) . . . . .	81
5.4	Overview photophysical properties of J-aggregates with surfactants . . . . .	86
5.5	Overview photophysical properties of J-aggregates with polymers . . . . .	86





---

# 10 Appendix

## 10.1 Supporting Information

In this chapter, the experimental procedures that were not carried successfully will be discussed in detail.

### 10.1.1 Attempts to couple alcohol at the boron center

#### Attempt 1

In a Schlenk flask 2,5,8,11-tetraoxatridecan-13-ol (11.98  $\mu\text{L}$ , 60-98  $\mu\text{mol}$ , 10 eq) were dissolved in dry DCM under inert atmosphere. NaH (1.17 mg, 8 eq) was added and the reaction was stirred for 30 min at room temperature. In a second Schlenk flask compound **43** (5.00 mg, 6.09  $\mu\text{mol}$ ) was dissolved in DCM and 1 M  $\text{BCl}_3$  in heptane (7.30  $\mu\text{L}$ , 7.30  $\mu\text{mol}$ , 1.2 eq) was added and stirred for 20 min. The color changed from blue to green. Afterwards the alcoholate was added to the second reaction mixture and stirred over night. The reaction progress was controlled via TLC and UV-VIS spectroscopy, the results indicate a decomposition to its ligand.

#### Attempt 2

The procedure was performed analogues to **Attempt 1**, except that the conversion to the alcoholate was carried out in toluene instead of DCM and during the chlorination step only 1.2 eq were added.

In a Schlenk flask 2,5,8,11-tetraoxatridecan-13-ol (11.98  $\mu\text{L}$ , 60-98  $\mu\text{mol}$ , 10 eq) were dissolved in dry toluene under inert atmosphere. NaH (1.17 mg, 8 eq) was added and the reaction was stirred for 30 min at room temperature. In a second Schlenk flask compound **43** (5.00 mg, 6.09  $\mu\text{mol}$ ) was dissolved in DCM and 1 M  $\text{BCl}_3$  in heptane (30.4  $\mu\text{L}$ , 3.4  $\mu\text{mol}$ , 5 eq) was added and stirred for 20 min. The color changed from blue to green. Afterwards the alcoholate was added to the second reaction mixture and stirred over night. The solution was extracted with water and dried over  $\text{Na}_2\text{SO}_4$ . After filtration, the solvents were removed. No product was isolated.

**Attempt 3**

5 mg (6.09  $\mu\text{mol}$ ) compound **43** were dissolved in dry DCM and 1 eq  $\text{BCl}_3$  was added. The solution stirred 20 min and a shift of absorption maxima (15 nm) was detected. 2,5,8,11-tetraoxatridecan-13-ol (12  $\mu\text{L}$ , 10 eq) was added and stirred for 1.5 hours. After reaction control, again 10 eq alcohol were added. On the next day the organic phase was washed with water, dried and removed. The product was tried to purify via flash column chromatography, however the dye reacts with the silica.

**10.1.2 Synthesis of Ethyl-4,7-dihydro-2H-4,7-ethanoisindole-1-carboxylate (35)**

480 mg (1.84 mmol) 2-Tosylbicyclo[2,2,2]octa-2,5-diene (**34**) were dissolved in dry THF (10 mL), ethyl isocynoactete (364  $\mu\text{L}$ , 3.32 mmol, 1.80 eq) and DBU (290  $\mu\text{L}$ , 1.94 mmol, 1.05 eq) were added. The reaction solution was stirred for 24 hours at room temperature. The reaction was controlled via TLC, no product was formed.

**10.1.3 Synthesis 14-(4-decyloxy)phenyl-7-7-difluoro-5,9-dimethyl-1,7,10,13-tetrahydro-4H-diethano[1,3,2]diazaborino diisindole (37)**

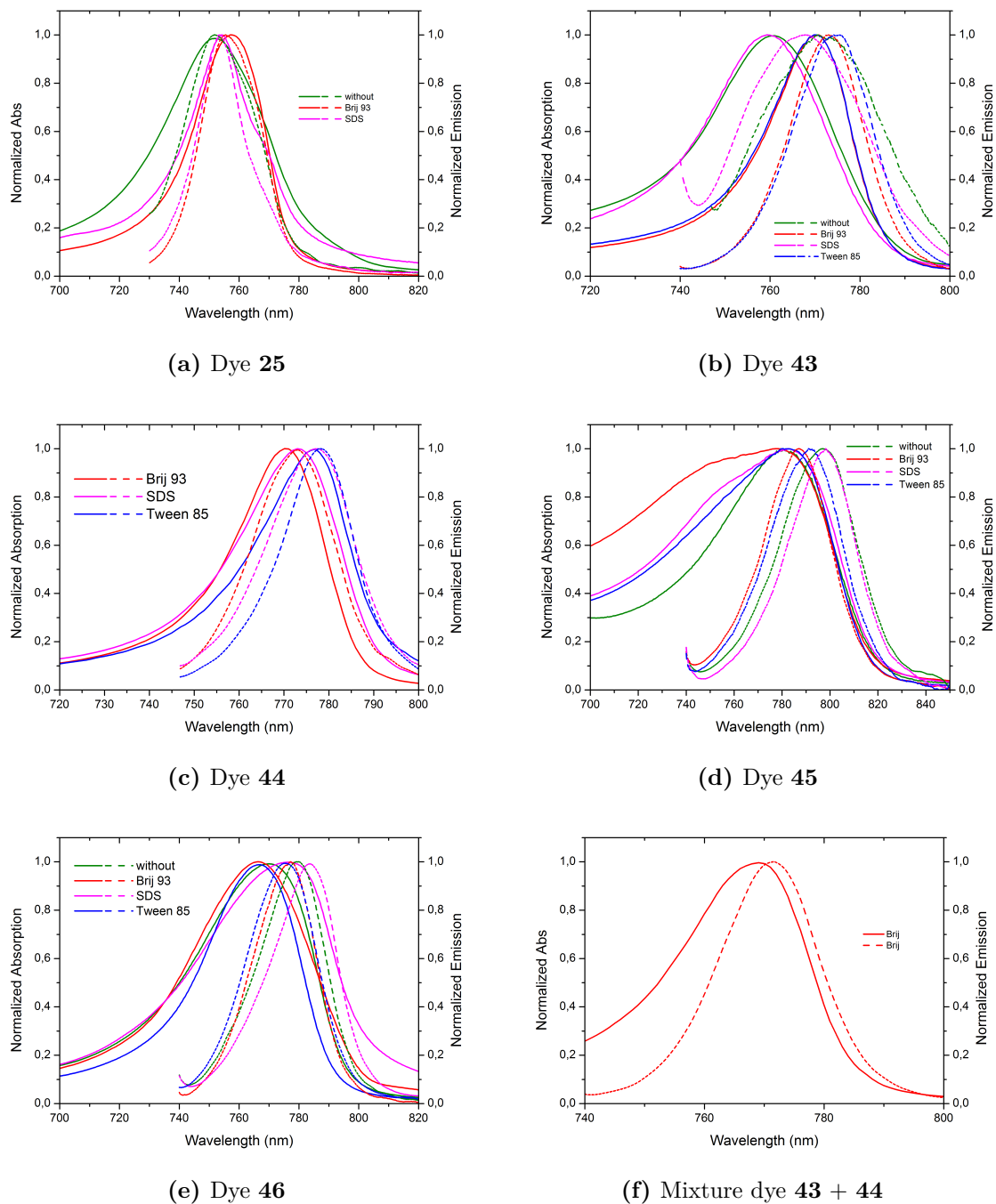
The reaction was carried out analogues to the second method described in 4.1.14.

Compound **35** (50.00 mg, 314.01  $\mu\text{mol}$ , 2 eq) was dissolved in dry DCM (16 mL) and small amount of dry ethanol (1.14 mL), 14 : 1, in a Schlenk tube under inert atmosphere. 4-(Decyloxy)benzaldehyde (45.00  $\mu\text{L}$ , 164.85  $\mu\text{mol}$ , 1.05eq) and a drop TFA were added. The mixture was stirred over night at room temperature.

After oxidation with DDQ (38.60 mg, 157.0  $\mu\text{mol}$ , 1 eq), which forms more side products compared to p-chloranil, DIPEA (274  $\mu\text{L}$ , 1.57 mmol, 10 eq) was added to guarantee a basic surrounding.  $\text{BF}_3$  diethyl etherate (291  $\mu\text{L}$ , 2.36 mmol, 15 eq) was added dropwise to the solution for the complexation. This did not work out, because the alcohol interferes with the complexation step. The right amount of base was added until the solution started to fluoresces. Afterwards the complexation with  $\text{BF}_3\text{OEt}_2$  was successful. The mixture was extracted with water, prepurified with a small column (silica, DCM) and the solvent was removed.

The reaction progress was monitored with TLC (CH : EA, 4 + 1).

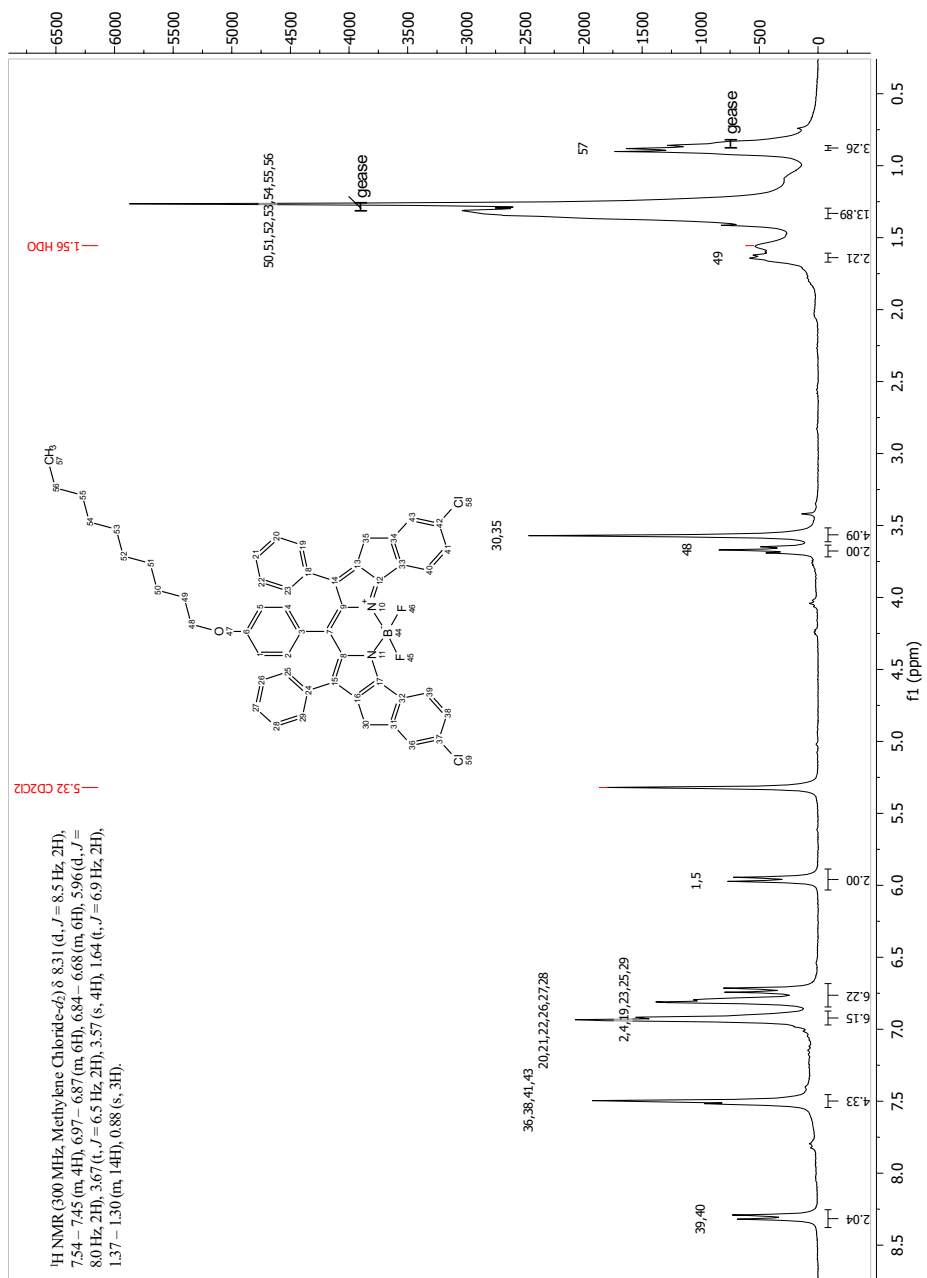
## 10.2 Remaining Absorption and Emission Spectra



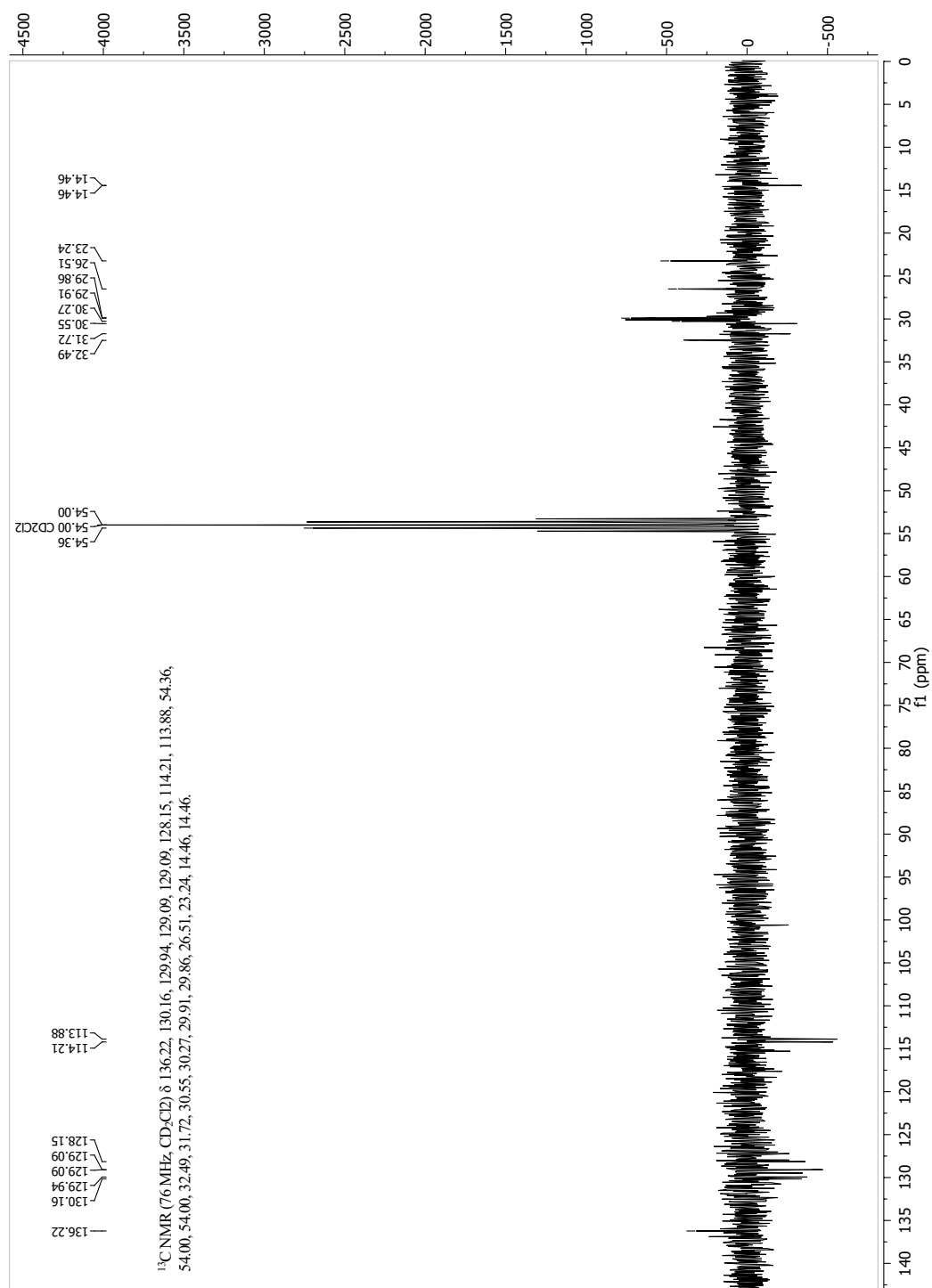
**Figure 10.1:** Absorption (solid line) and Emission (dashed line) spectra of dyes in water in presence of different surfactants

## 10.3 NMR Spectra

## 10.3.1 Compound 21

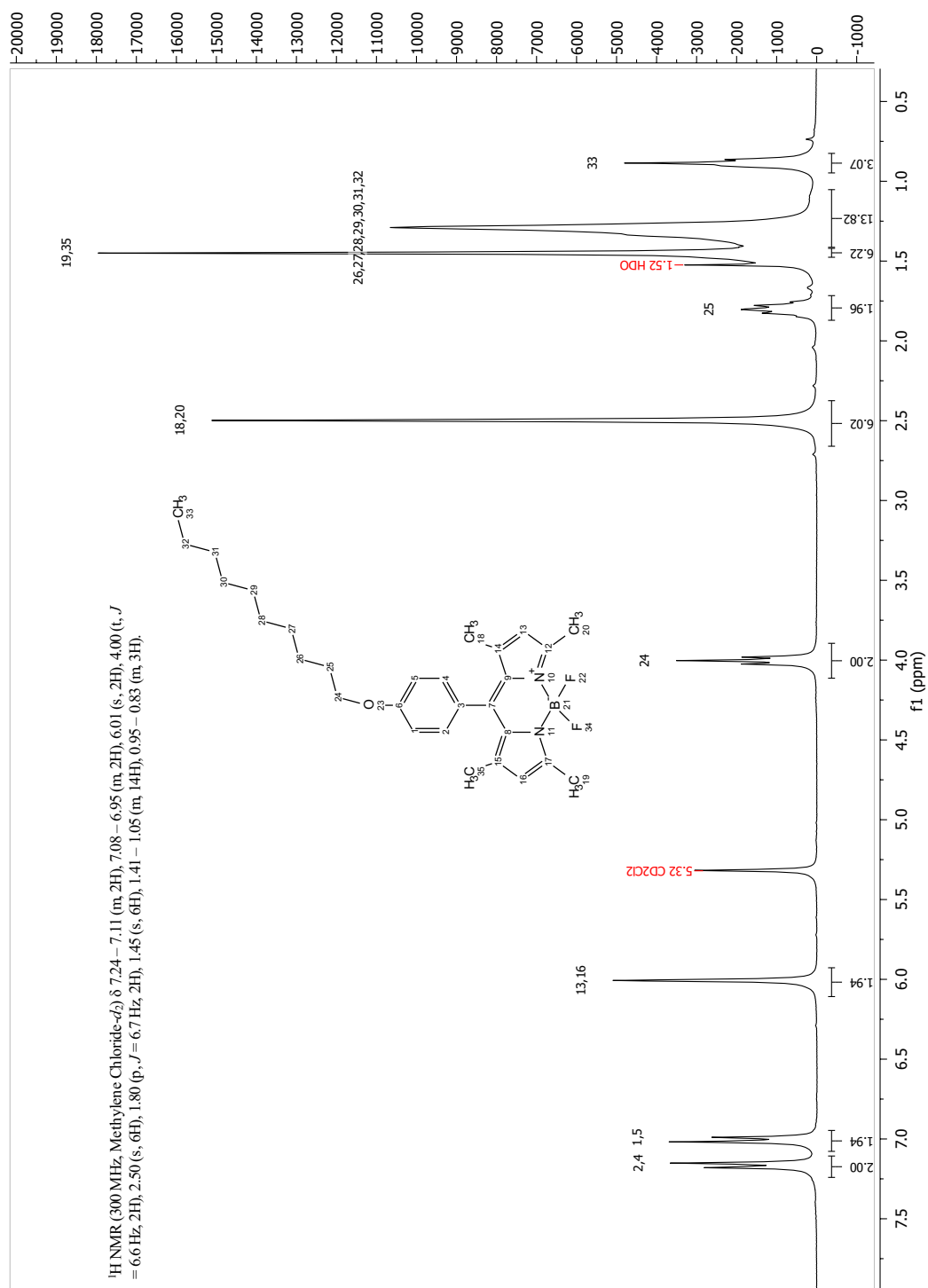


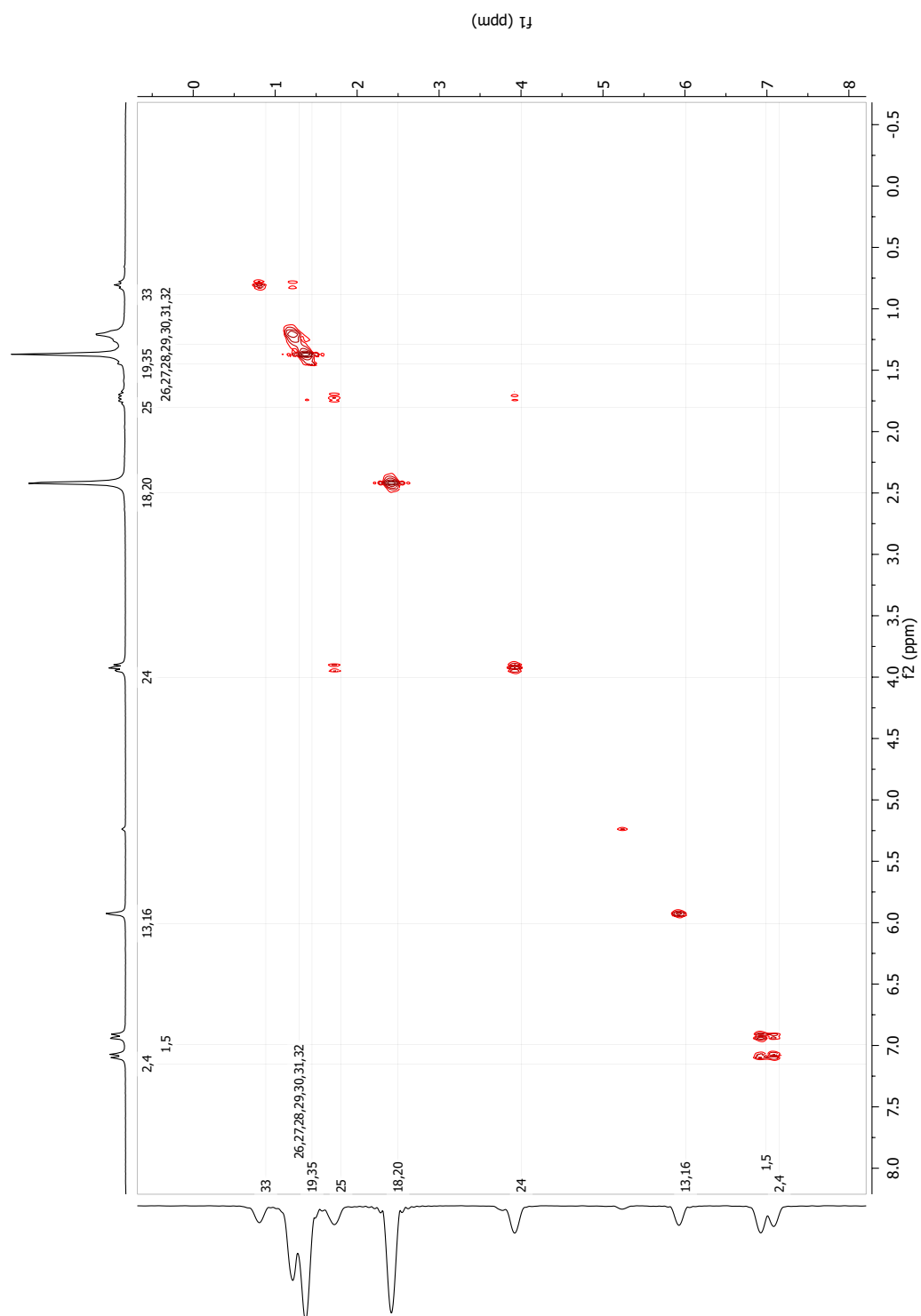
**Figure 10.2:** <sup>1</sup>H NMR spectrum (300 MHz, Methylene Chloride) of Cl-rigid m-decyloxy BODIPY 21



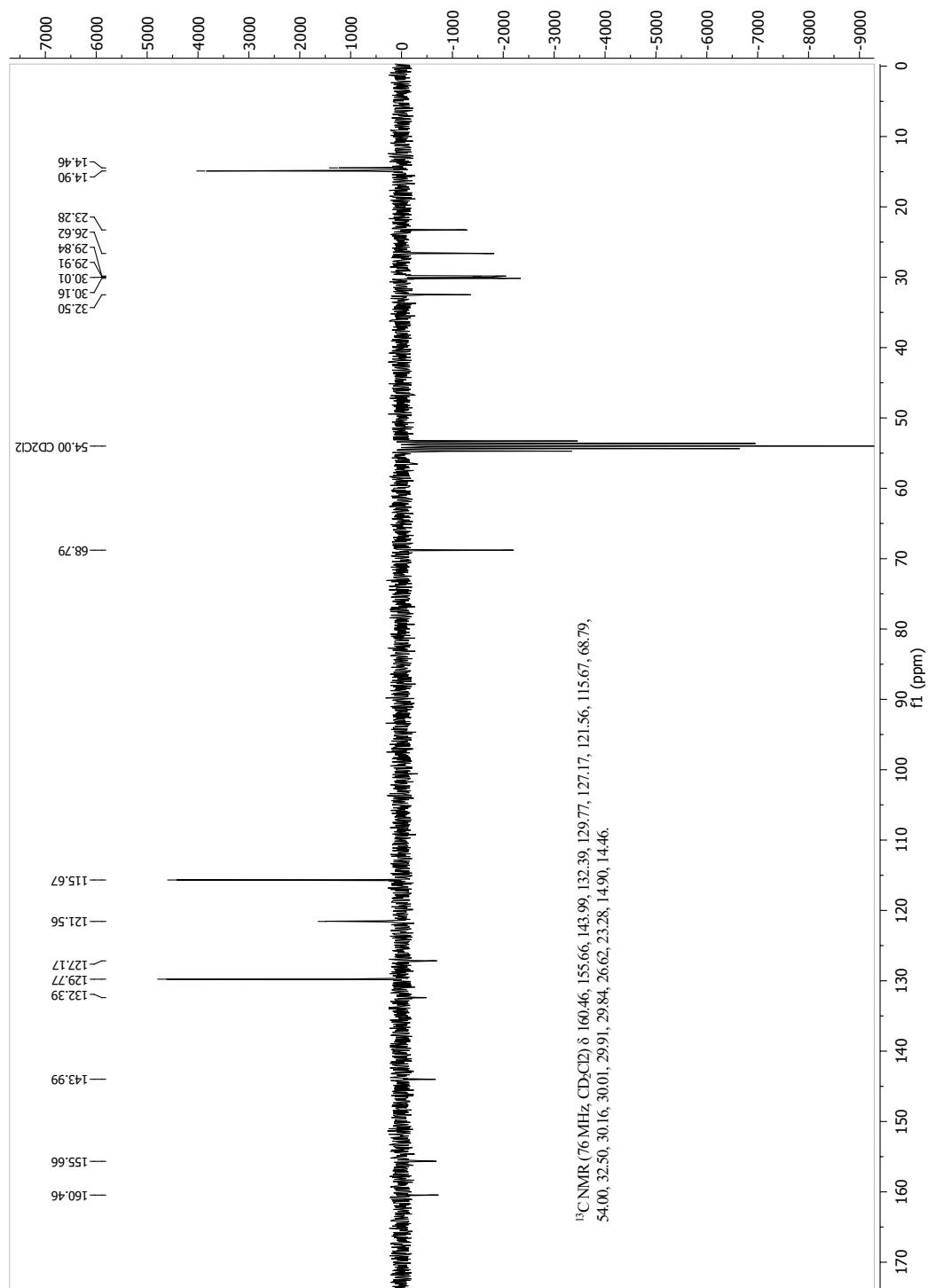
**Figure 10.3:** APT spectrum (76 MHz, Methylene Chloride) of compound **21**

## 10.3.2 Compound 22

Figure 10.4: <sup>1</sup>H NMR (300 MHz, Methylene Chloride) of compound 22



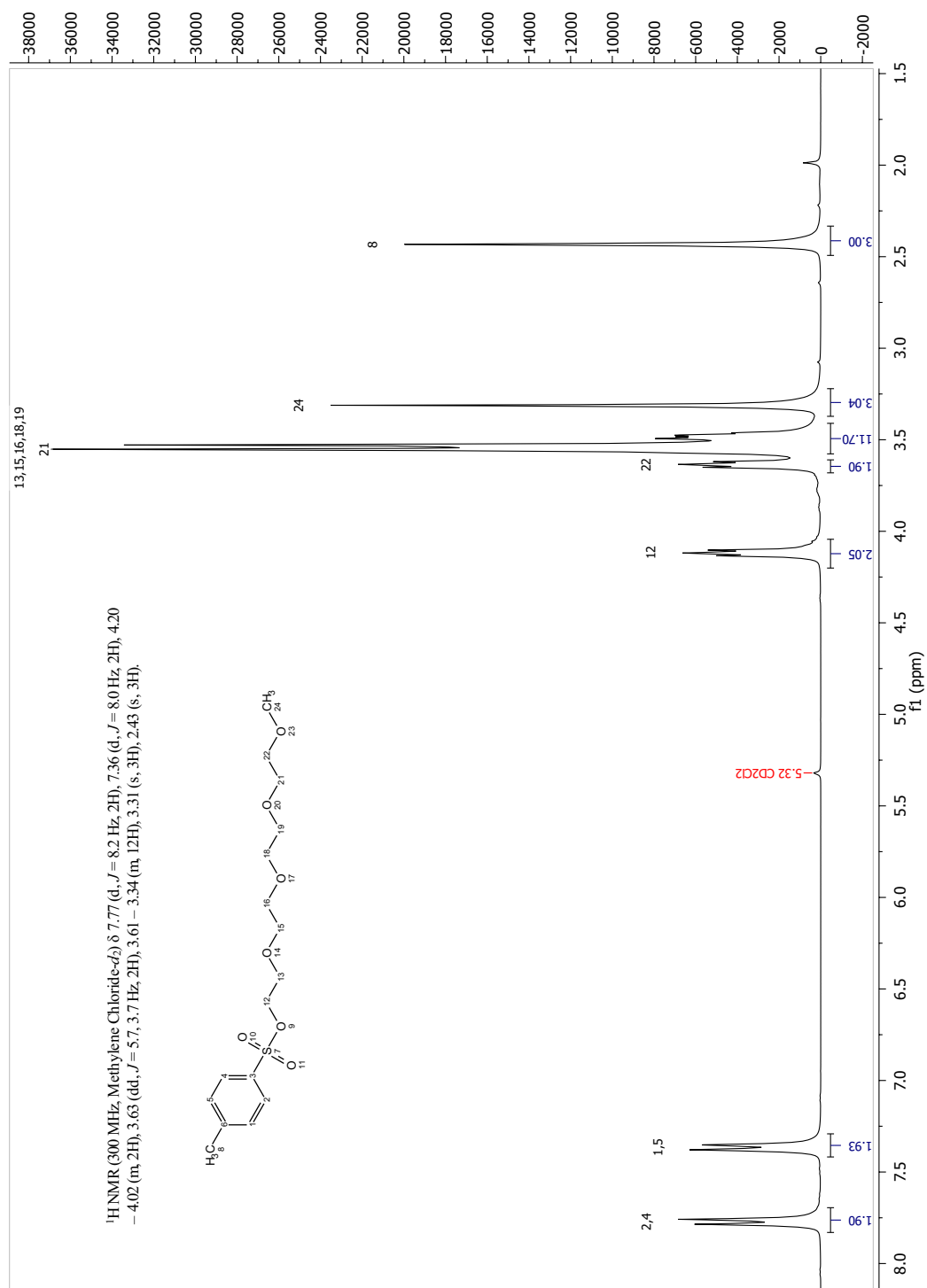
**Figure 10.5:** COSY measurement (300 MHz, Methylene Chloride) of compound **22**

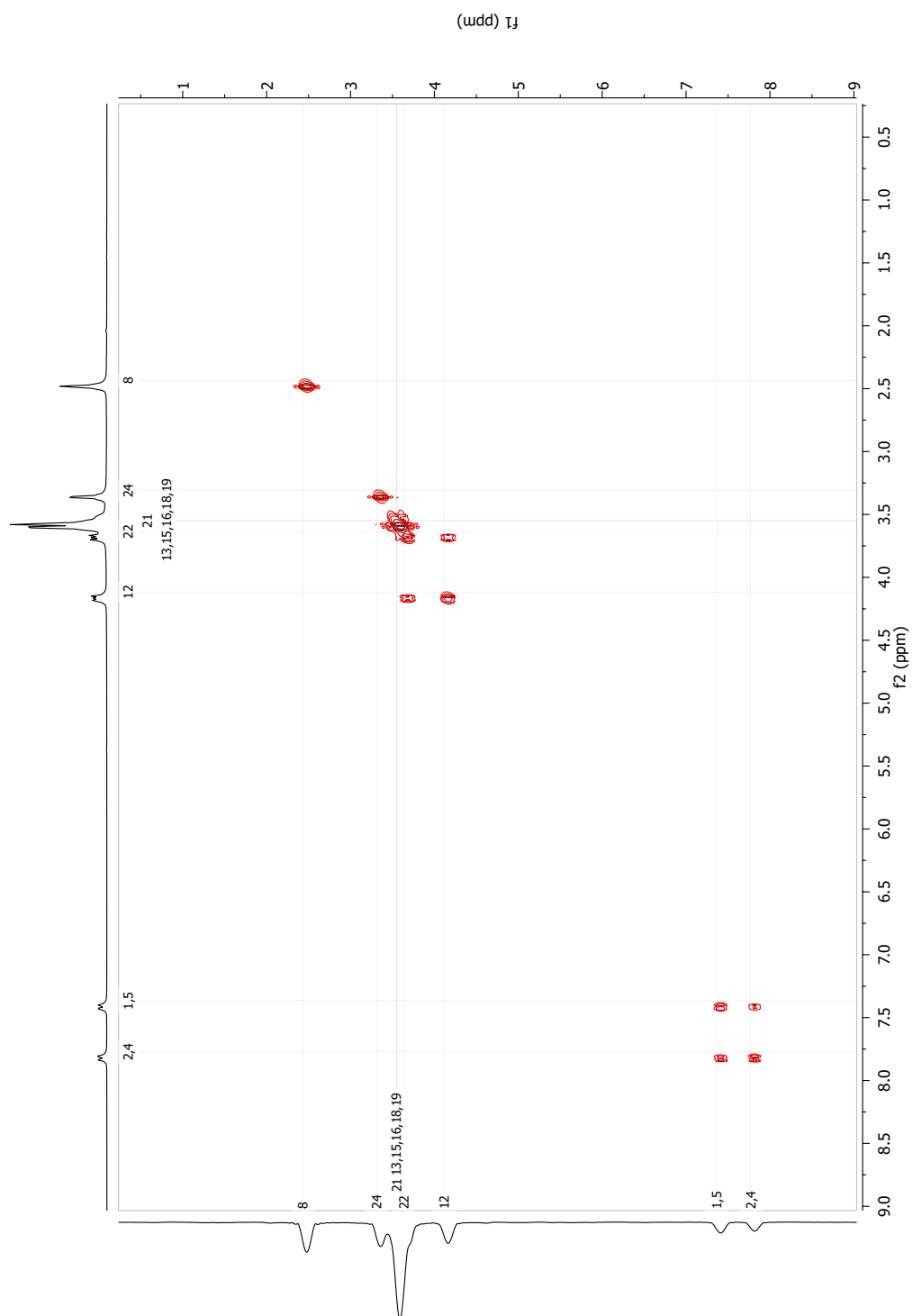


**Figure 10.6:** APT measurement (76 MHz, Methylene Chloride) of compound **22**



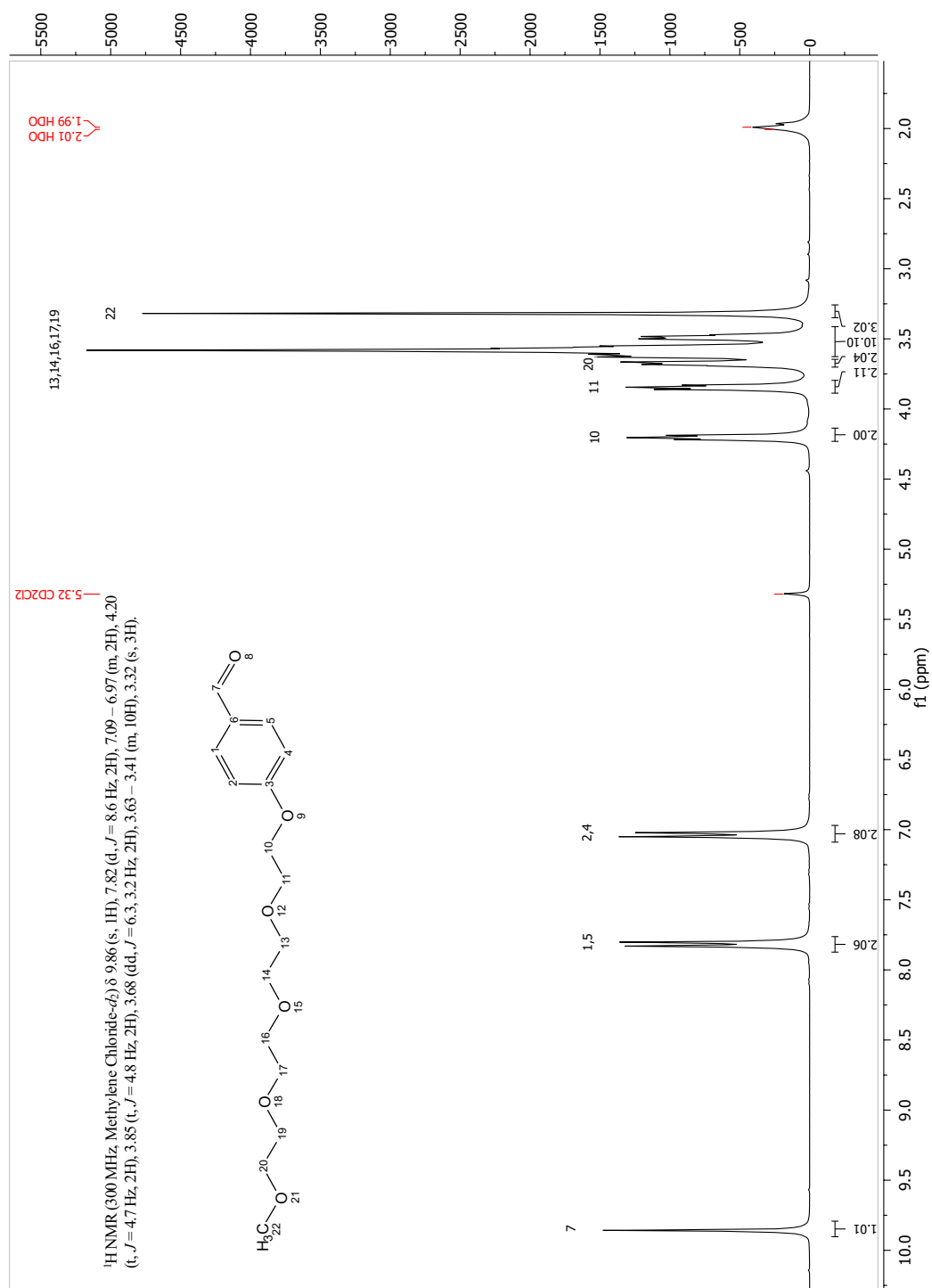
## 10.3.3 Compound 23

Figure 10.7: <sup>1</sup>H NMR spectrum (300 MHz, Methylene Chloride) of Tosyl TEG (23)



**Figure 10.8:** COSY spectrum (300 MHz, Methylene Chloride) of Tosyl TEG (**23**)

## 10.3.4 Compound 24



**Figure 10.9:** <sup>1</sup>H NMR spectrum (300 MHz, Methylene Chloride) of TEG benzaldehyde (**24**)

## 10.3.5 Compound 25

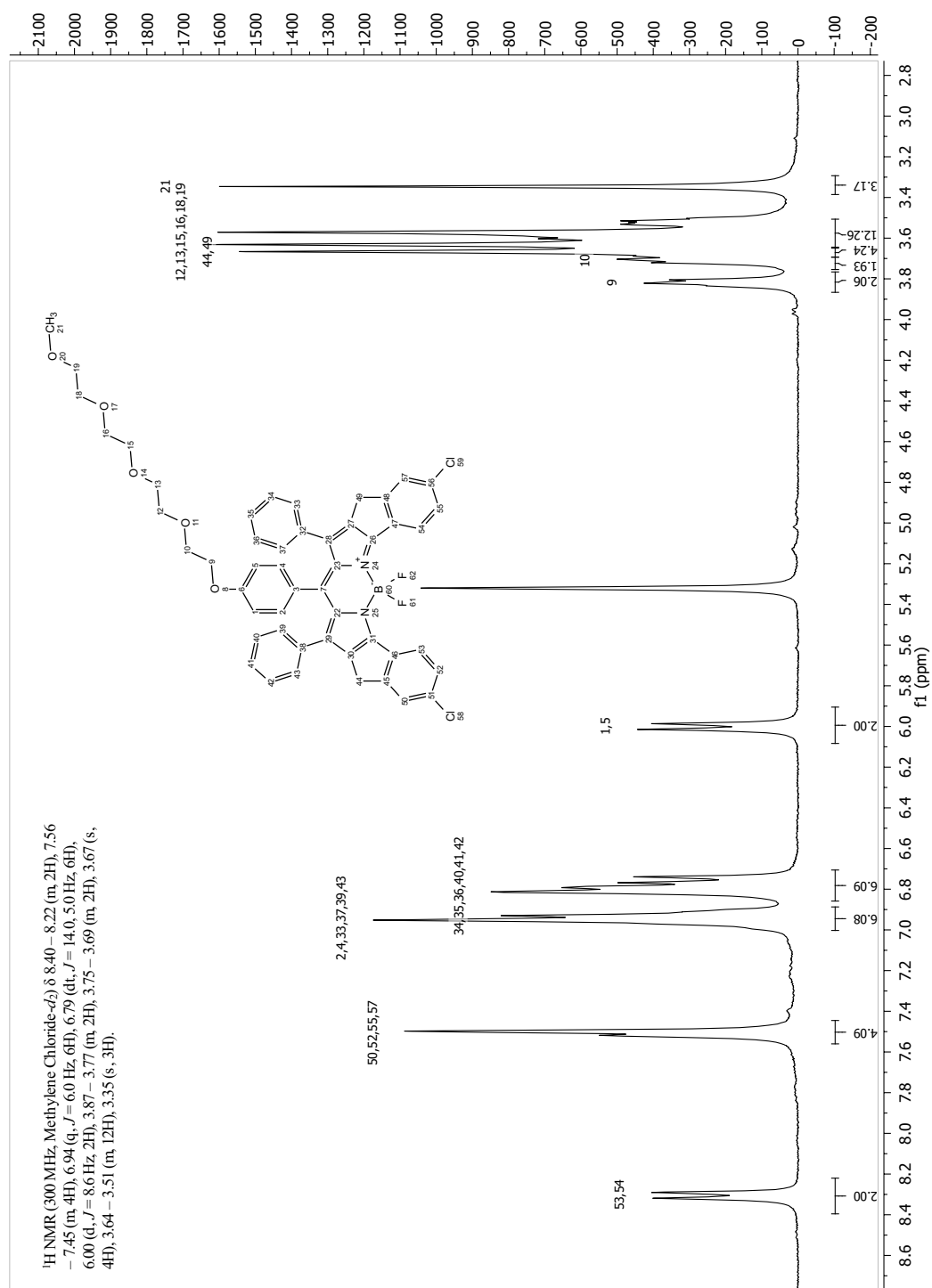


**Figure 10.10:** <sup>1</sup>H NMR spectrum (300 MHz, Methylene Chloride) of Cl-rigid m-TEG BODIPY (25)

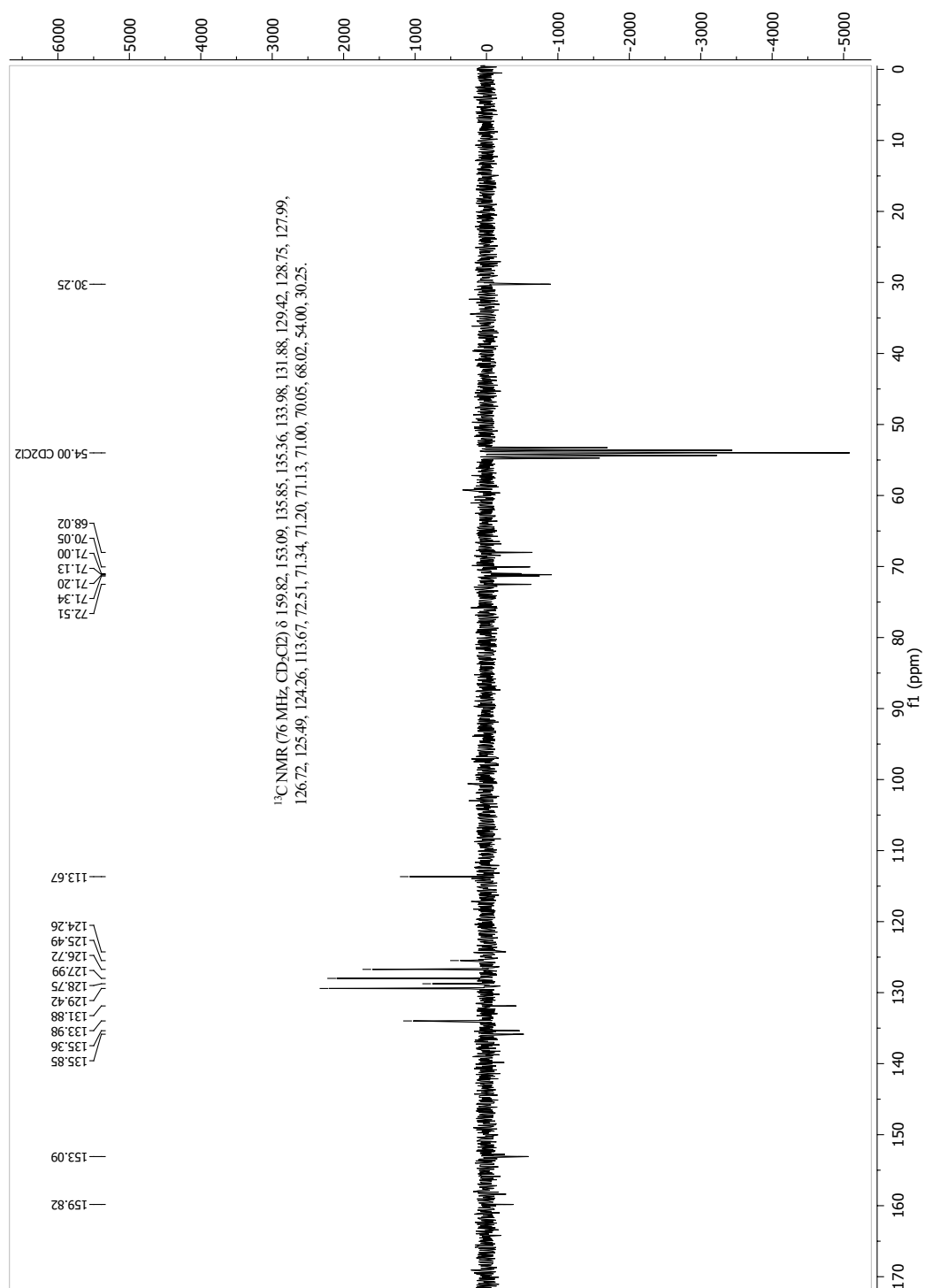
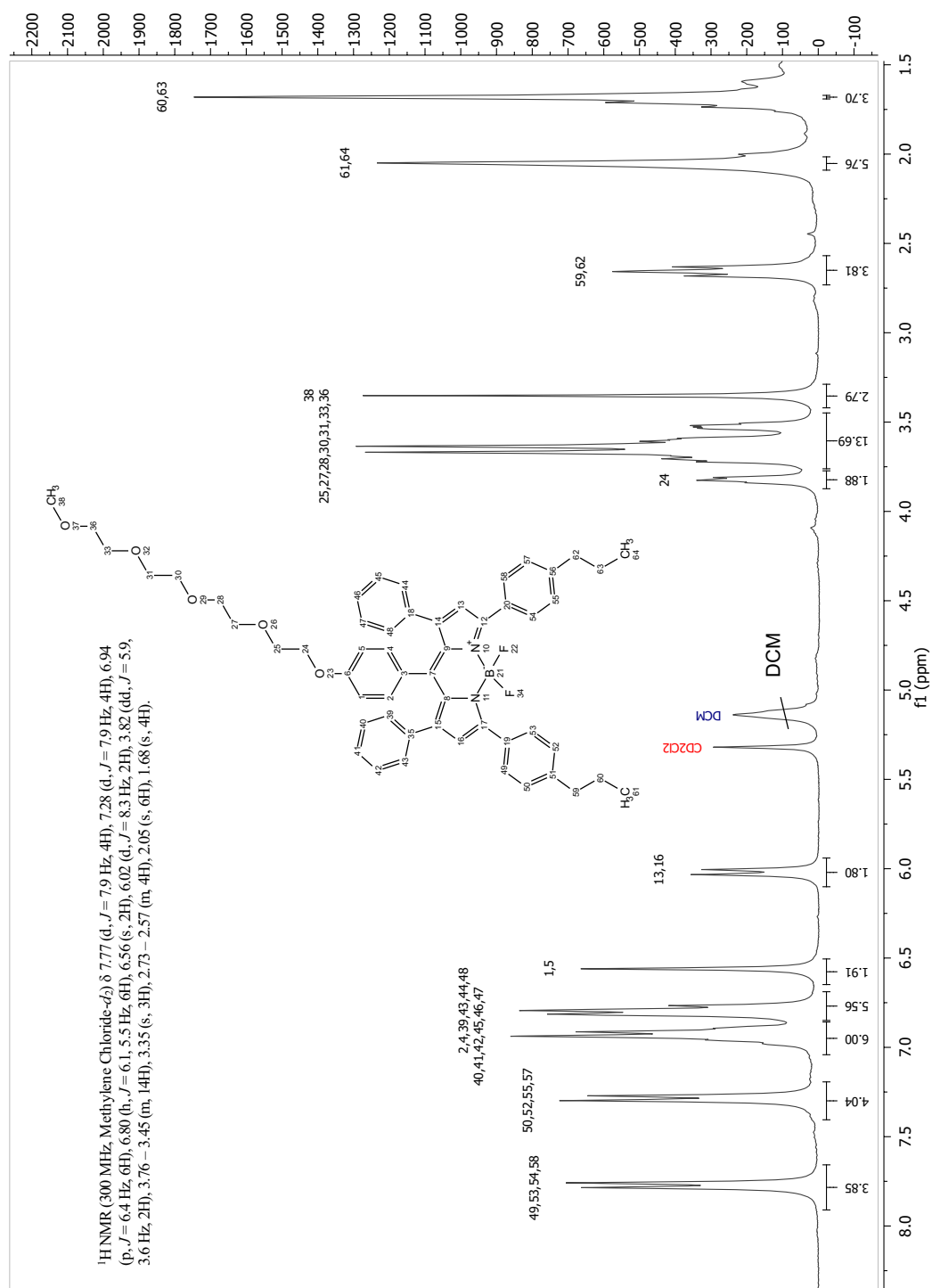
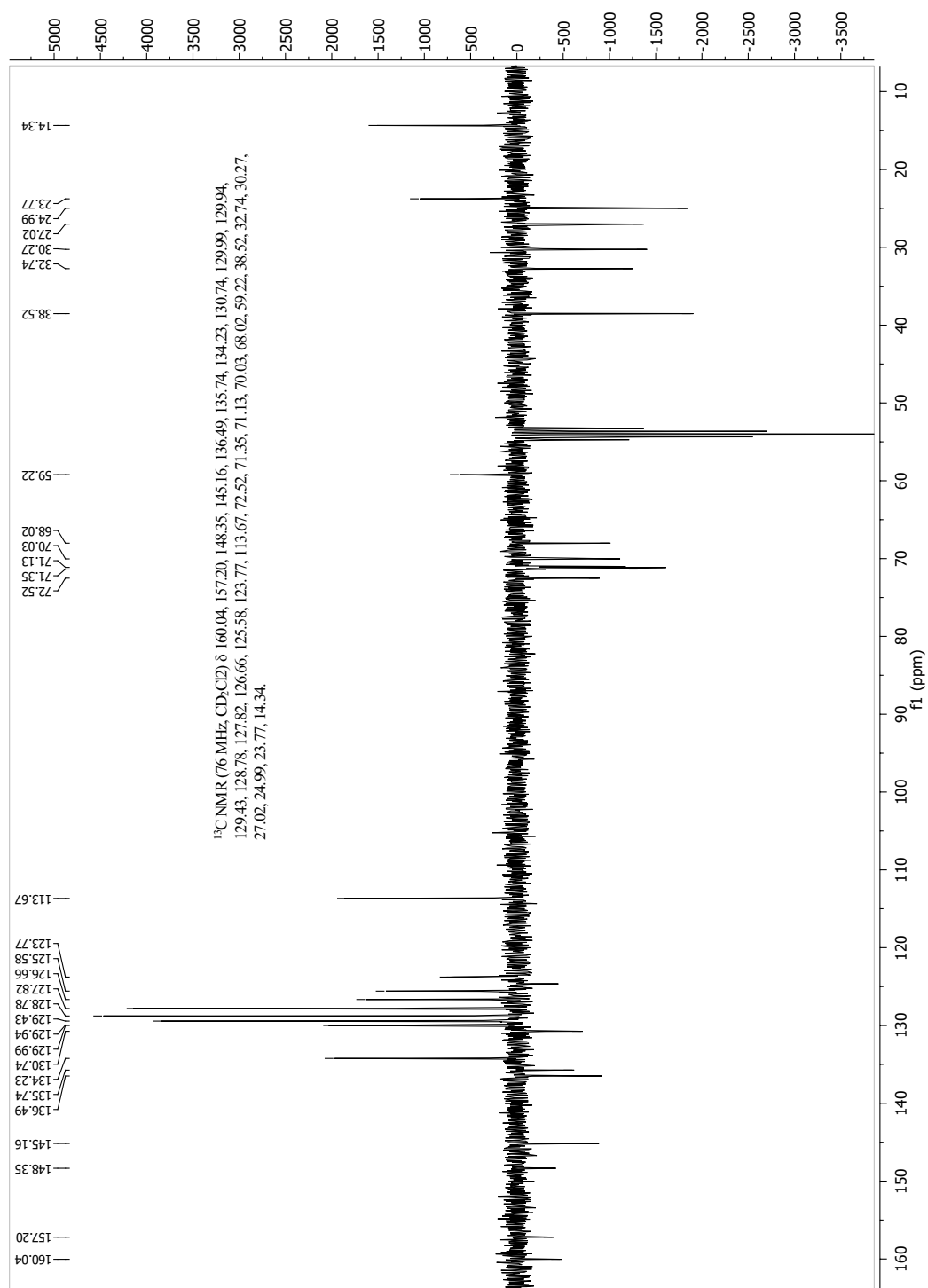


Figure 10.11: APT spectrum (76 MHz, Methylene Chloride) of compound (25)

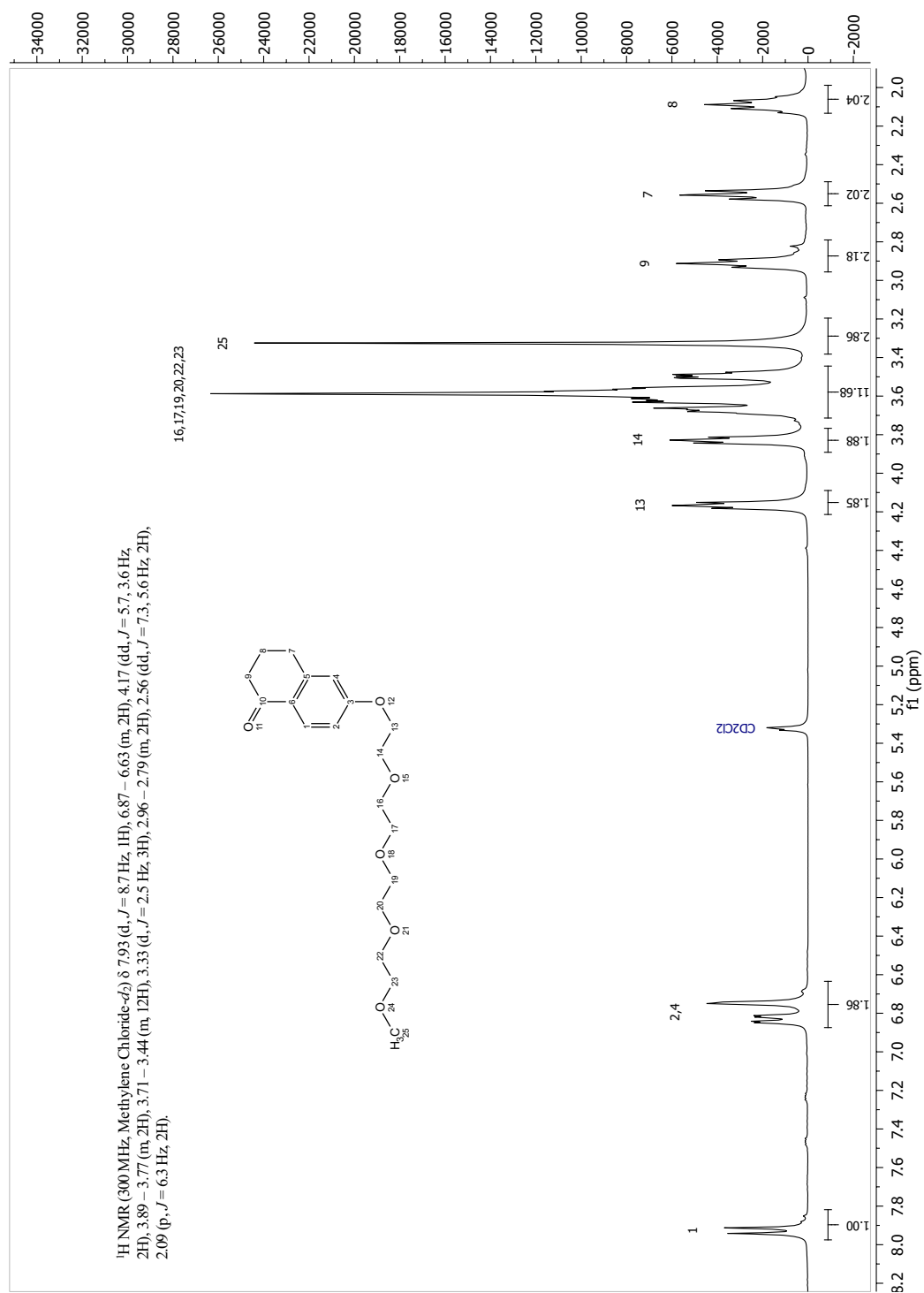
## 10.3.6 Compound 27

Figure 10.12: <sup>1</sup>H NMR spectrum (300 MHz, Methylene Chloride) of compound 27



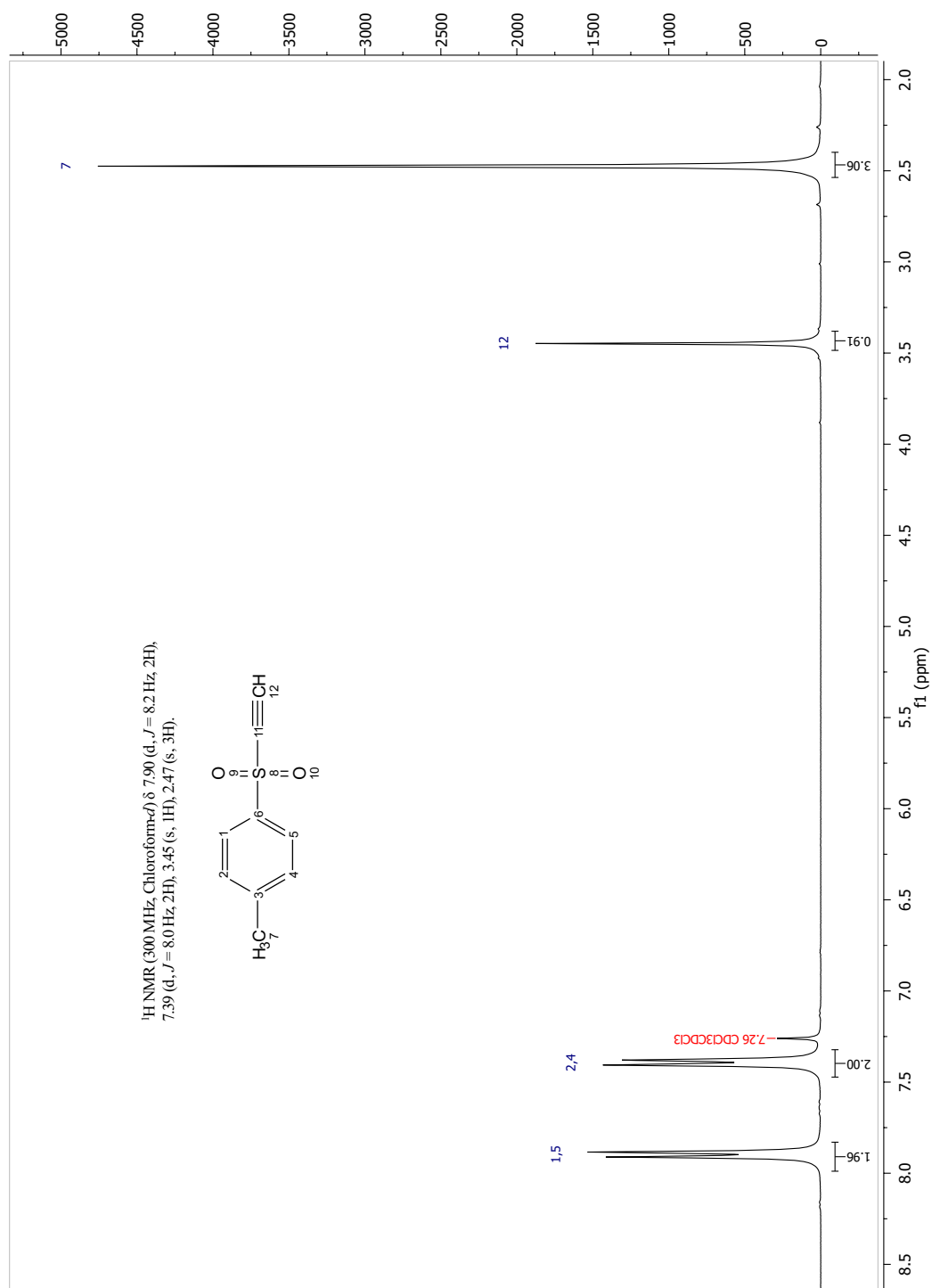
**Figure 10.13:** APT spectrum (76 MHz, Methylene Chloride) of compound (27)

## 10.3.7 Compound 28

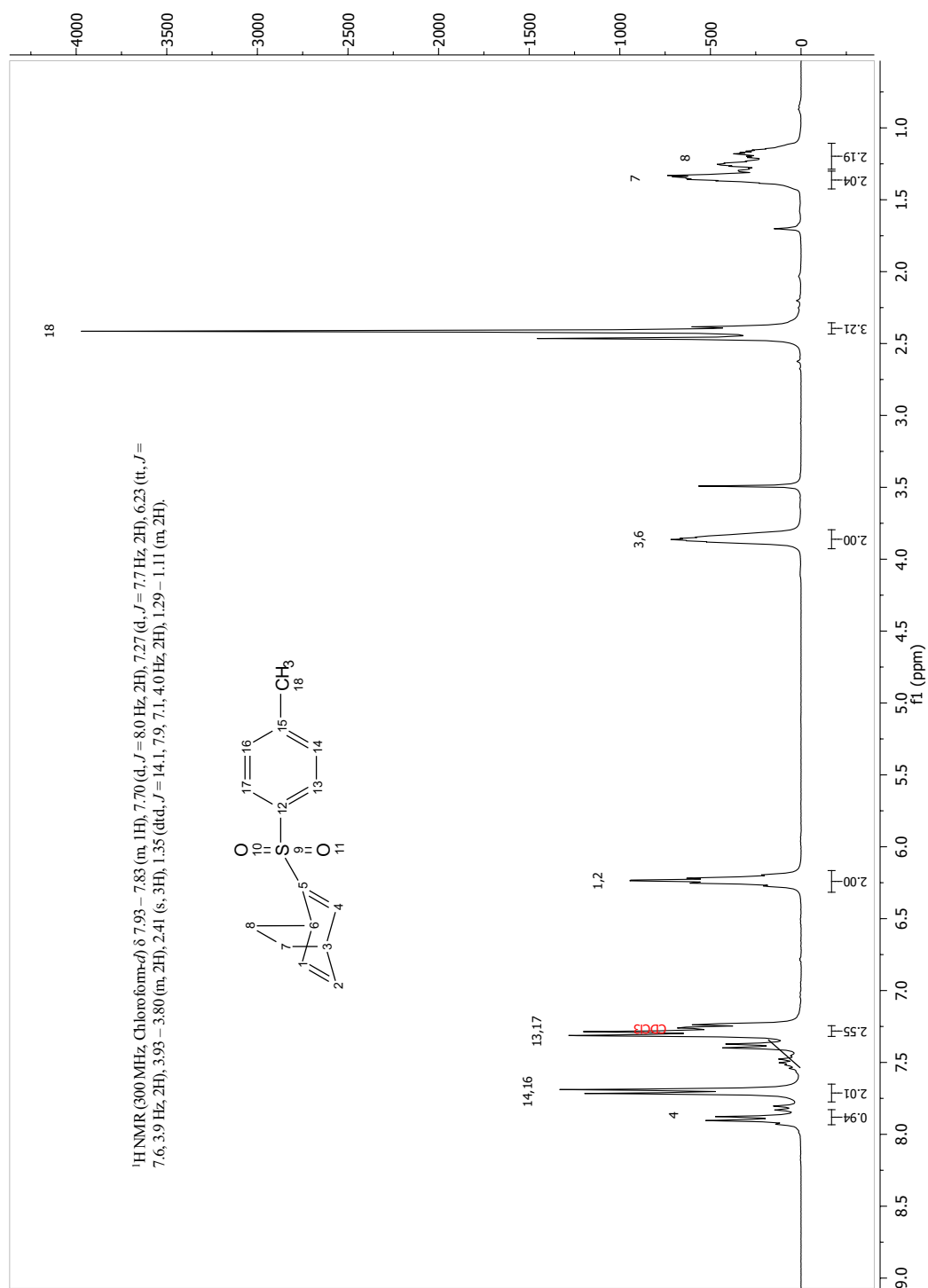
Figure 10.14:  $^1\text{H}$  NMR spectrum (300 MHz, Methylene Chloride) of compound (28)



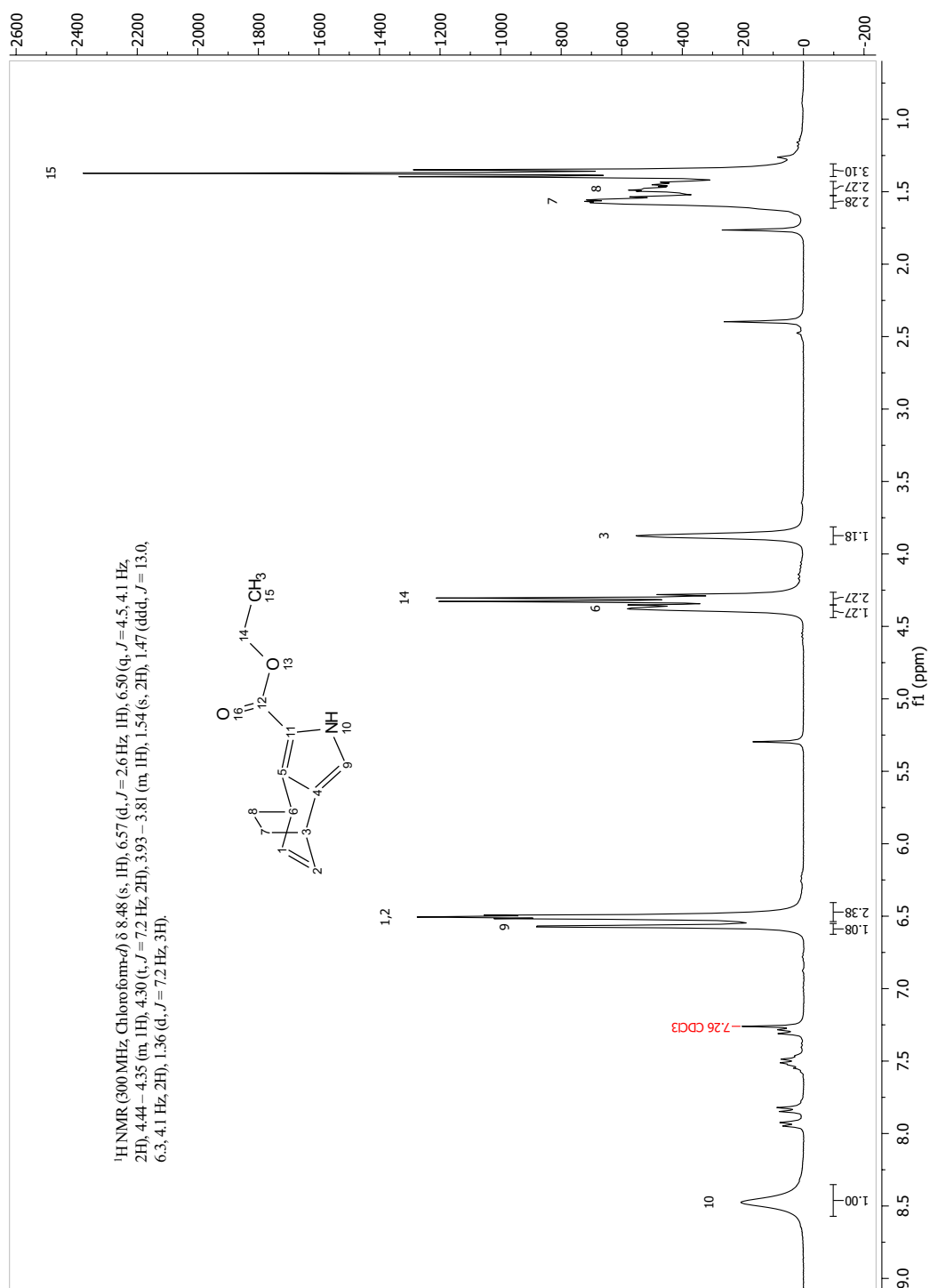
## 10.3.8 Compound 33

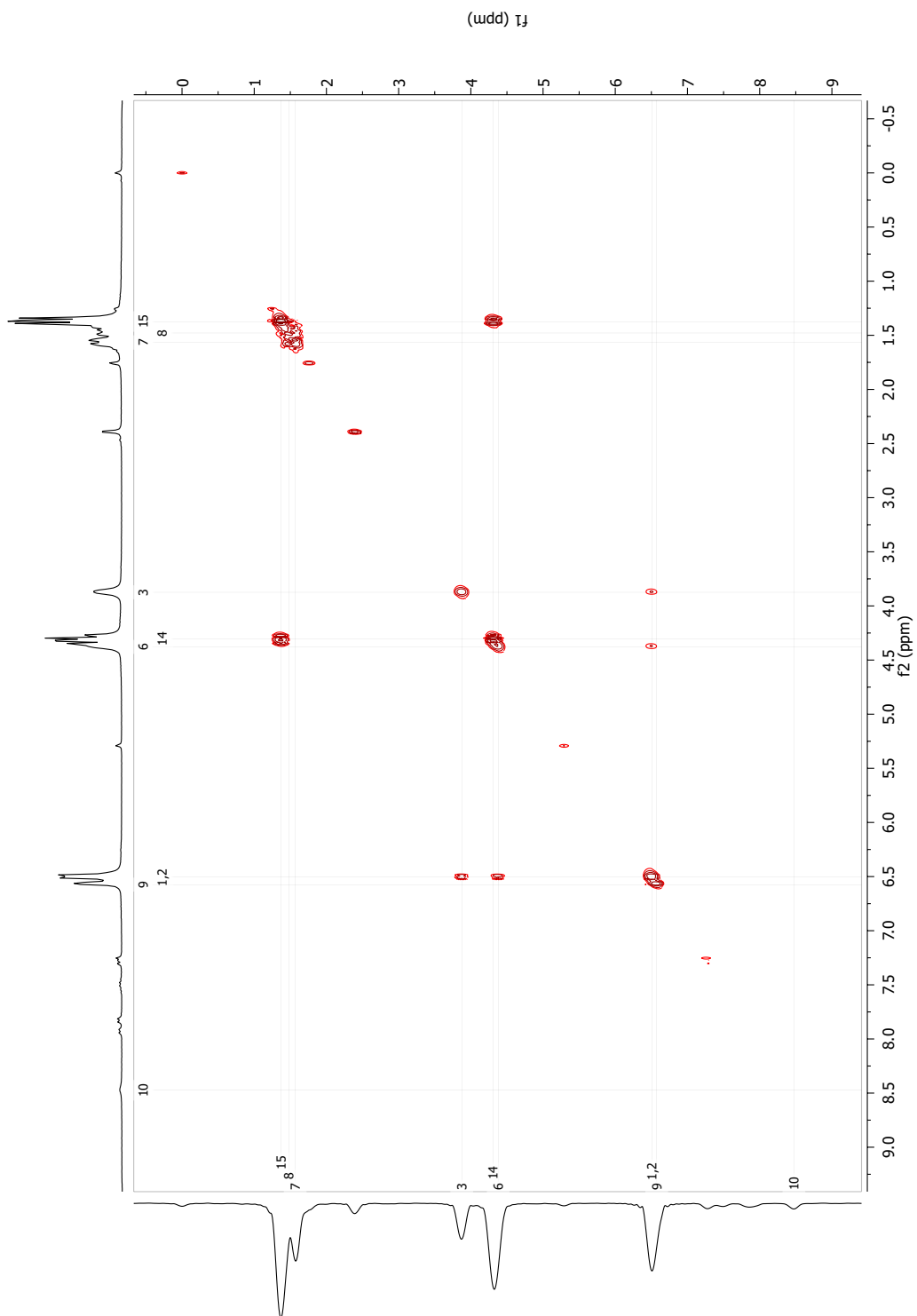
**Figure 10.15:** <sup>1</sup>H NMR spectrum (300 MHz, Chloroform) of p-Tolyl ethynyl sulfone (**33**)

## 10.3.9 Compound 34

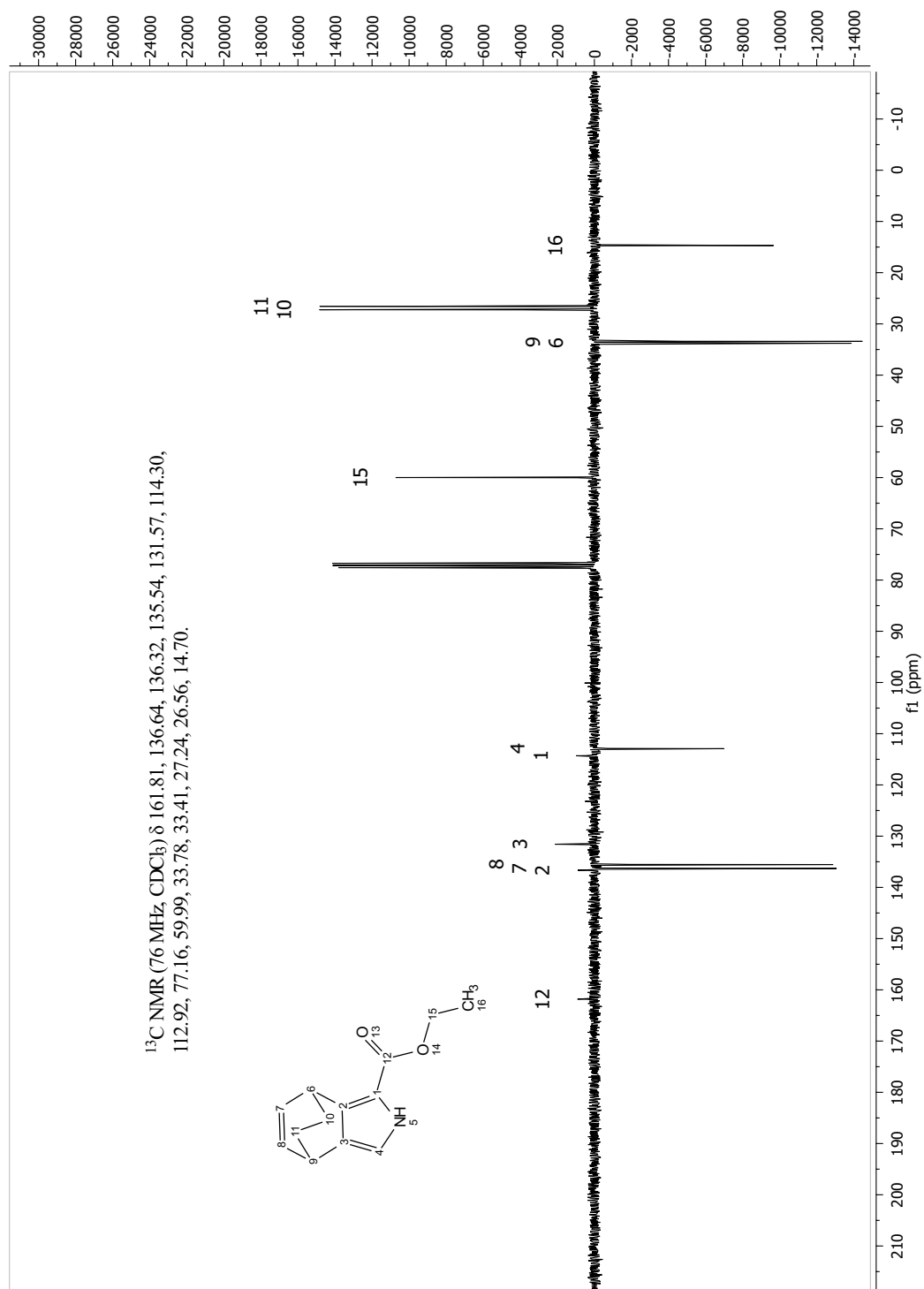
Figure 10.16: <sup>1</sup>H NMR spectrum (300 MHz, Chloroform) of compound 34

## 10.3.10 Compound 35

Figure 10.17: <sup>1</sup>H NMR spectrum (300 MHz, Chloroform) of BCOD fused pyrrole (**35**)

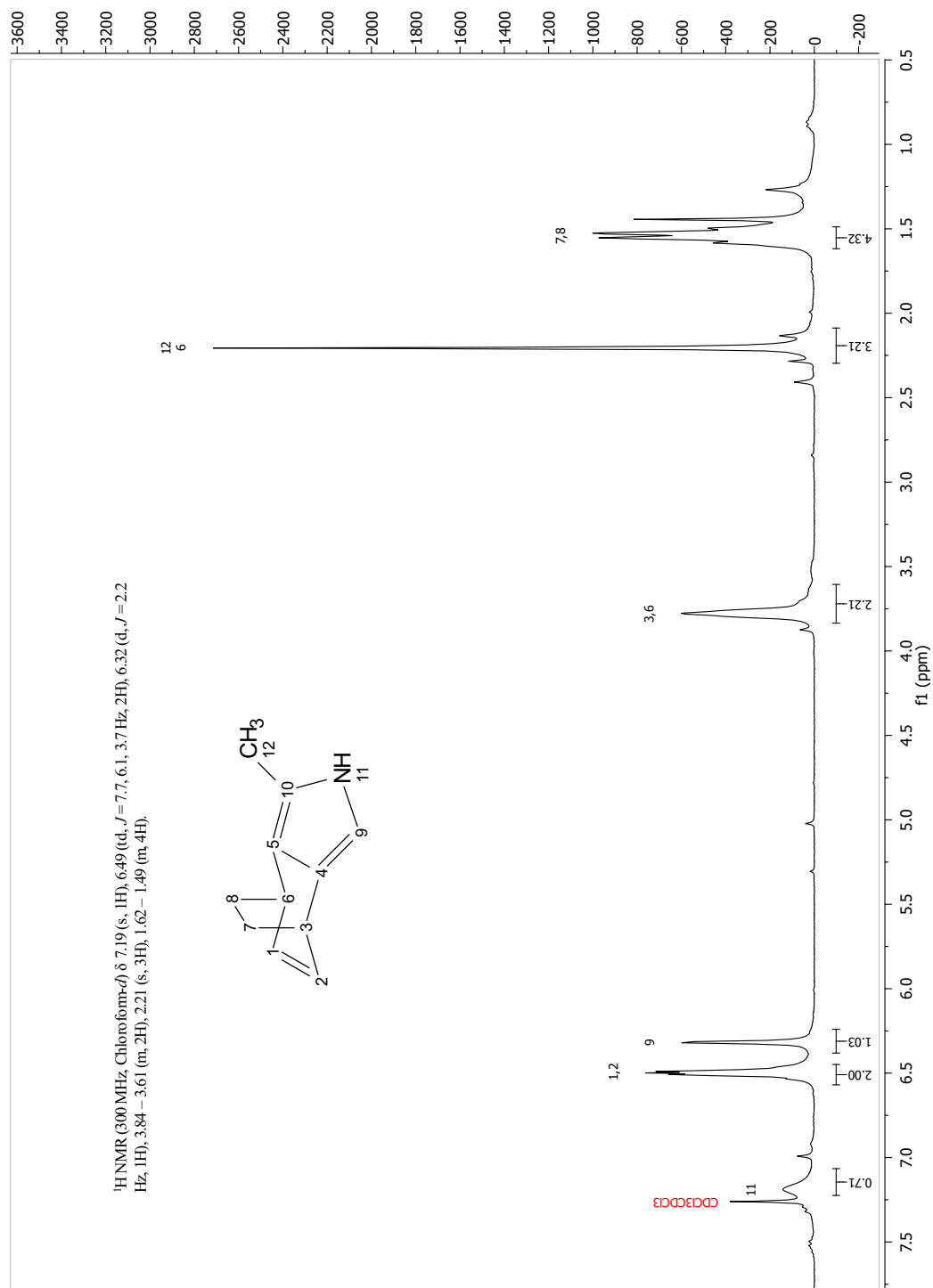


**Figure 10.18:** COSY spectrum (300 MHz, Chloroform) of BCOD fused pyrrole (**35**)

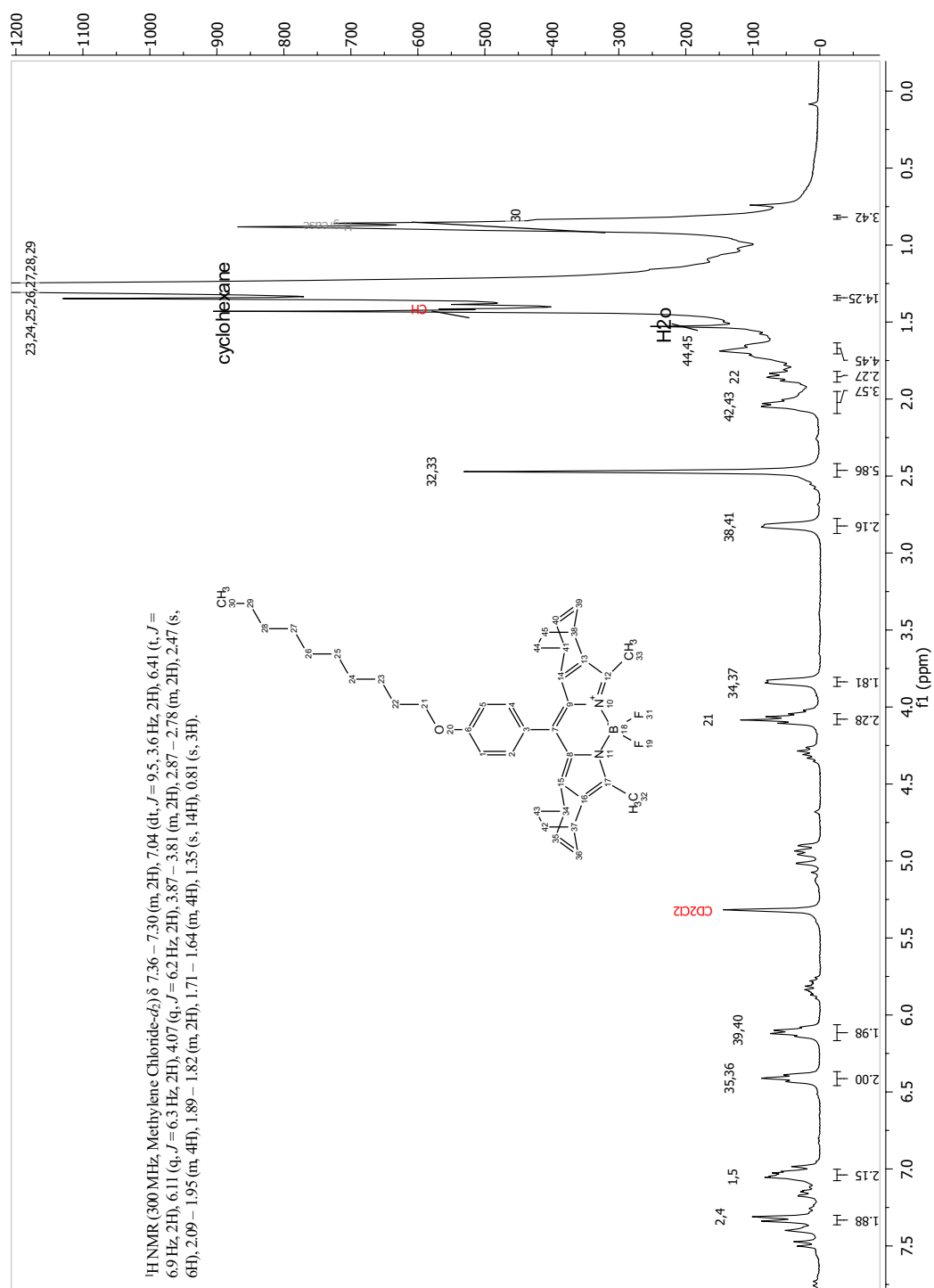


**Figure 10.19:** APT spectrum (76 MHz, Chloroform) of BCOD fused pyrrole (**35**)

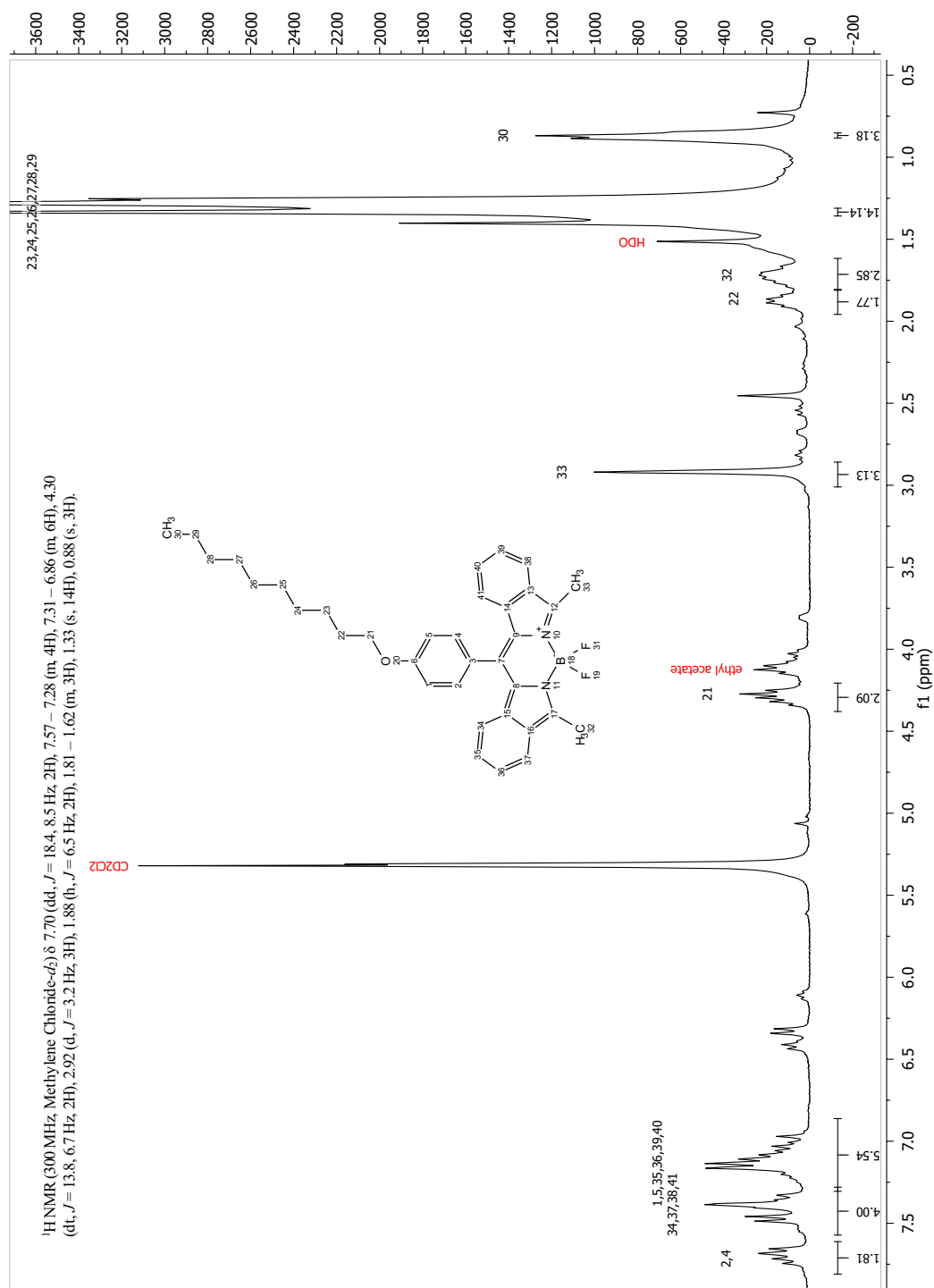
## 10.3.11 Compound 36

Figure 10.20: <sup>1</sup>H NMR spectrum (300 MHz, Chloroform) of compound 36

## 10.3.12 Compound 37

Figure 10.21: <sup>1</sup>H NMR spectrum (300 MHz, Methylene Chloride) of compound 37

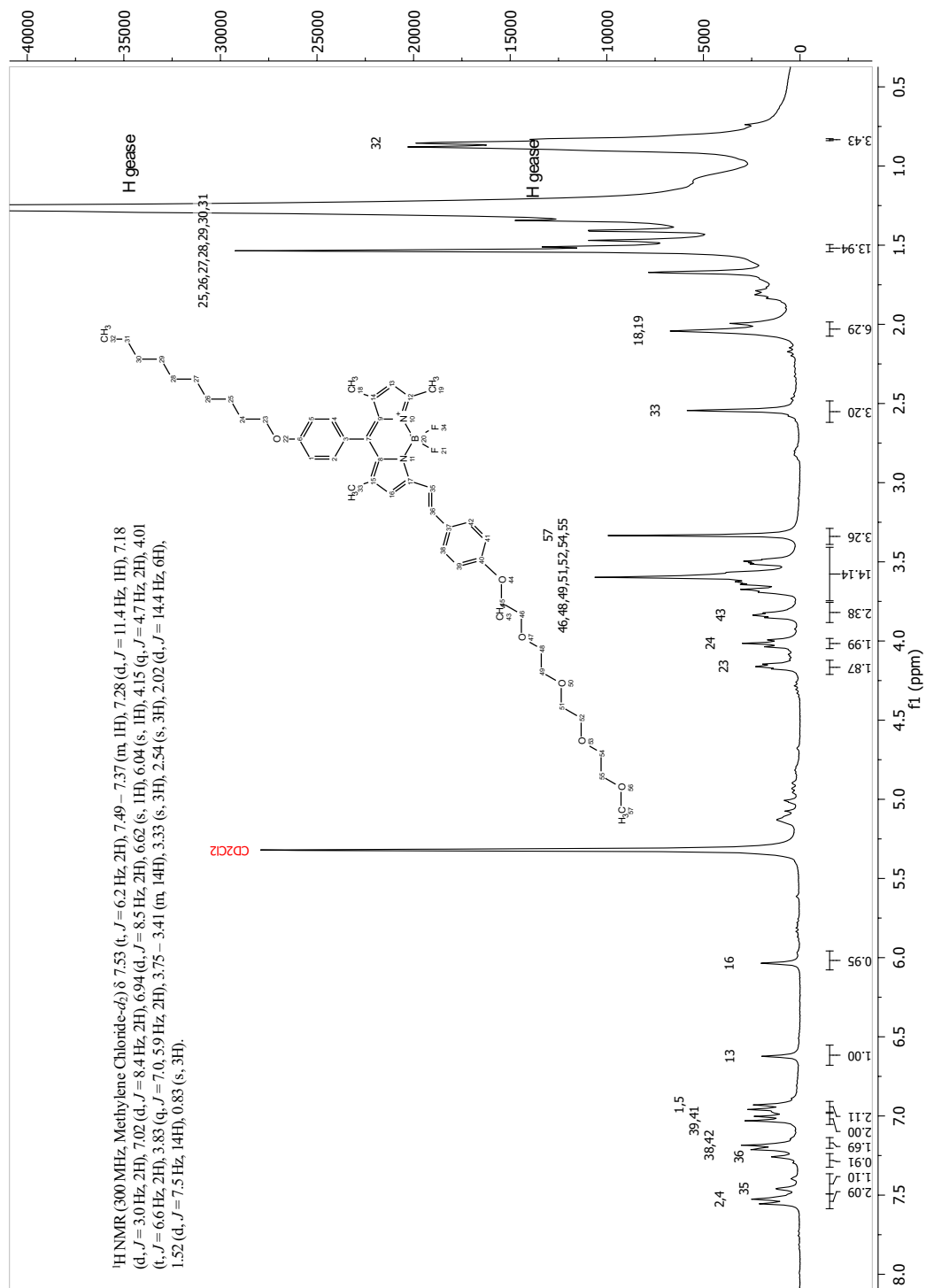
## 10.3.13 Compound 38



**Figure 10.22:**  $^1\text{H}$  NMR spectrum (300 MHz, Methylene Chloride) of the retro Diels-Alder reaction (**38**)



## 10.3.14 Compound 42

Figure 10.23: <sup>1</sup>H NMR spectrum (300 MHz, Methylene Chloride) of compound 42

## 10.3.15 Compound 43

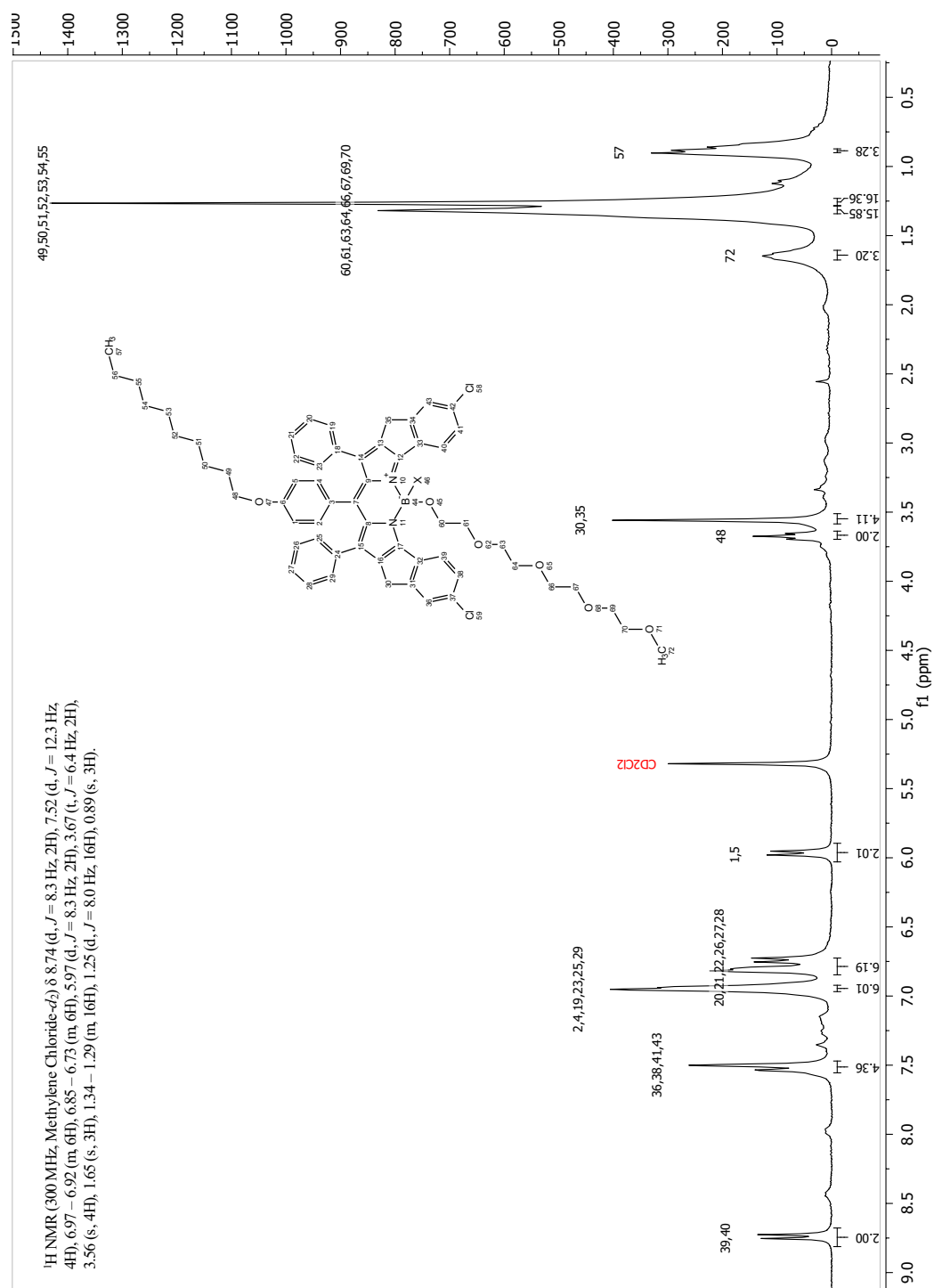


**Figure 10.24:** <sup>1</sup>H NMR spectrum (300 MHz, Methylene Chloride) of C-rigid m-decyloxy B-TEG BODIPY (**43**)

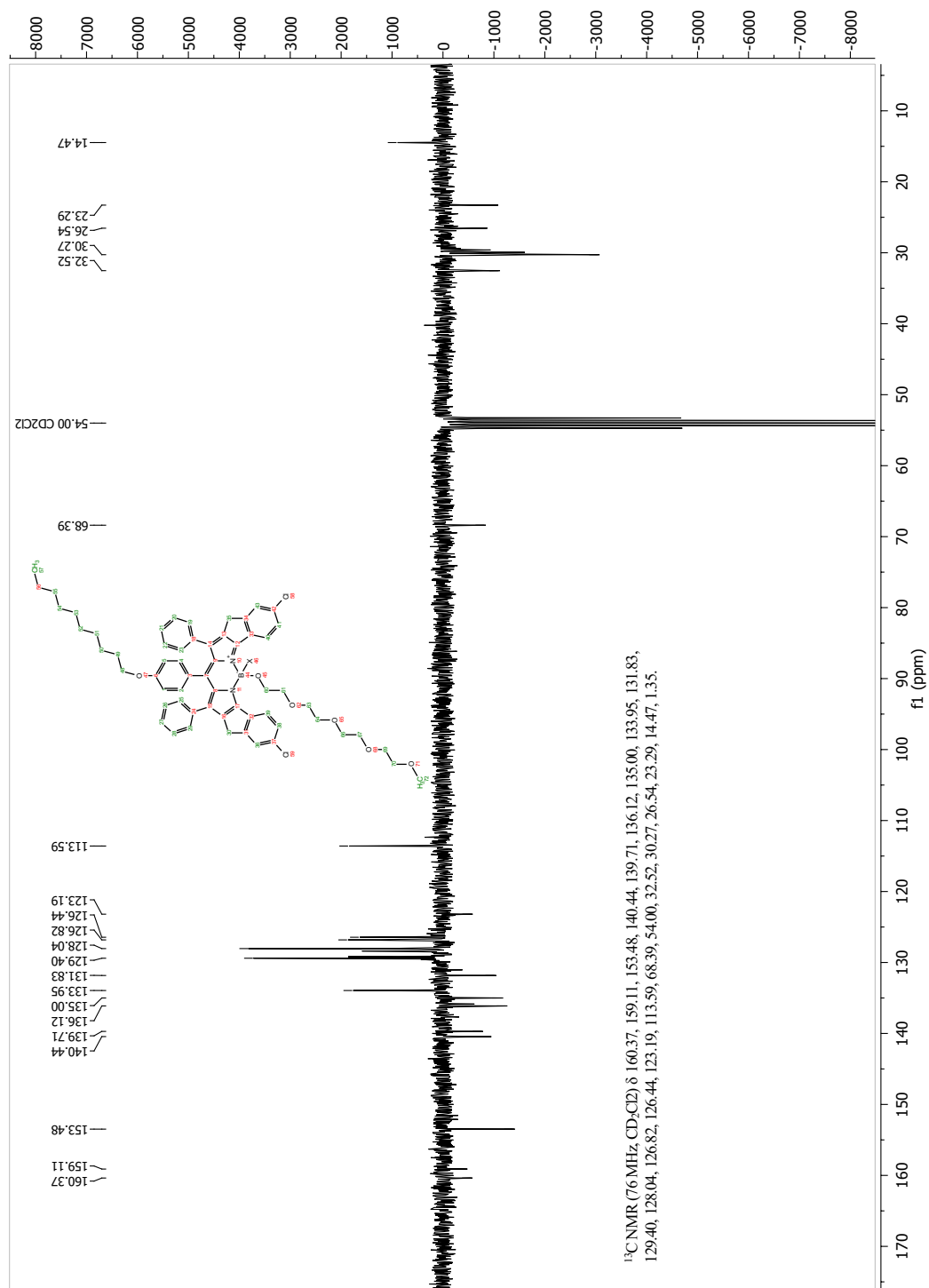
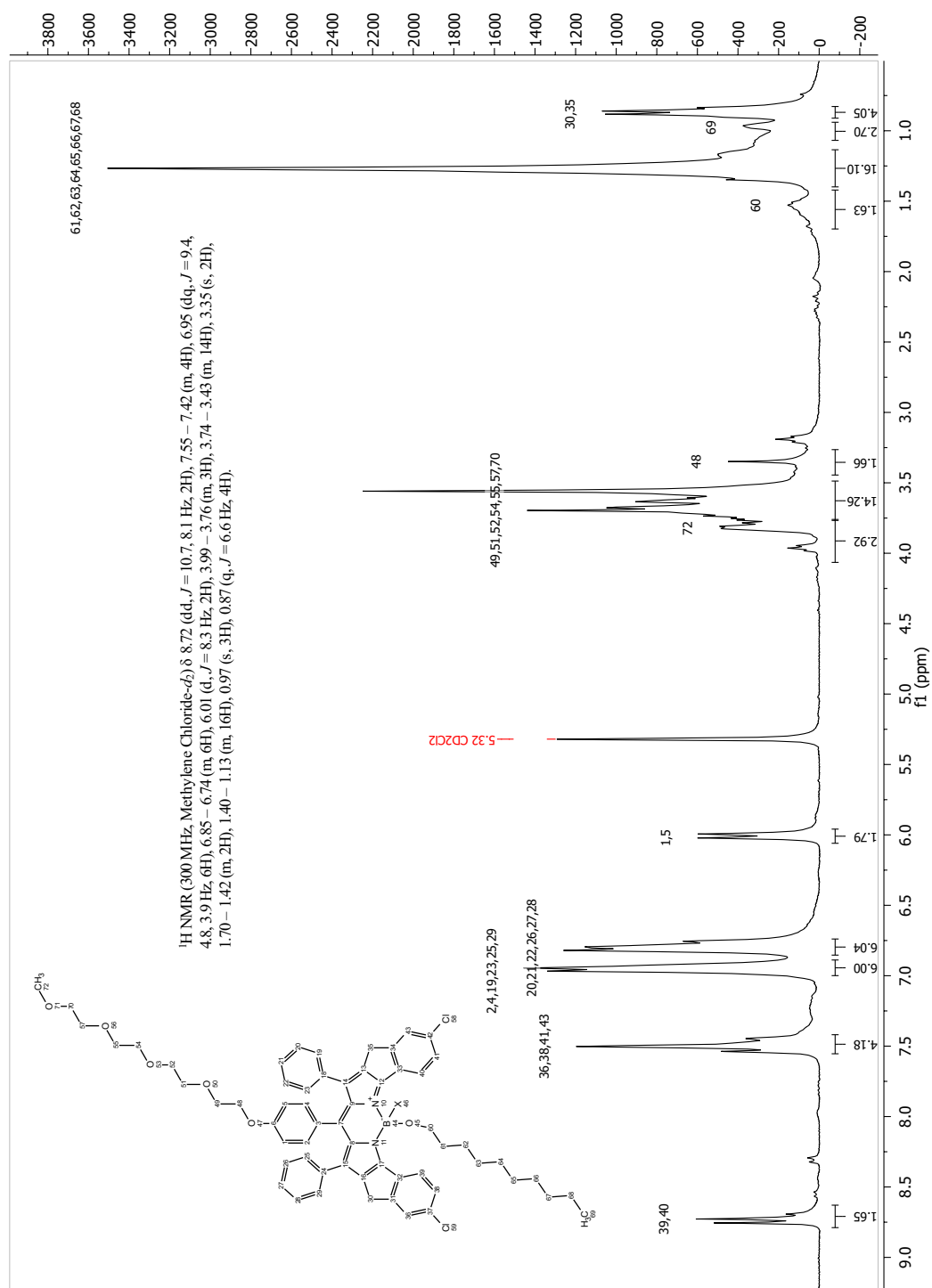


Figure 10.25: APT spectrum (76 MHz, Methylene Chloride) of compound (43)

## 10.3.16 Compound 44



**Figure 10.26:** <sup>1</sup>H NMR spectrum (300 MHz, Methylene Chloride) of Cl-rigid m-TEG BODIPY (44)

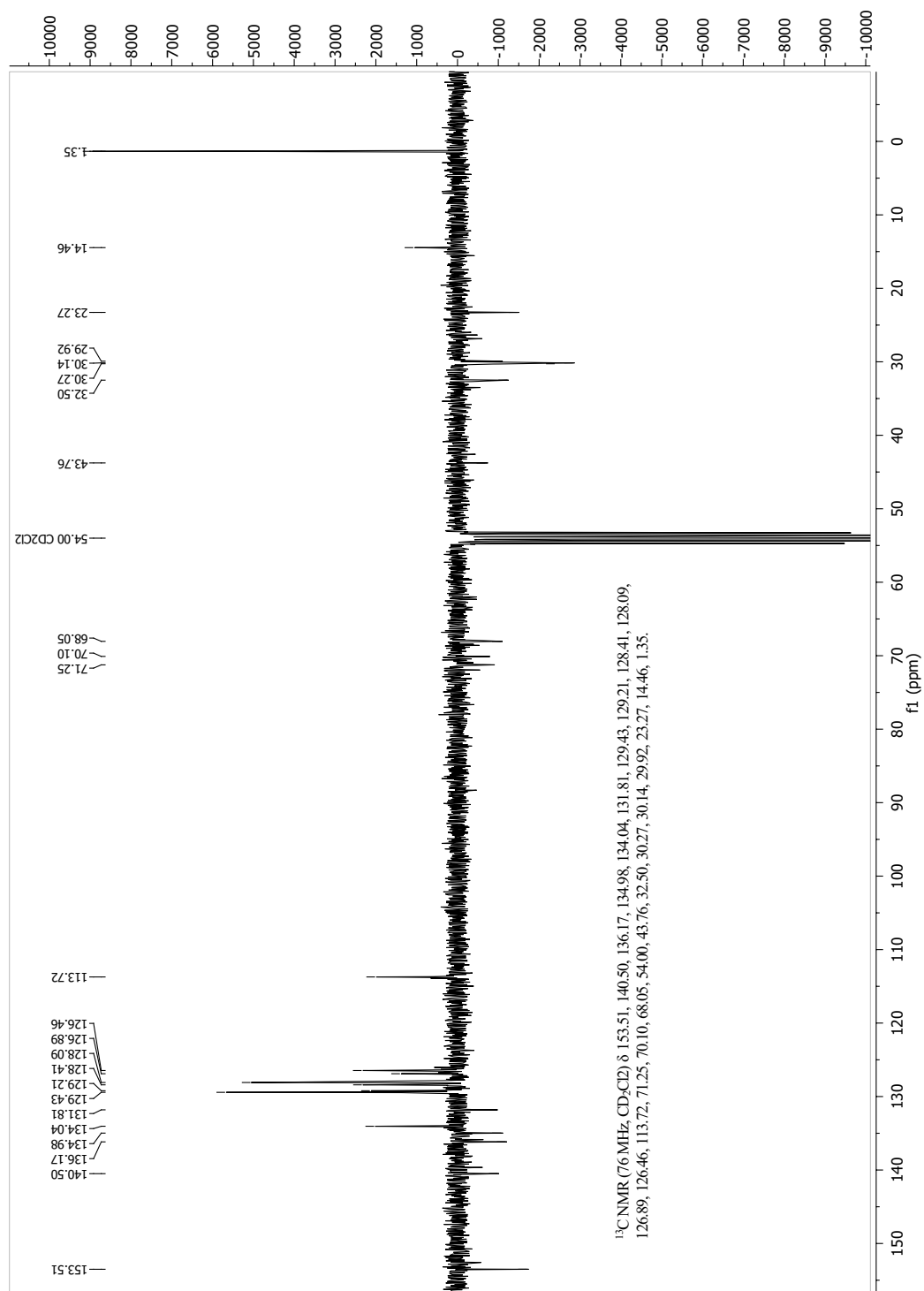
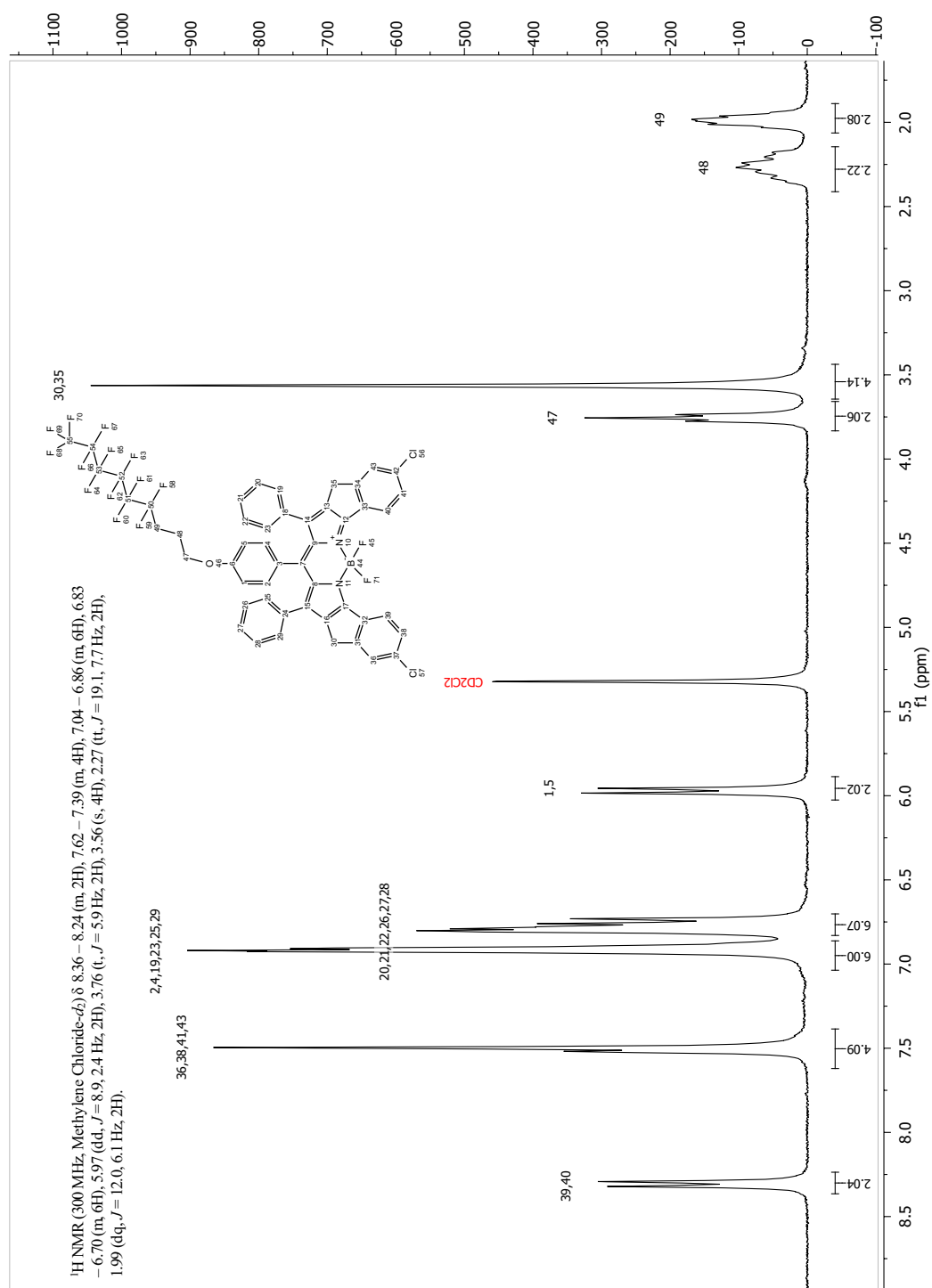


Figure 10.27: APT spectrum (76 MHz, Methylene Chloride) of compound (44)

## 10.3.17 Compound 45



**Figure 10.28:** <sup>1</sup>H NMR spectrum (300 MHz, Methylene Chloride) of Cl-rigid m-perfluoro BODIPY (45)

## 10.3.18 Compound 47

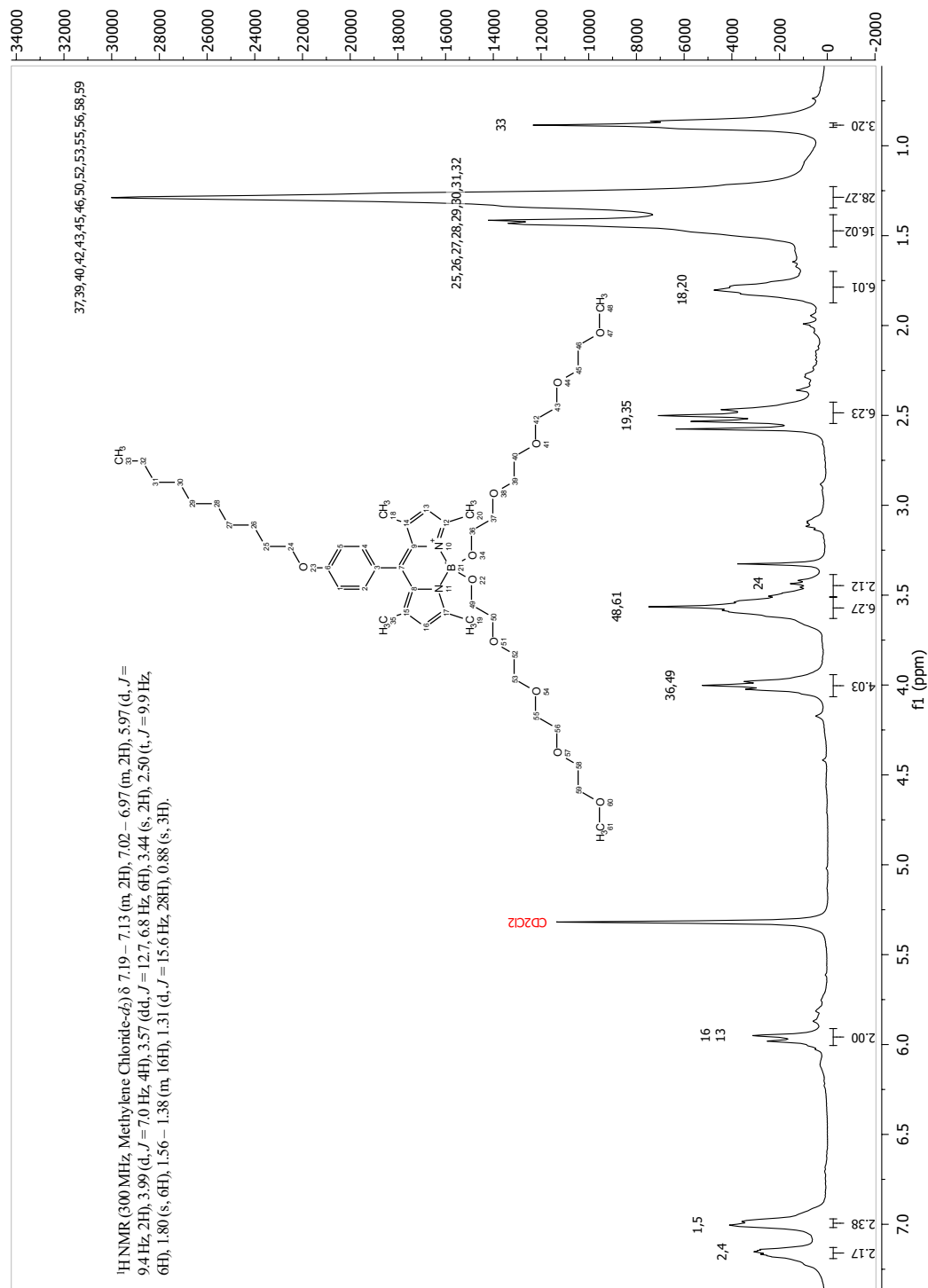


**Figure 10.29:** <sup>1</sup>H NMR spectrum (300 MHz, Methylene Chloride) of tetramethyl m-decyloxy B-TEG BODIPY (47)

## 10.4 MS Data

## 10.4.1 Compound 21

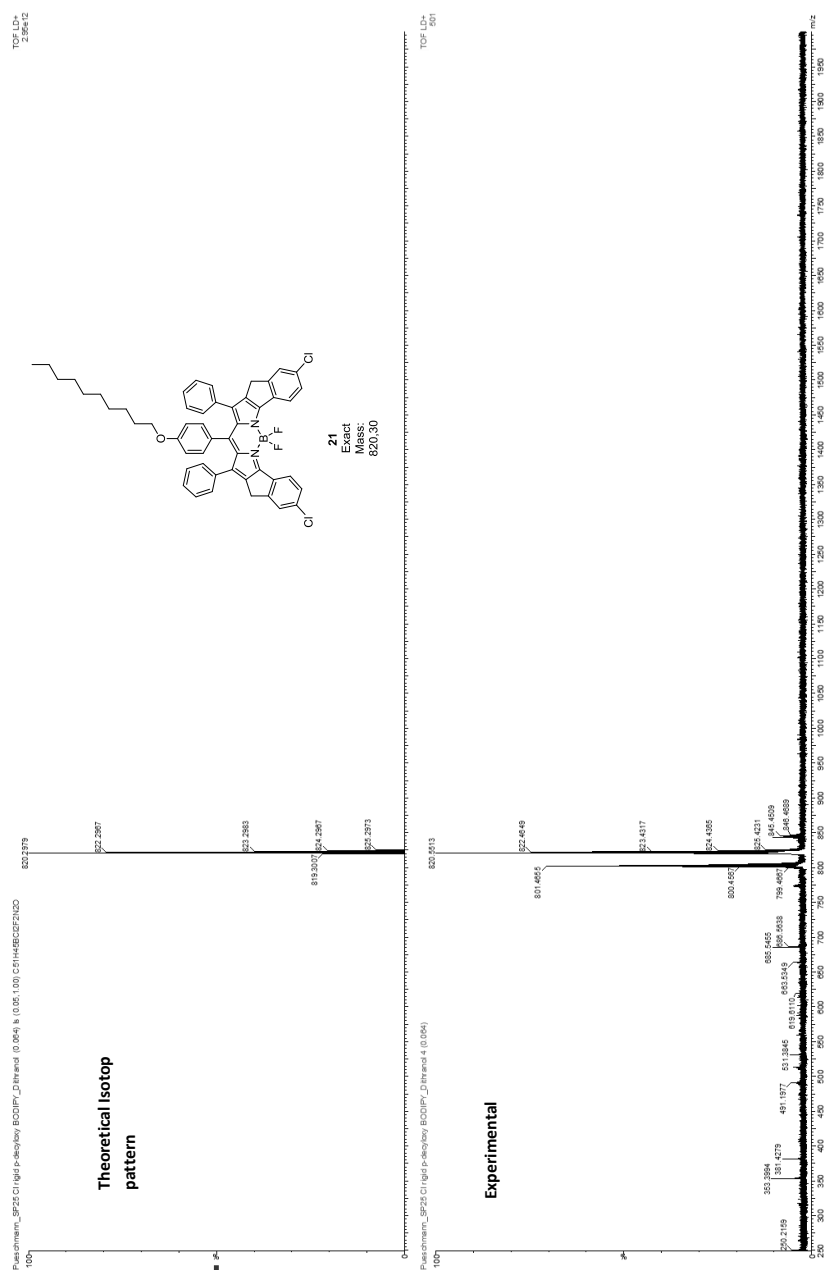


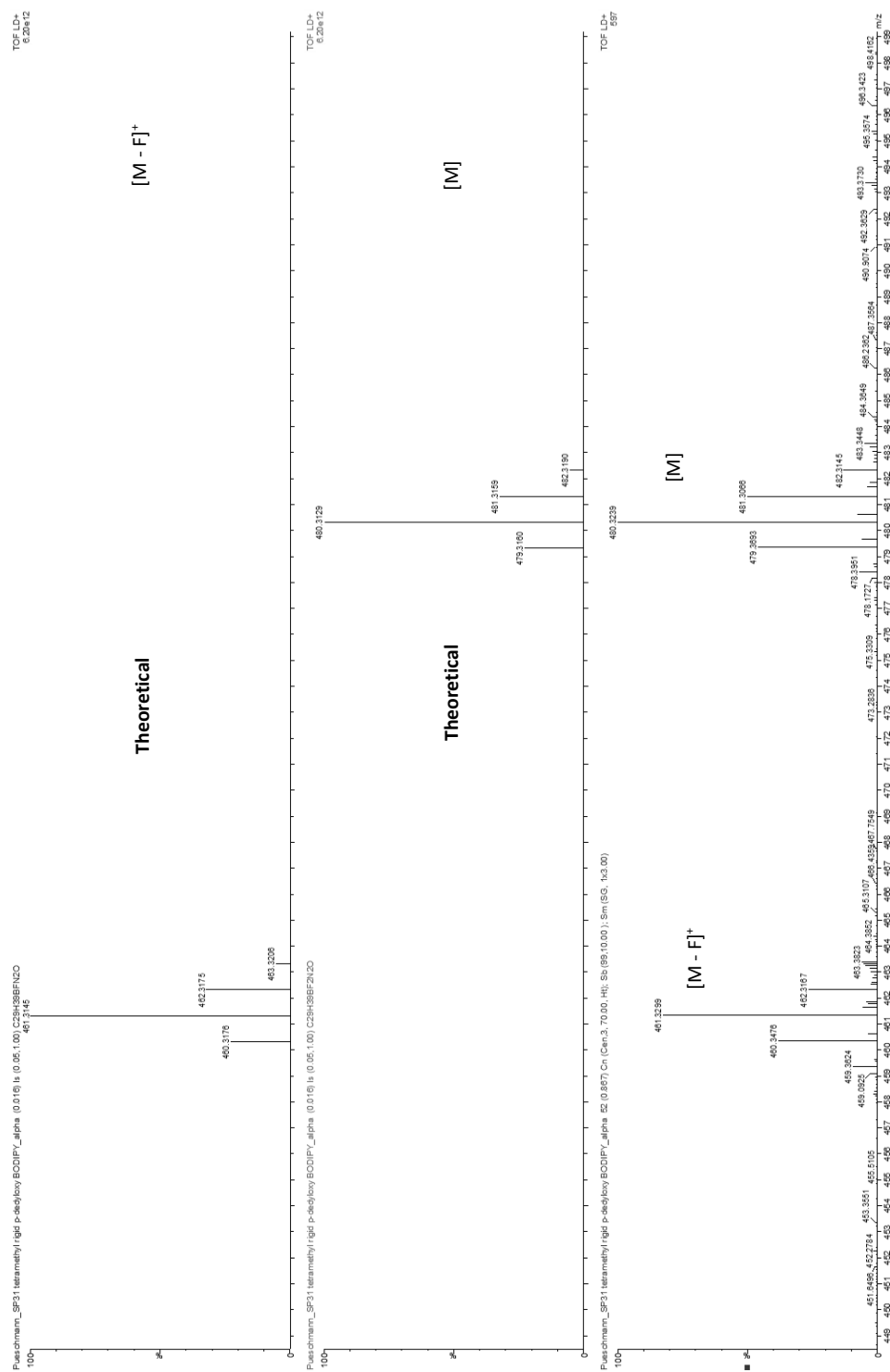
**Figure 10.30:** whole MALDI-TOF spectrum of compound **21** in dithranol matrix with the corresponding isotope pattern





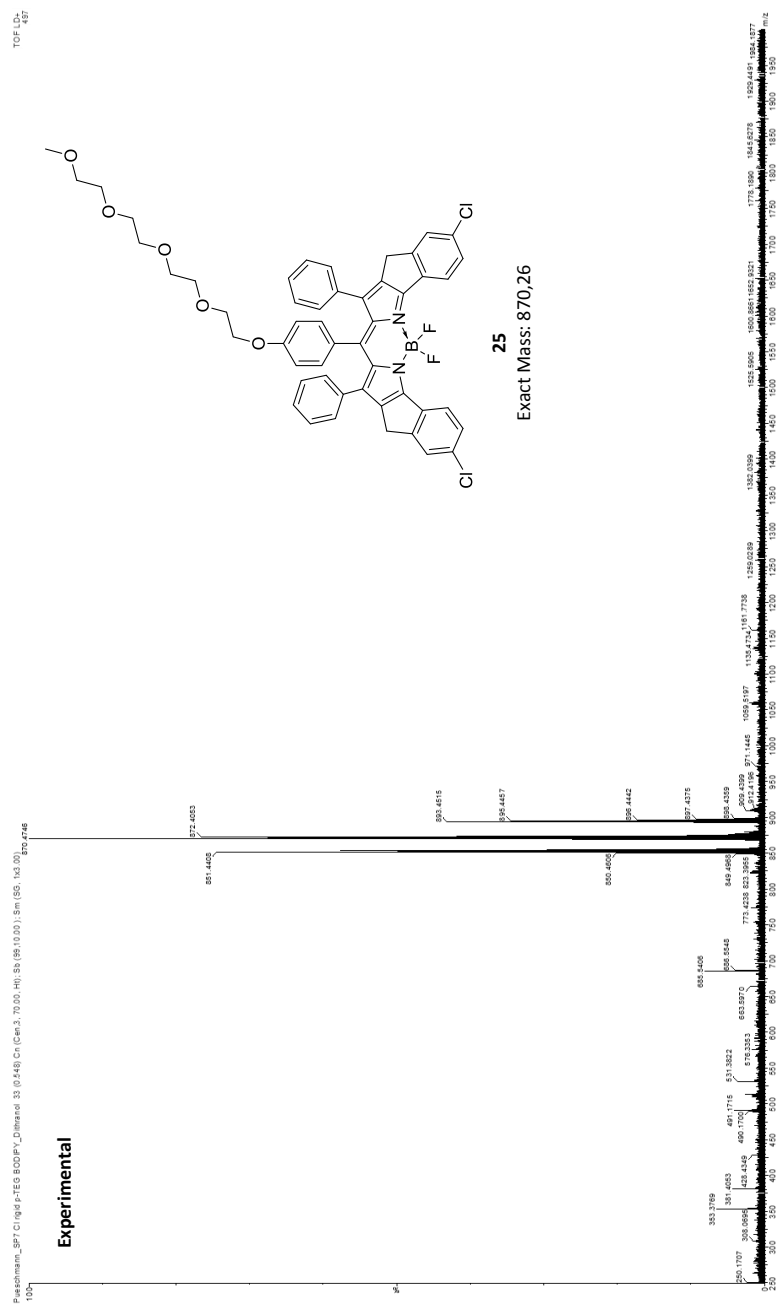
**Figure 10.31:** MALDI-TOF spectrum of compound **21** in dithranol matrix with the corresponding isotope pattern





**Figure 10.33:** MALDI-TOF spectrum of compound 22 in alpha matrix with the corresponding isotope pattern

## 10.4.3 Compound 25

Figure 10.34: MALDI-TOF of compound **25** in dithranol matrix

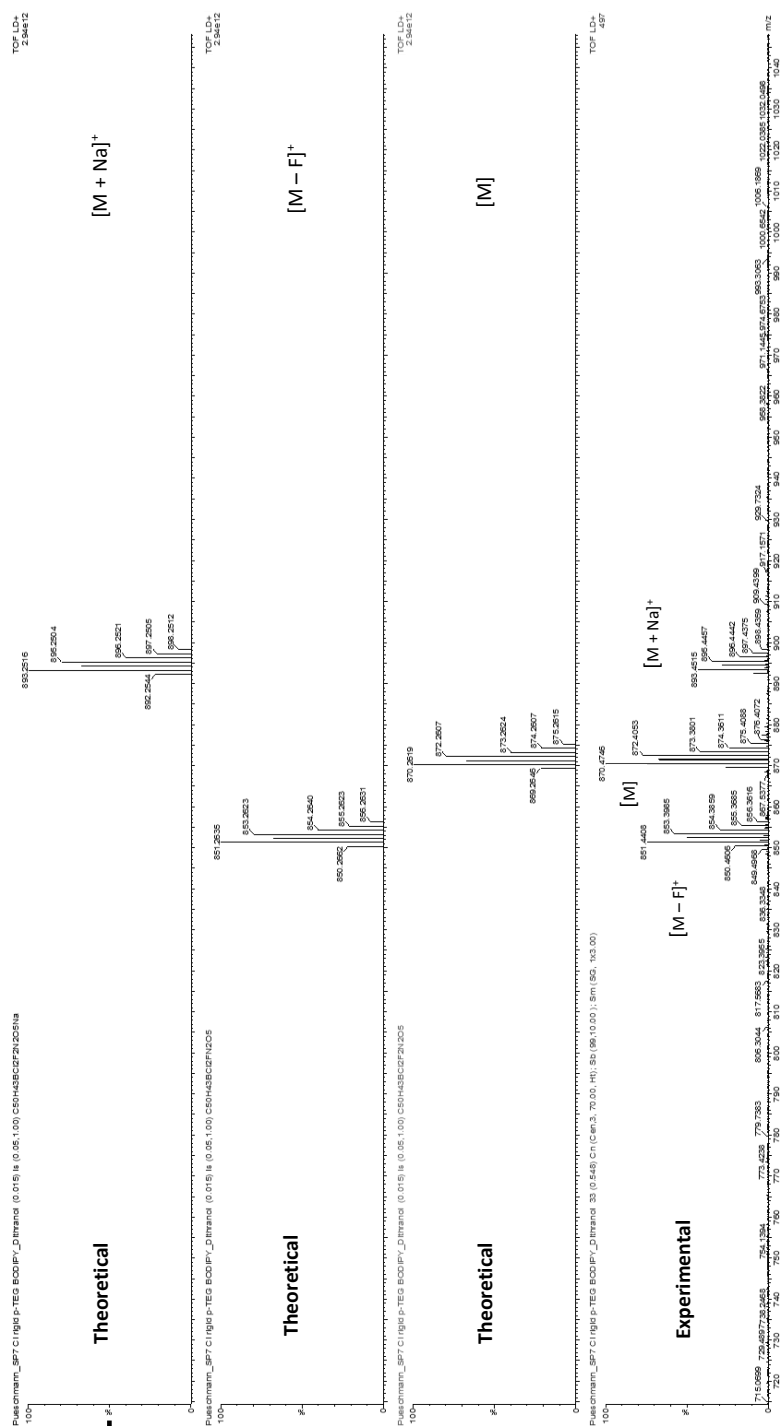


**Figure 10.35:** MALDI-TOF of m-TEG BODIPY (25) in dithranol matrix with corresponding isotope pattern

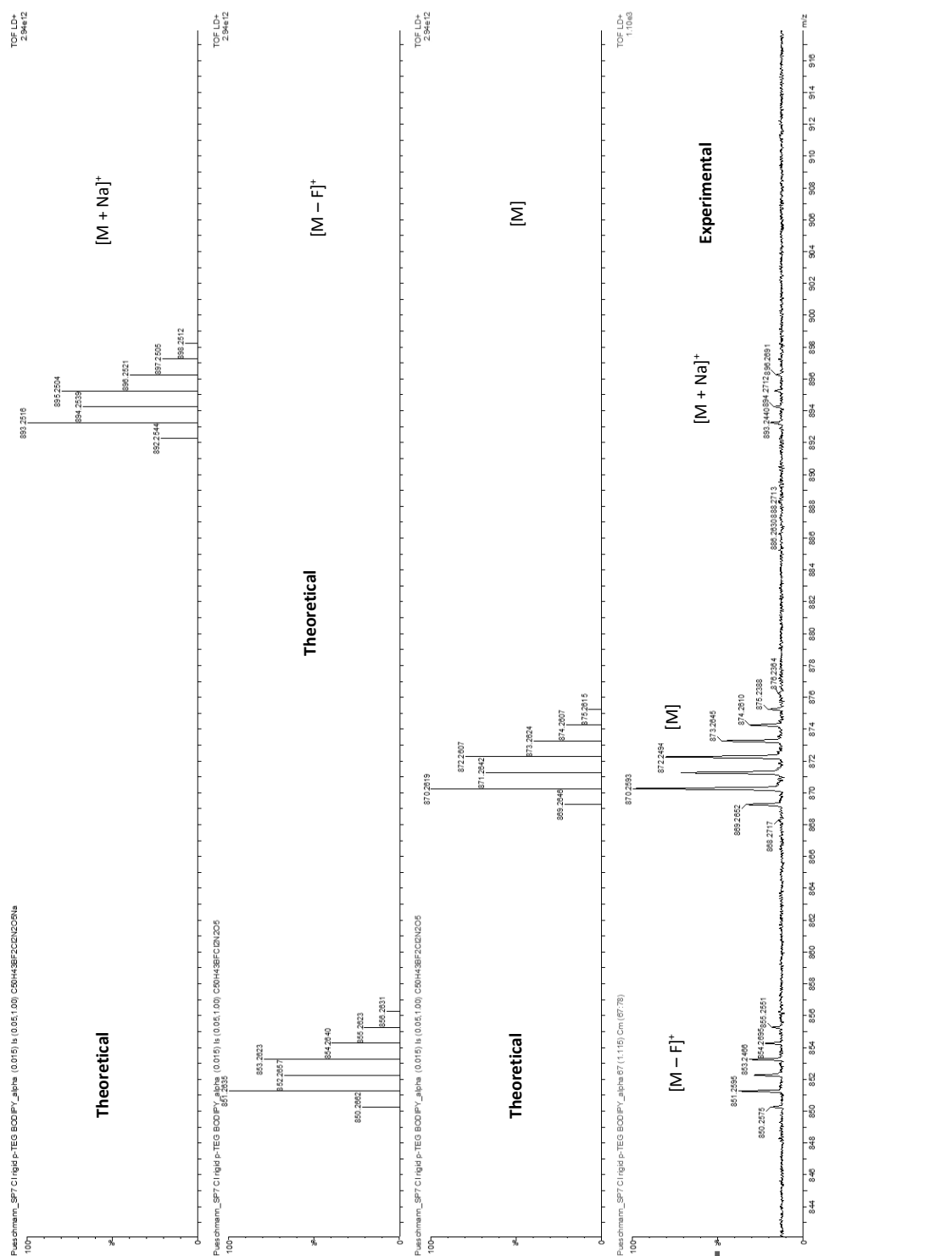


**Figure 10.36:** MALDI-TOF of m-TEG BODIPY (**25**) in alpha matrix with corresponding isotope pattern

## 10.4.4 Compound 27

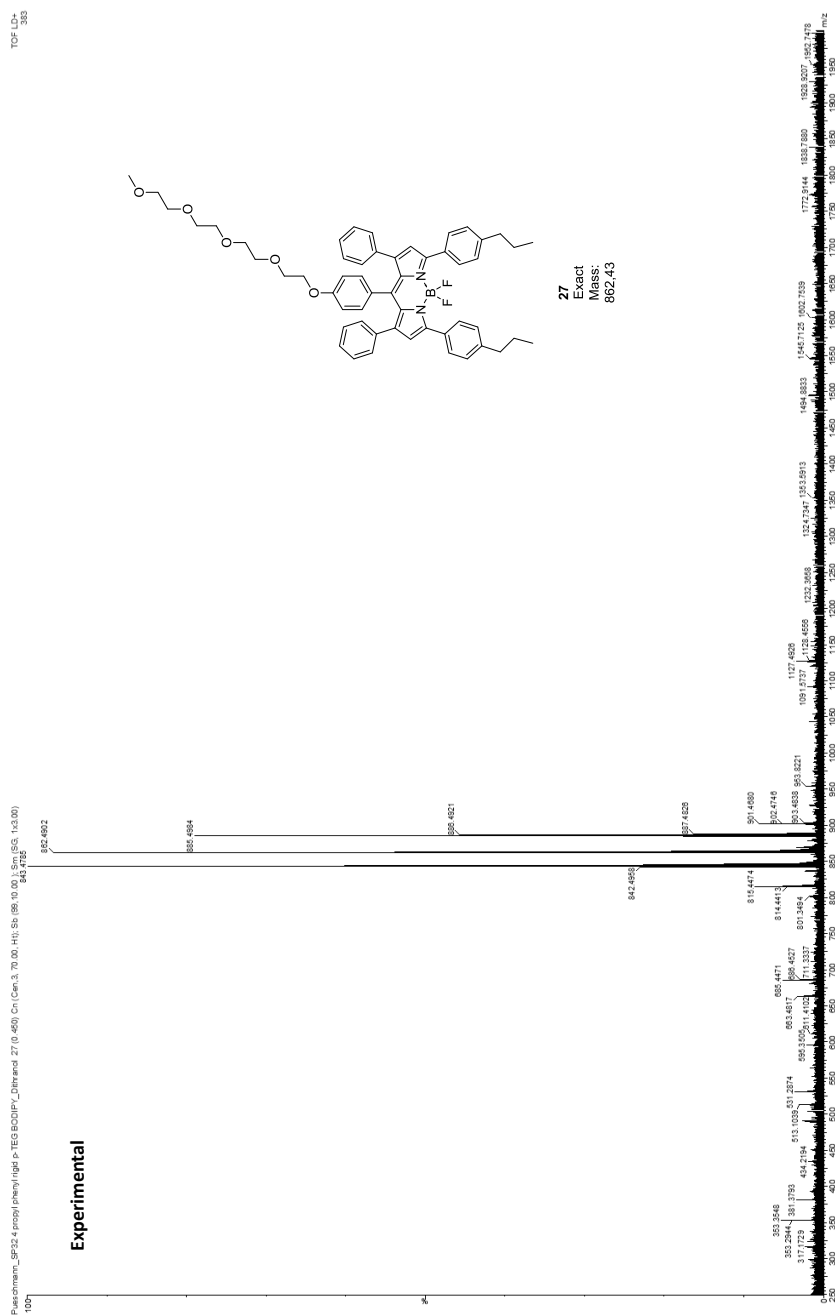
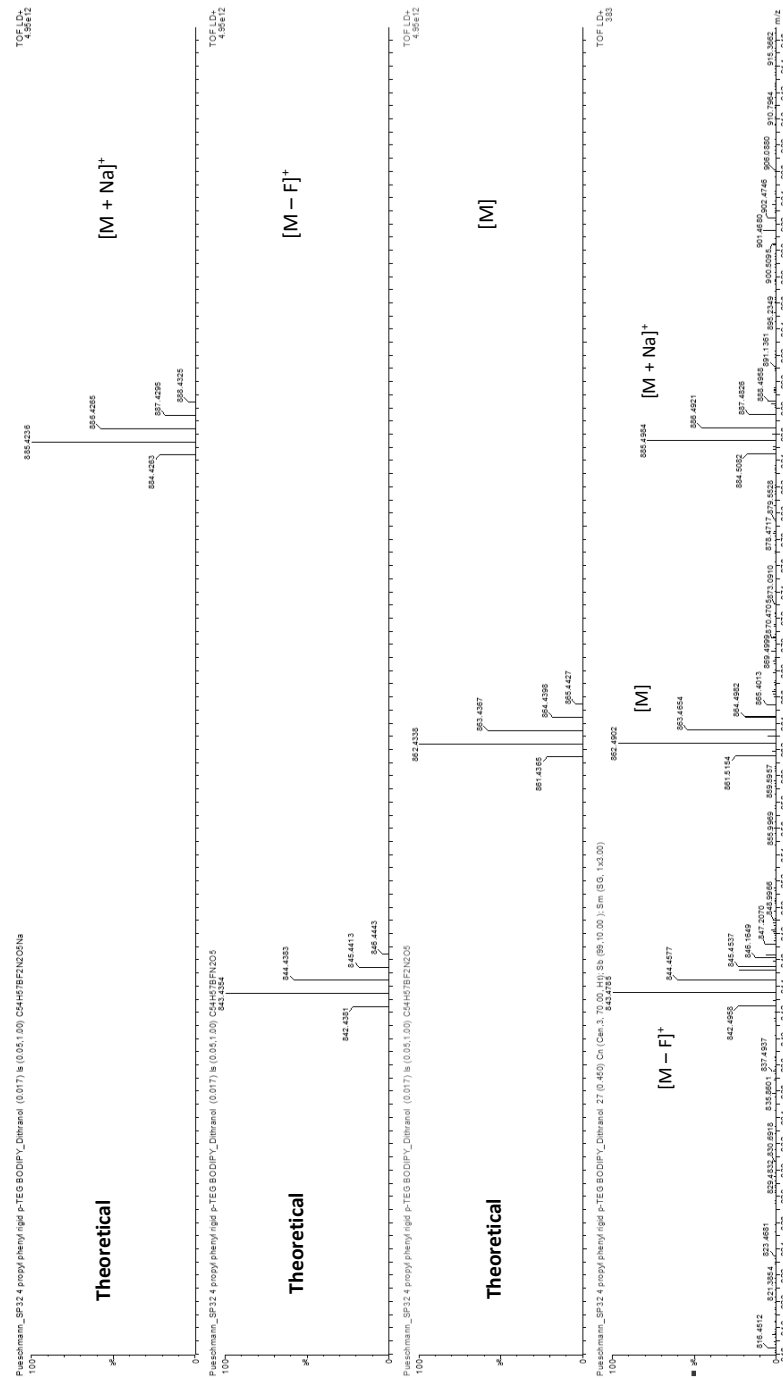
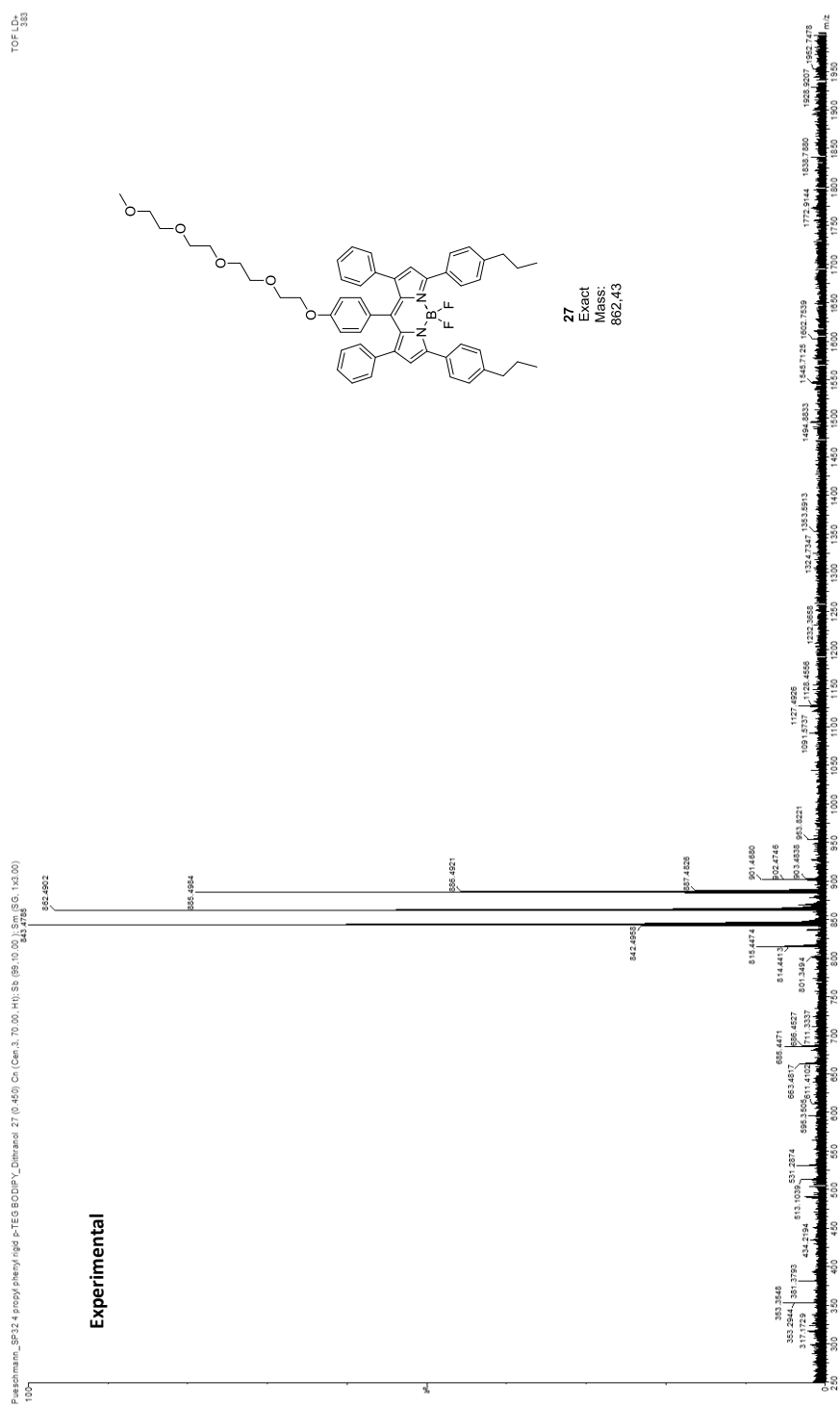


Figure 10.37: Experimental MALDI-TOF of compound 27 in dithranol matrix



**Figure 10.38:** MALDI-TOF of compound **27** in dithranol matrix with corresponding isotope pattern





**Figure 10.39:** Experimental MALDI-TOF of compound **27** in alpha matrix with corresponding isotope pattern

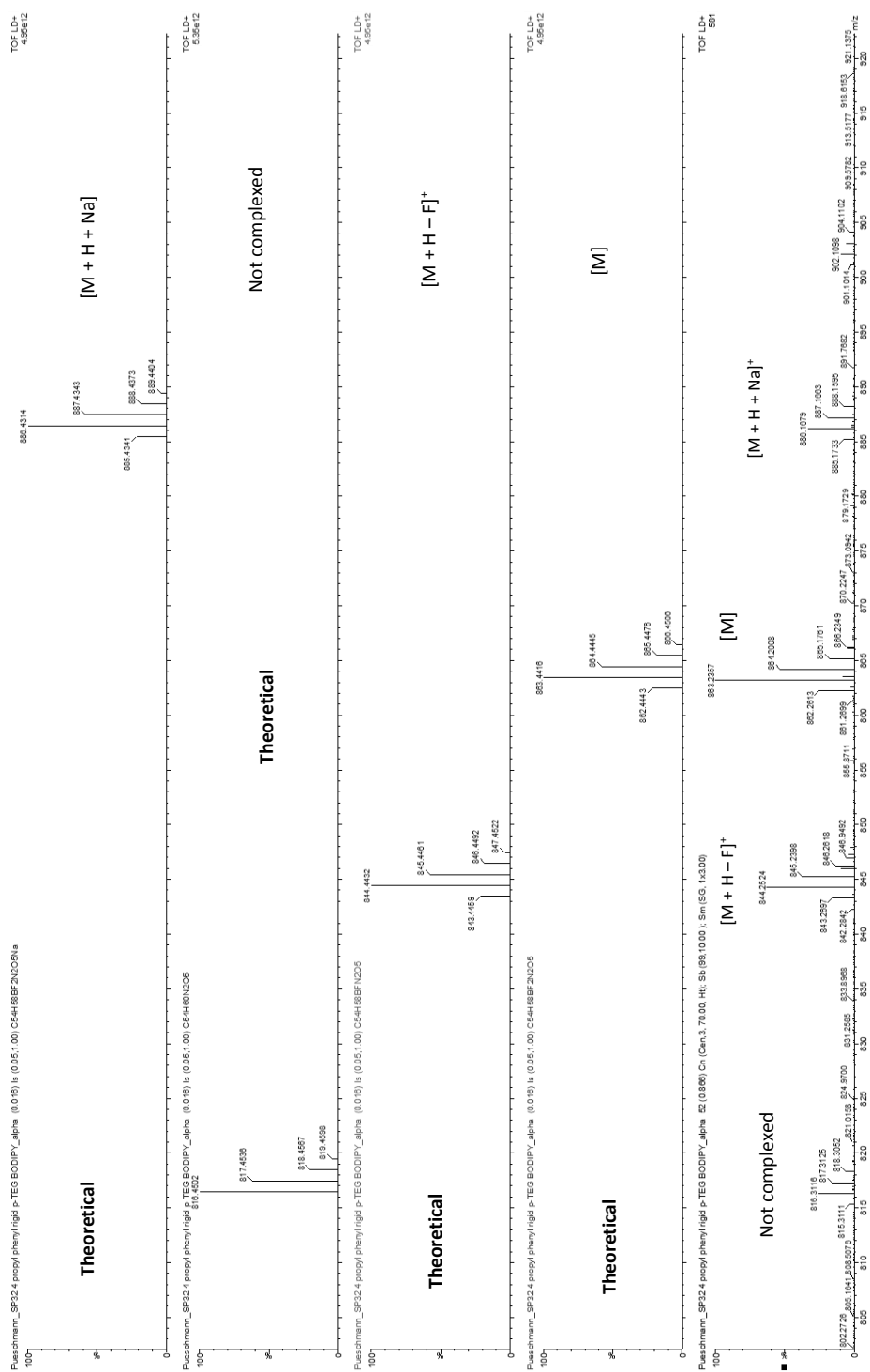


**Figure 10.40:** MALDI-TOF of compound **27** in alpha matrix with corresponding isotope pattern

## 10.4.5 Compound 38

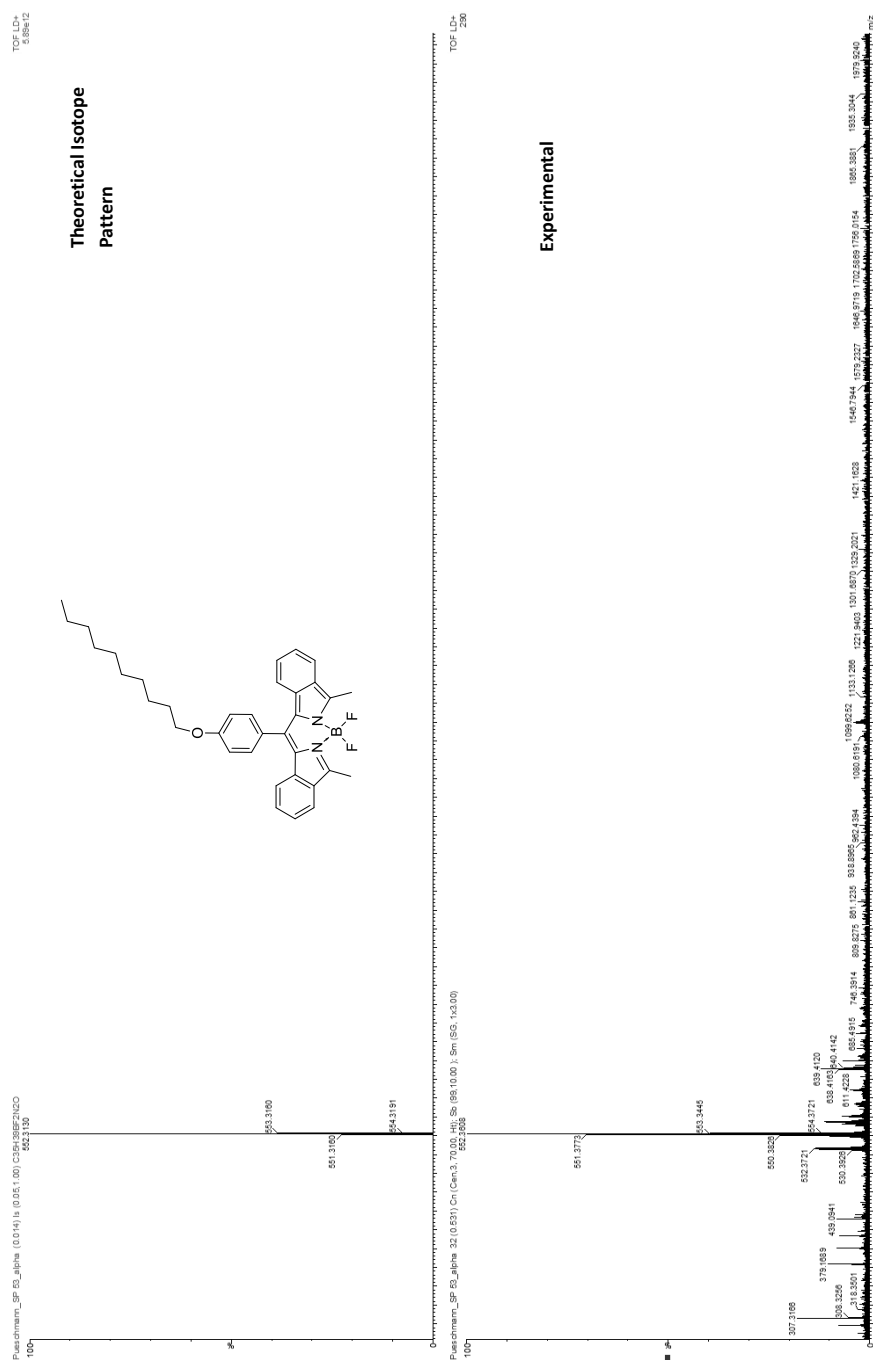


**Figure 10.41:** MALDI-TOF of compound 38 in alpha matrix with corresponding isotope pattern

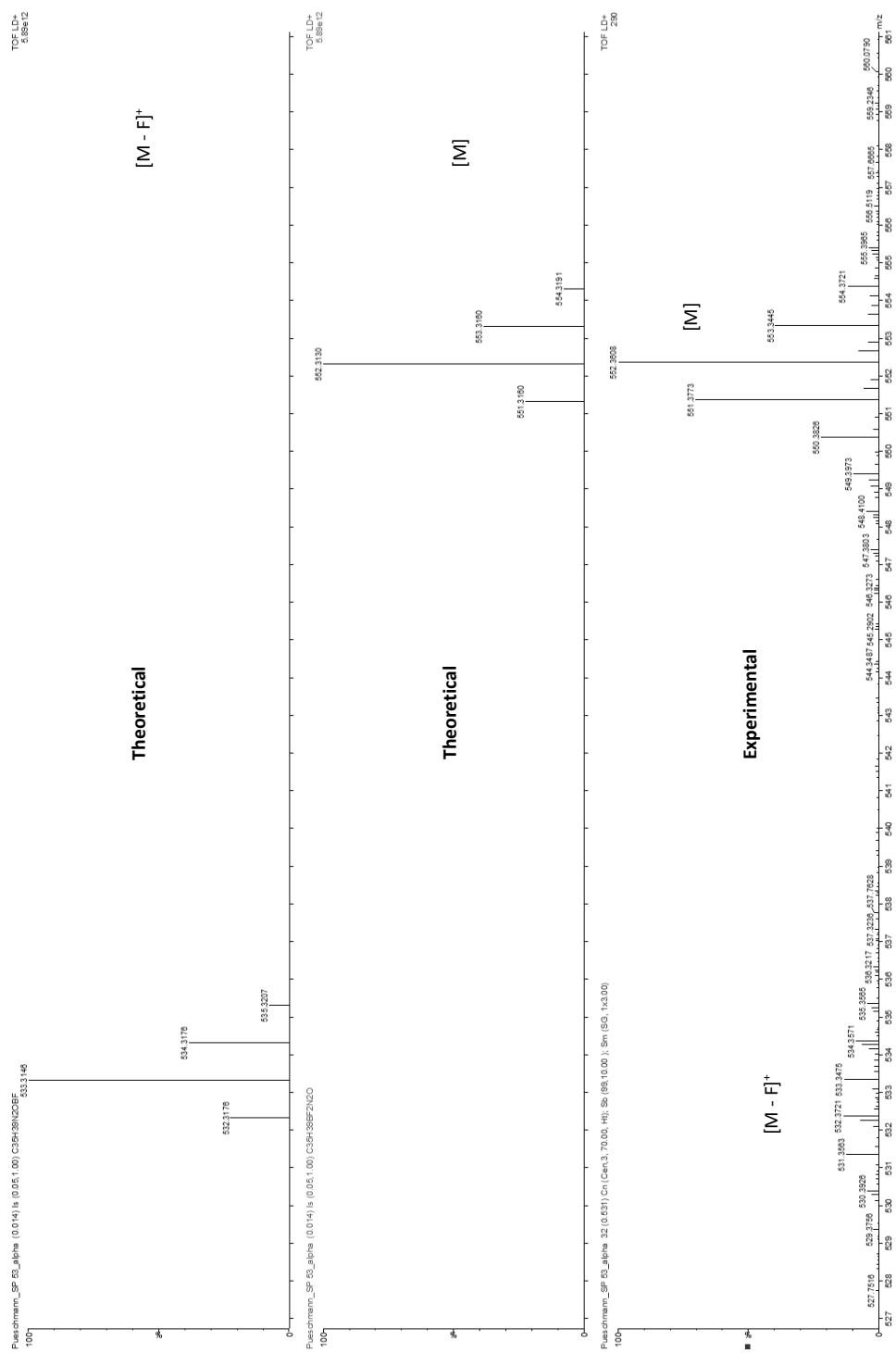


**Figure 10.42:** MALDI-TOF of compound **38** in alpha matrix with corresponding isotope pattern

## 10.4.6 Compound 43

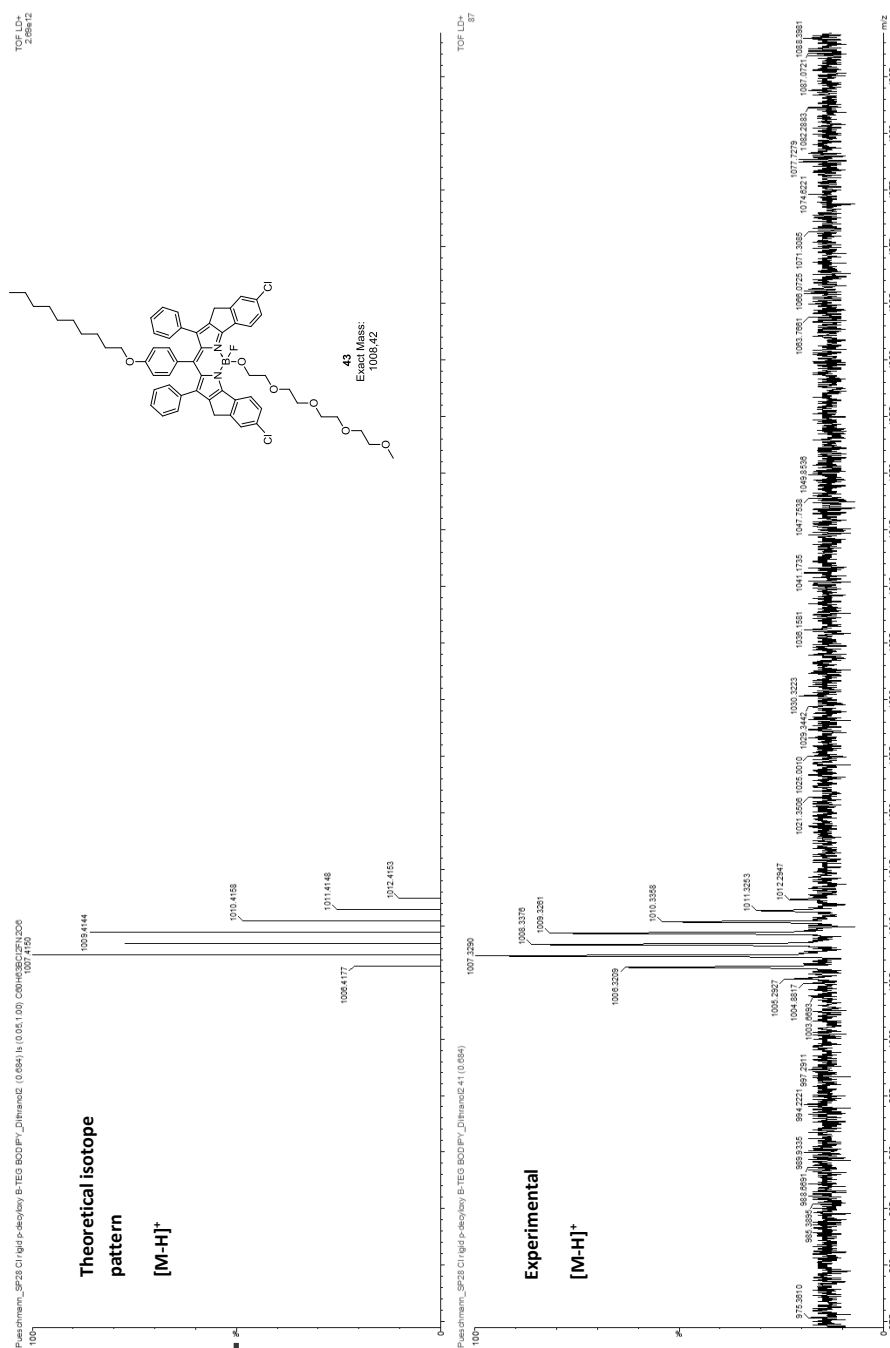


Figure 10.43: MALDI-TOF of 43 in dithranol matrix with corresponding isotope pattern

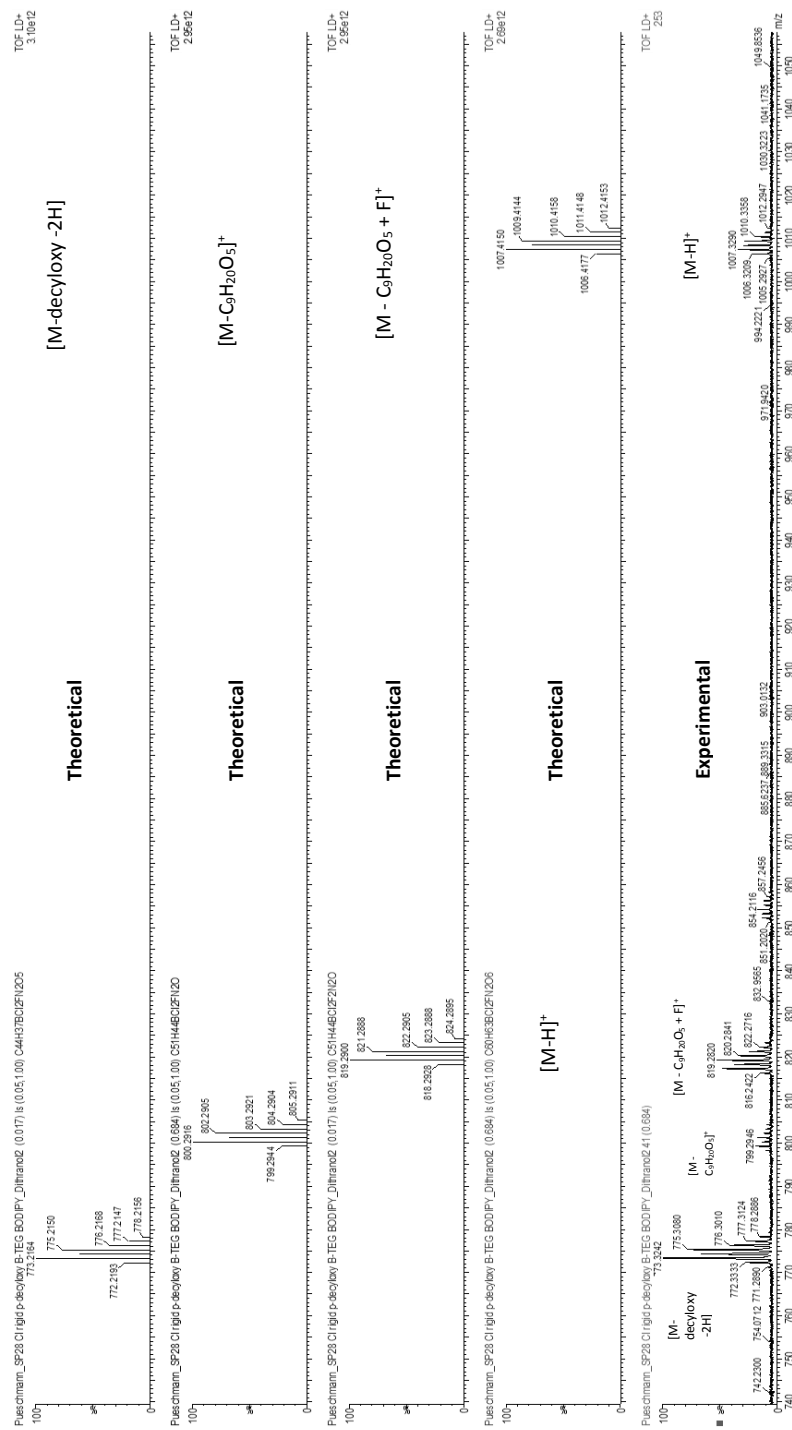
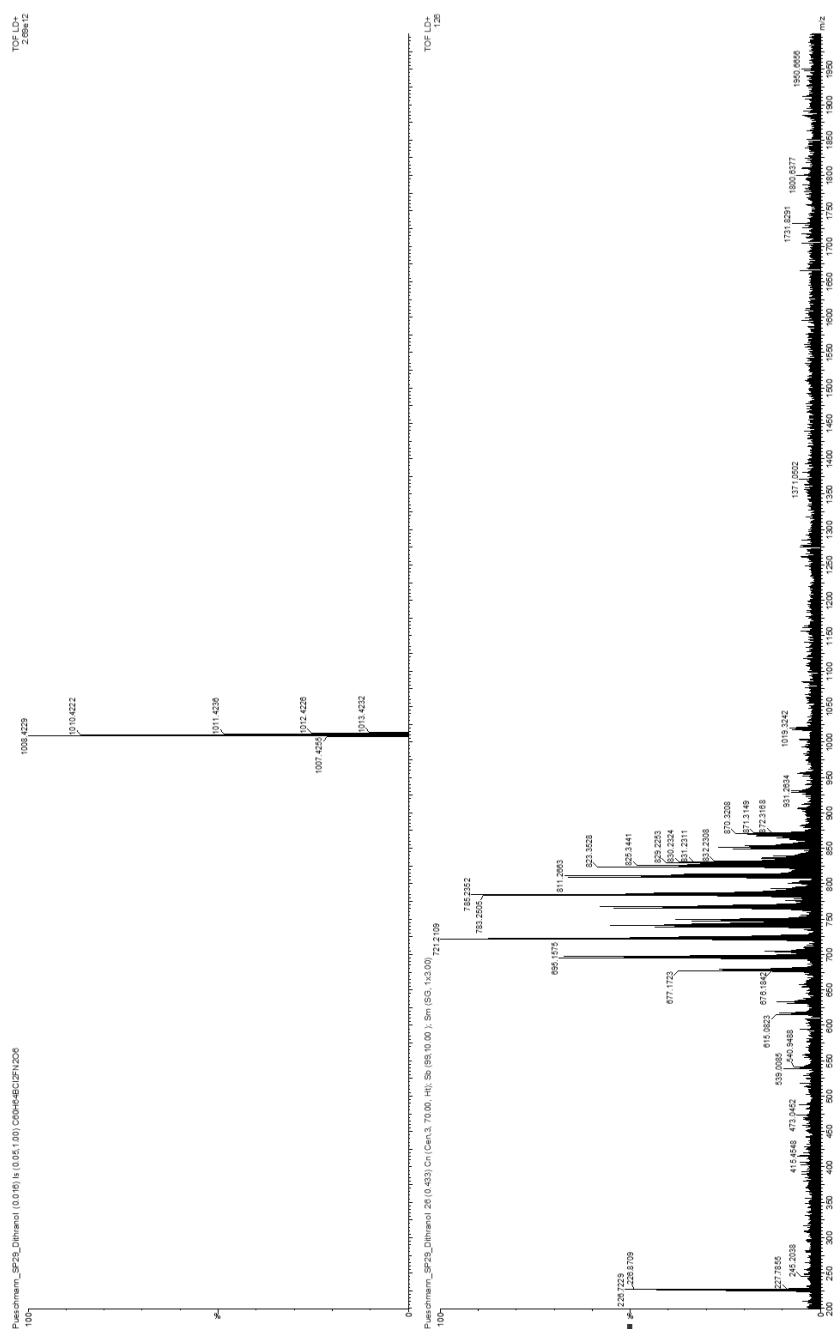


Figure 10.44: MALDI-TOF of 43 in dithranol matrix with corresponding isotope pattern

## 10.4.7 Compound 44



**Figure 10.45:** MALDI-TOF of 44 in dithranol matrix with corresponding isotope pattern shows only defragmentation

## 10.4.8 Compound 45

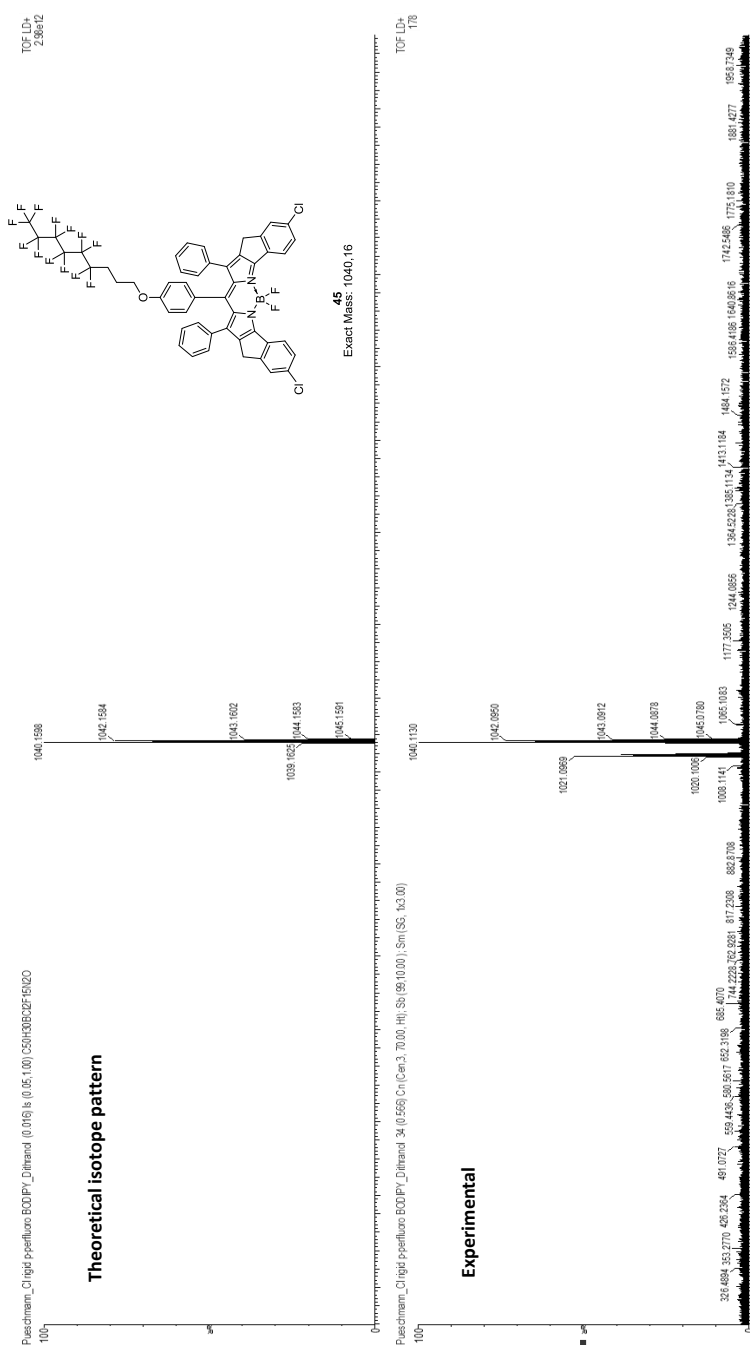


**Figure 10.46:** MALDI-TOF of m-perfluoro BODIPY (45) in dithranol matrix with corresponding isotope pattern



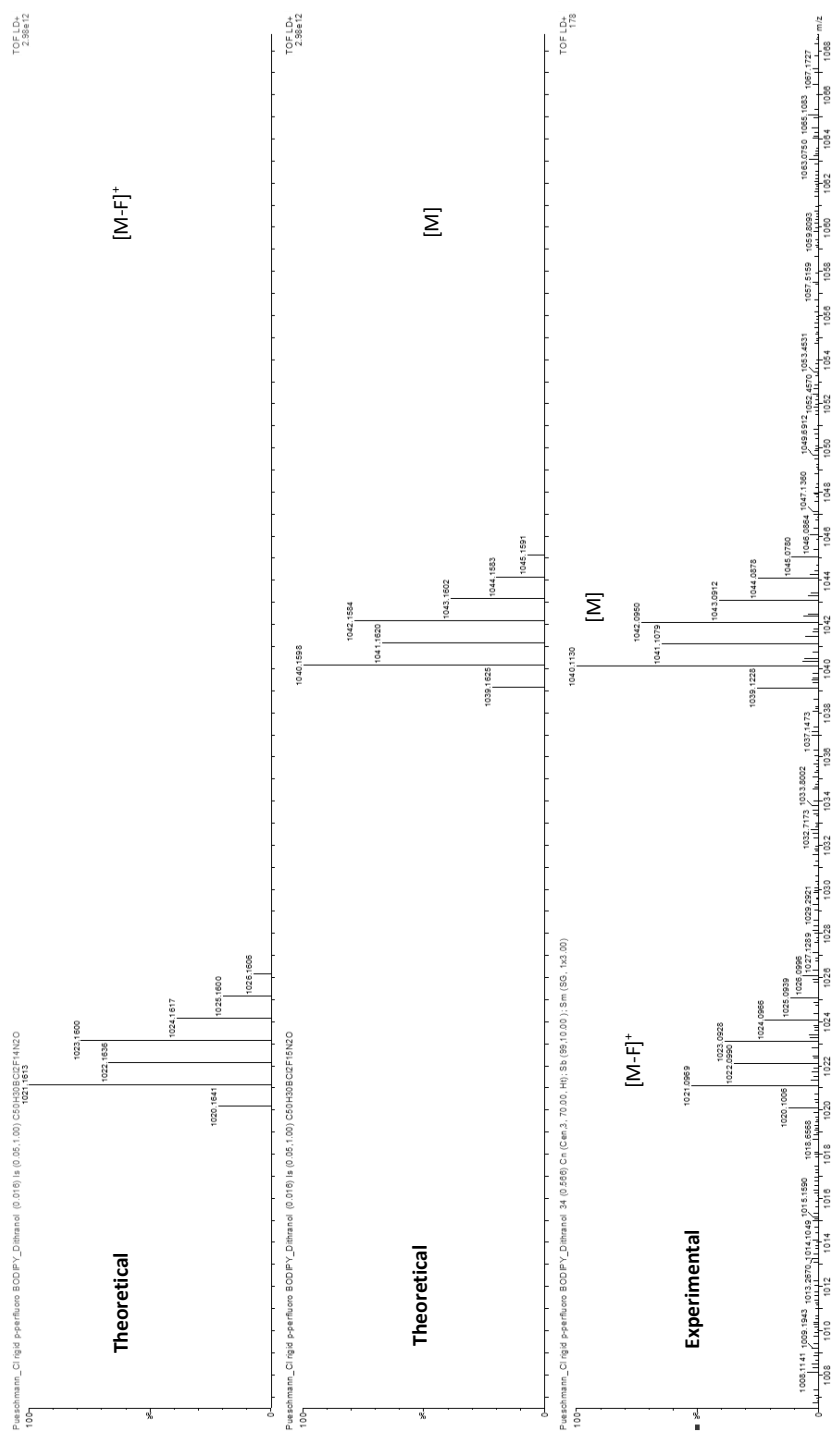


**Figure 10.47:** MALDI-TOF of m-perfluoro BODIPY (45) in dithranol matrix with corresponding isotope pattern

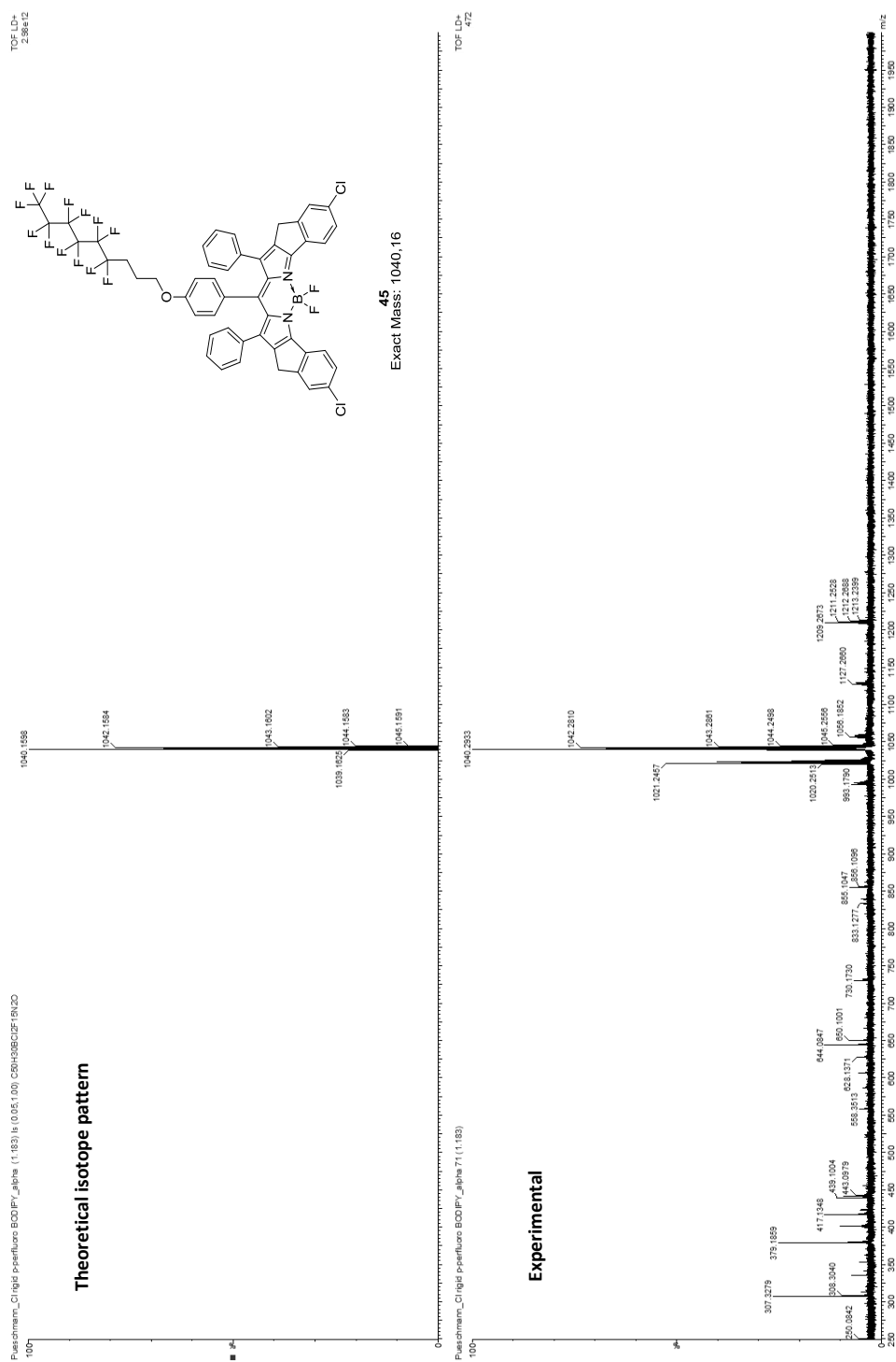


**Figure 10.48:** MALDI-TOF of m-perfluoro BODIPY (**45**) in alpha matrix with corresponding isotope pattern

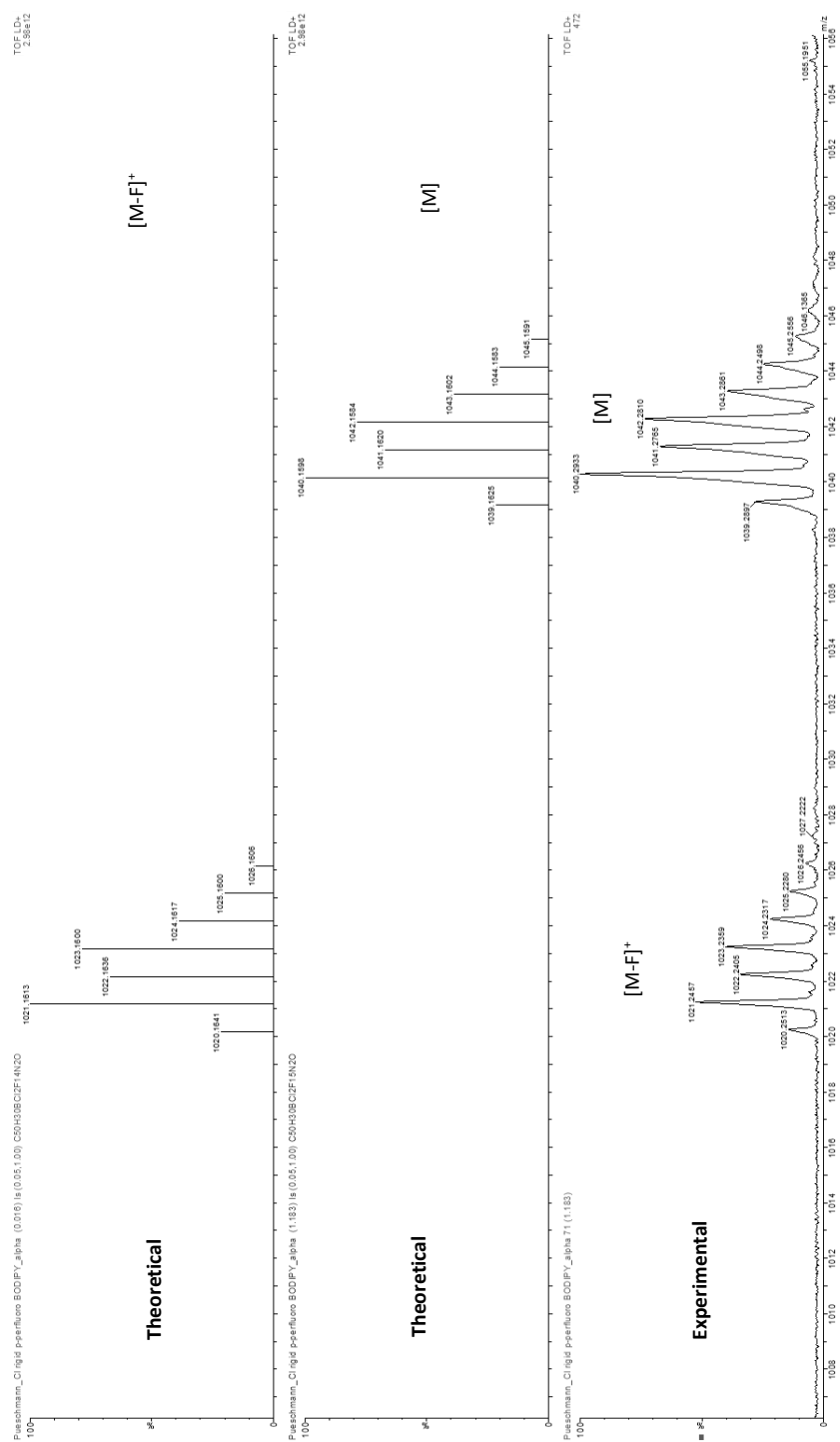


**Figure 10.49:** MALDI-TOF of m-perfluoro BODIPY (45) in alpha matrix with corresponding isotope pattern

## 10.4.9 Compound 46

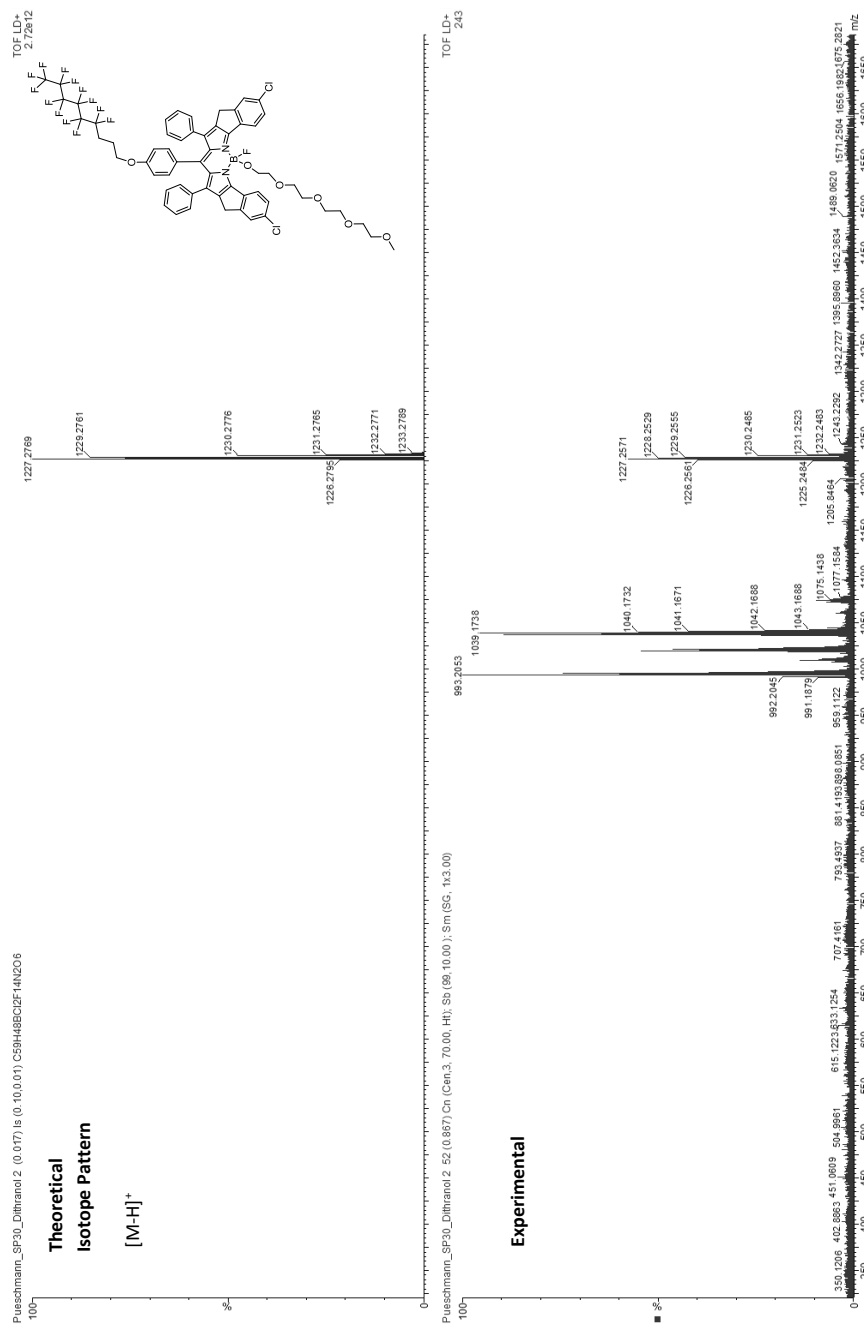


**Figure 10.50:** MALDI-TOF of m-perfluoro B-TEG BODIPY (**46**) in dithranol matrix with corresponding isotope pattern



**Figure 10.51:** MALDI-TOF of m-perfluoro B-TEG BODIPY (46) in dithranol matrix with corresponding isotope pattern

### 10.4.10 Compound 47

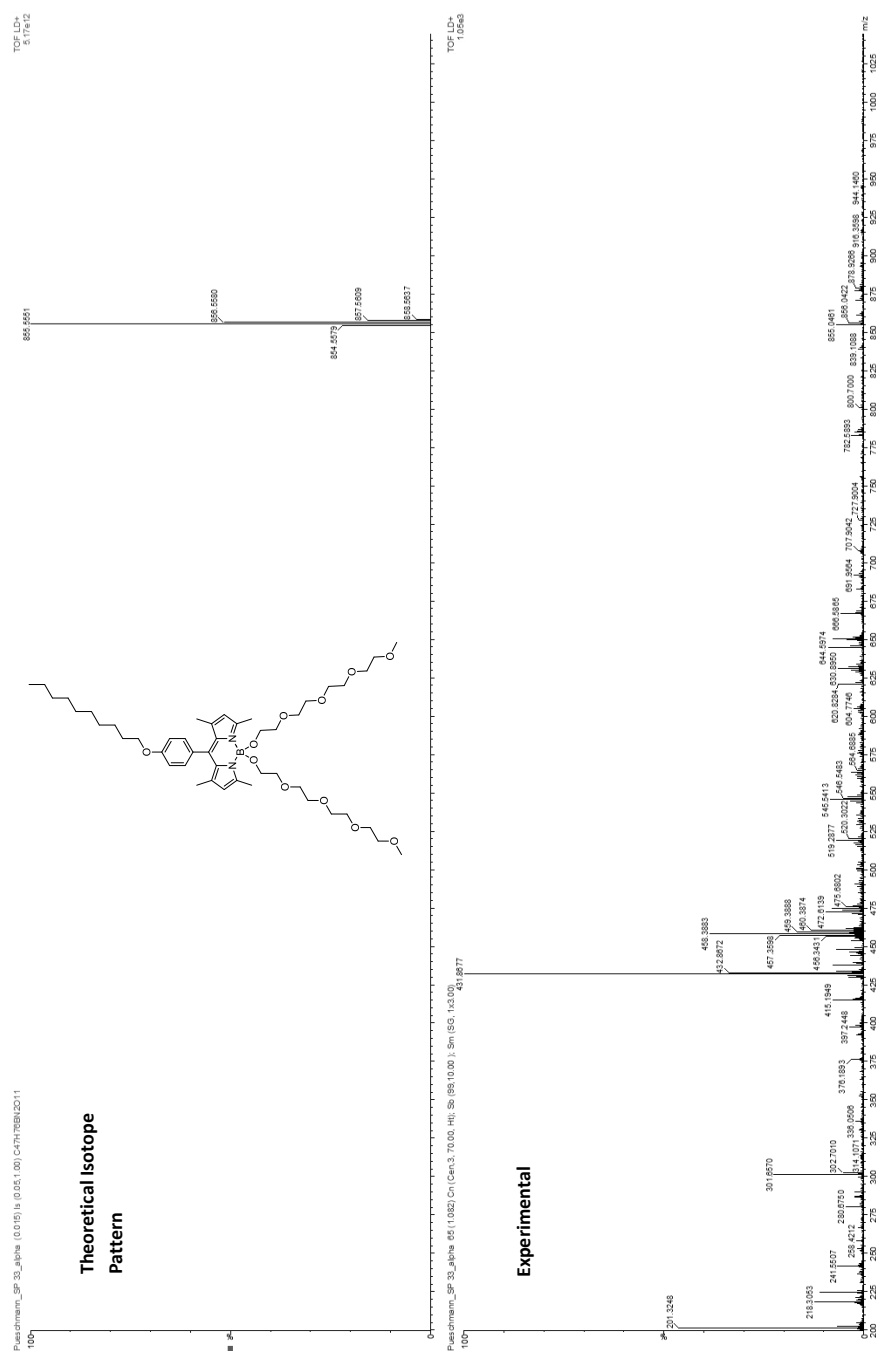


Figure 10.52: MALDI-TOF of compound 47 in alpha matrix with corresponding isotope pattern



Figure 10.53: MALDI-TOF of compound 47 in alpha matrix with corresponding isotope pattern showing mostly defragmentation